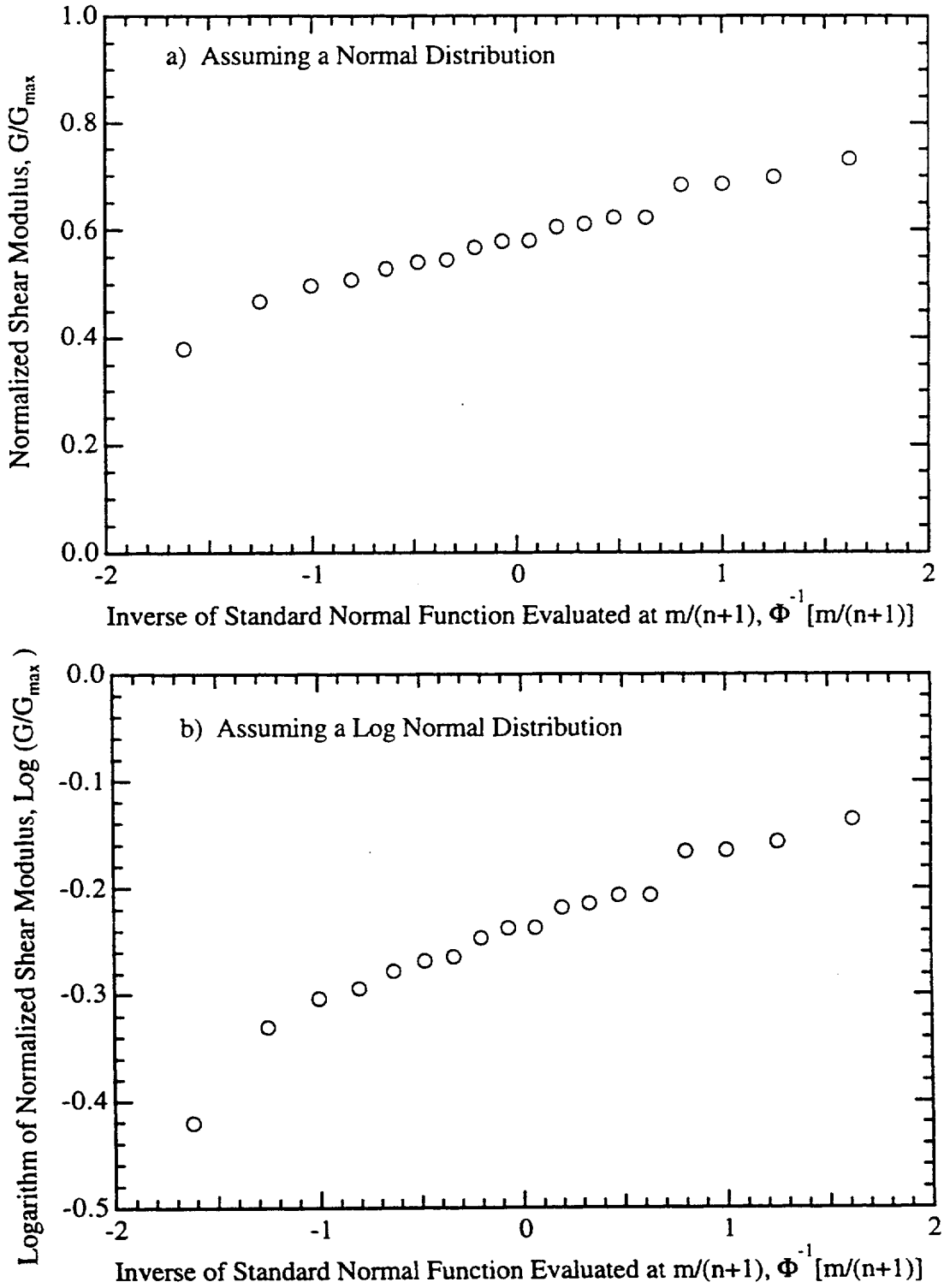


Fig. 89 Evaluation of the Distribution of $G/G_{max}$ Values at $\gamma$ = 0.03% for the Tobacco Road and Snapp Sands

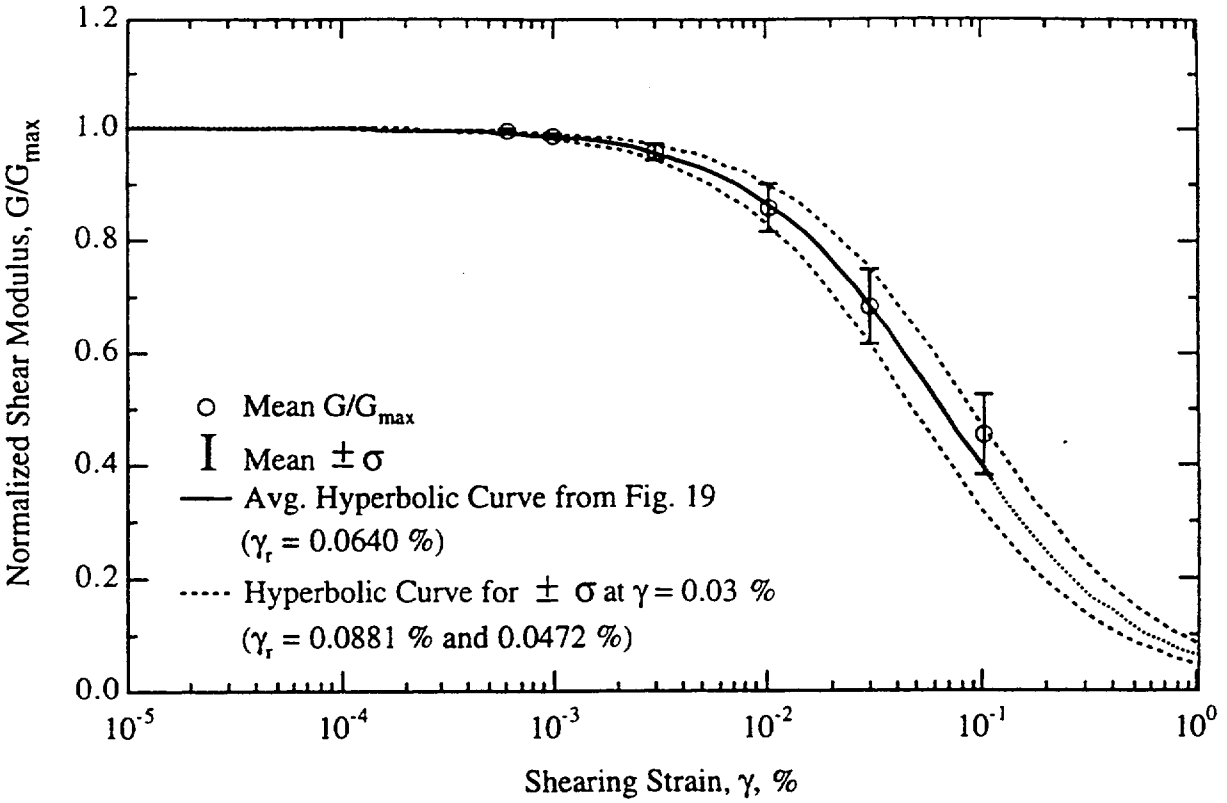


Fig. 90 Statistical Evaluation of the $G/G_{max}$ Values for the Dry Branch Sands

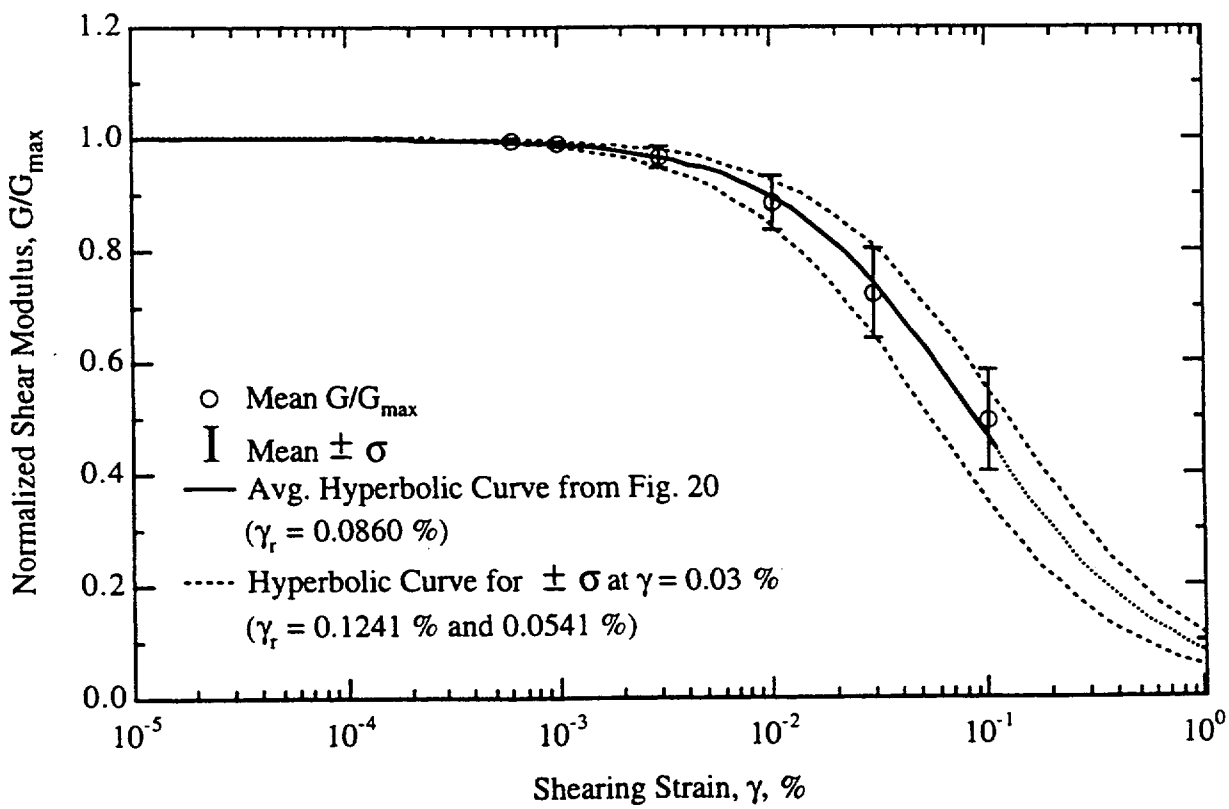


Fig. 91 Statistical Evaluation of the $G/G_{max}$ Values for the Santee Sands

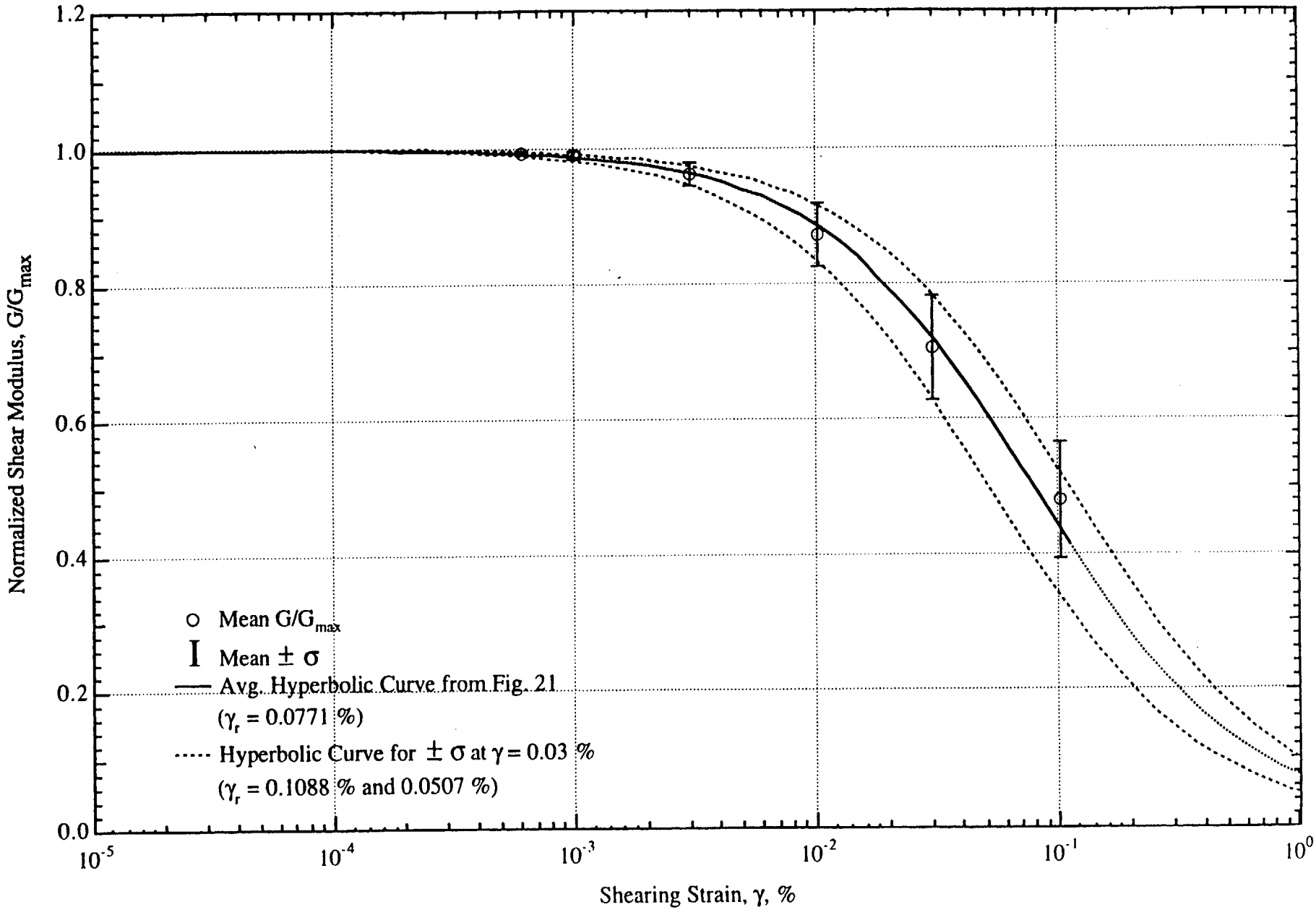


Fig. 92 Statistical Evaluation of the G/Gmax Values for the Combined Dry Branch and Santee Sands

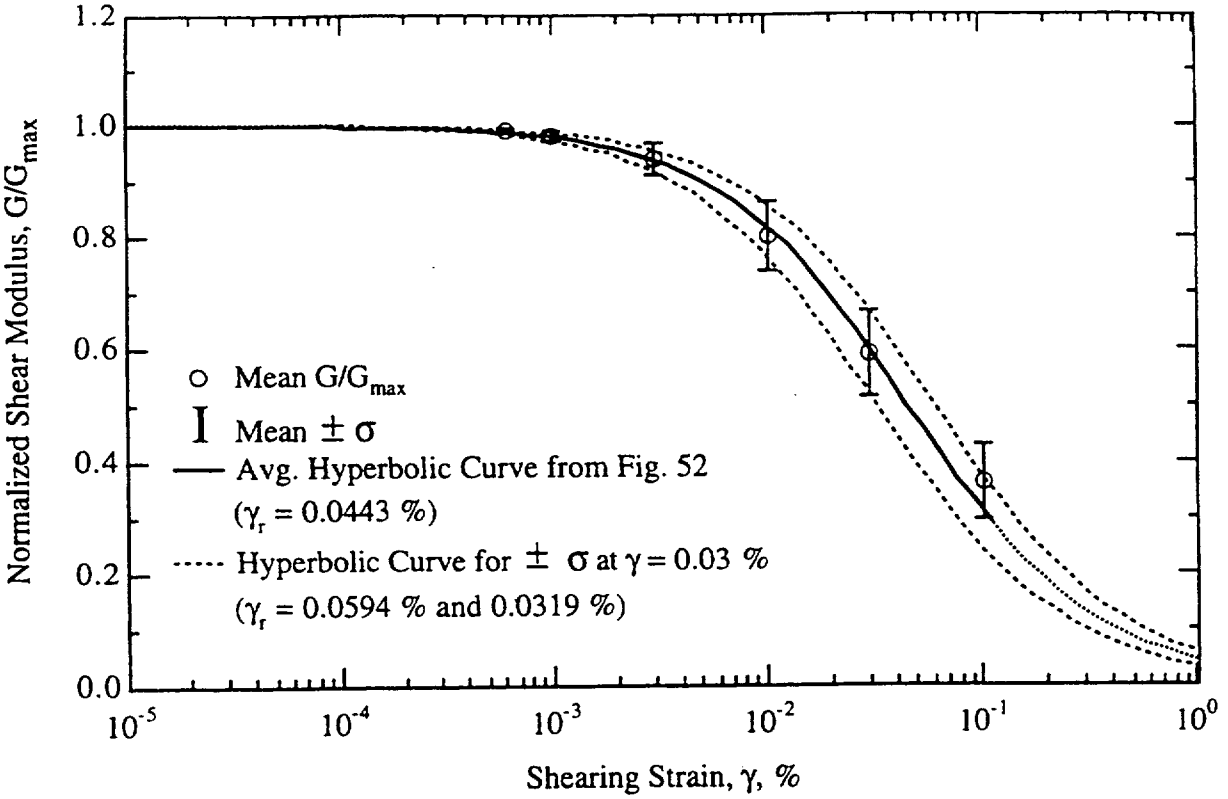


Fig. 93 Statistical Evaluation of the $G/G_{max}$ Values of the Tobacco Road Sands

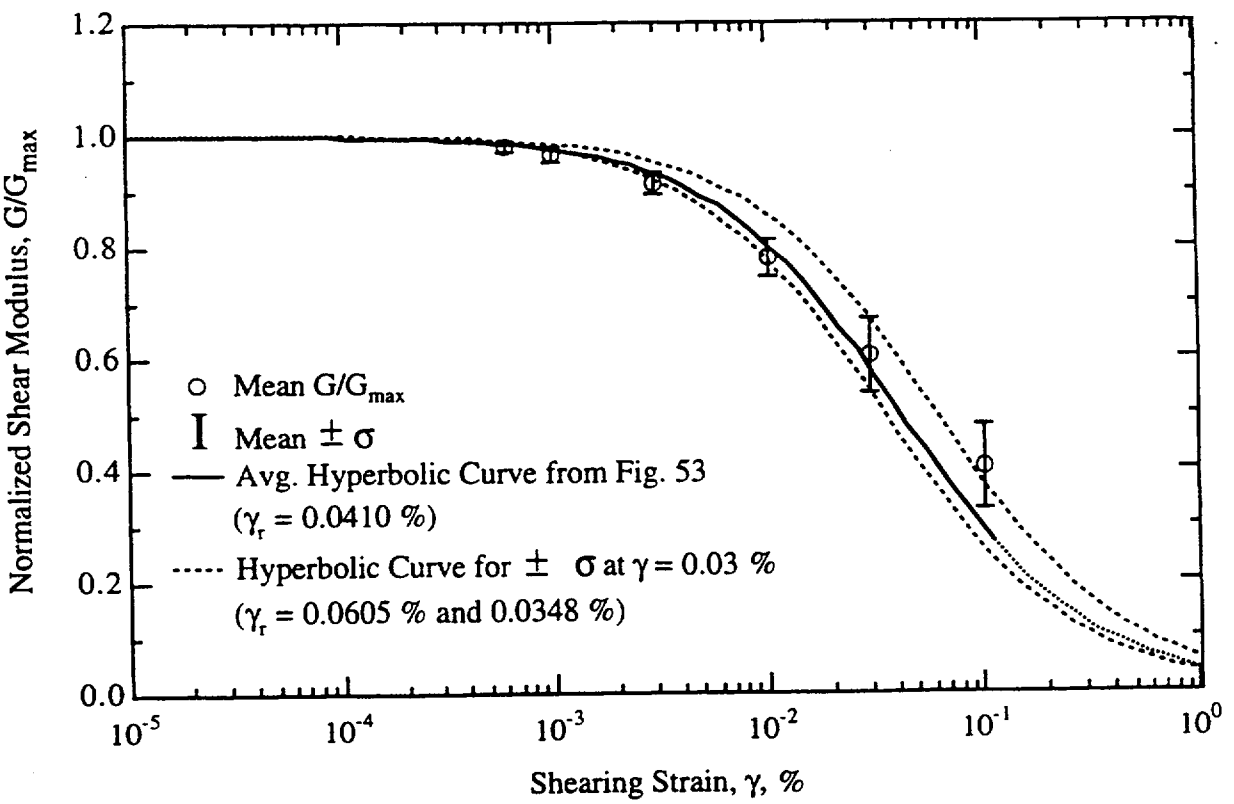


Fig. 94 Statistical Evaluation of the $G/G_{max}$ Values of the Snapp Sands

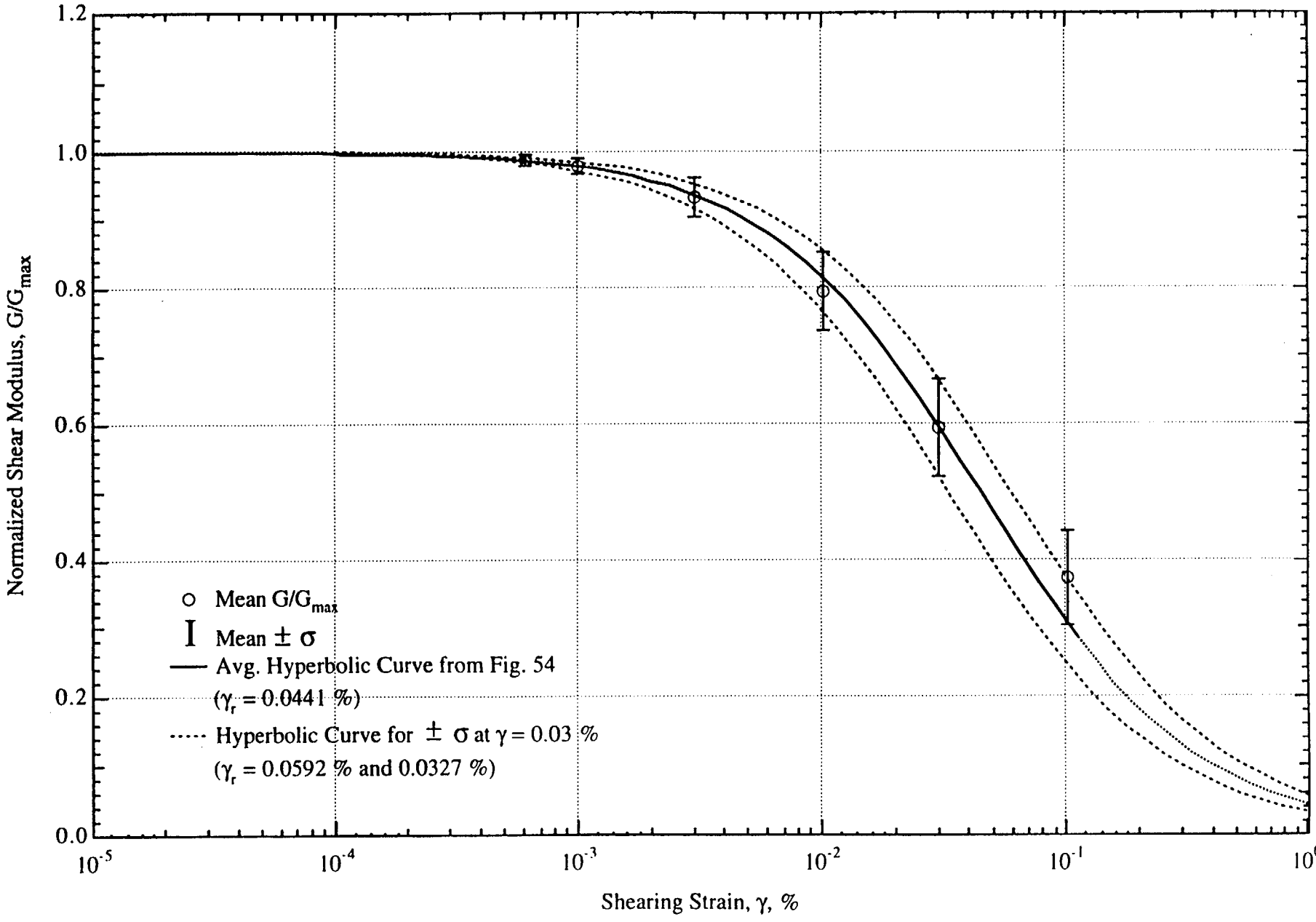


Fig. 95 Statistical Evaluation of the $G/G_{max}$ Values for the Combined Tobacco Road and Snapp Sands

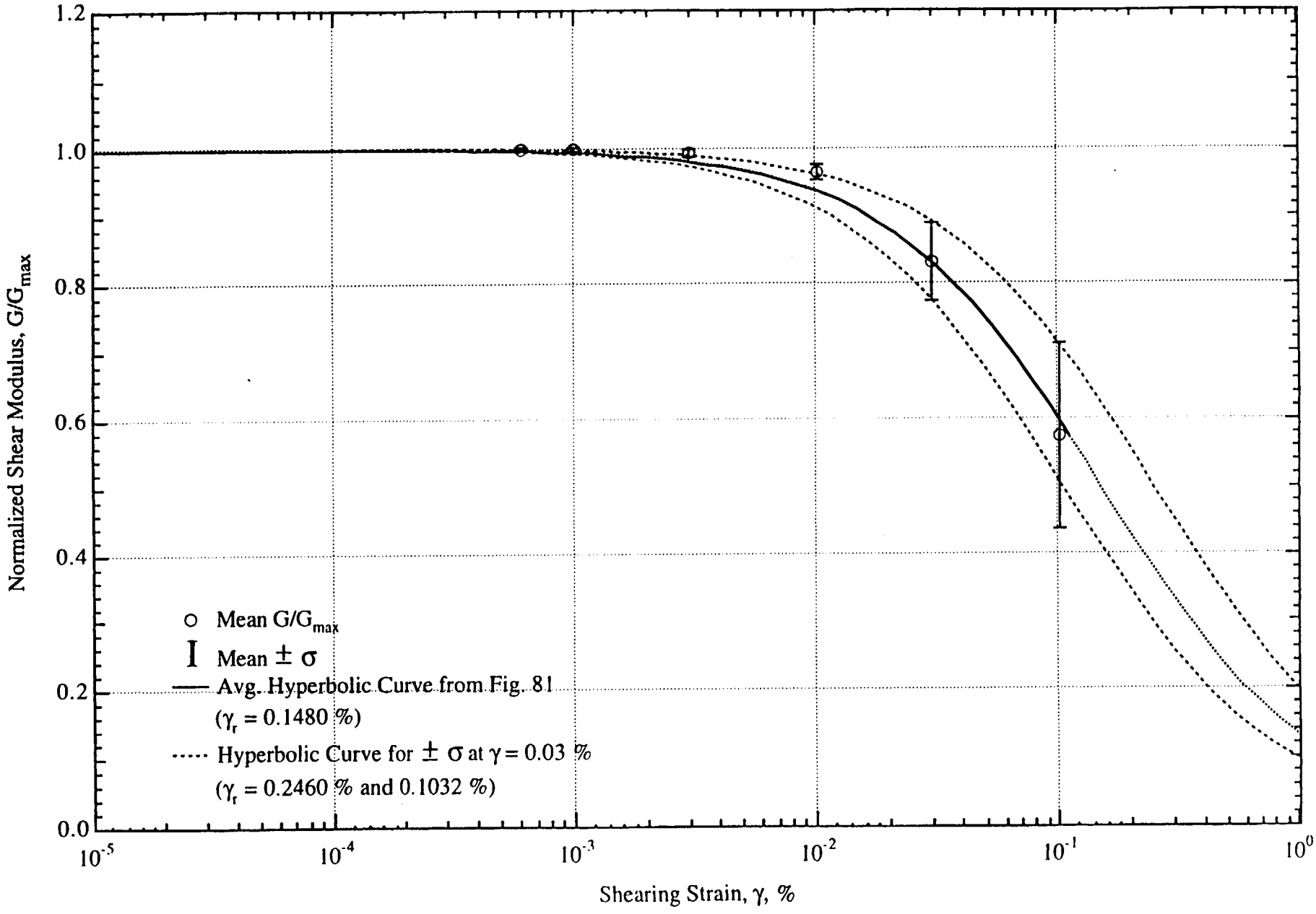


Fig. 96 Statistical Evaluation of the $G/G_{max}$ Values for the Shallow Clays

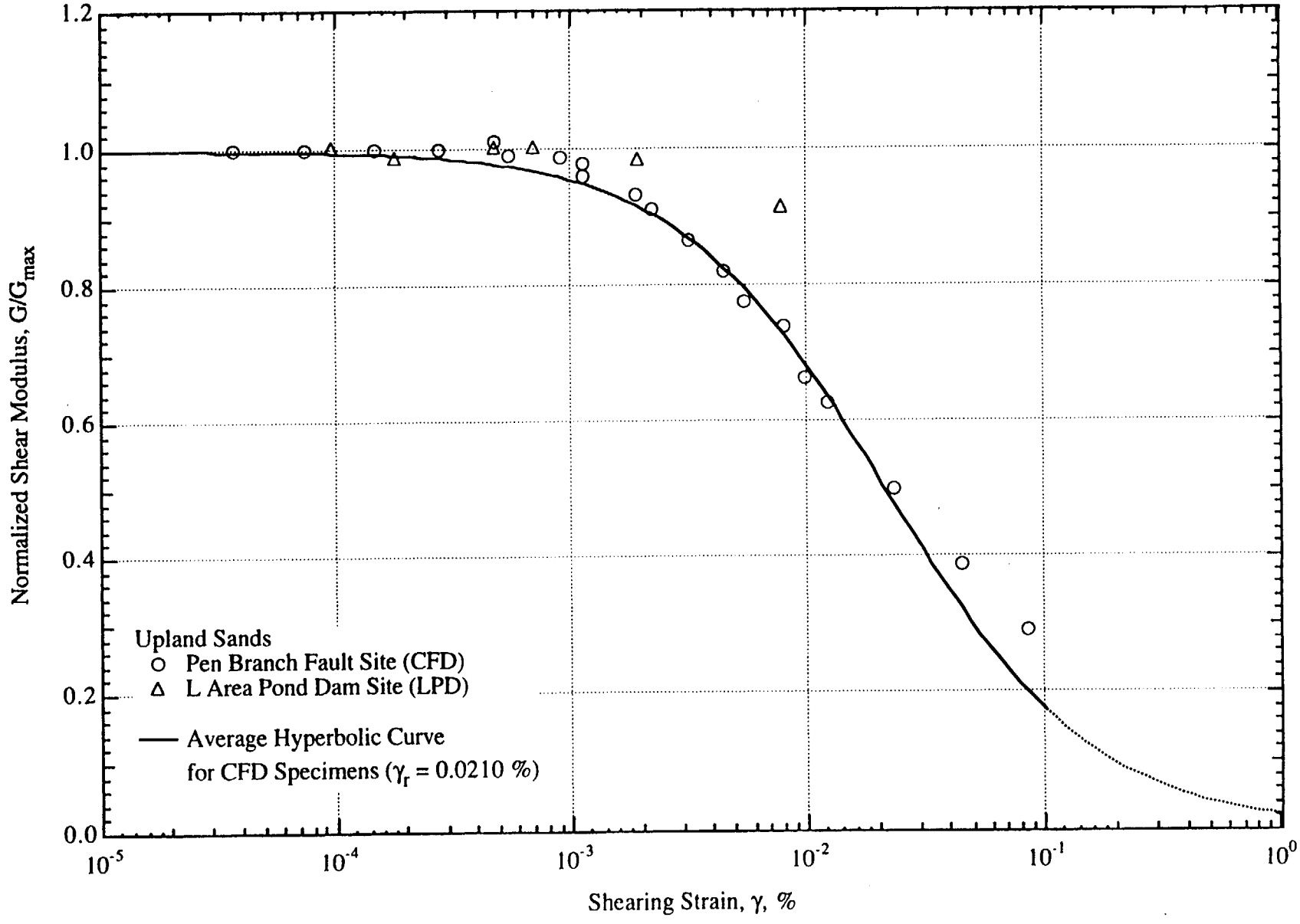


Fig. 97 Summary Plot of All $G/G_{max}$ - log $\gamma$ Relationships Determined by Resonant Column Testing with the Specimens Confined At or Near the In-Situ Mean Effective Stress for the Upland Sands

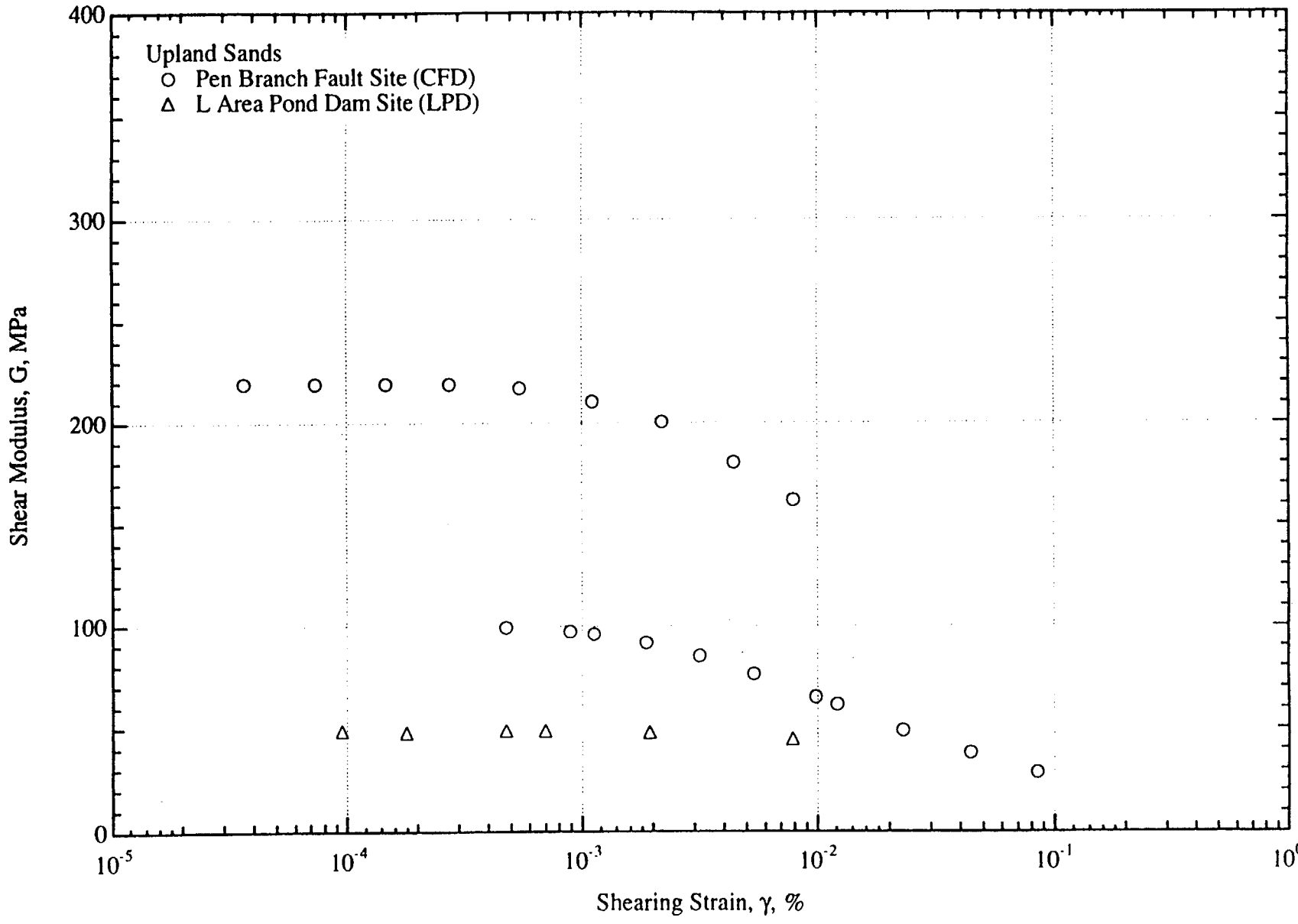


Fig. 98 Summary Plot of All G - log γ Relationships Determined by Resonant Column Testing with the Specimens Confined At or Near the In-Situ Mean Effective Stress for the Upland Sands

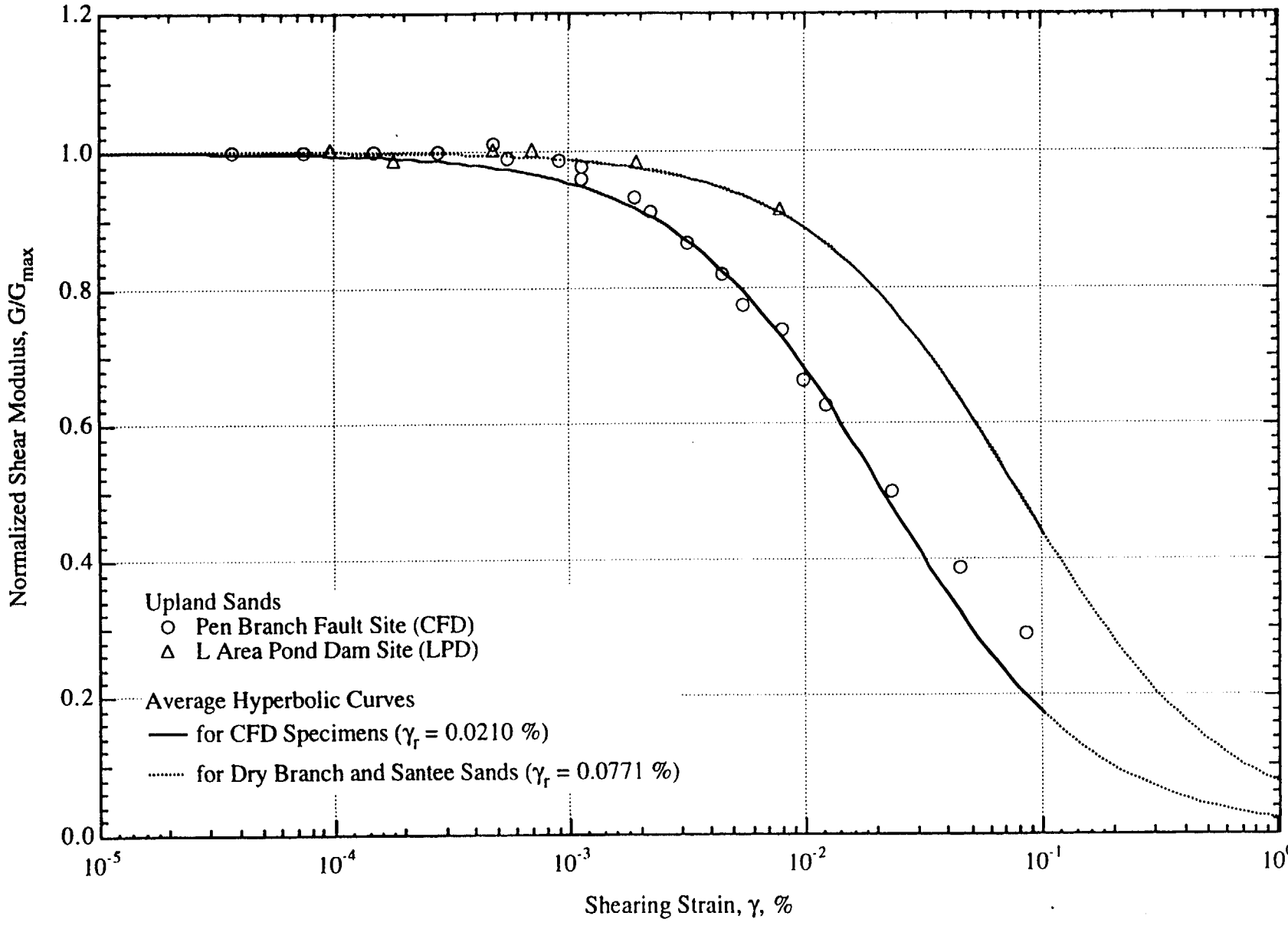


Fig. 99 Comparison of the $G/G_{max}$ - log $\gamma$ Relationship Determined by Resonant Column Testing of the Softer Upland Sand Specimen with the Average Recommended Hyperbolic Relationship for Dry Branch and Santee Sands

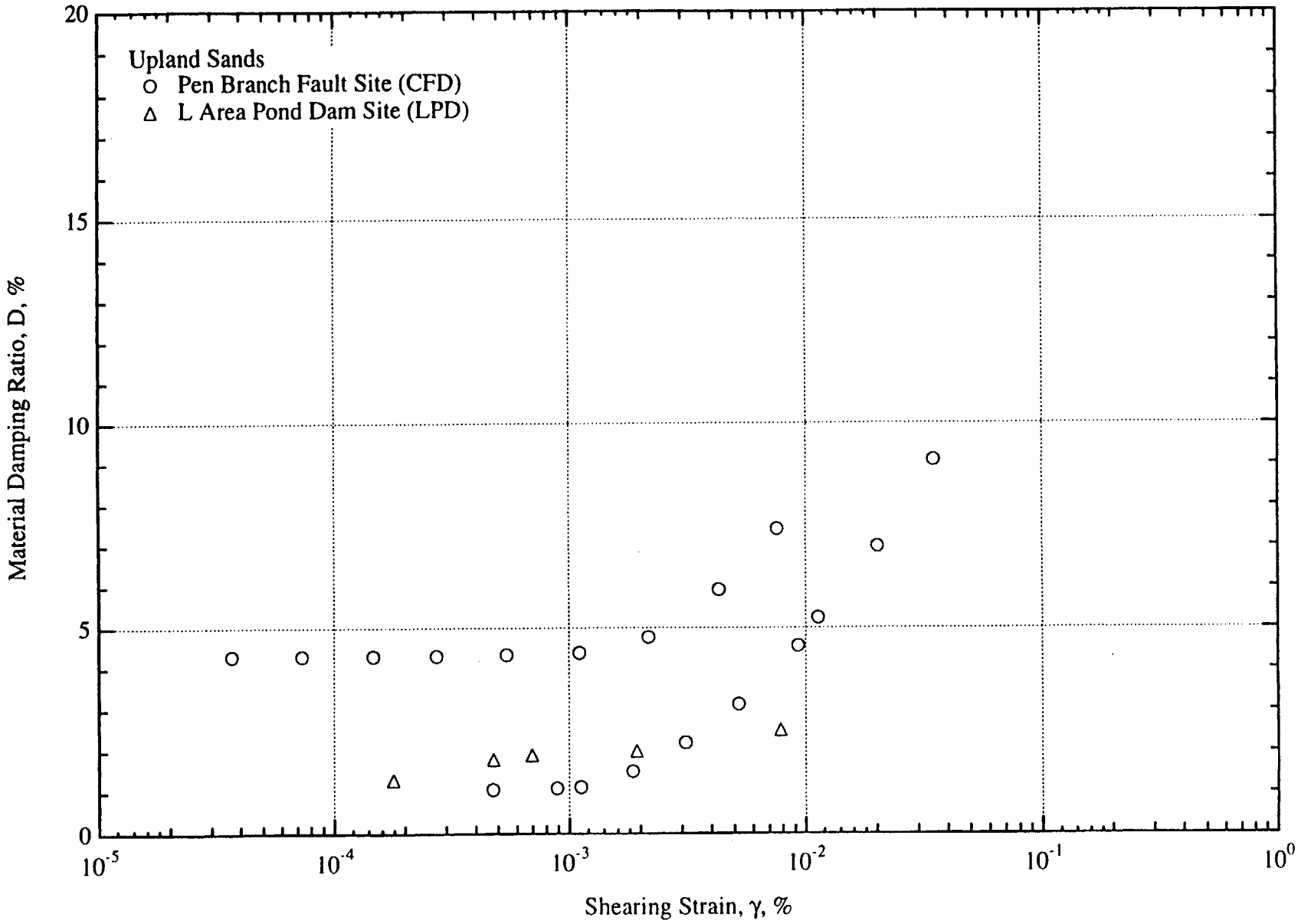


Fig. 100 Summary Plot of All D - log γ Relationships Determined by Resonant Column Testing with the Specimens Confined At or Near the In-Situ Mean Effective Stress for the Upland Sands

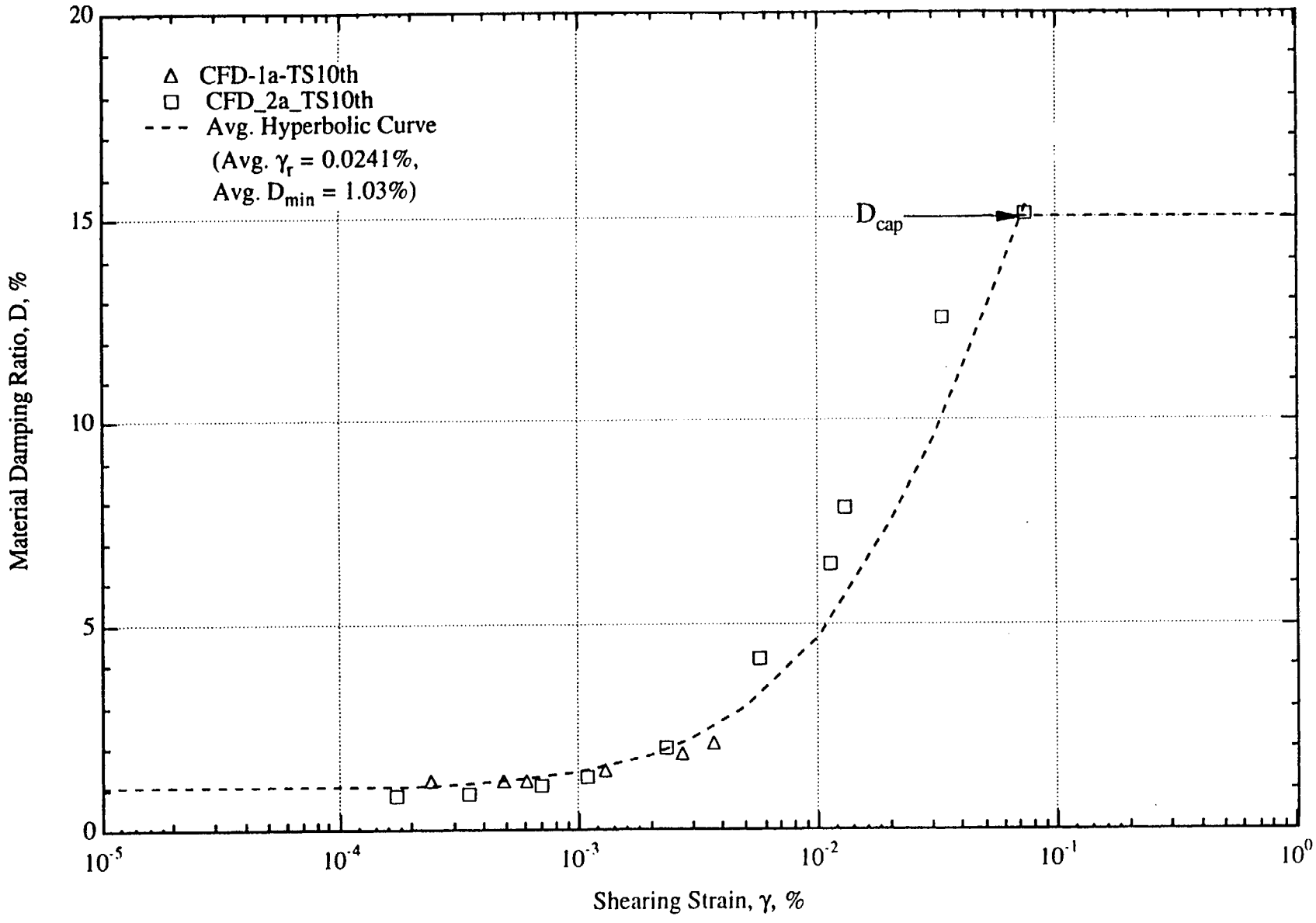


Fig. 101 Comparison of the D - log γ Relationships Measured in the Tenth Cycle of TS Testing with the Recommended Average Hyperbolic Relationship for Stiff Upland Sands

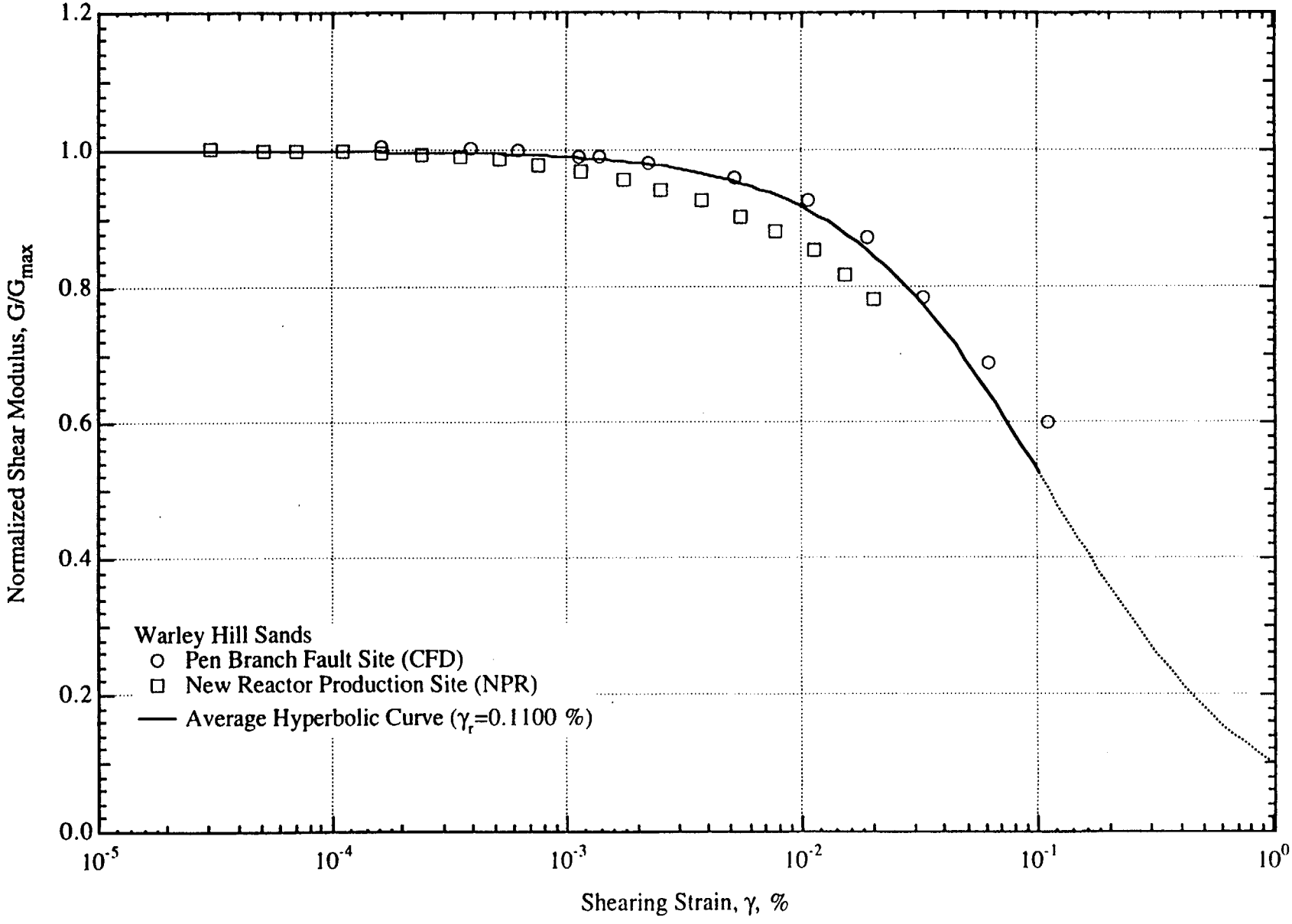


Fig. 102 Summary Plot of All $G/G_{max}$ - log $\gamma$ Relationships Determined by Resonant Column Testing with the Specimens Confined At or Near the In-Situ Mean Effective Stress for the Warley Hill Sands

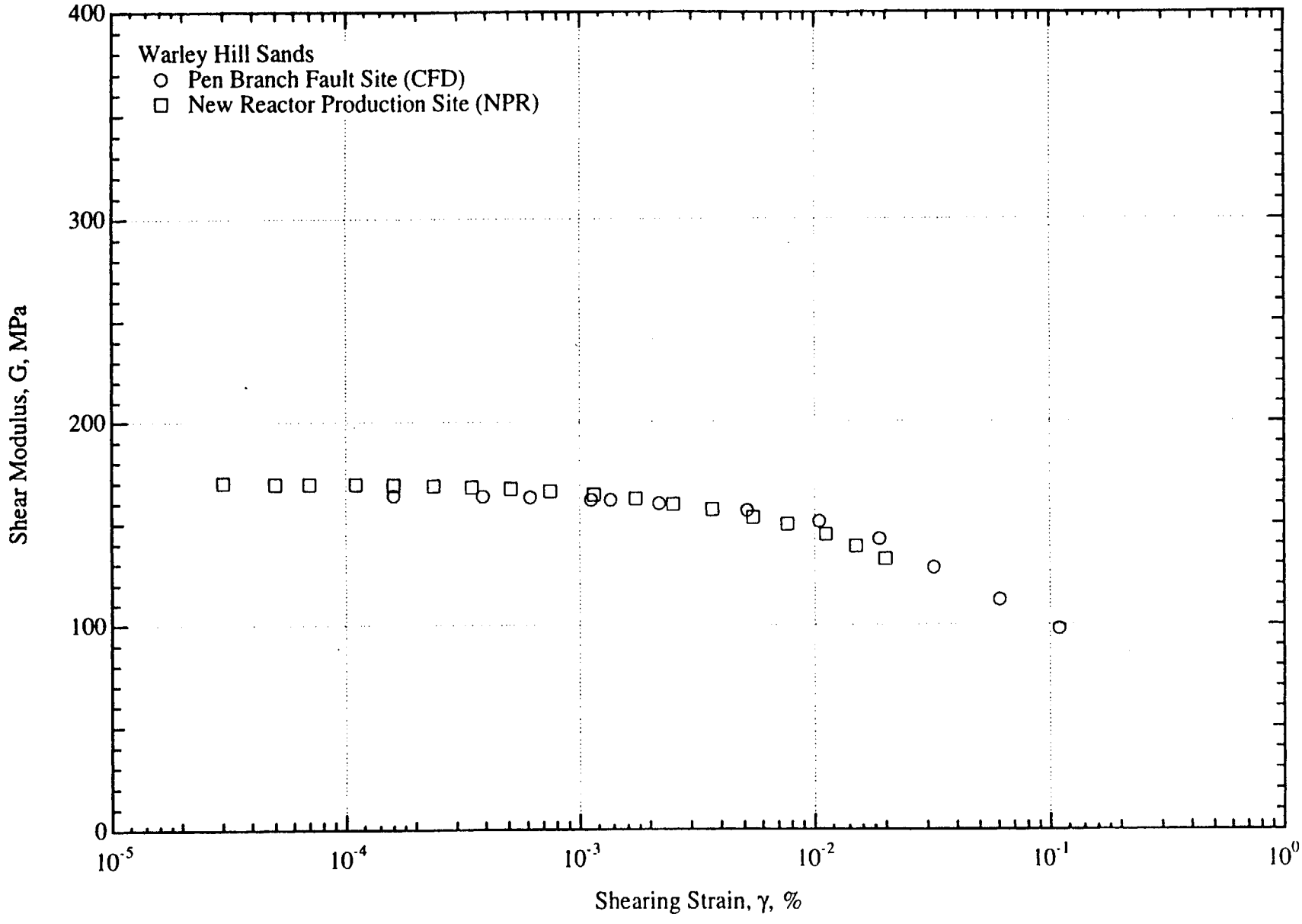


Fig. 103 Summary Plot of All G - log γ Relationships Determined by Resonant Column Testing with the Specimens Confined At or Near the In-Situ Mean Effective Stress for the Warley Hill Sands

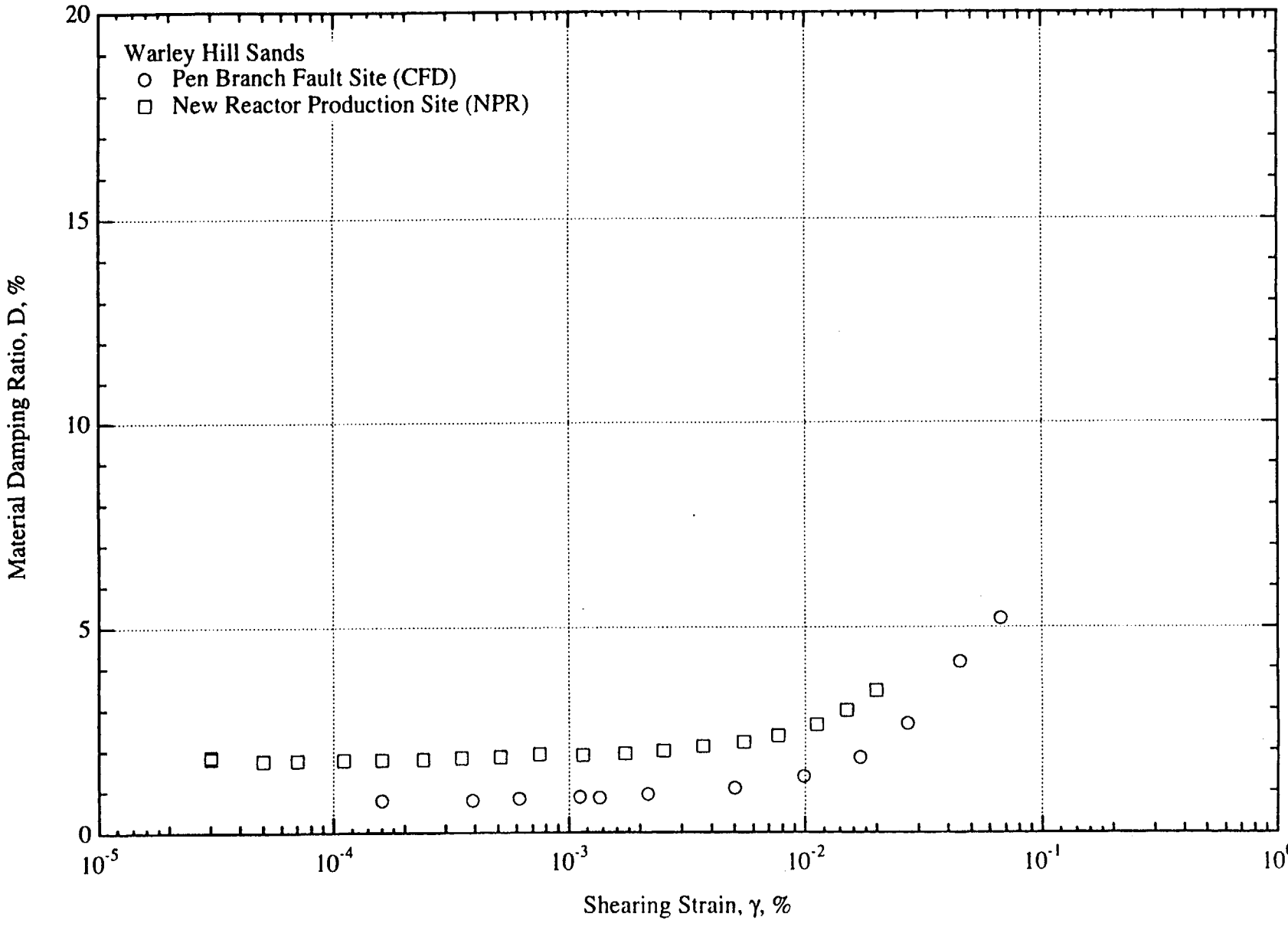


Fig. 104 Summary Plot of All D - log γ Relationships Determined by Resonant Column Testing with the Specimens Confined At or Near the In-Situ Mean Effective Stress for the Warley Hill Sands

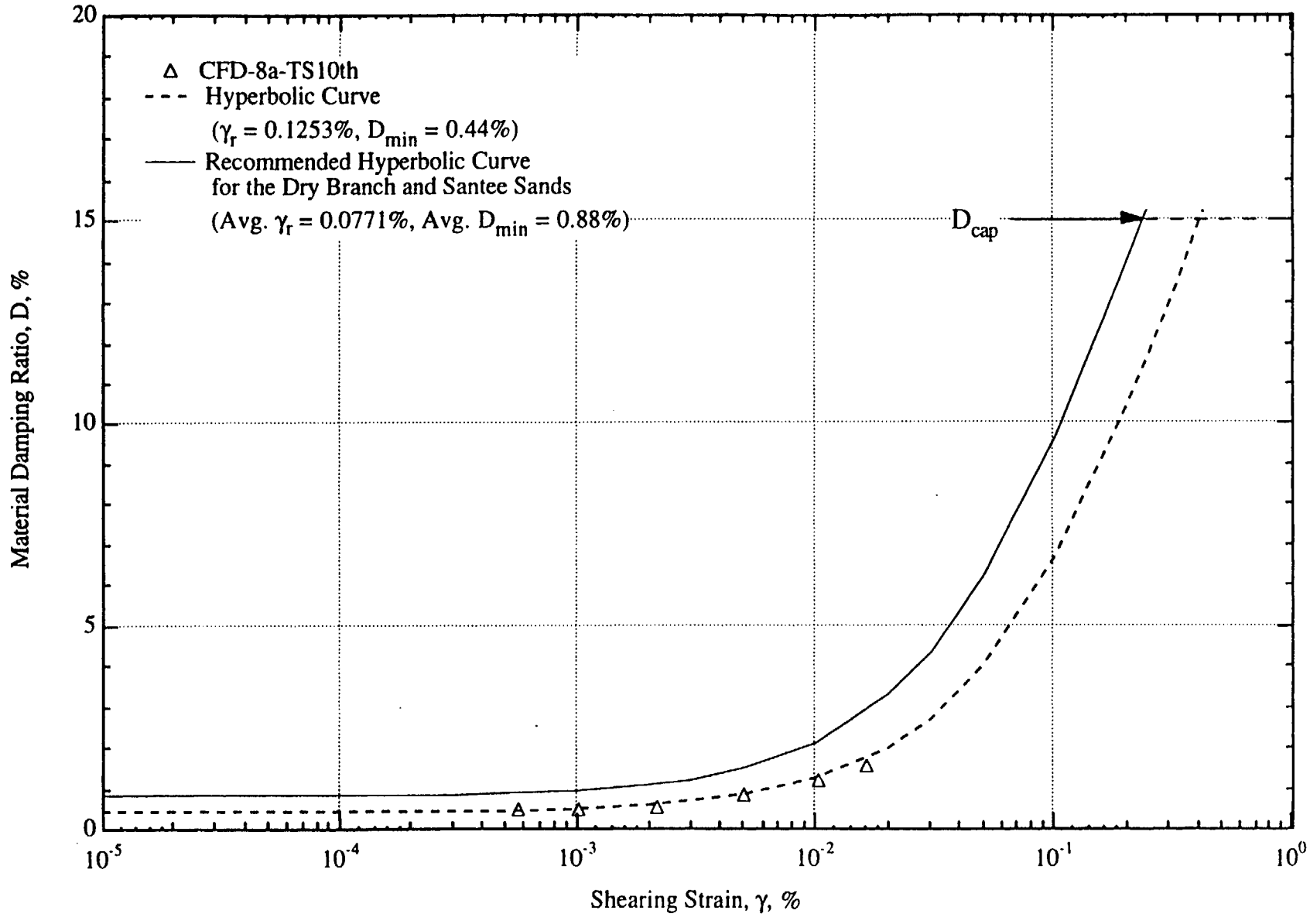


Fig. 105 Comparison of the D - log γ Relationship Measured in the Tenth Cycle of TS Testing for the Warley Hill Specimen with an Average Hyperbolic Relationship Warley Hill Sands and the Recommended Average Hyperbolic Relationship for the Dry Branch

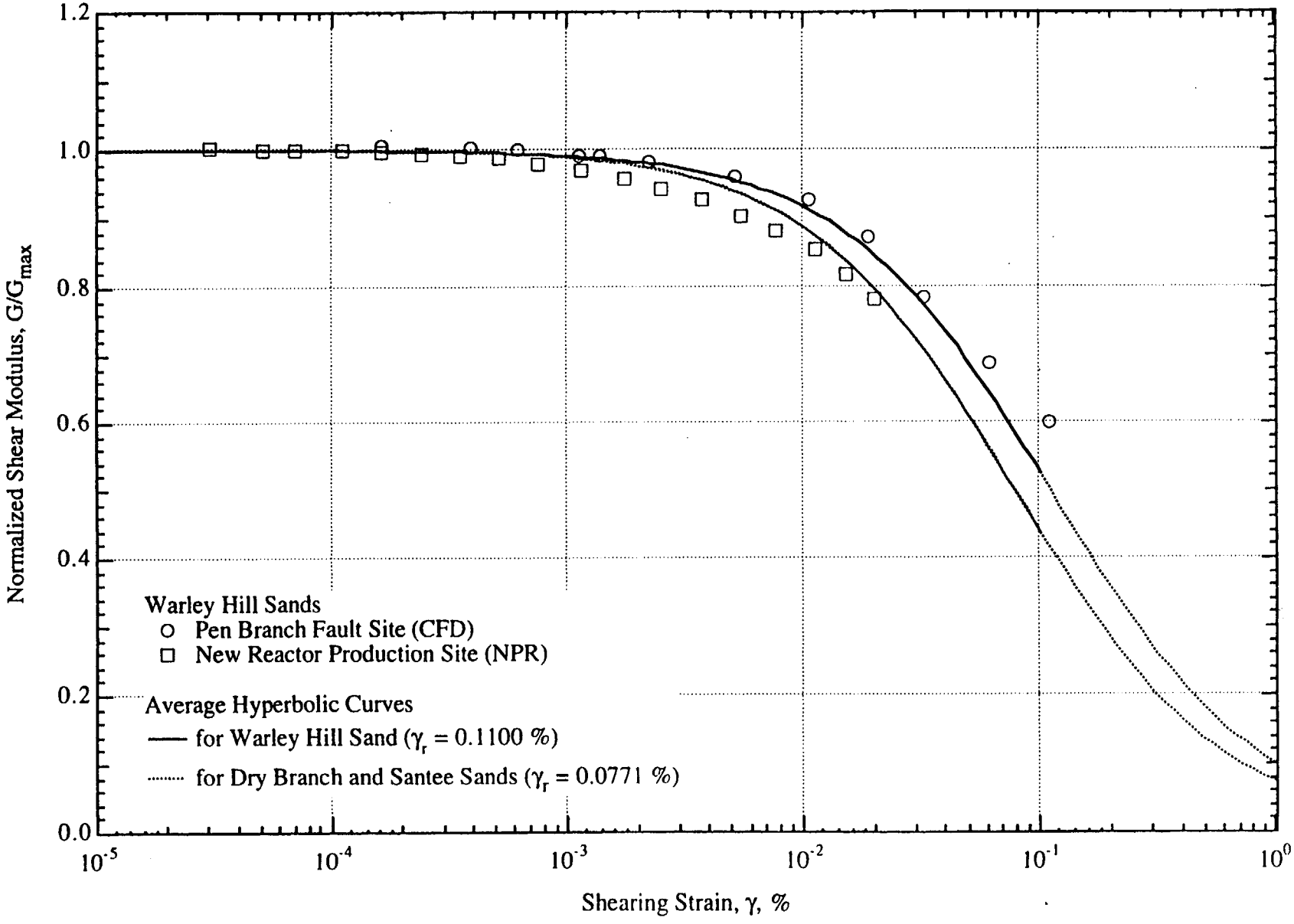


Fig. 106 Comparison of an Average Hyperbolic $G/G_{max}$ - log γ Relationship for the Warley Hill Sands with the Recommended Average Hyperbolic Relationship for the Dry Branch and Santee Sands

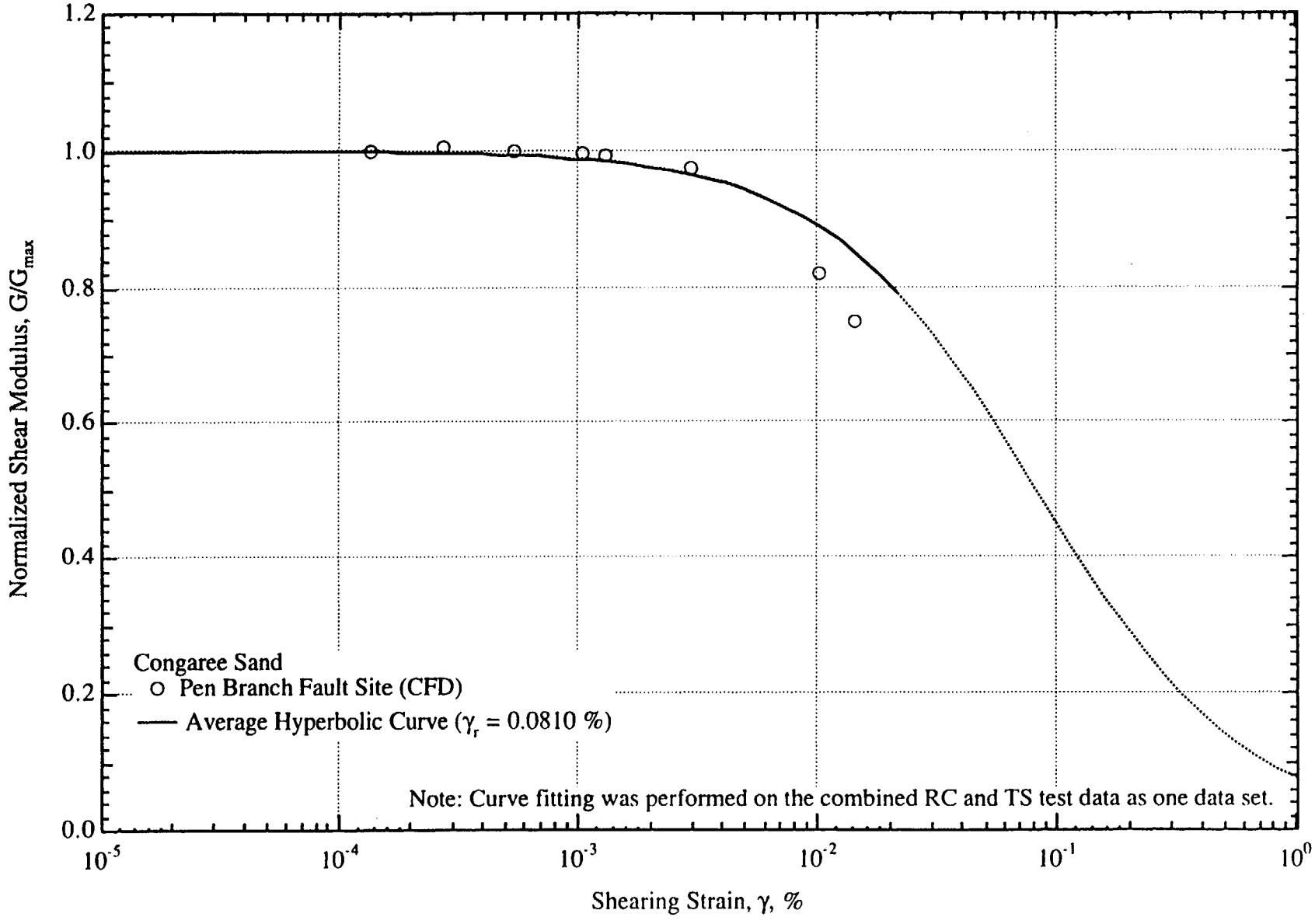


Fig. 107 Plot of the $G/G_{max}$ - log $\gamma$ Relationship Determined by Resonant Column Testing with a Specimen Confined At or Near the In-Situ Mean Effective Stress for the Congaree Sand

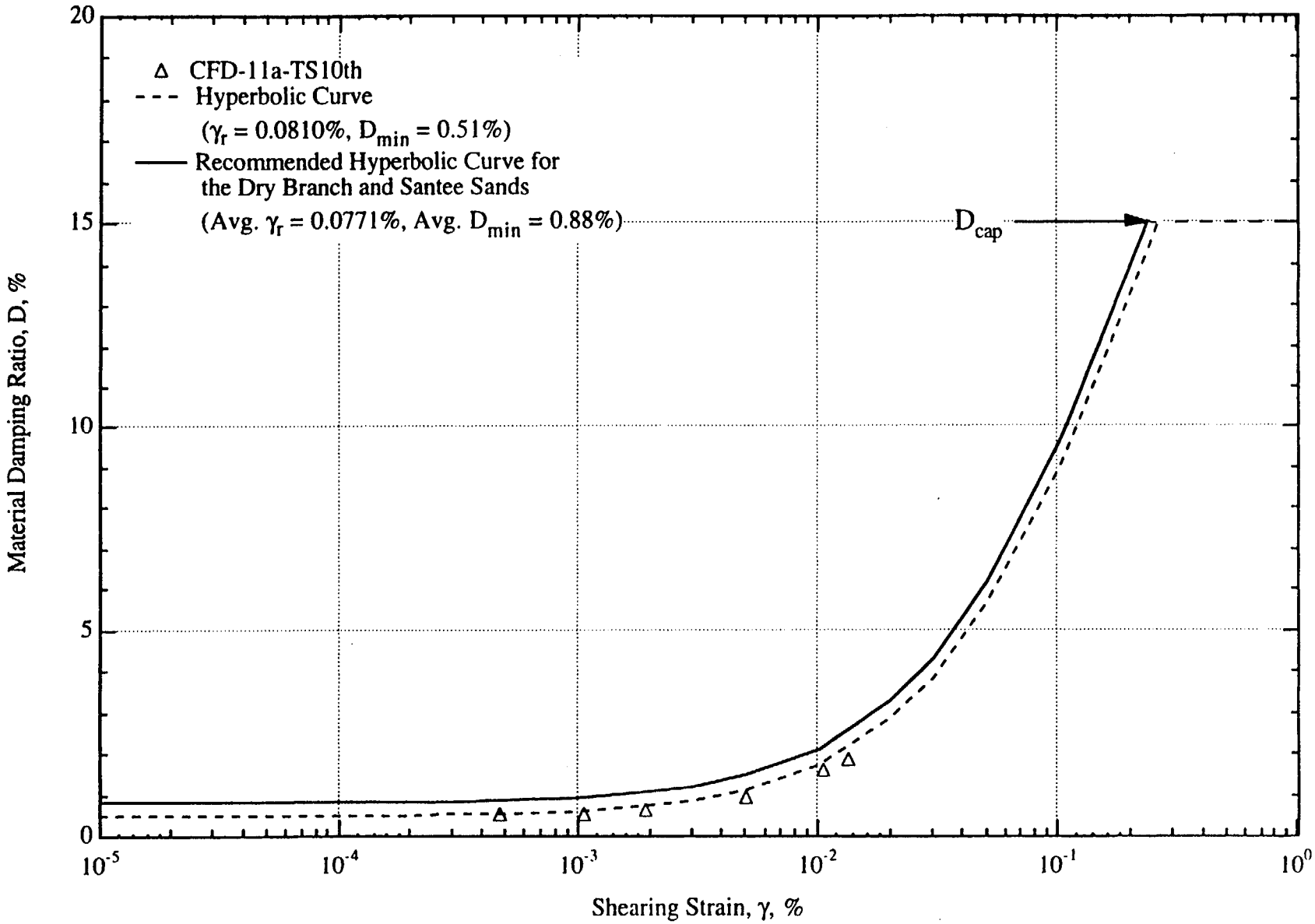


Fig. 108 Comparison of the D - log γ Relationship Measured in the Tenth Cycle of TS Testing for the Congaree Specimen with an Average Hyperbolic Relationship for Congaree Sands and with the Recommended Average Hyperbolic Relationship for the Dry Branch and Santee Sands

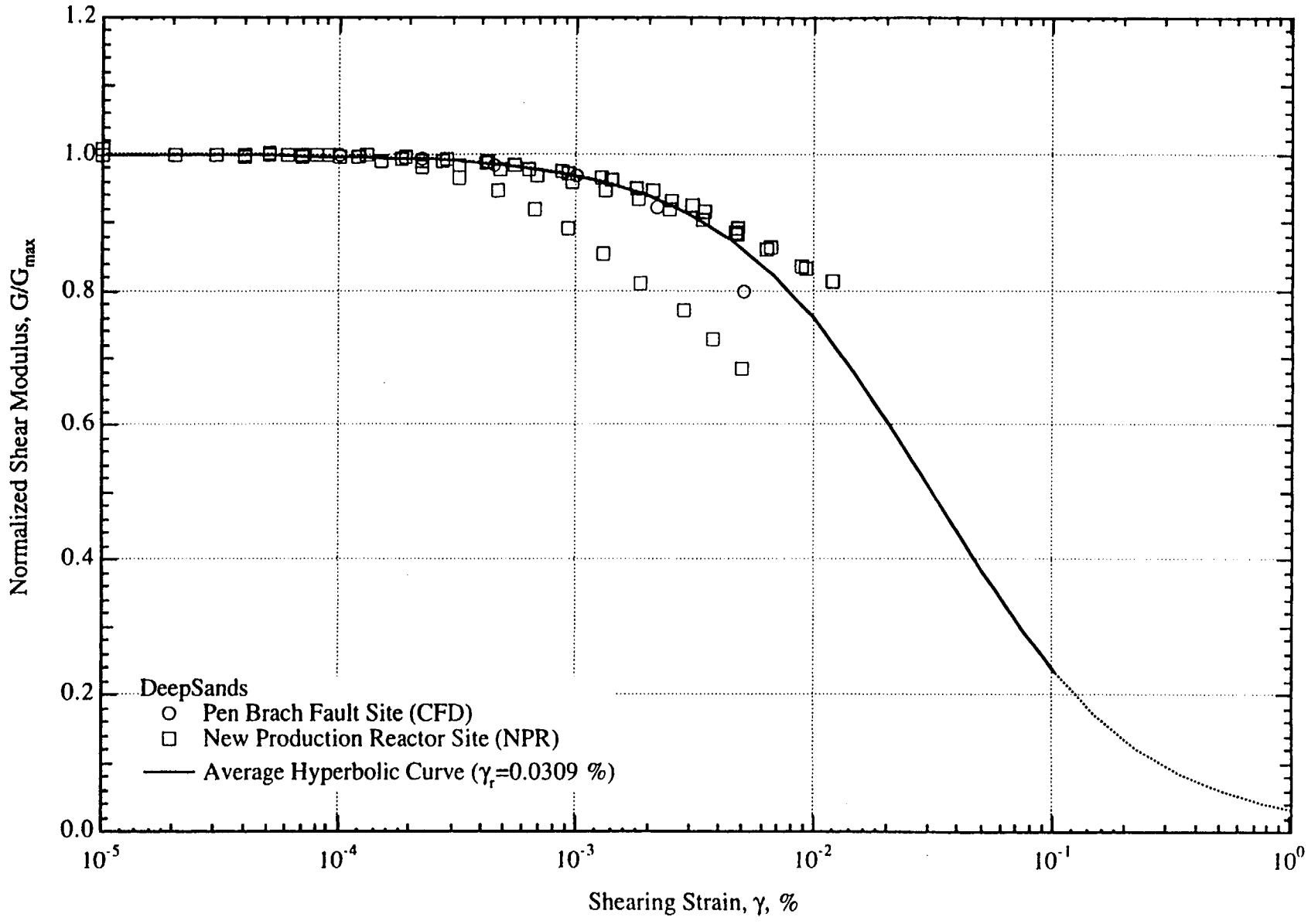


Fig. 109 Summary Plot of All $G/G_{max}$ - log $\gamma$ Relationships Determined by RCTS Testing with the Specimens Confined At or Near the In-Situ Mean Effective Stress for the Deep Sands

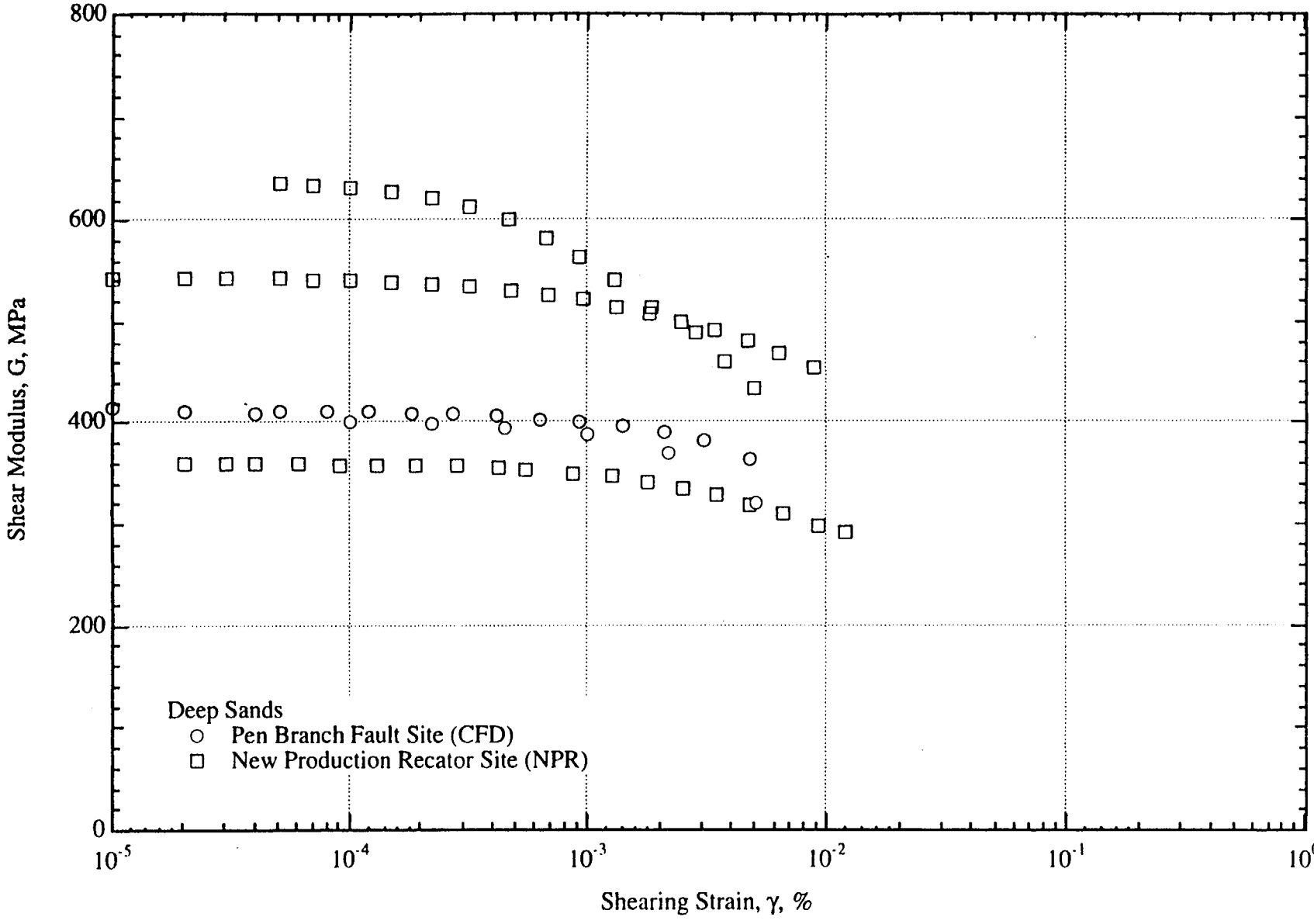


Fig. 110 Summary Plot of All G - log γ Relationships Determined by RCTS Testing with the Specimens Confined At or Near the In-Situ Mean Effective Stress for the Deep Sands

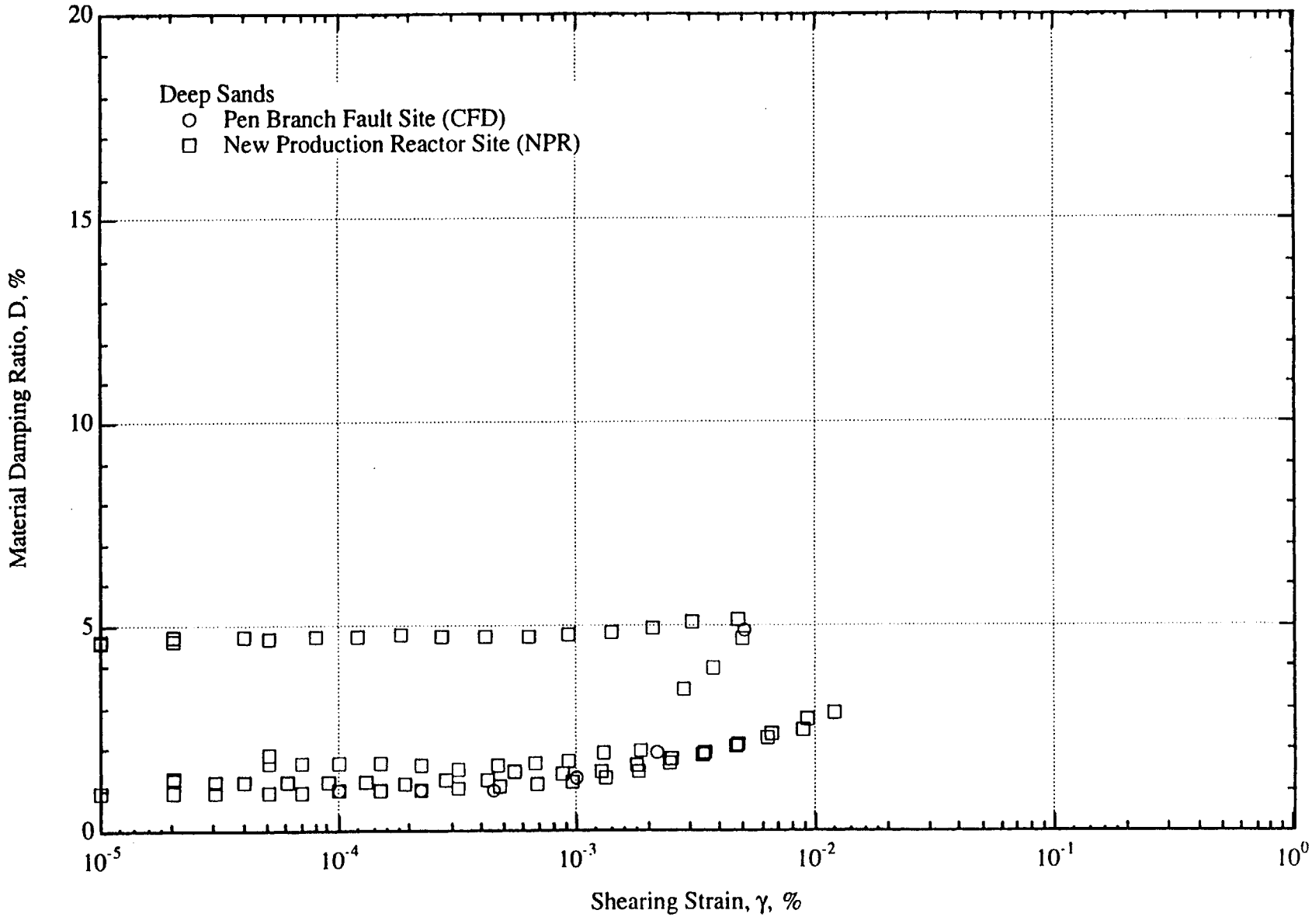


Fig. 111 Summary Plot of All D - log γ Relationships Determined by RCTS Testing with the Specimens Confined At or Near the In-Situ Mean Effective Stress for the Deep Sands

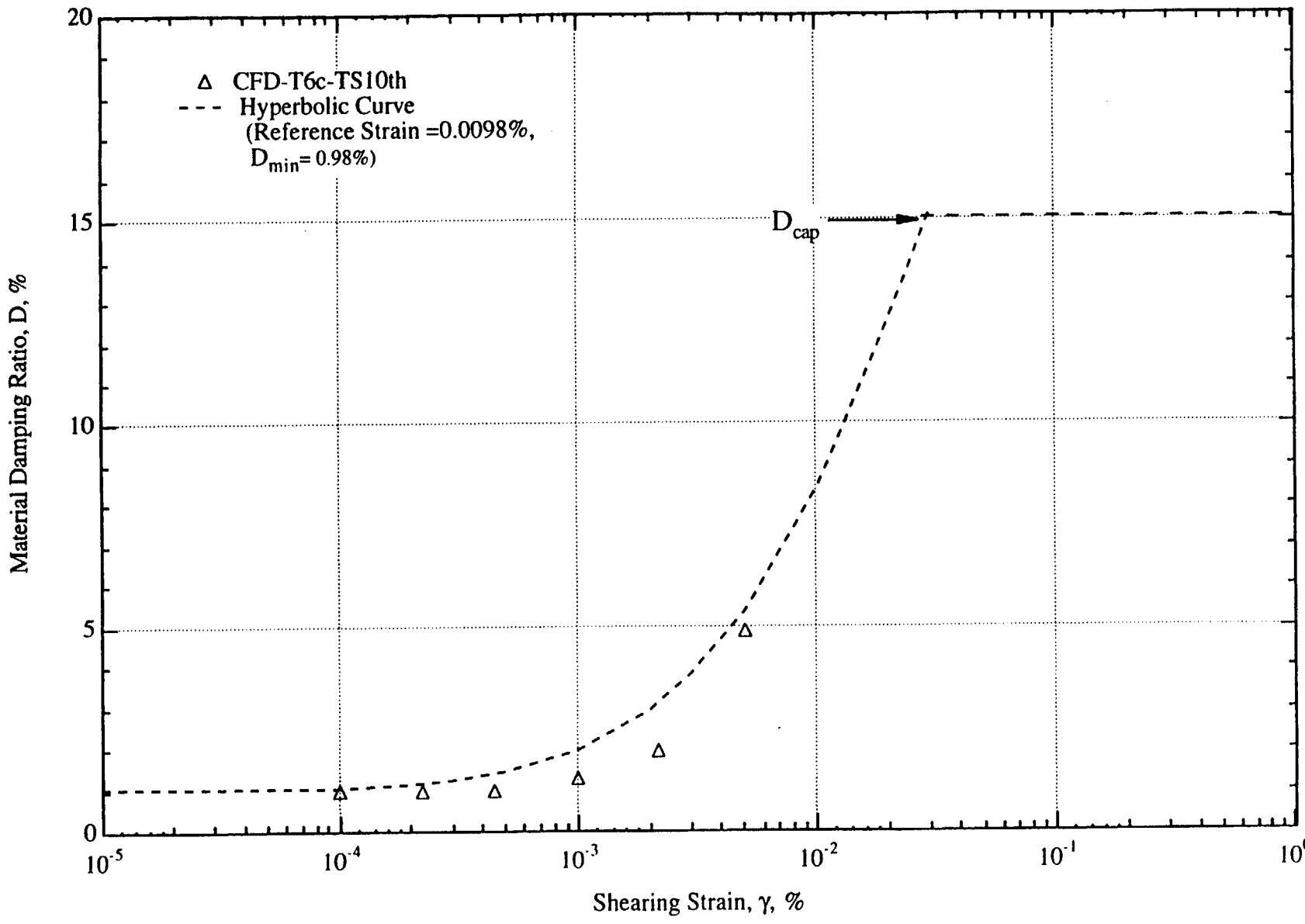


Fig. 112 Comparison of the D - log γ Relationship Measured in the Tenth Cycle of TS Testing with an Average Hyperbolic Curve for the Deep Sands

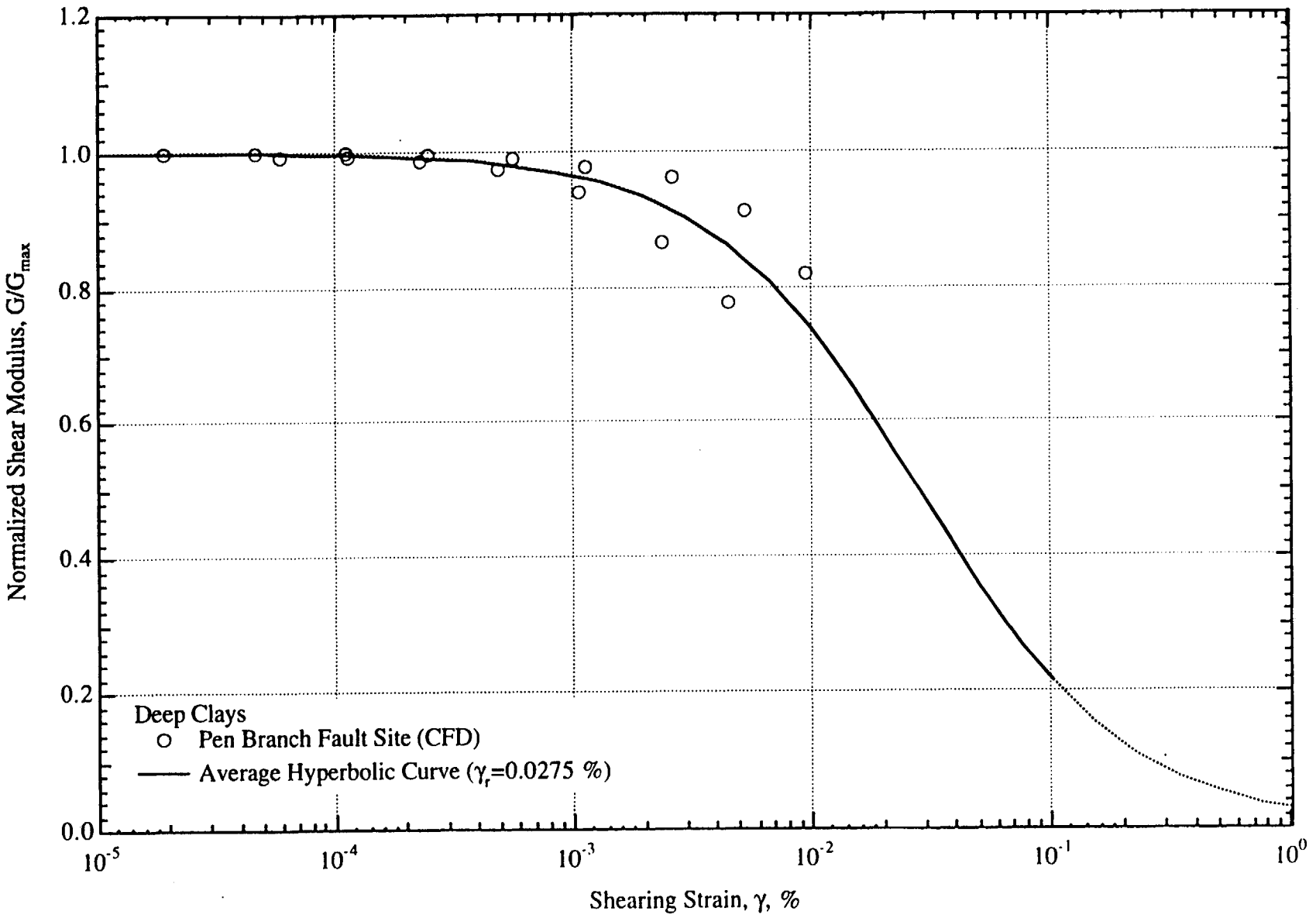


Fig. 113 Summary Plot of All $G/G_{max}$ - log $\gamma$ Relationships Determined by RCTS Testing with the Specimens Confined At or Near the In-Situ Mean Effective Stress for the Deep Clays

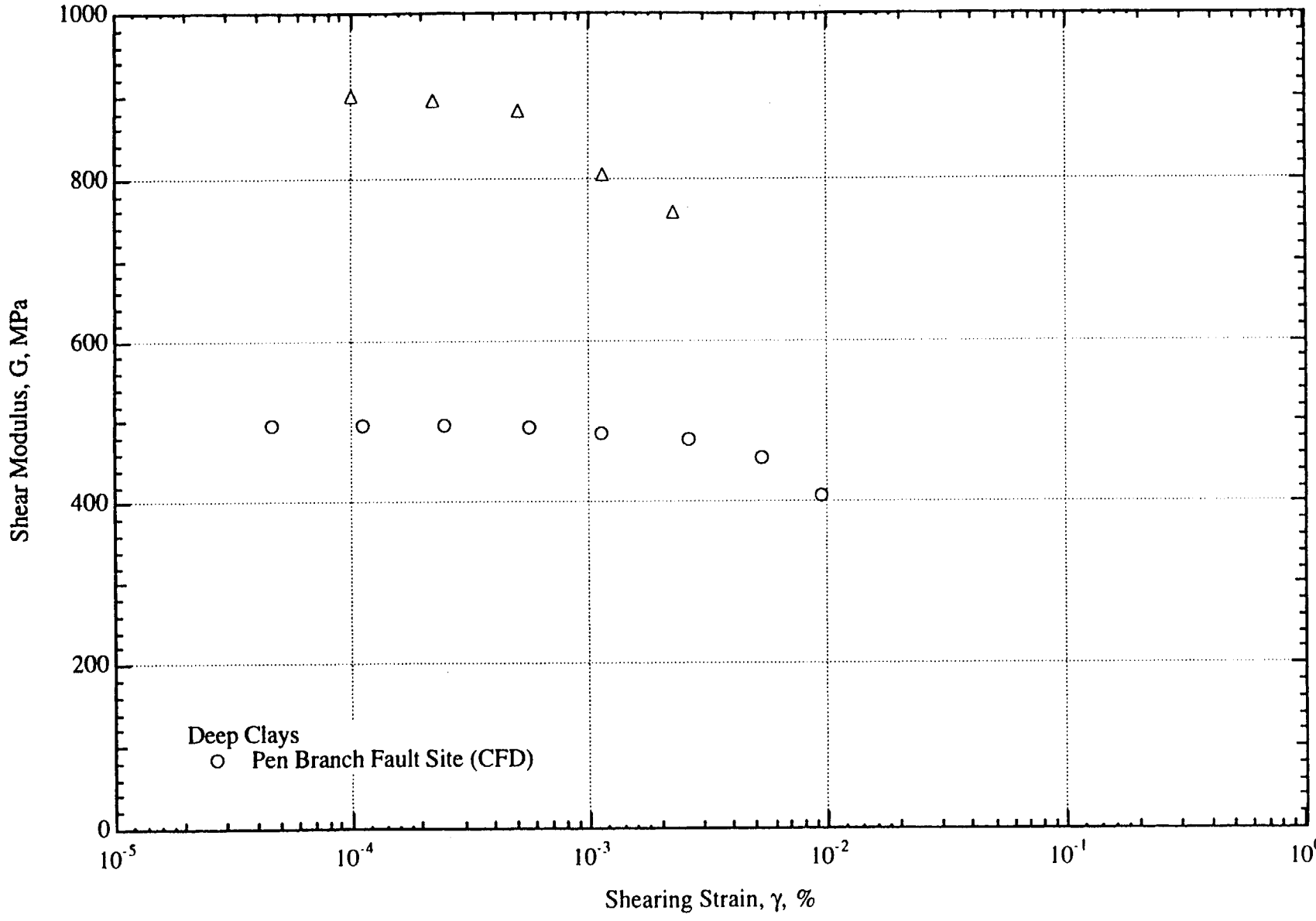


Fig. 114 Summary Plot of All G - log γ Relationships Determined by RCTS Testing with the Specimens Confined At or Near the In-Situ Mean Effective Stress for the Deep Clays

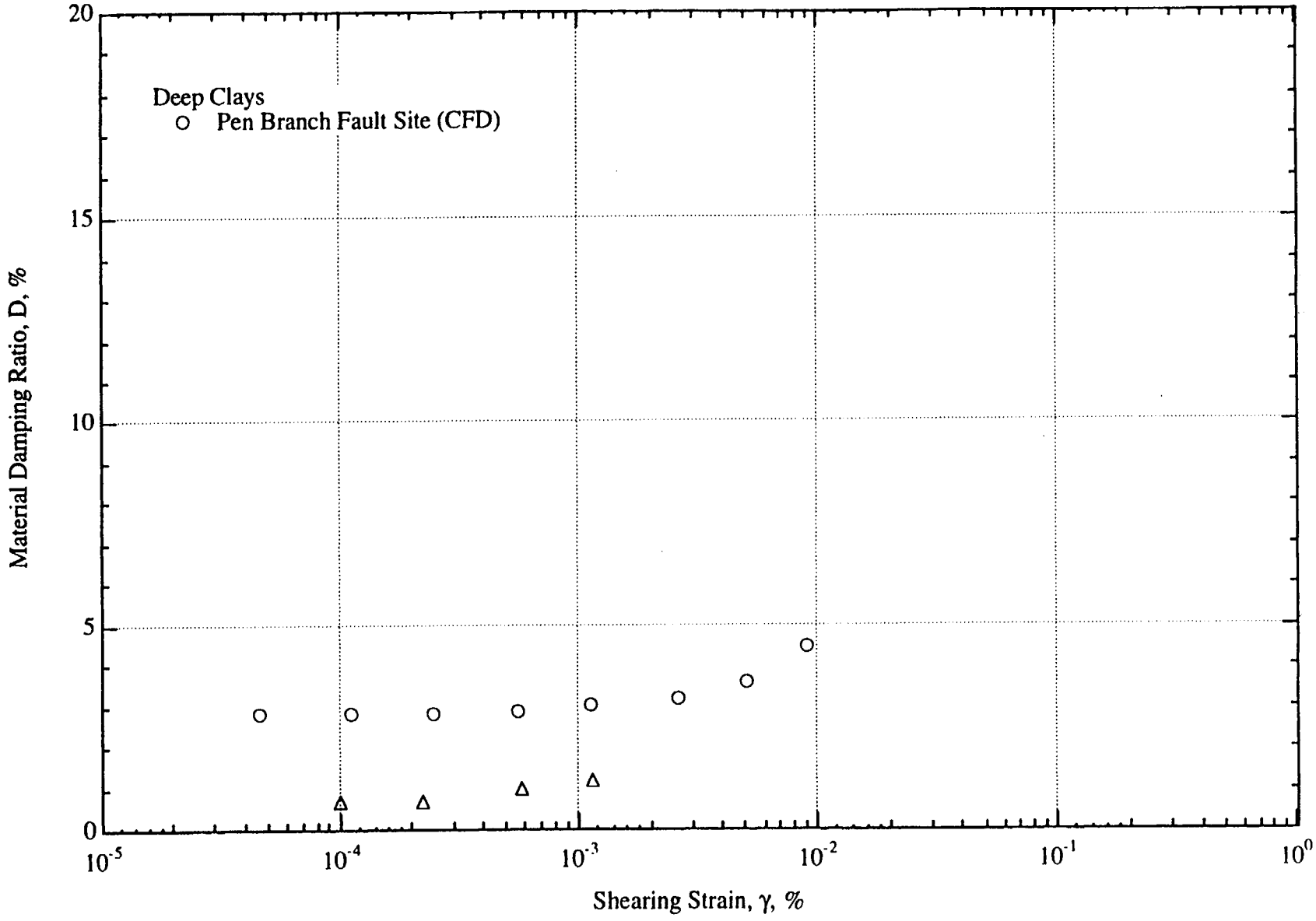


Fig. 115 Summary Plot of All D - log γ Relationships Determined by RCTS Testing with the Specimens Confined At or Near the In-Situ Mean Effective Stress for the Deep Clays

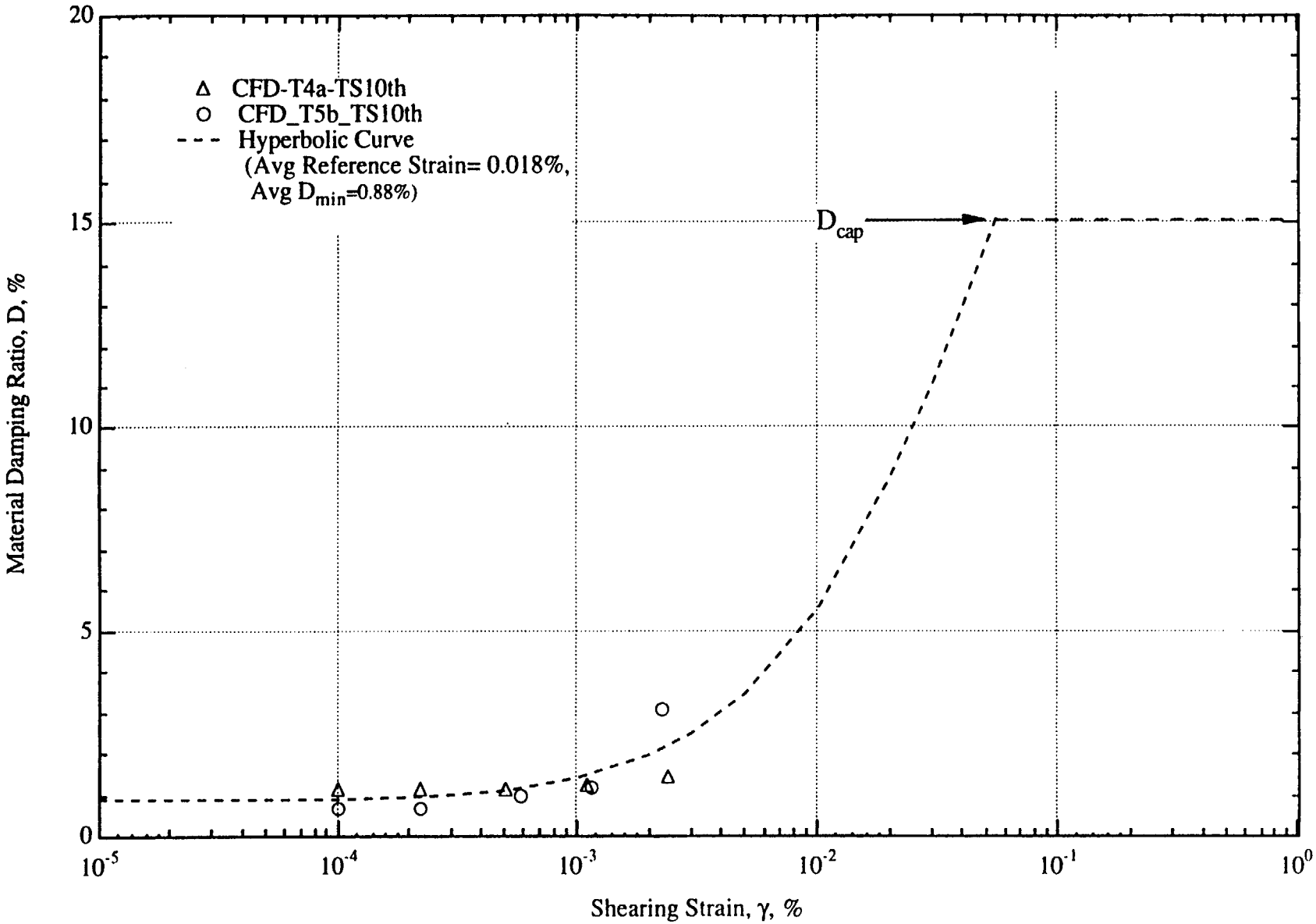


Fig. 116 Comparison of the D - log γ Relationships Measured in the Tenth Cycle of TS Testing with an Average Hyperbolic Curve for the Deep Clays

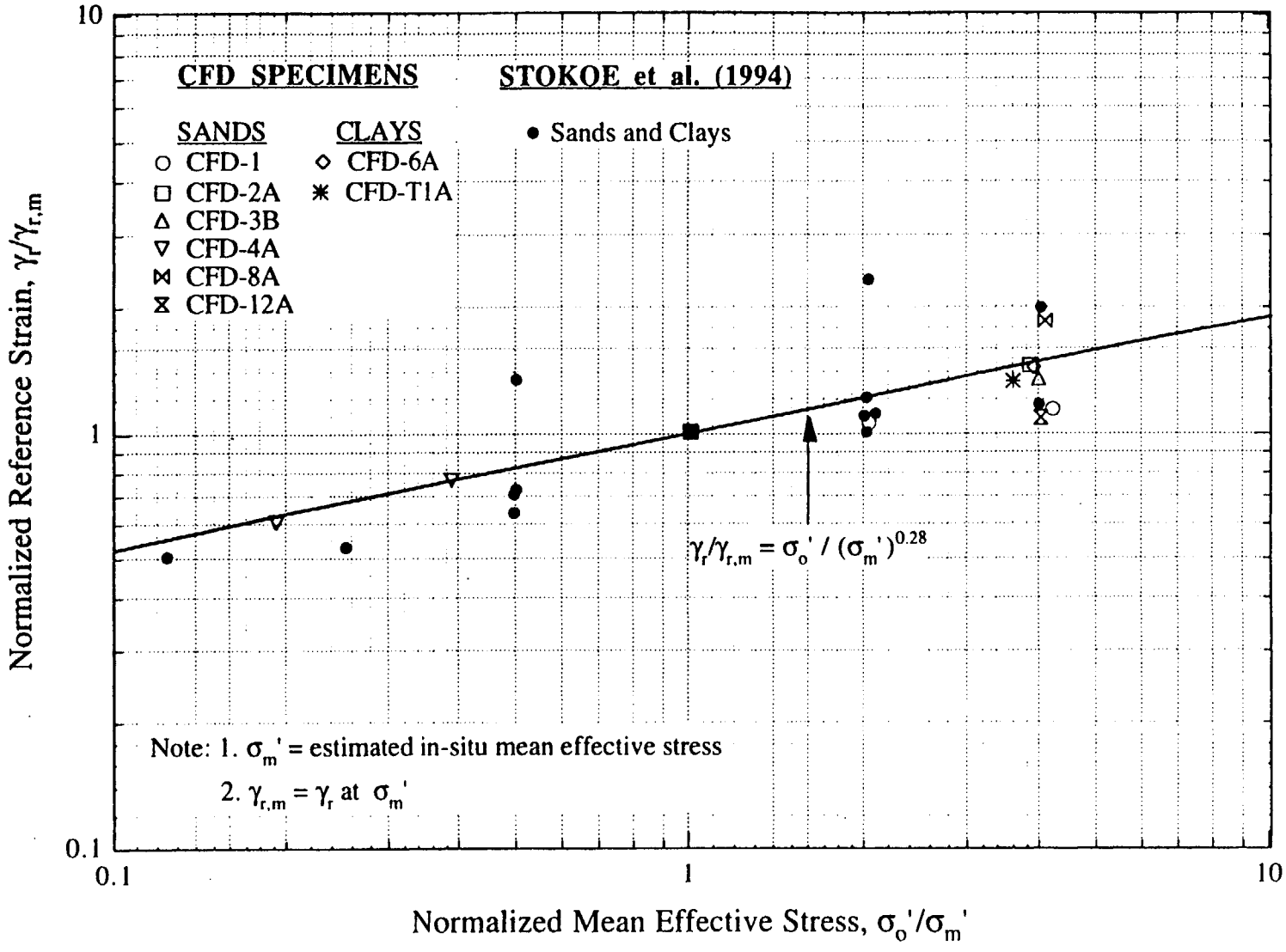


Fig. 117 Variation of Reference Strain with Mean Effective Stress Determined from Shallow Sands and Clays

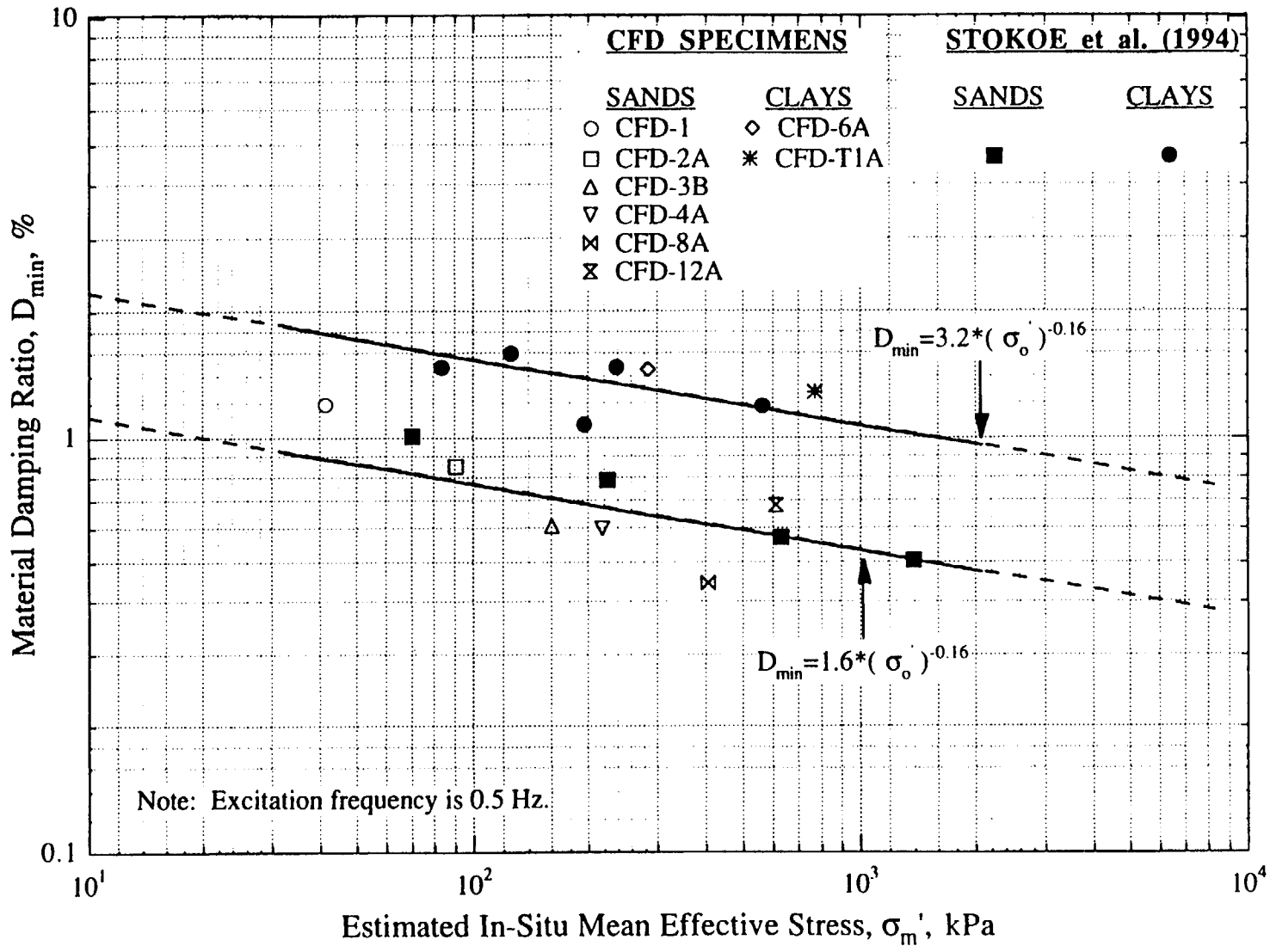


Fig. 118 Variation of $D_{min}$ Measured in the Torsional Shear Test with the Estimated In-Situ Mean Effective Stress

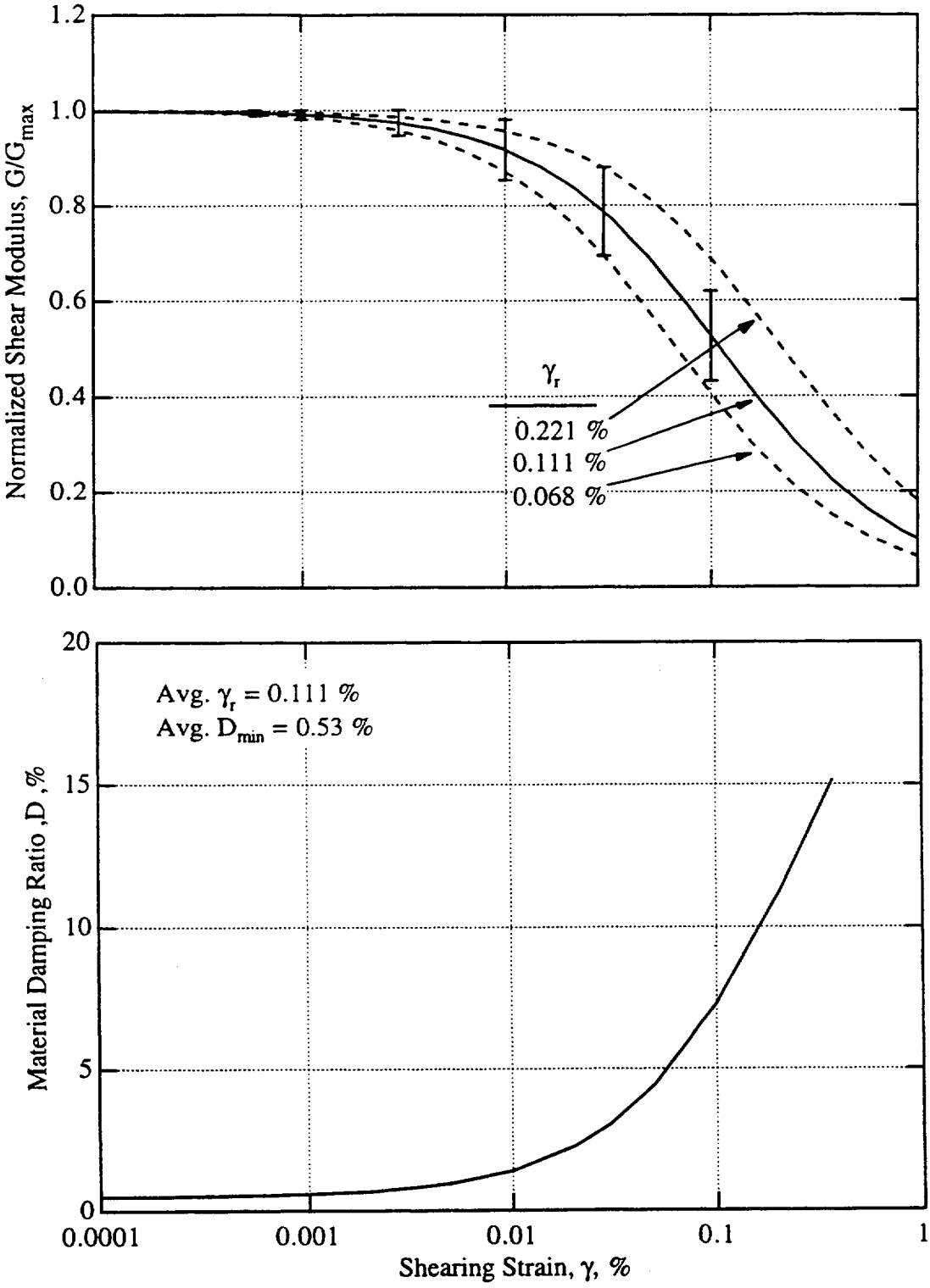


Fig. 119 Predicted $G/G_{max}$ - log $\gamma$ and D - log $\gamma$ Relationships for Deep Sands at a Depth of 750 ft (228.6 m) by Extrapolating the Shallow Sands Correction

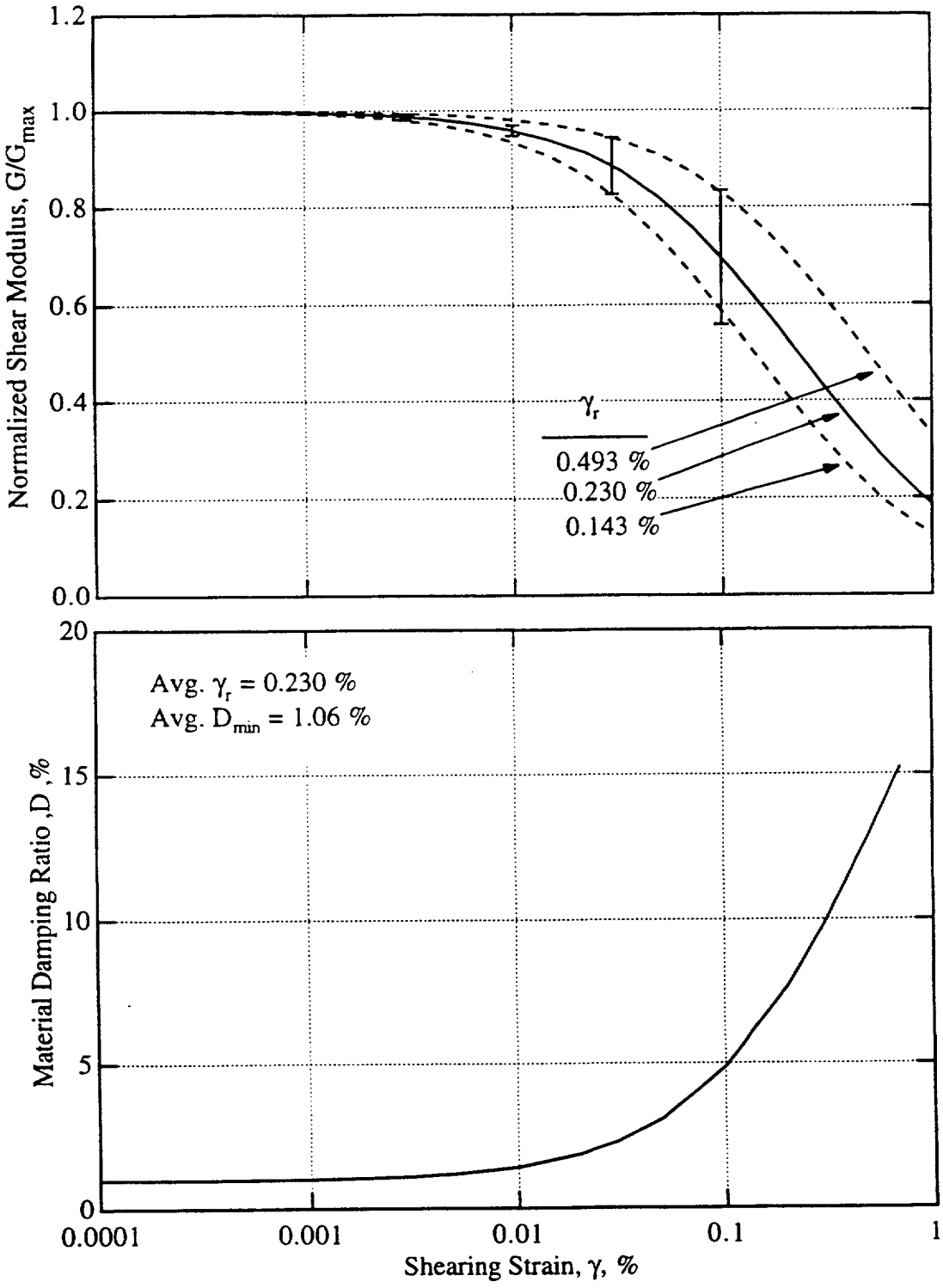


Fig. 120 Predicted $G/G_{max}$ - log $\gamma$ and D - log $\gamma$ Relationships for Deep Clays at a Depth of 750 ft (228.6 m) by Extrapolating the Shallow Clays Correction

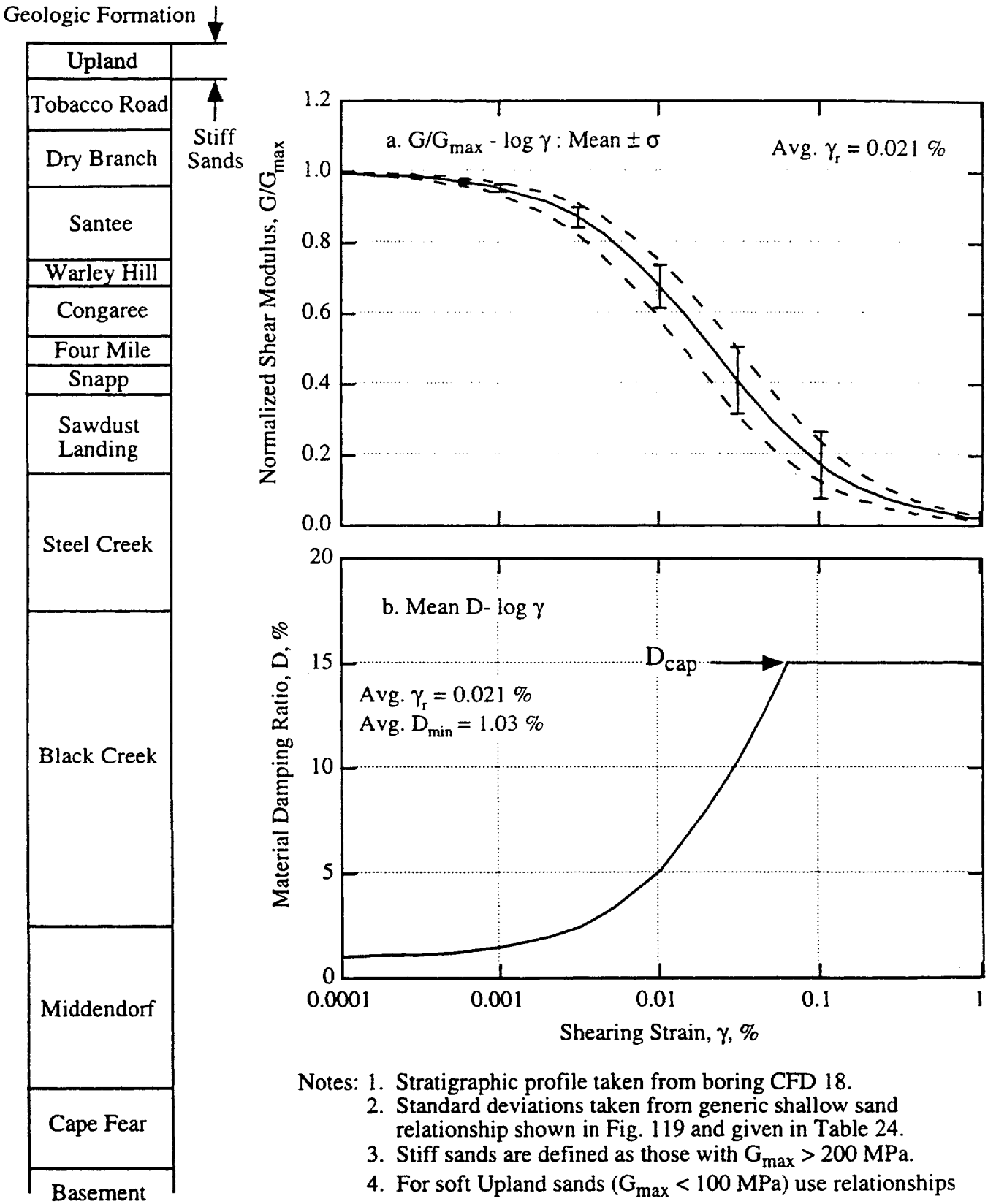


Notes: 1. Stratigraphic profile taken from boring CFD 18.
2. Standard deviations taken from generic shallow sand relationship shown in Fig. 119 and given in Table 24.
3. Stiff sands are defined as those with $G_{max}$ > 200 MPa.
4. For soft Upland sands ($G_{max}$ < 100 MPa) use relationships shown in Fig. 123.
5. Values of D evaluated at f ≤1 Hz.

Fig. 121 Recommended Generic $G/G_{max}$ - log γ and D - log γ Relationships for Stiff Upland Sands at SRS

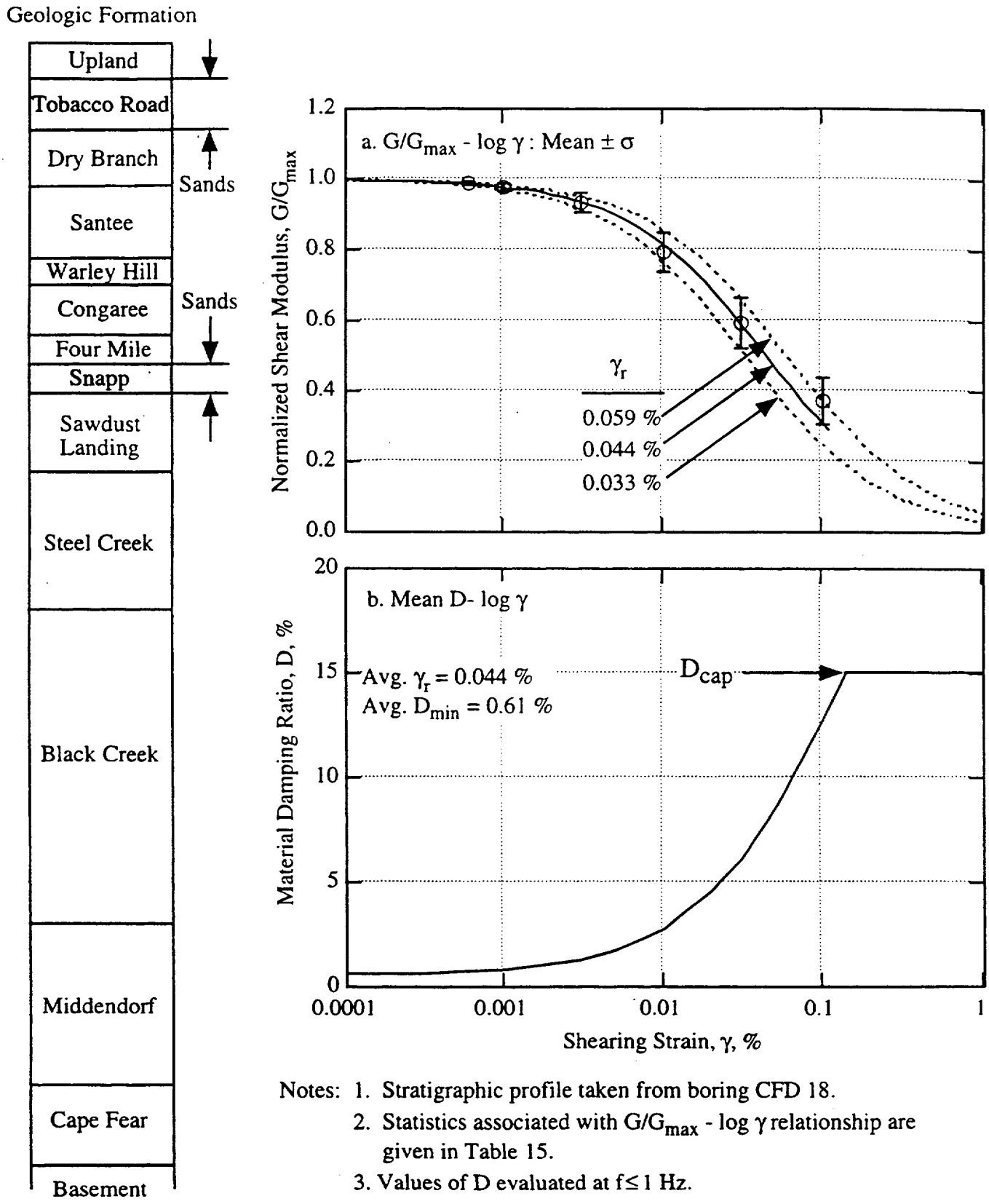


Notes: 1. Stratigraphic profile taken from boring CFD 18.
2. Statistics associated with $G/G_{max}$ - log γ relationship are given in Table 15.
3. Values of D evaluated at f≤1 Hz.

Fig. 122 Recommended Generic $G/G_{max}$ - log γ and D - log γ Relationships for Tobacco Road and Snapp Sands at SRS

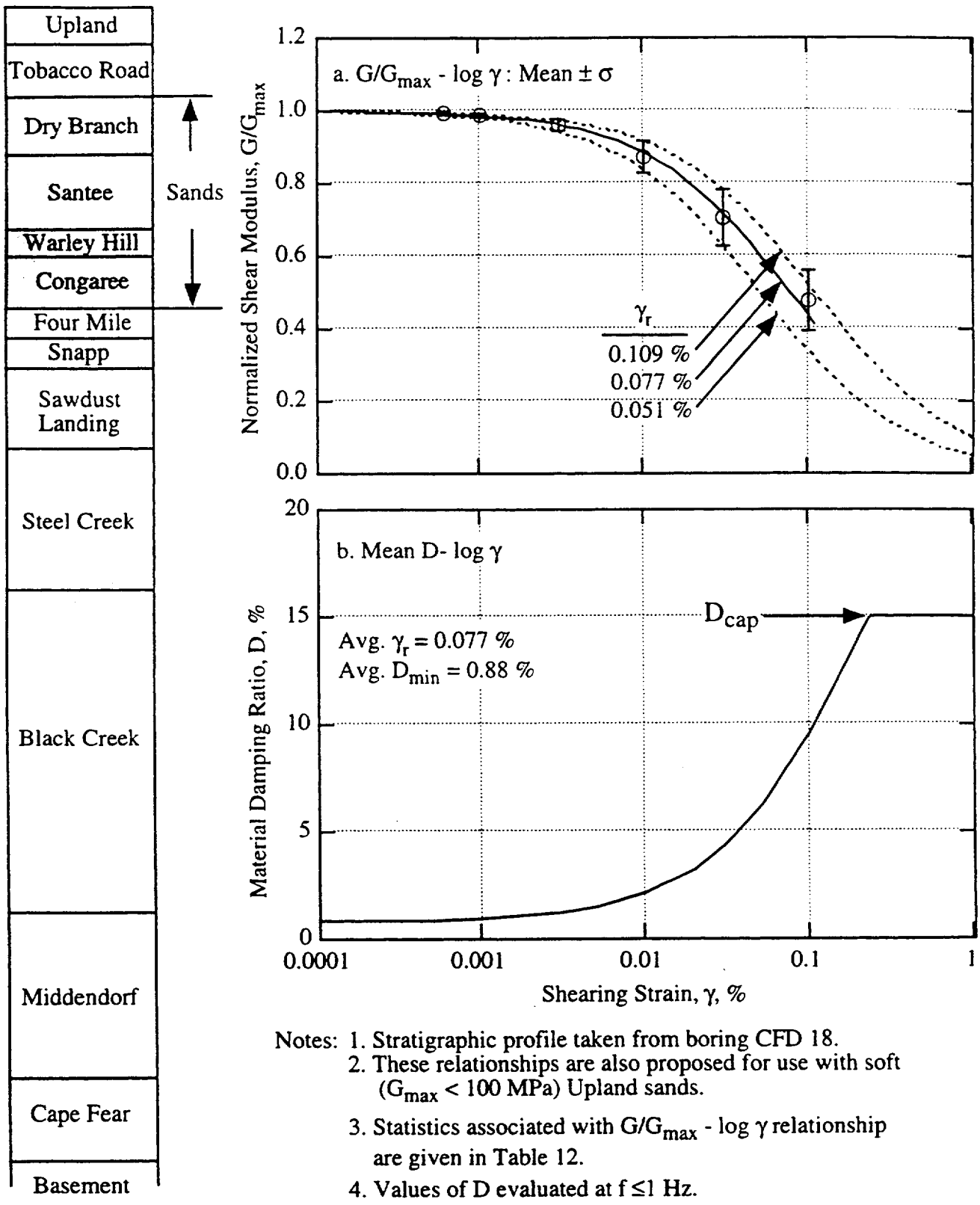


Notes: 1. Stratigraphic profile taken from boring CFD 18.
2. These relationships are also proposed for use with soft ($G_{max}$ < 100 MPa) Upland sands.
3. Statistics associated with $G/G_{max}$ - log γ relationship are given in Table 12.
4. Values of D evaluated at f ≤1 Hz.

Fig. 123 Recommended Generic $G/G_{max}$ - log γ and D - log γ Relationships for Dry Branch, Santee, Warlev Hill and Congaree Sands at SRS

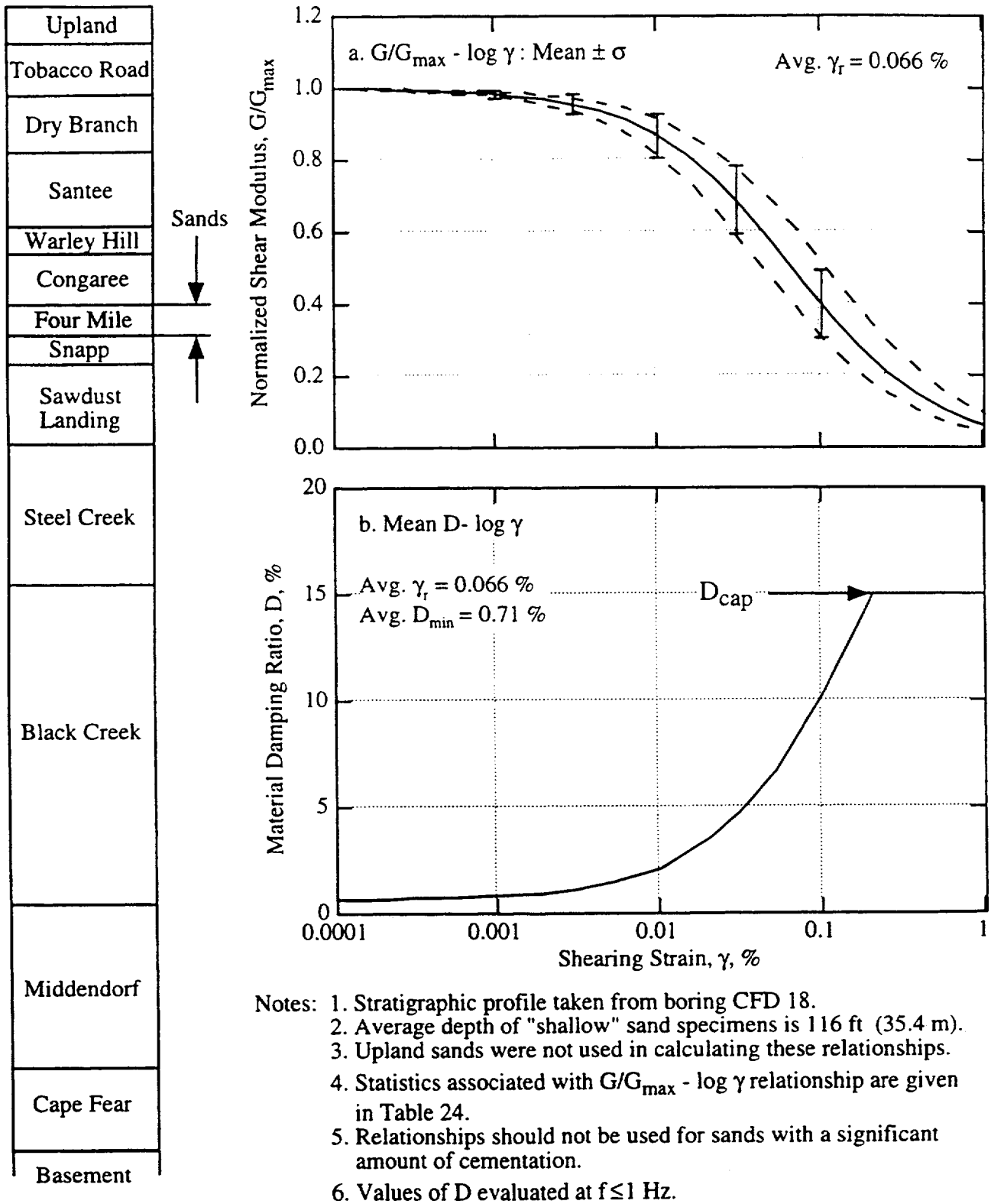


Notes:
1. Stratigraphic profile taken from boring CFD 18.
2. Average depth of "shallow" sand specimens is 116 ft (35.4 m).
3. Upland sands were not used in calculating these relationships.
4. Statistics associated with $G/G_{max}$ - log γ relationship are given in Table 24.
5. Relationships should not be used for sands with a significant amount of cementation.
6. Values of D evaluated at f ≤ 1 Hz.

Fig. 124 Recommended Generic $G/G_{max}$ - log γ and D - log γ Relationships for Four Mile Sands and Any Other Unrepresented Shallow Sand Formation at SRS

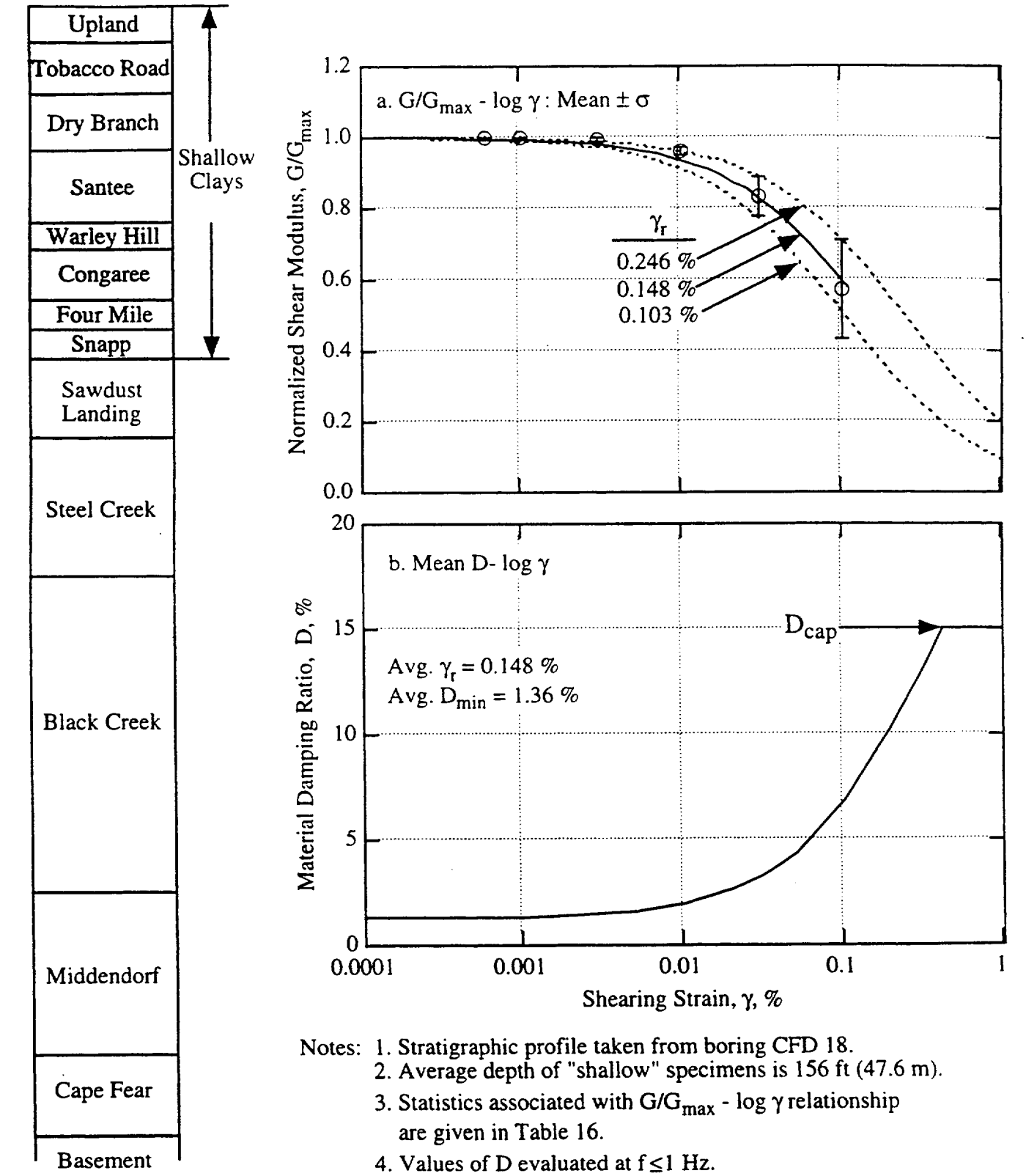


Notes: 1. Stratigraphic profile taken from boring CFD 18.
2. Average depth of "shallow" specimens is 156 ft (47.6 m).
3. Statistics associated with $G/G_{max}$ - log γ relationship are given in Table 16.
4. Values of D evaluated at f ≤ 1 Hz.

Fig. 125 Recommended Generic $G/G_{max}$ - log γ and D - log γ Relationships for Shallow Clays at SRS

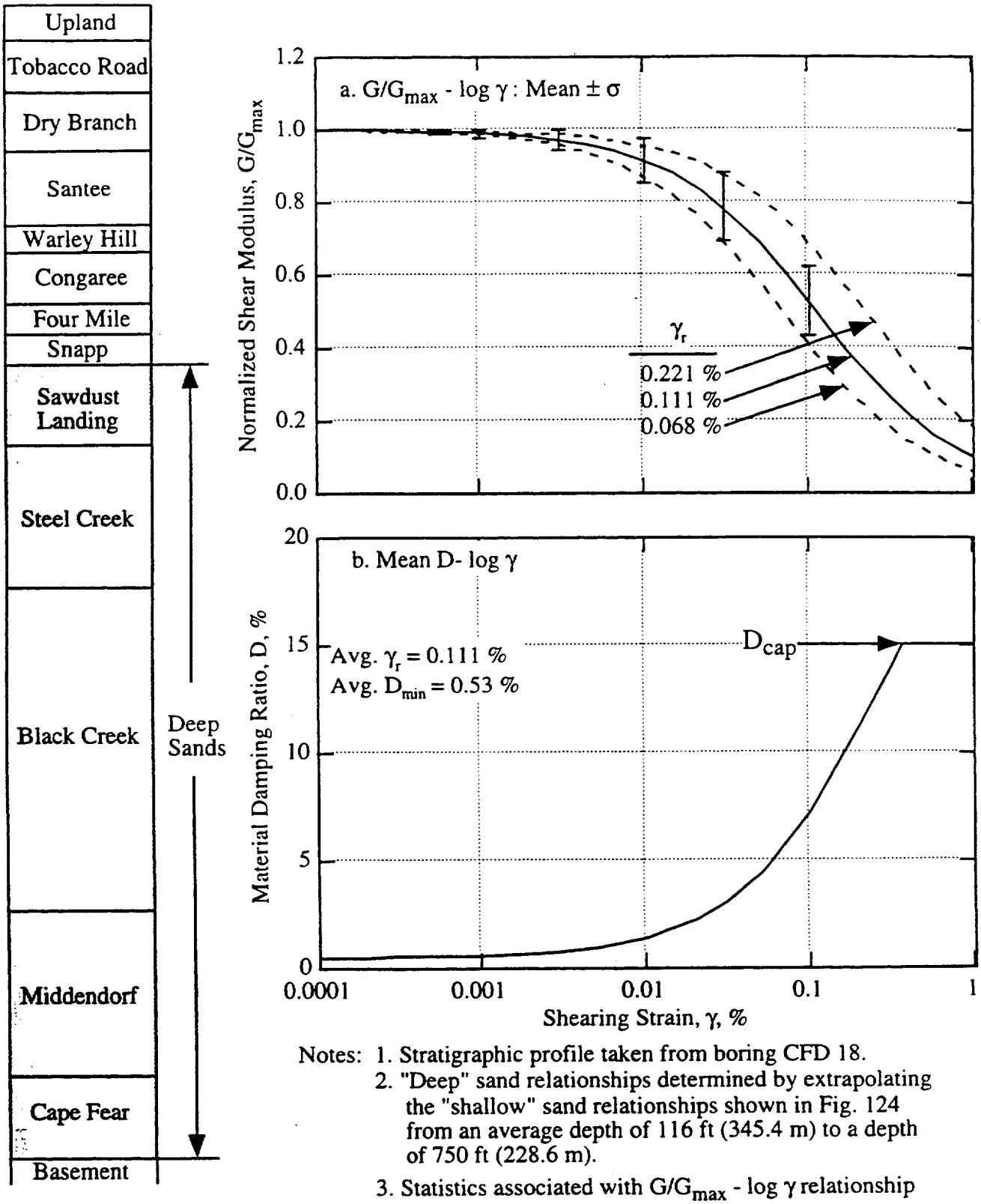


Notes:
1. Stratigraphic profile taken from boring CFD 18.
2. "Deep" sand relationships determined by extrapolating the "shallow" sand relationships shown in Fig. 124 from an average depth of 116 ft (345.4 m) to a depth of 750 ft (228.6 m).
3. Statistics associated with $G/G_{max}$ - log $\gamma$ relationship are given in Table 24.
4. Values of D evaluated at f≤1 Hz.

Fig. 126 Recommended Generic $G/G_{max}$ - log $\gamma$ and D - log $\gamma$ Relationships for the Deep Sands at SRS

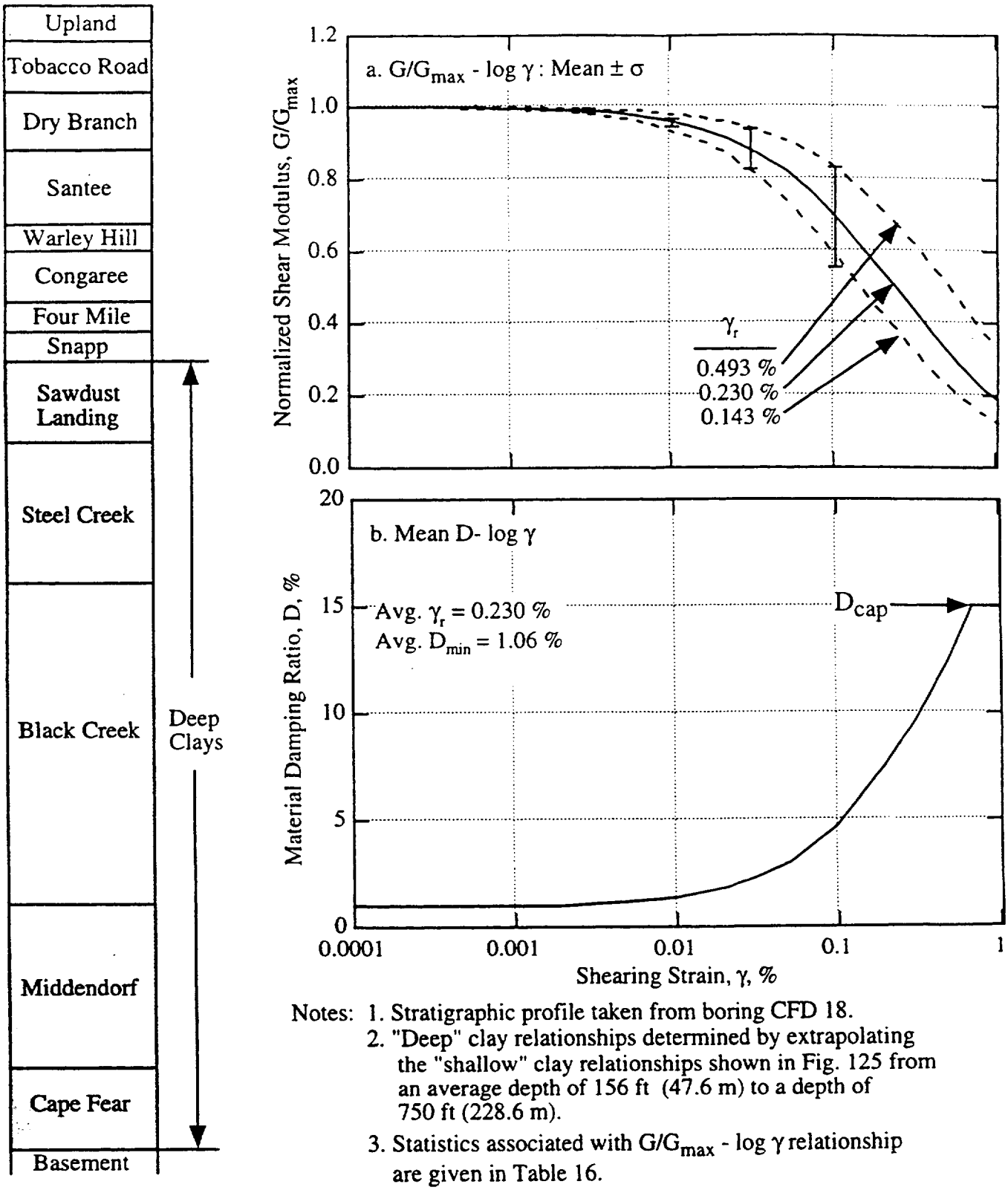


Notes: 1. Stratigraphic profile taken from boring CFD 18.
2. "Deep" clay relationships determined by extrapolating the "shallow" clay relationships shown in Fig. 125 from an average depth of 156 ft (47.6 m) to a depth of 750 ft (228.6 m).
3. Statistics associated with $G/G_{max}$ - log γ relationship are given in Table 16.
4. Values of D evaluated at f ≤ 1 Hz.

Fig. 127 Recommended Generic $G/G_{max}$ - log γ and D - log γ Relationships for the Deep Clays at SRS

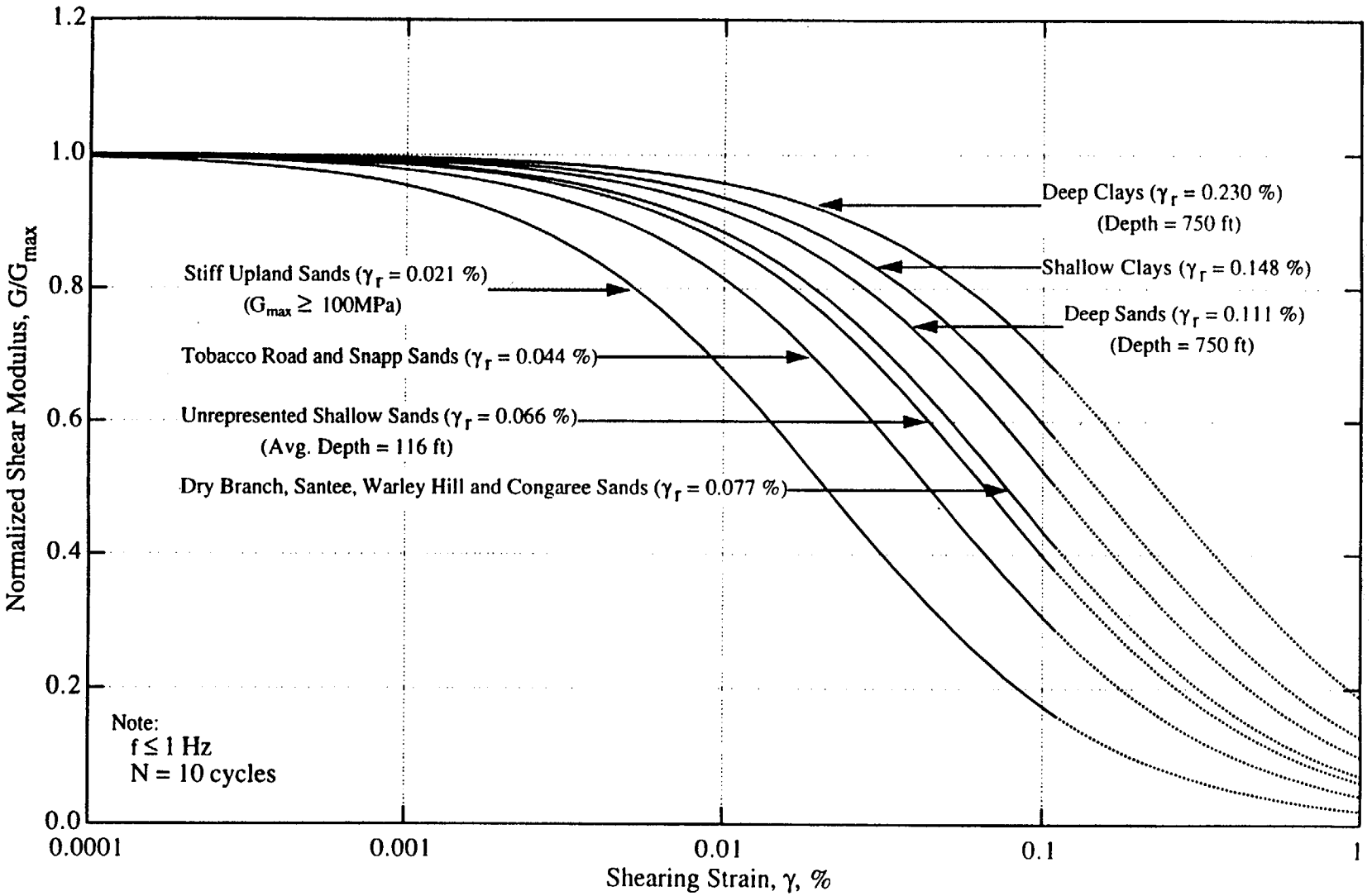


Fig. 128 Summary Plot of the Average Recommended $G/G_{max}$ - log $\gamma$ Relationships for Soils at the Savannah River Site

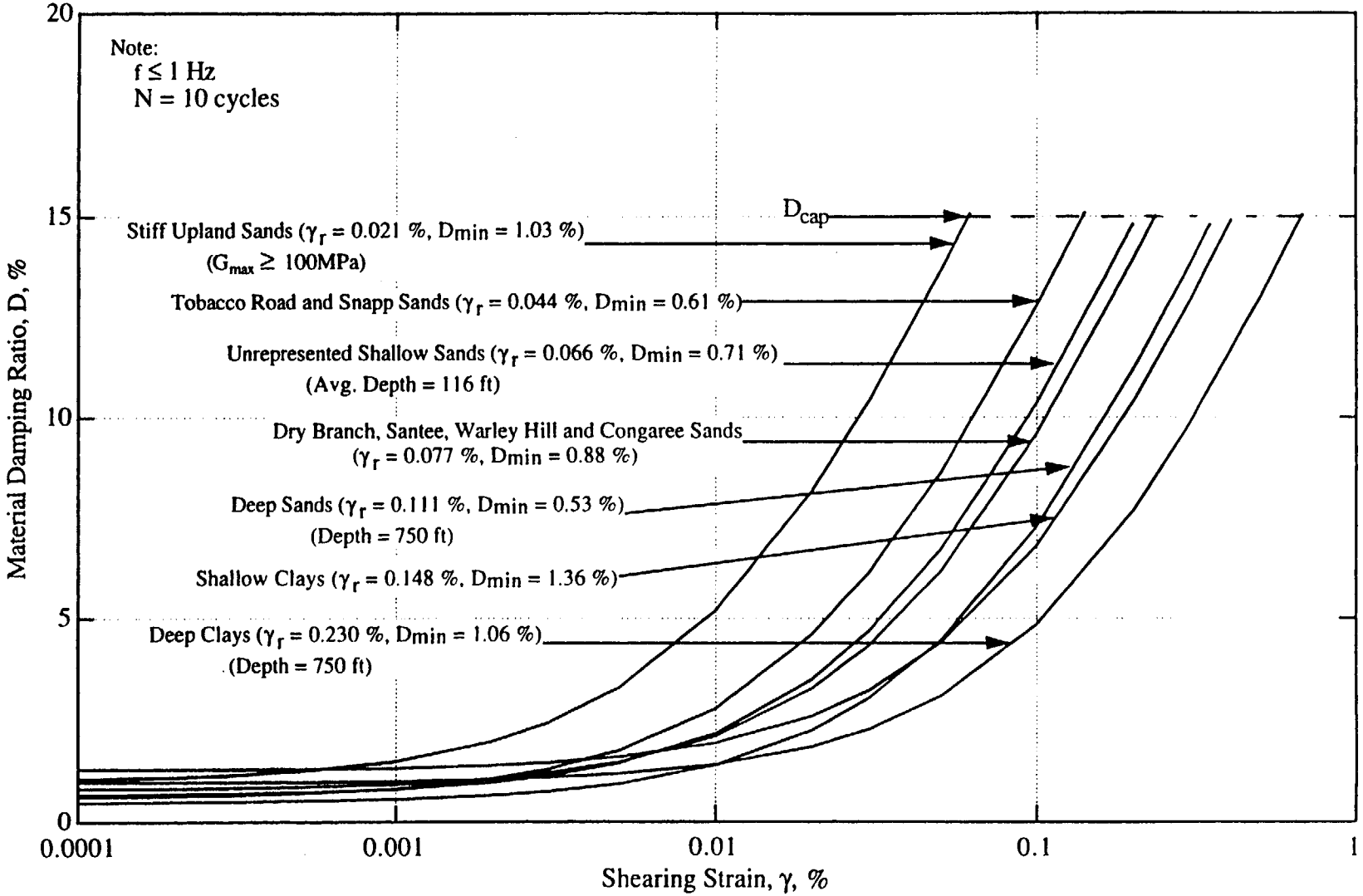


Fig. 129 Summary Plot of the Average Recommended D - log γ Relationships for Soils at the Savannah River Site

# Appendix A

# Data That Were Deleted From The Correlation Study

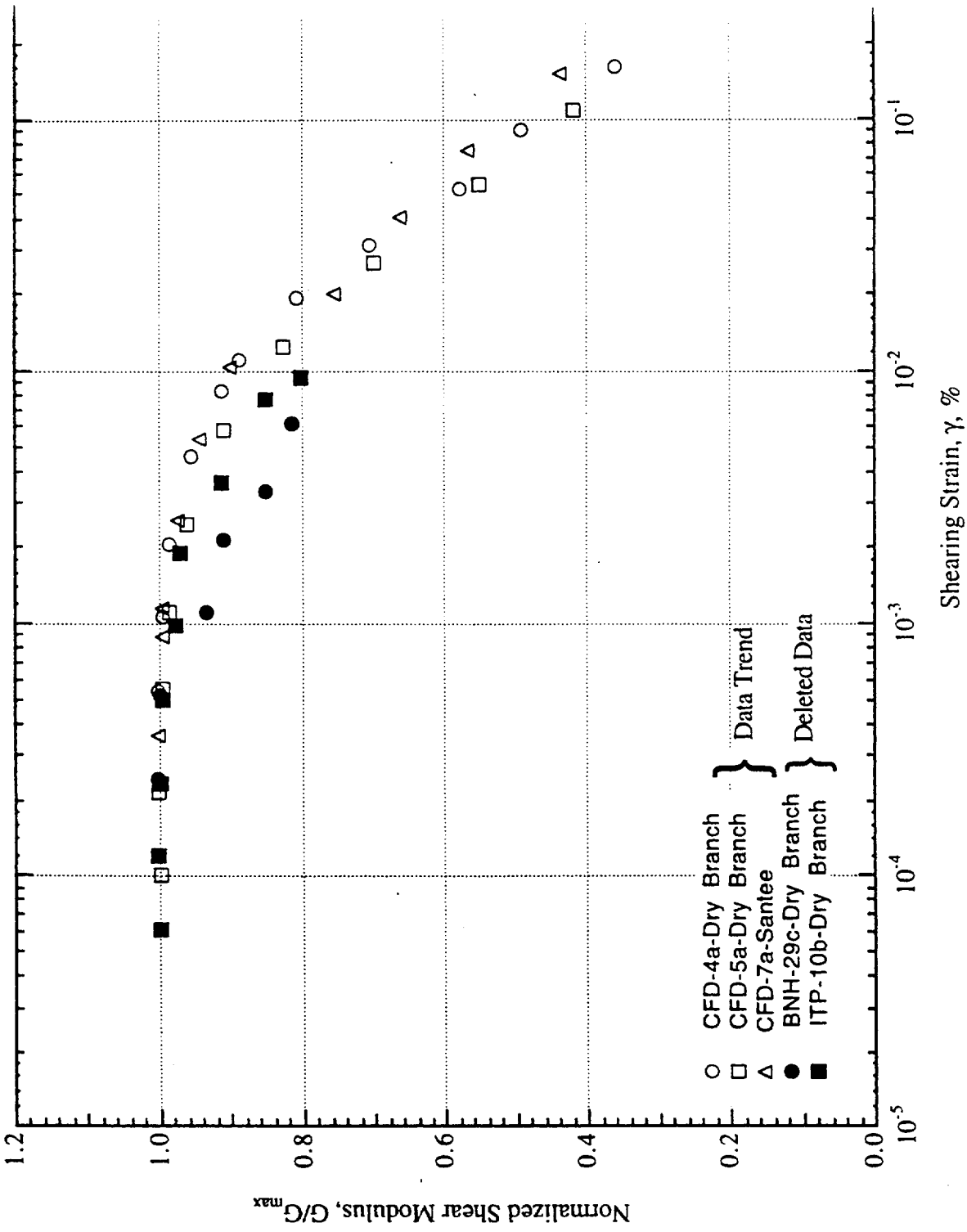


Fig. A.1 Dry Branch and Santee Sands: G/G$_{max}$ - log γ Relationships Deleted from the Corr

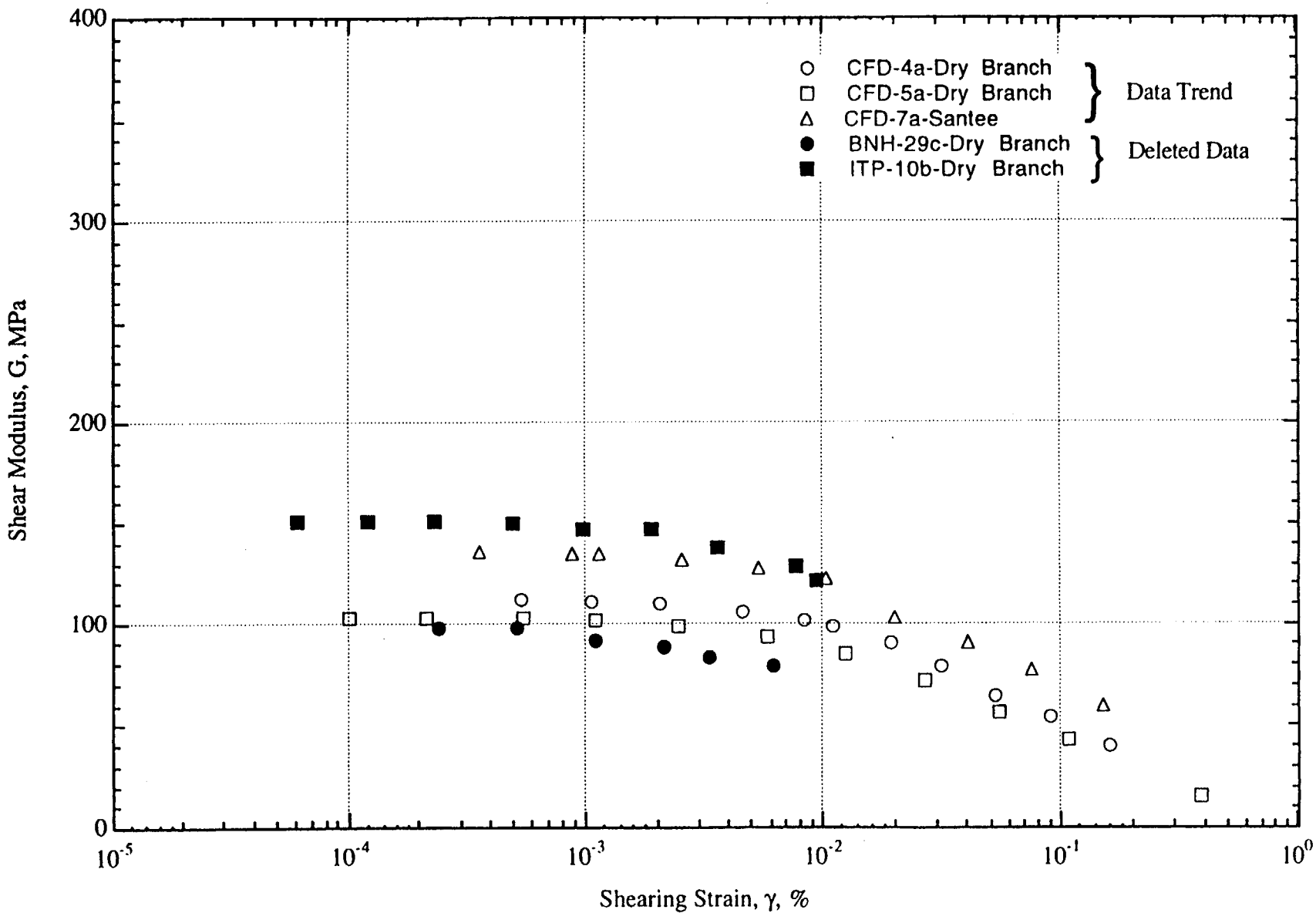


Fig. A.2 Dry Branch and Santee Sands: G - log γ Relationships Deleted from the Correlation

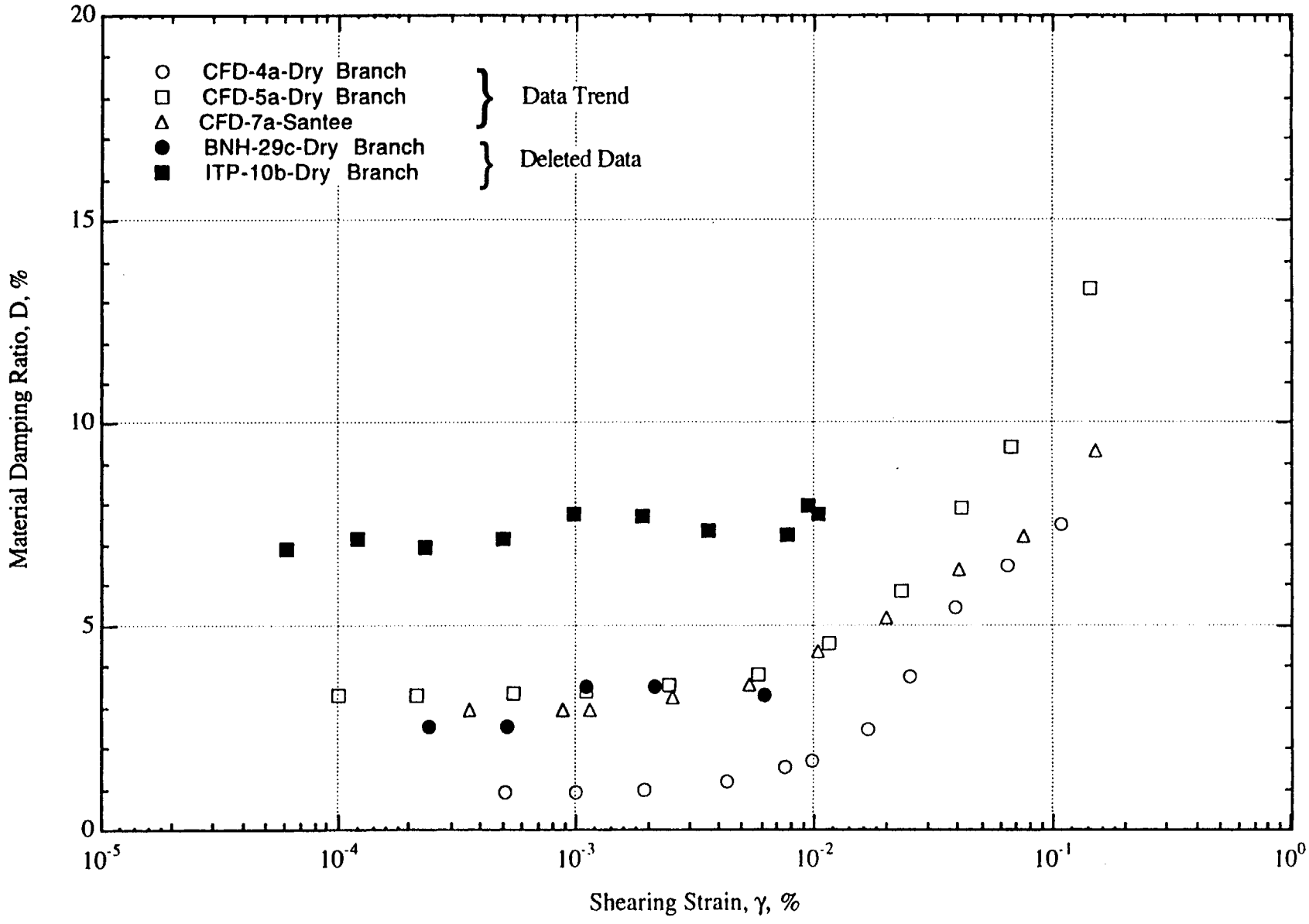


Fig. A.3 Dry Branch and Santee Sands: D - log γ Relationships Deleted from the Correlation

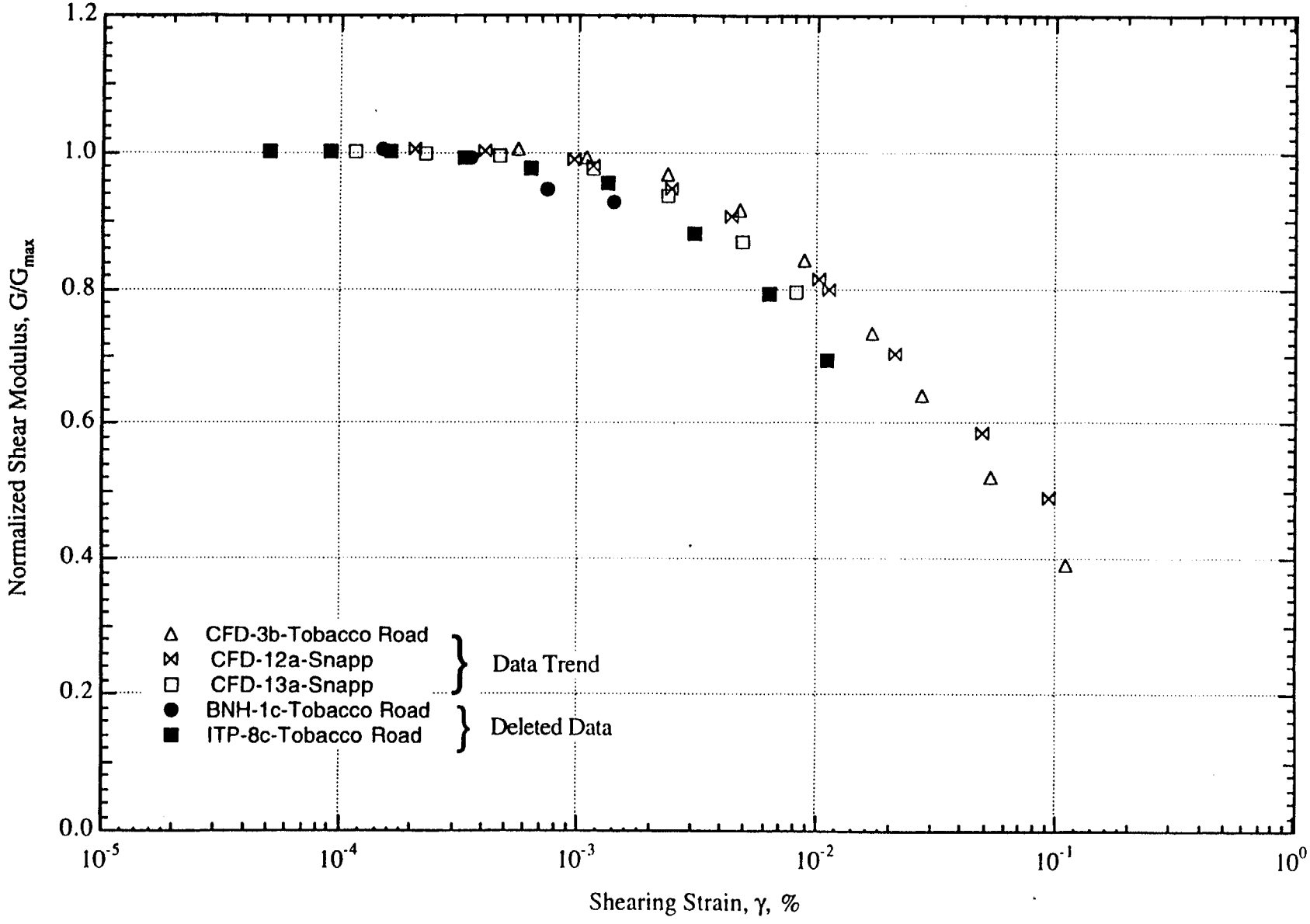


Fig. A.4 Tobacco Road and Snapp Sands: $G/G_{max}$ - log $\gamma$ Relationships Deleted From the Correlation

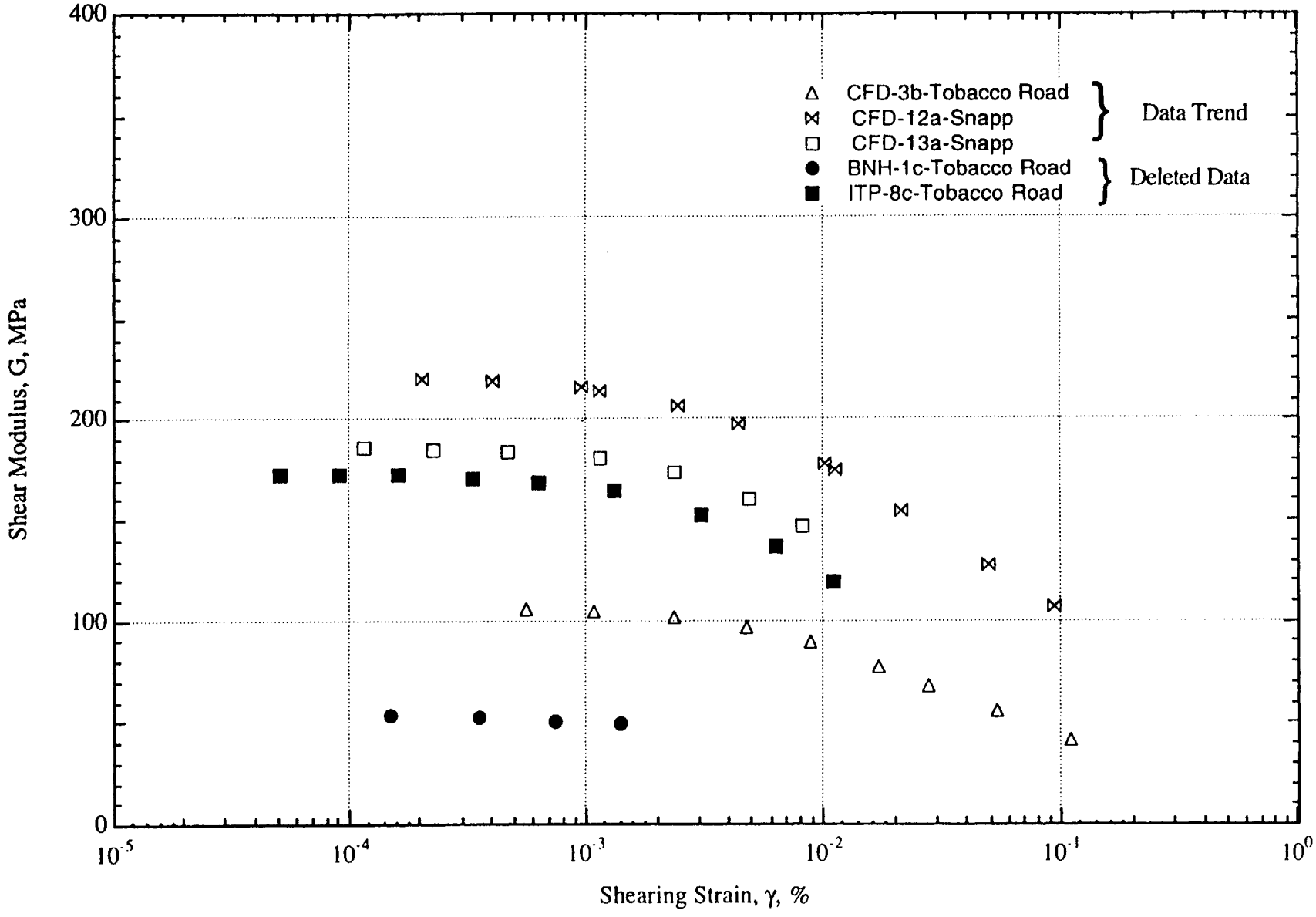


Fig. A.5 Tobacco Road and Snapp Sands: G - log γ Relationships Deleted From the Correlation

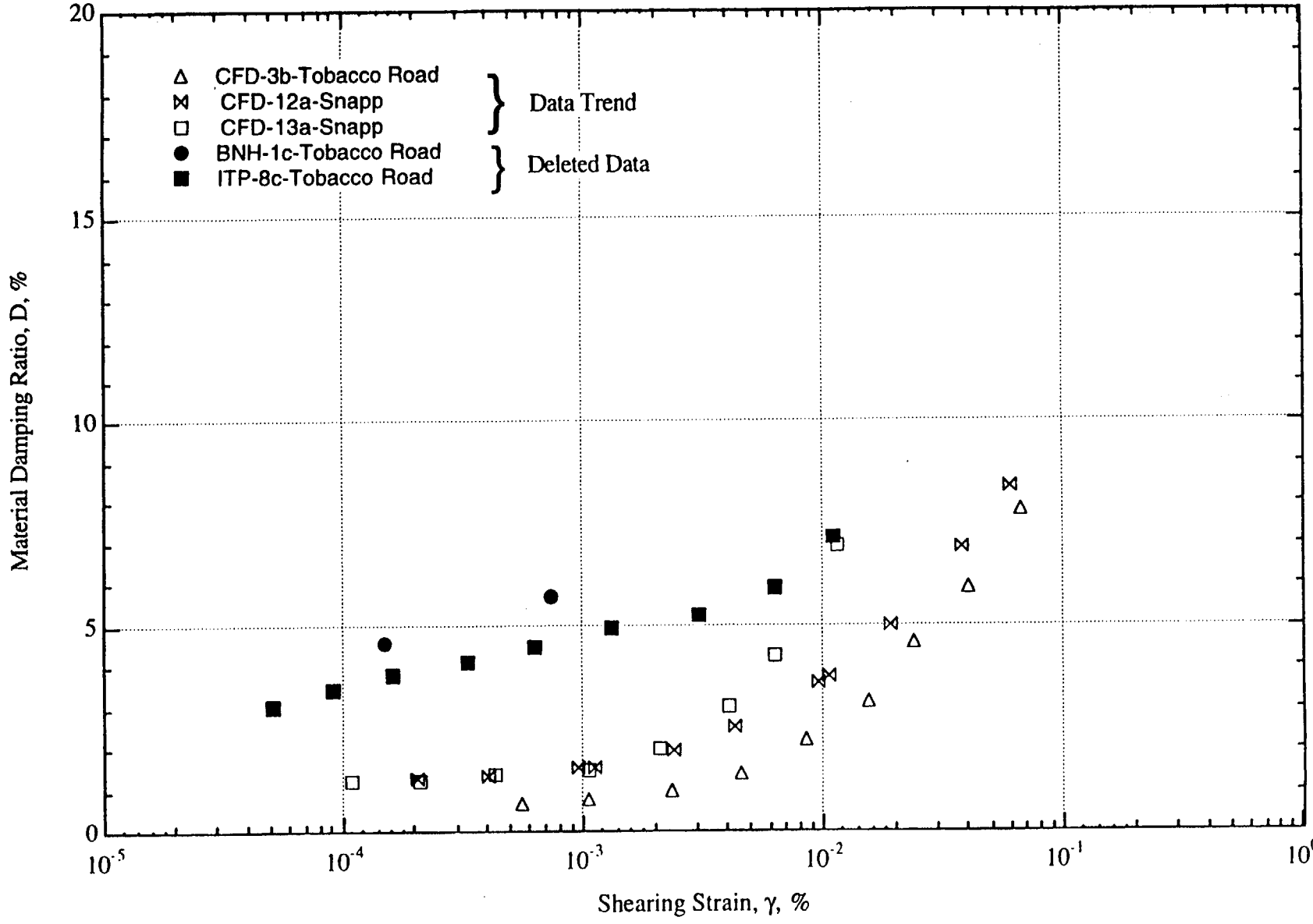


Fig. A.6 Tobacco Road and Snapp Sands: D - log γ Relationships Deleted From the Correlation

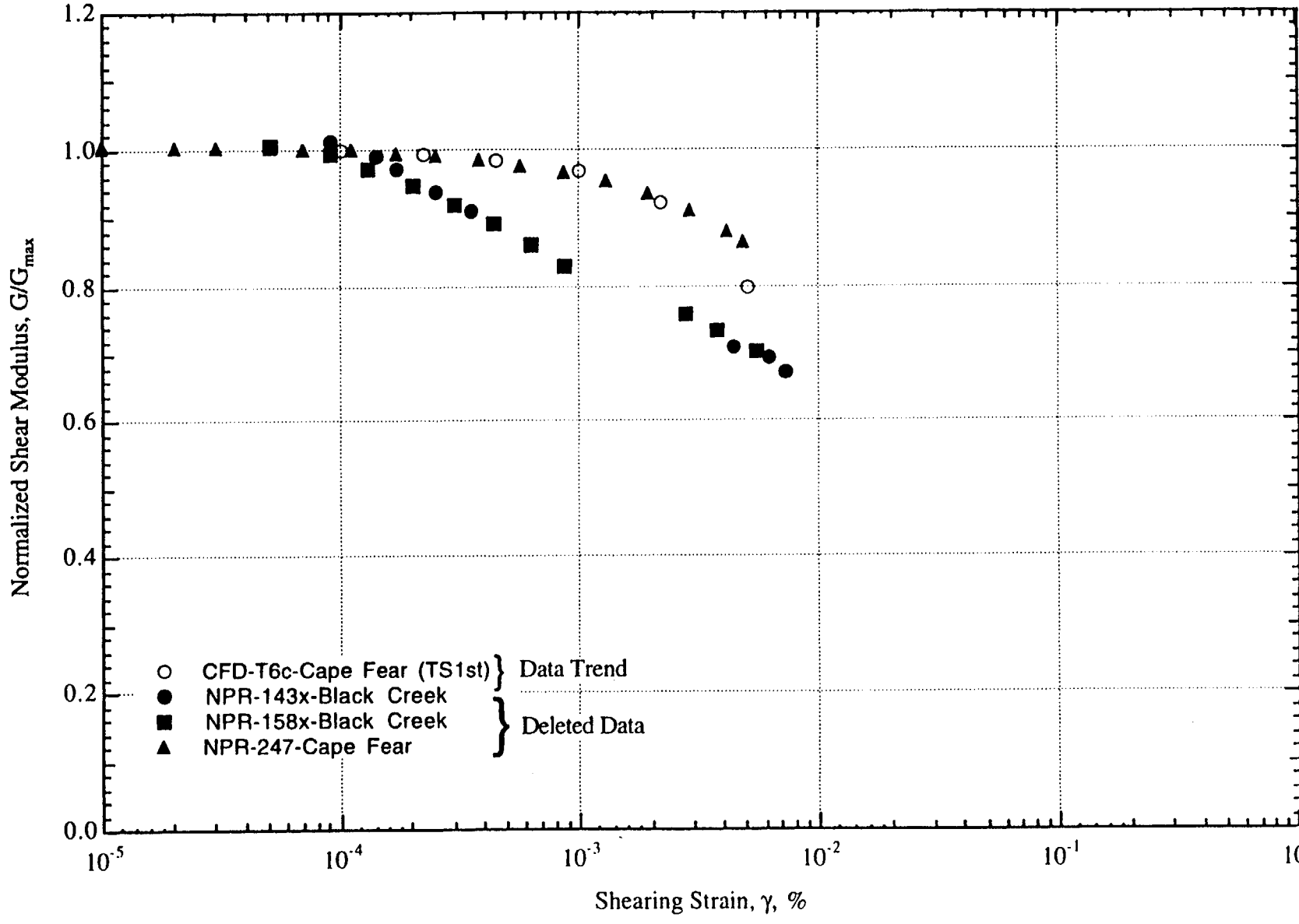


Fig. A.7 Deep Sands: $G/G_{max}$ - log $\gamma$ Relationships Deleted From the Correlation

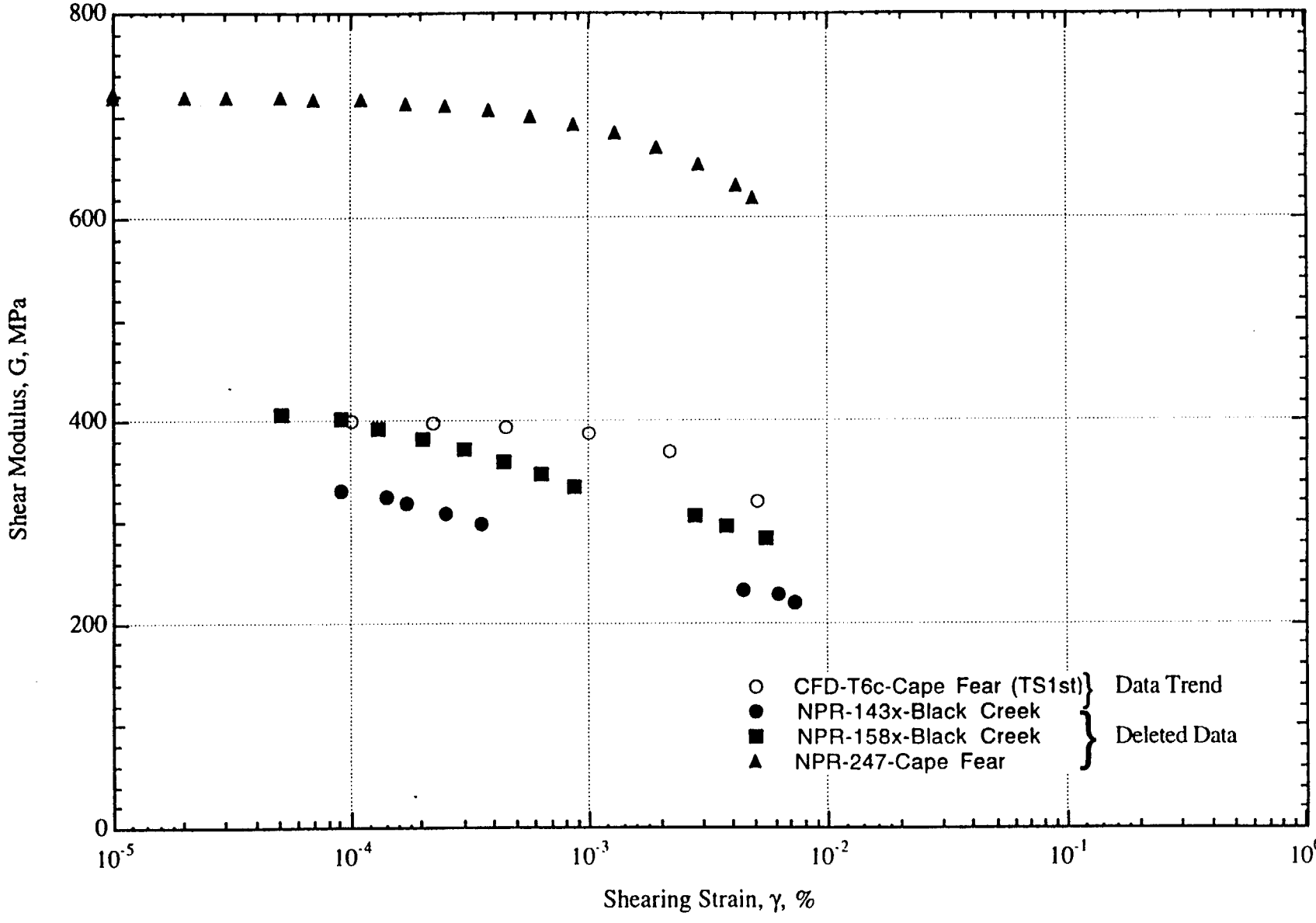


Fig. A.8 Deep Sands: G - log γ Relationships Deleted From the Correlation

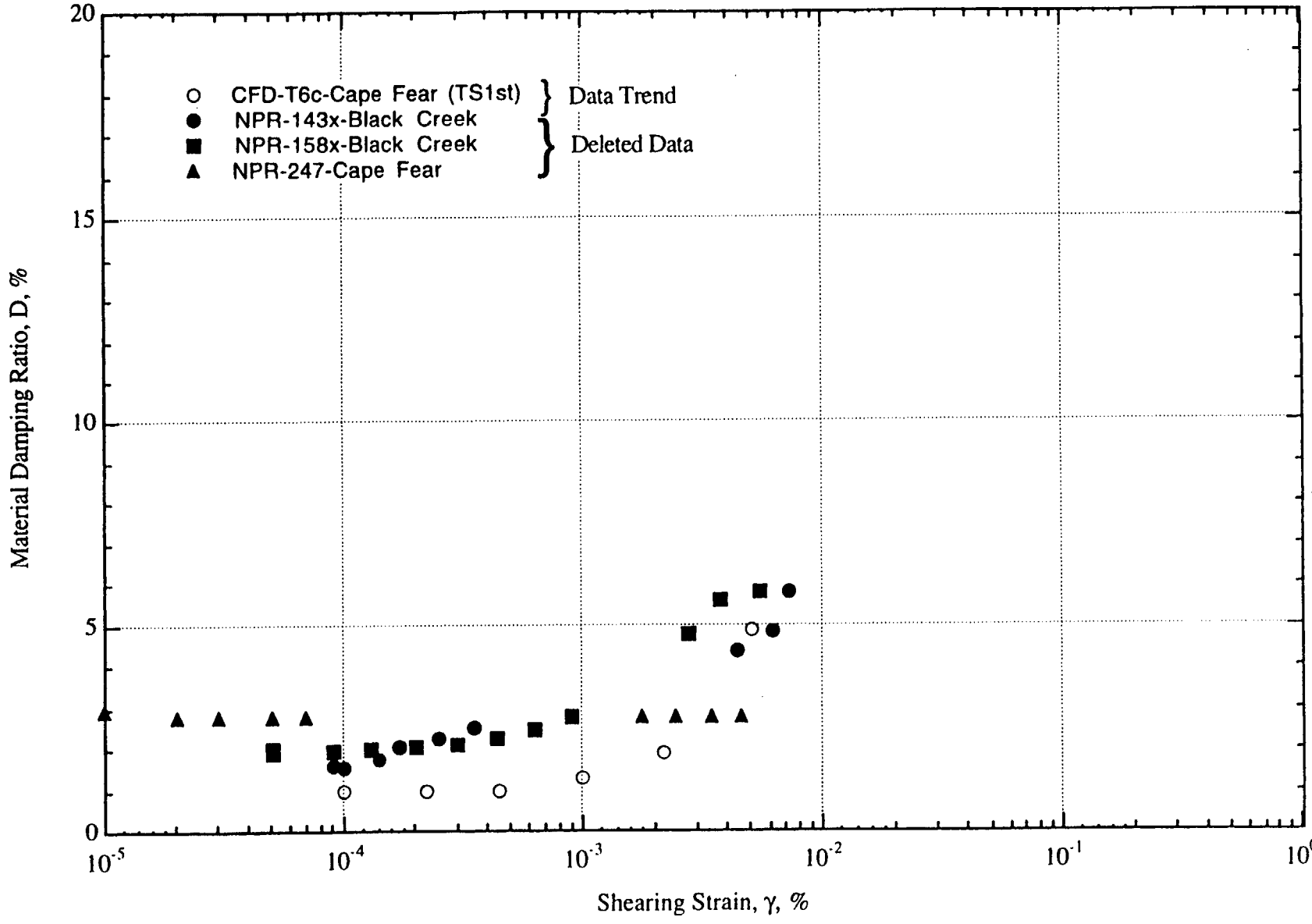


Fig. A.9 Deep Sands: D - log γ Relationships Deleted From the Correlation

# Appendix B

# Nonlinear Dynamic Properties of Similar Soils Evaluated With The RCTS Equipment at UTA

## Table B. 1. Initial Properties of Specimens Presented in Appendix B

| Sample Number | Depth ft (m) | Soil/Rock Type (Unified Soil Classification) | LL % | PI % | $D_{10}$ mm | $D_{30}$ mm | $D_{60}$ mm | $R_{200}$[1] % | Water Content % | Total Unit Weight pcf(g/cm$^3$) | Void Ratio e | Dia. cm | Height cm | Specific Gravity $G_S$[2] | Degree of Saturation % |
|---|---|---|---|---|---|---|---|---|---|---|---|---|---|---|---|
| T1 [6] | 17.5 (5.3) | Silty Sand (SM) | non-plastic | | - | - | 0.11 | 66 | 19.9 | 120 (1.92) | 0.69 | 5.03 | 10.07 | 2.65 | 76 |
| T2 [6] | 30 (9.1) | Sand with Silt (SP-SM) | non-plastic | | 0.10 | 0.18 | 0.26 | 91 | 21.3 | 120 (1.92) | 0.67 | 3.78 | 7.58 | 2.65 | 84 |
| T3 [6] | 60 (18.3) | Fat Clay (CH) | 51 | 26 | - | - | - | 1 | 50.2 | 108 (1.73) | 1.34 | 5.11 | 10.10 | 2.70 | 100[3] |
| G2-1 [7] | 20 (6.1) | Lean Clay (CL) | 43 | 23 | - | - | - | 14 | 27.0 | 121(1.94) | 0.76 | 3.81 | 7.62 | 2.70 | 96 |
| G5-1 [7] | 120 (36.6) | Sandy Silt (ML) | non- plastic | | - | - | - | 38 | 19.1 | 131(2.10) | 0.51 | 3.82 | 7.52 | 2.65 | 100 |
| HQ146 [4, 8] | 662 (202) | Basalt | - | - | - | - | - | - | - | 143(2.29) | 0.20 | 2.54 | 4.99 | 2.75 | 0[5] |

1. $R_{200}$ = Percent of soil sample by weight remaining on #200 sieve
2. Specific gravity was assumed.
3. Degree of saturation slightly exceeds 100 %.
4. Epoxy glue was used to fix the specimen to the end platens of the test equipment.
5. Degree of saturation was assumed because water content was not determined.
6. From Geotechnical Engineering Report GR93-4, Geotechnical Engineering Center, Civil Engineering Department, The University of Texas at Austin
7. From Geotechnical Engineering Report GR93-5, Geotechnical Engineering Center, Civil Engineering Department, The University of Texas at Austin
8. From Geotechnical Engineering Report GR93-7, Geotechnical Engineering Center, Civil Engineering Department, The University of Texas at Austin

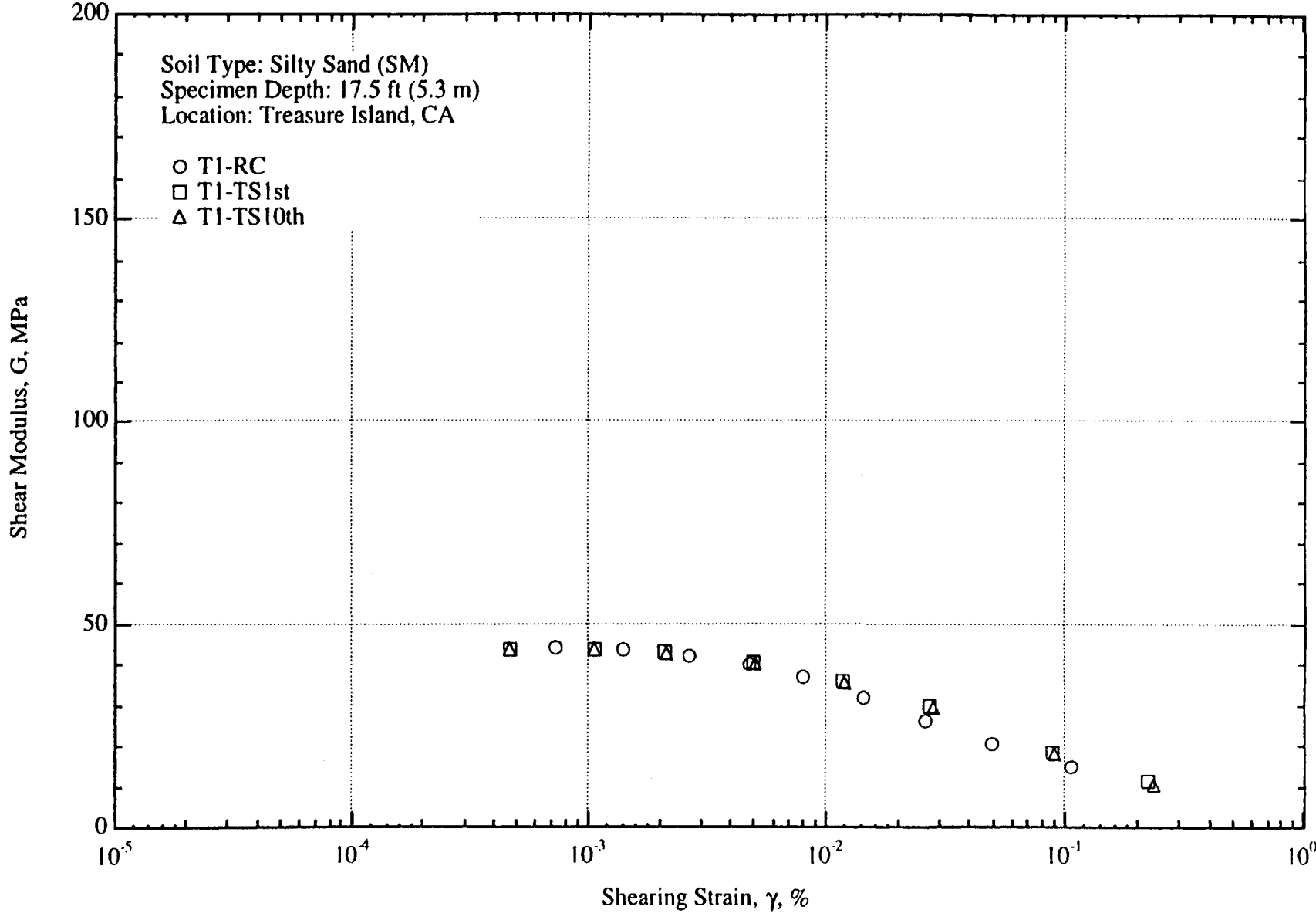


Fig. B.1 Variation in Shear Modulus with Shearing Strain at an Effective Confining Pressure of 6 psi (=864 psf=41 kPa) from RCTS Tests of Sample T1

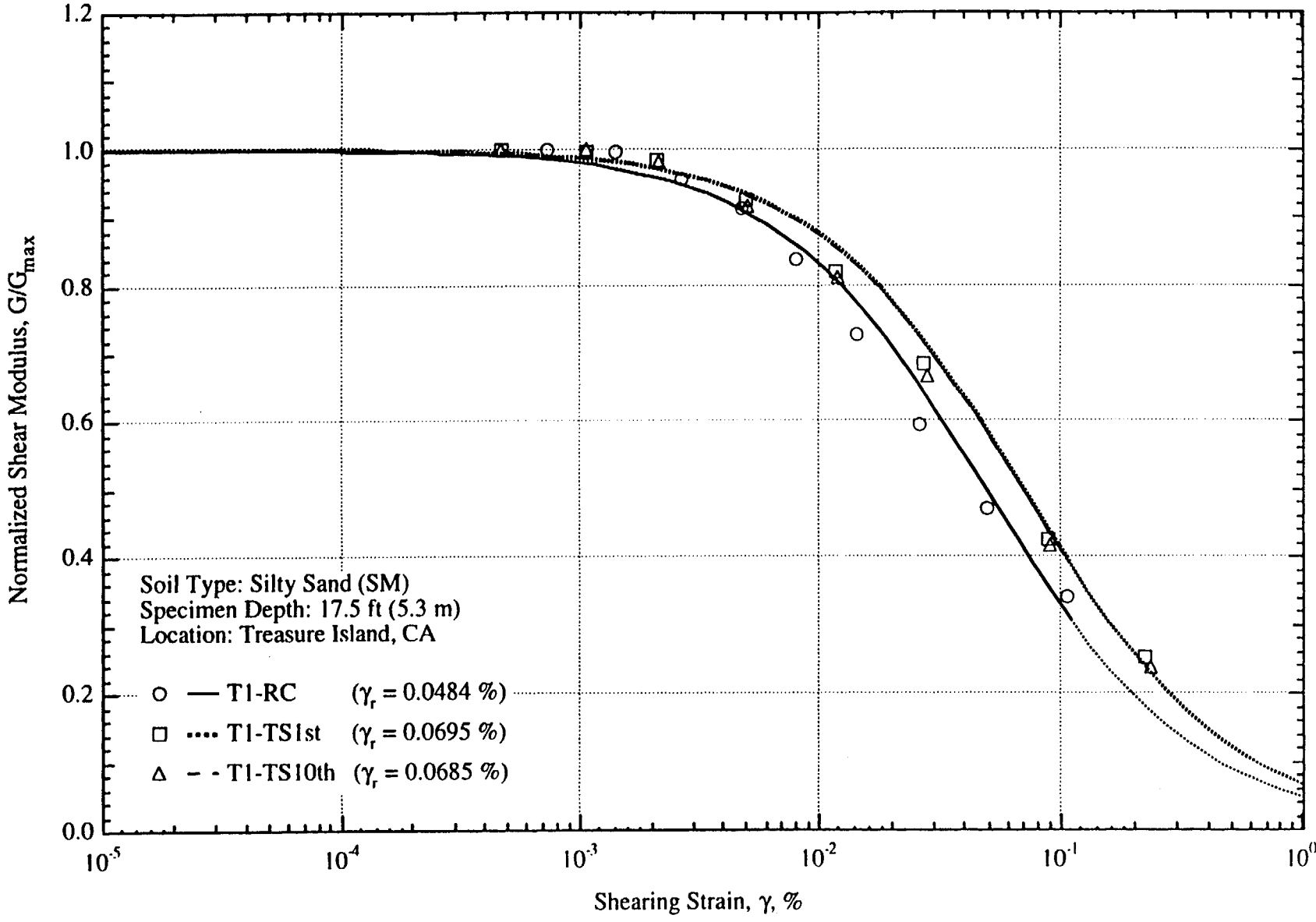


Fig. B.2 Variation in Normalized Shear Modulus with Shearing Strain at an Effective Confining Pressure of 6 psi(=864 psf=41 kPa) from RCTS Tests of Sample T1

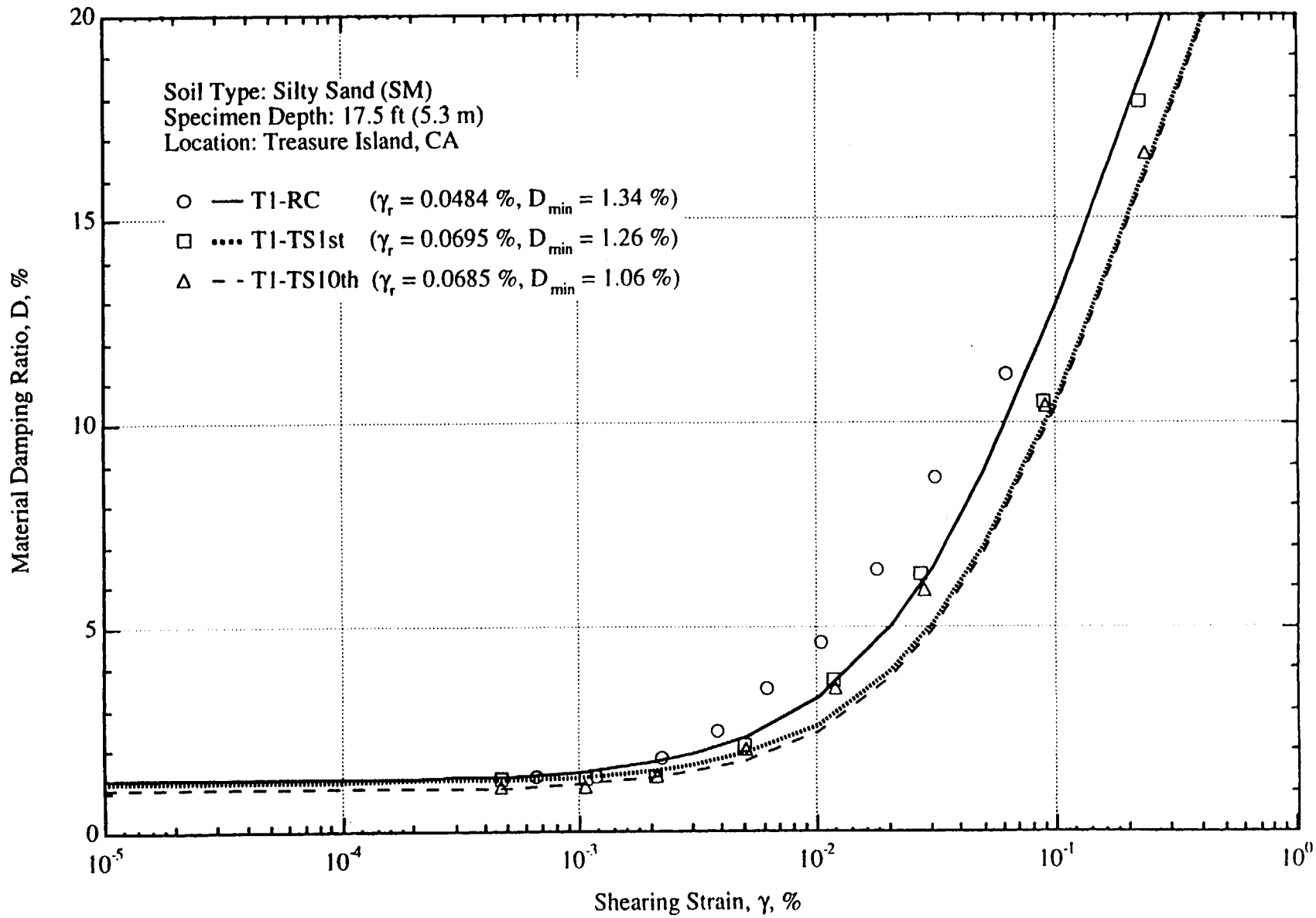


Fig. B.3 Variation in Material Damping Ratio with Shearing Strain at an Effective Confining Pressure of 6 psi(=864 psf=41 kPa) from RCTS Tests of Sample T1

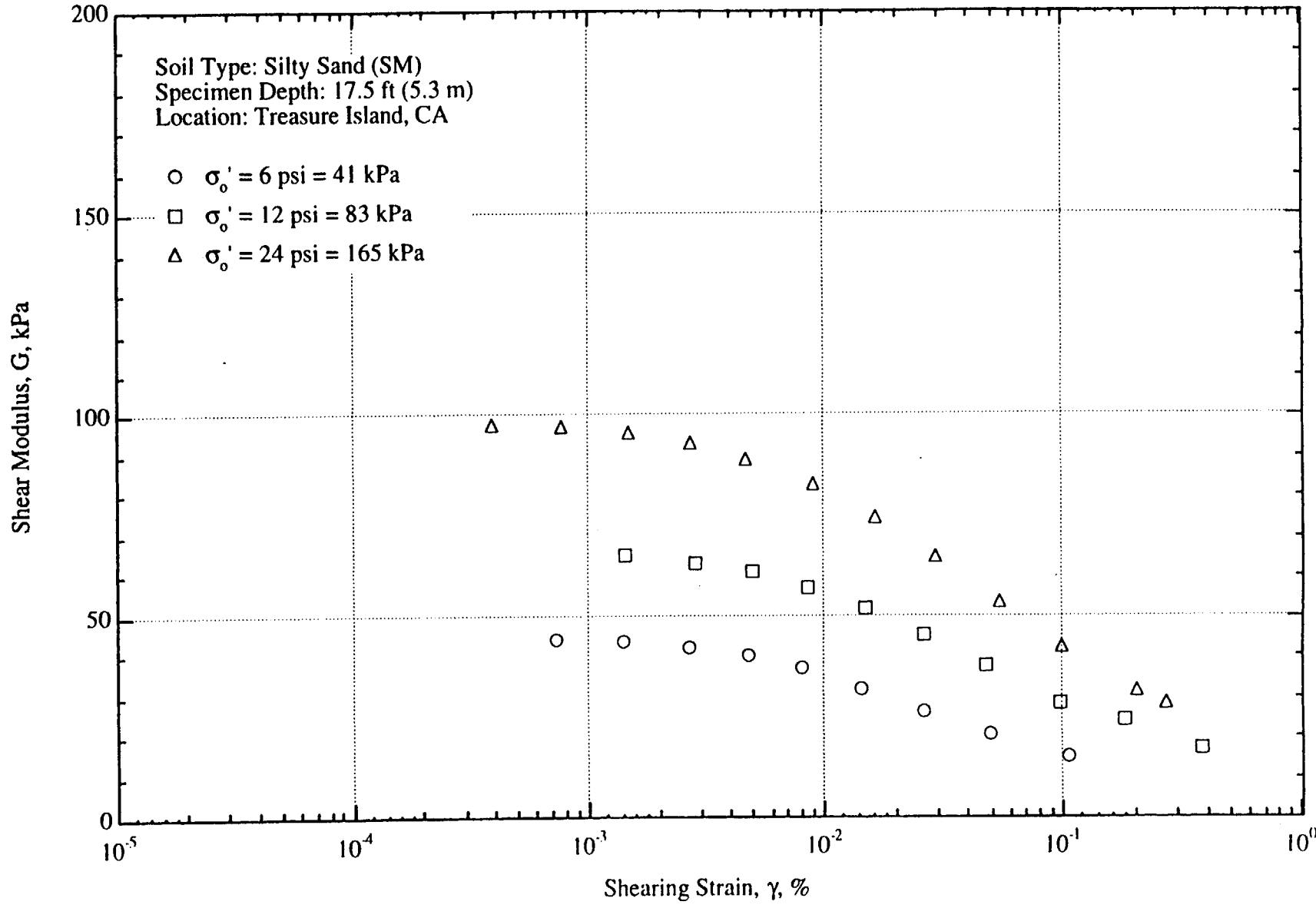


Fig. B.4 Variation in Shear Modulus with Shearing Strain and Effective Confining Pressure from Resonant Column Tests of Sample T1

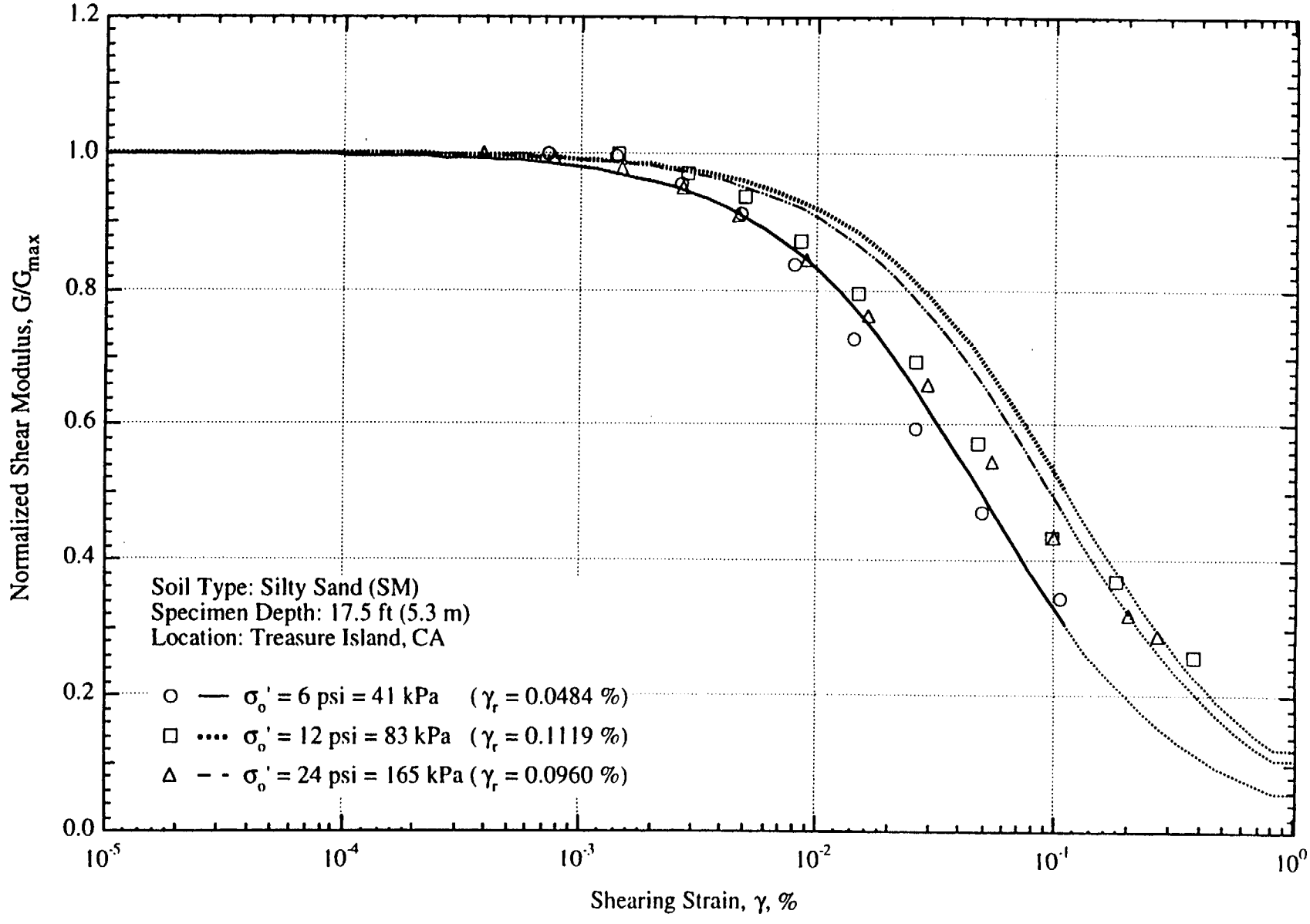


Fig. B.5 Comparison of the Variation in Normalized Shear Modulus with Shearing Strain and Effective Confining Pressure from Resonant Column Tests of Sample T1

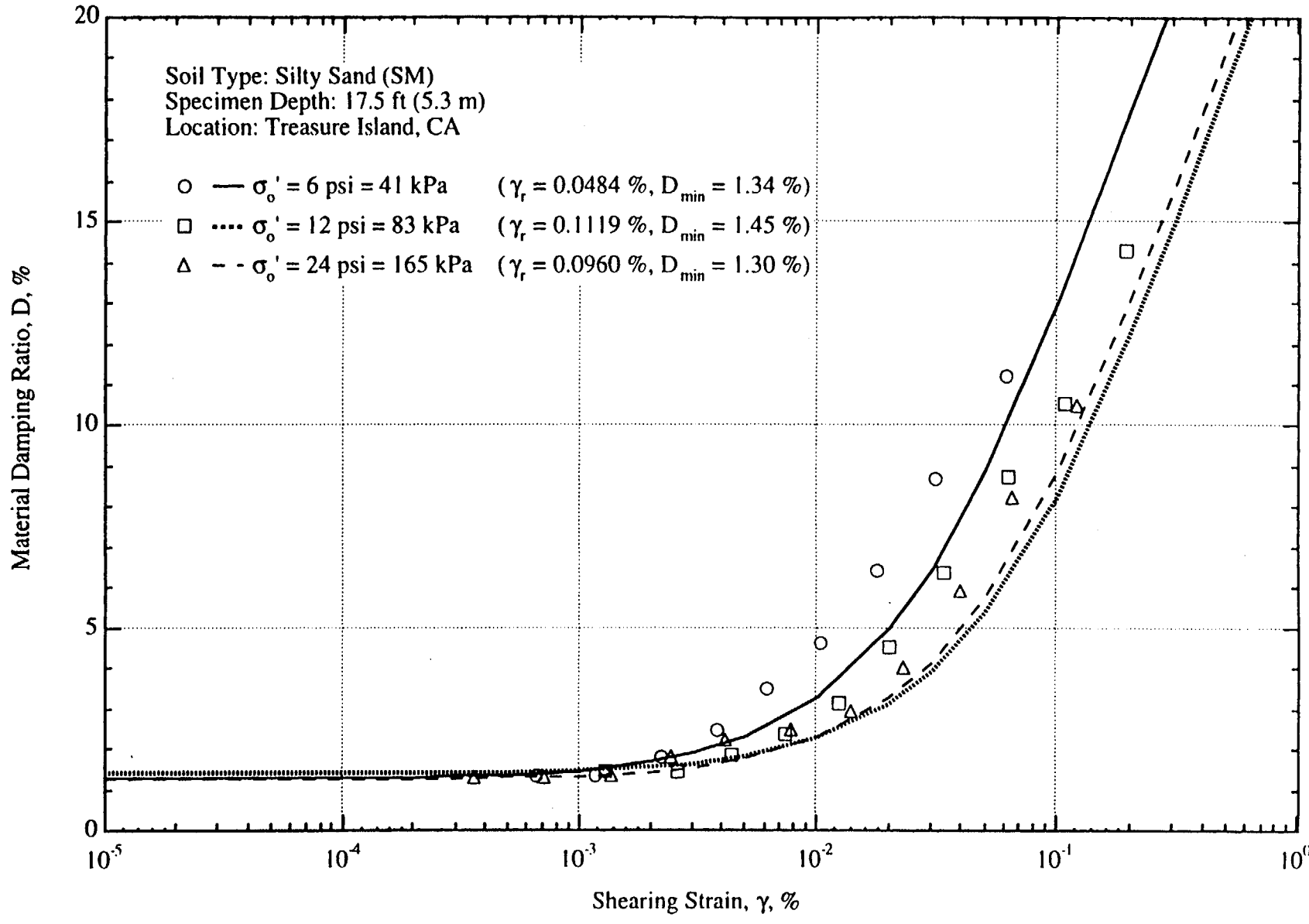


Fig. B.6 Variation in Material Damping Ratio with Shearing Strain and Effective Confining Pressure from Resonant Column Tests of Sample T1

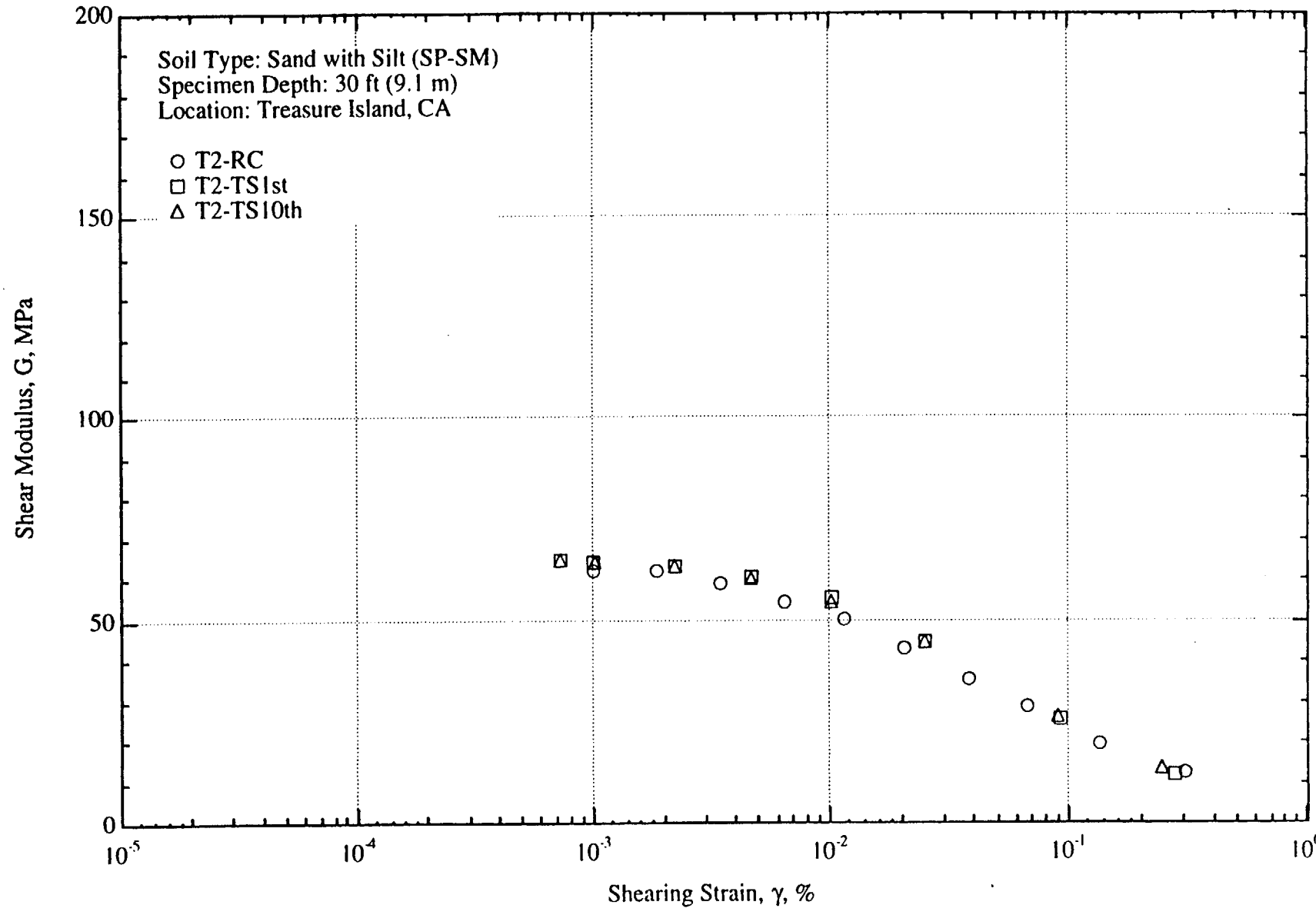


Fig. B.7 Variation in Shear Modulus with Shearing Strain at an Effective Confining Pressure of 10 psi (=1.44 ksf=69 kPa) from RCTS Tests of Sample T2

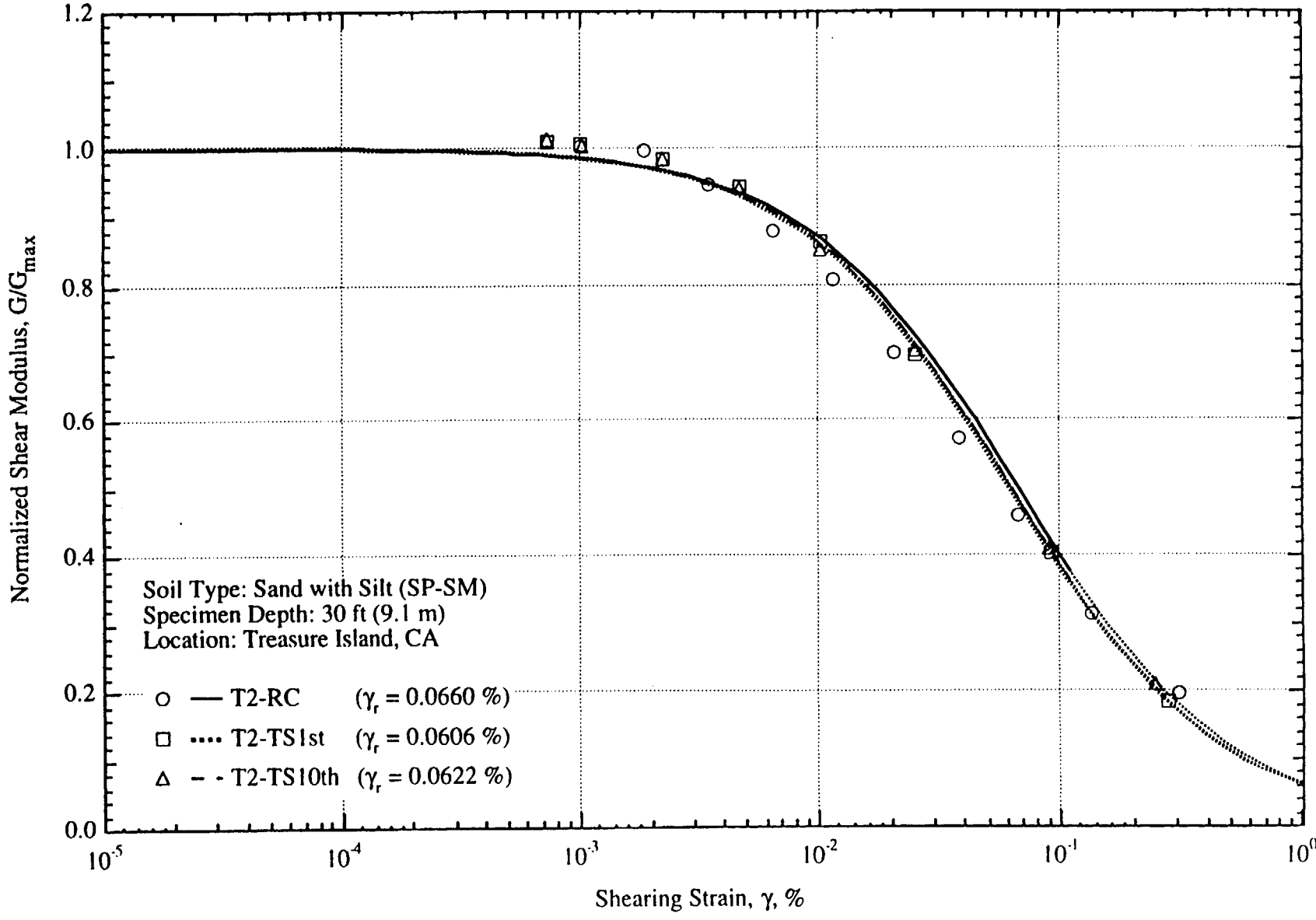


Fig. B.8 Variation in Normalized Shear Modulus with Shearing Strain at an Effective Confining Pressure of 10 psi(=1.44 ksf=69 kPa) from RCTS Tests of Sample T2

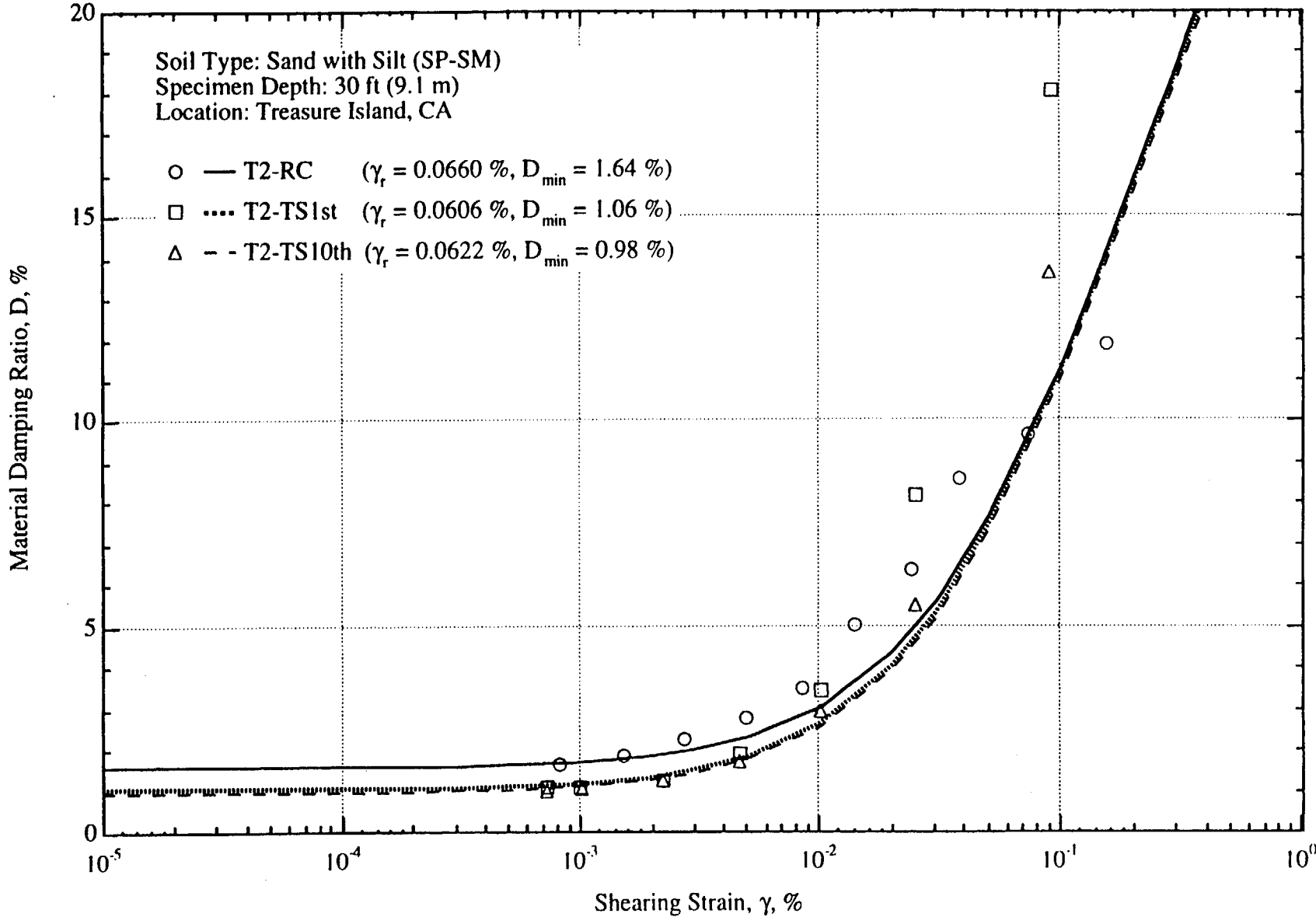


Fig. B.9 Variation in Material Damping Ratio with Shearing Strain at an Effective Confining Pressure of 10 psi(=1.44 ksf=69 kPa) from RCTS Tests of Sample T2

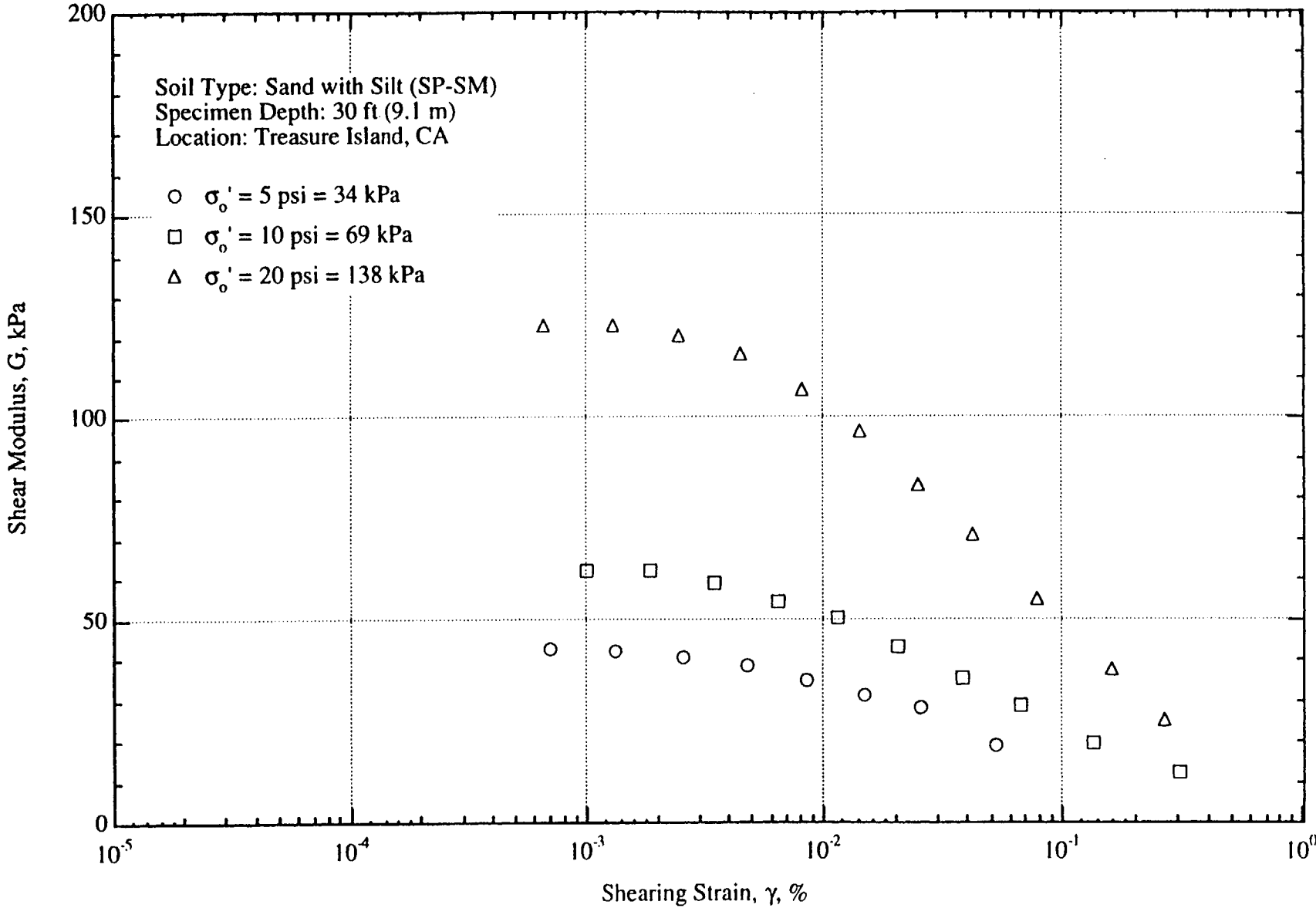


Fig. B.10 Variation in Shear Modulus with Shearing Strain and Effective Confining Pressure from Resonant Column Tests of Sample T2

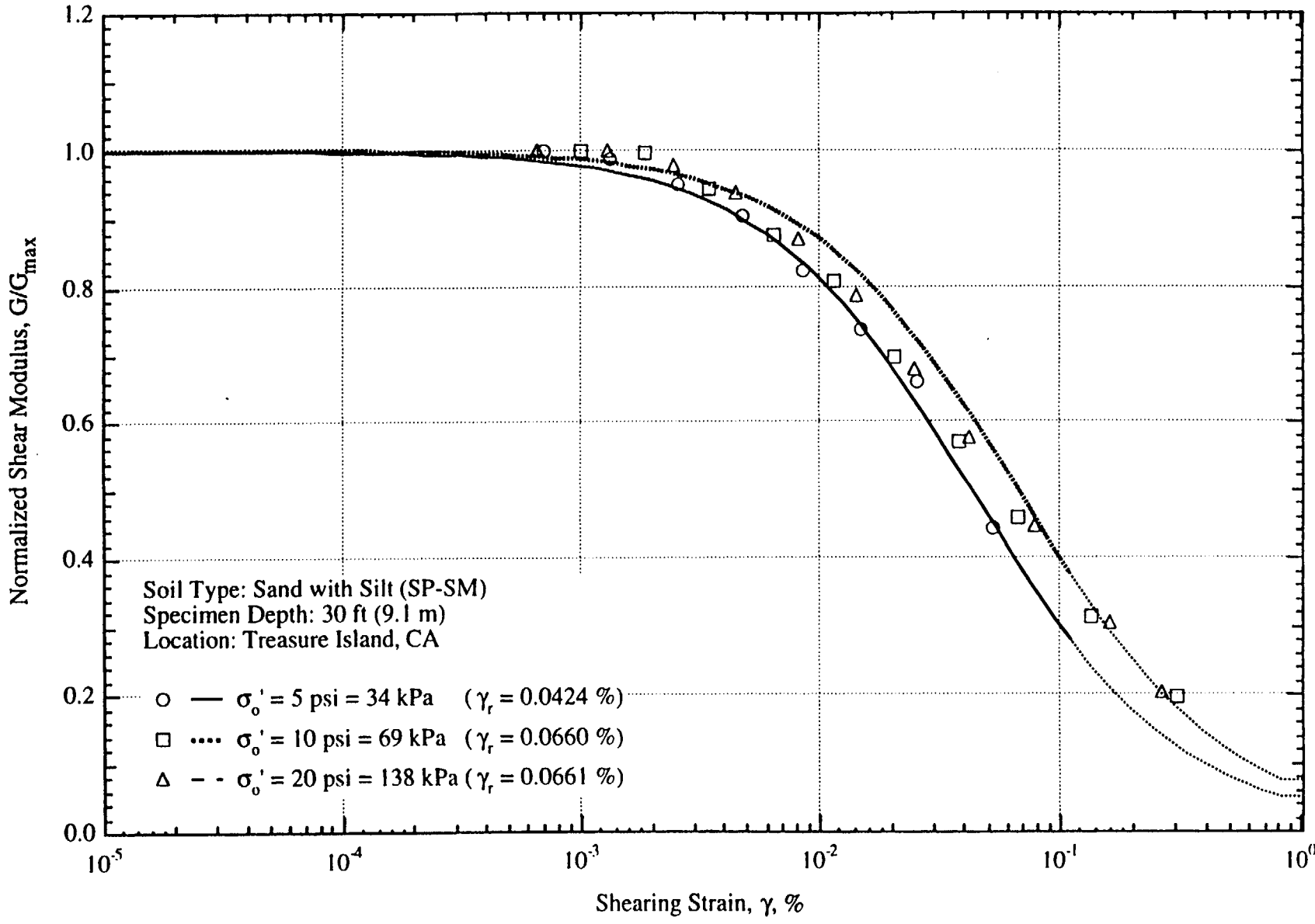


Fig. B.11 Comparison of the Variation in Normalized Shear Modulus with Shearing Strain and Effective Confining Pressure from Resonant Column Tests of Sample T2

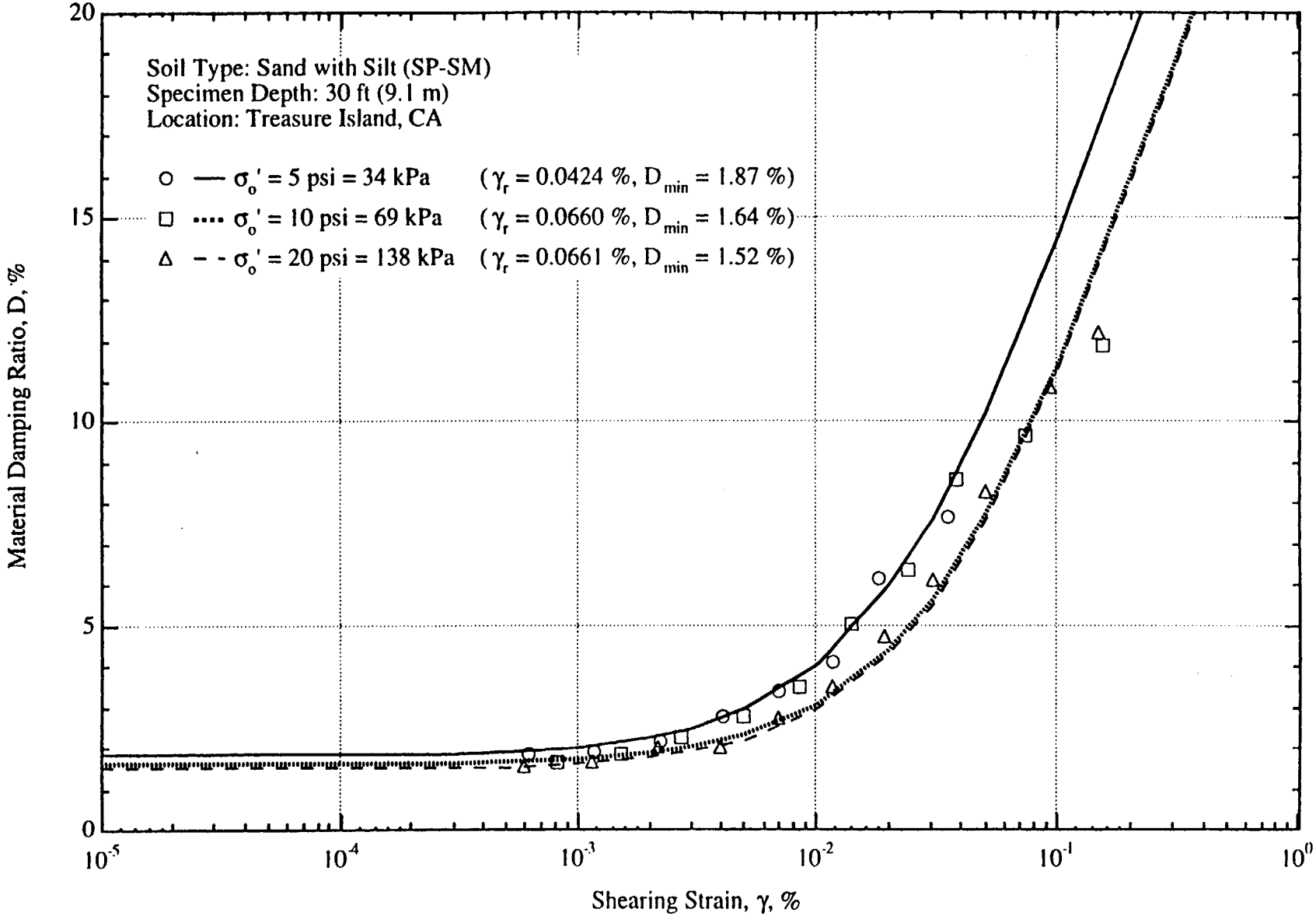


Fig. B.12 Variation in Material Damping Ratio with Shearing Strain and Effective Confining Pressure from Resonant Column Tests of Sample T2

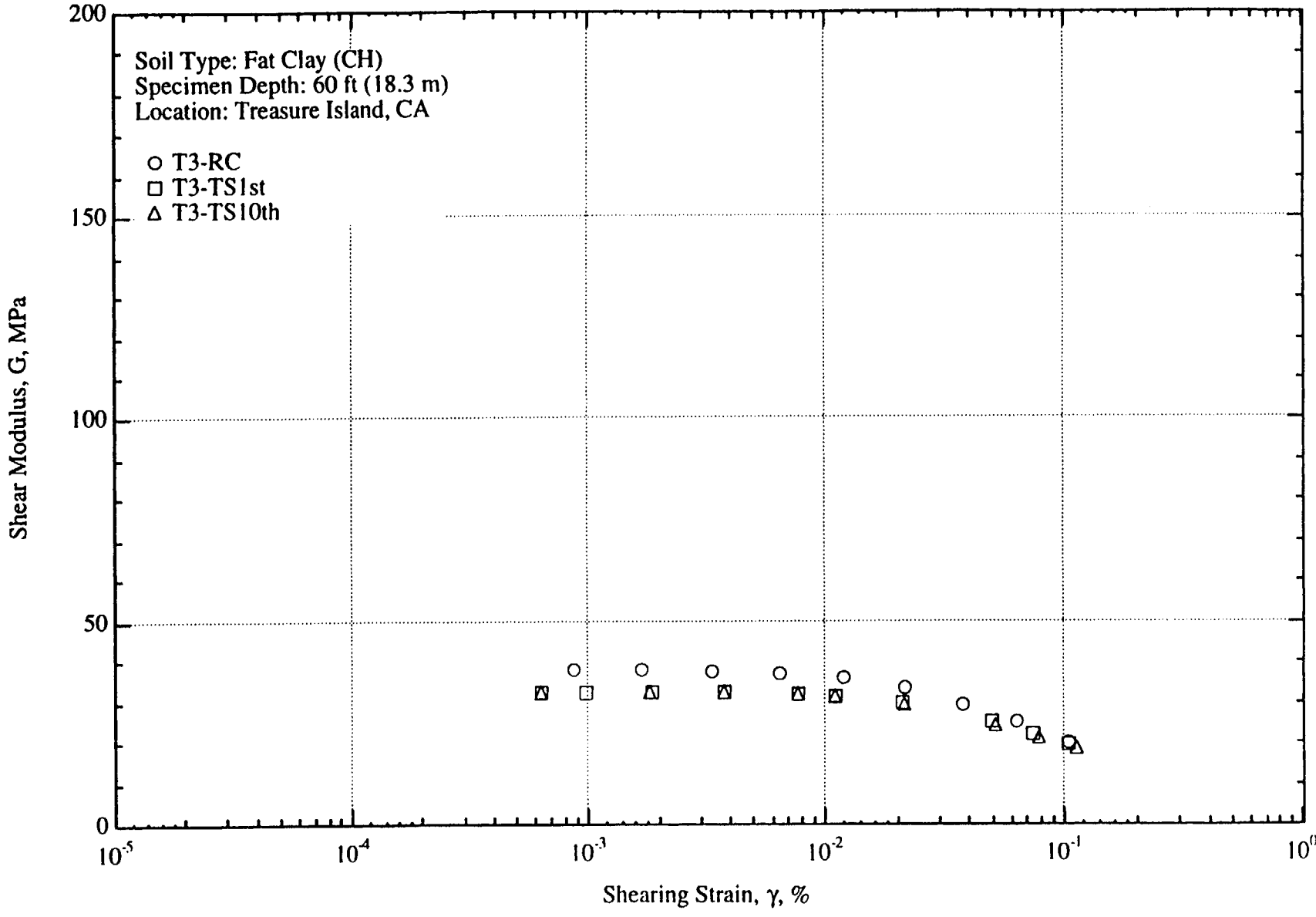


Fig. B.13 Variation in Shear Modulus with Shearing Strain at an Effective Confining Pressure of 18 psi (=2.59 ksf=124 kPa) from RCTS Tests of Sample T3

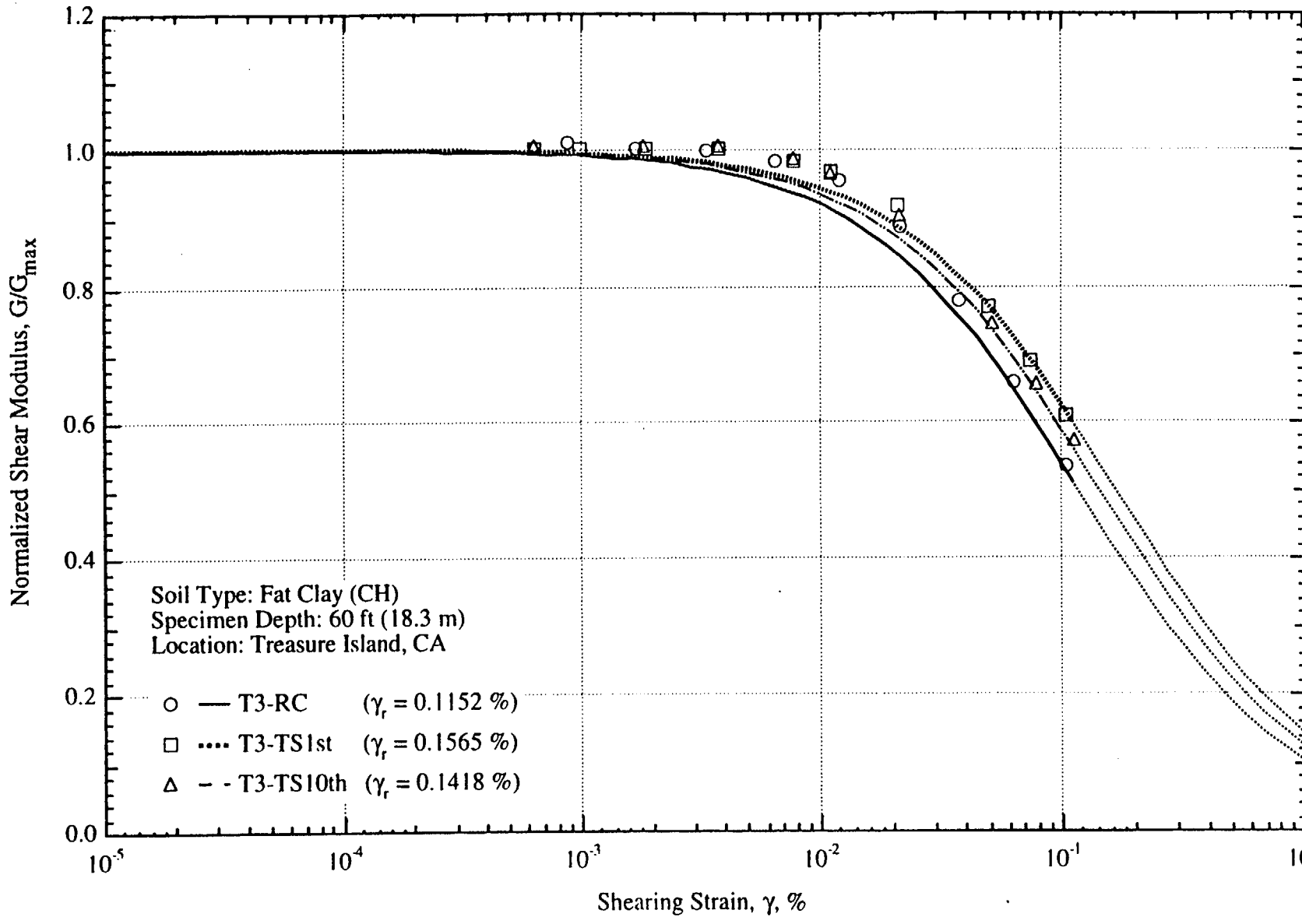


Fig. B.14 Variation in Normalized Shear Modulus with Shearing Strain at an Effective Confining Pressure of 18 psi(=2.59 ksf=124 kPa) from RCTS Tests of Sample T3

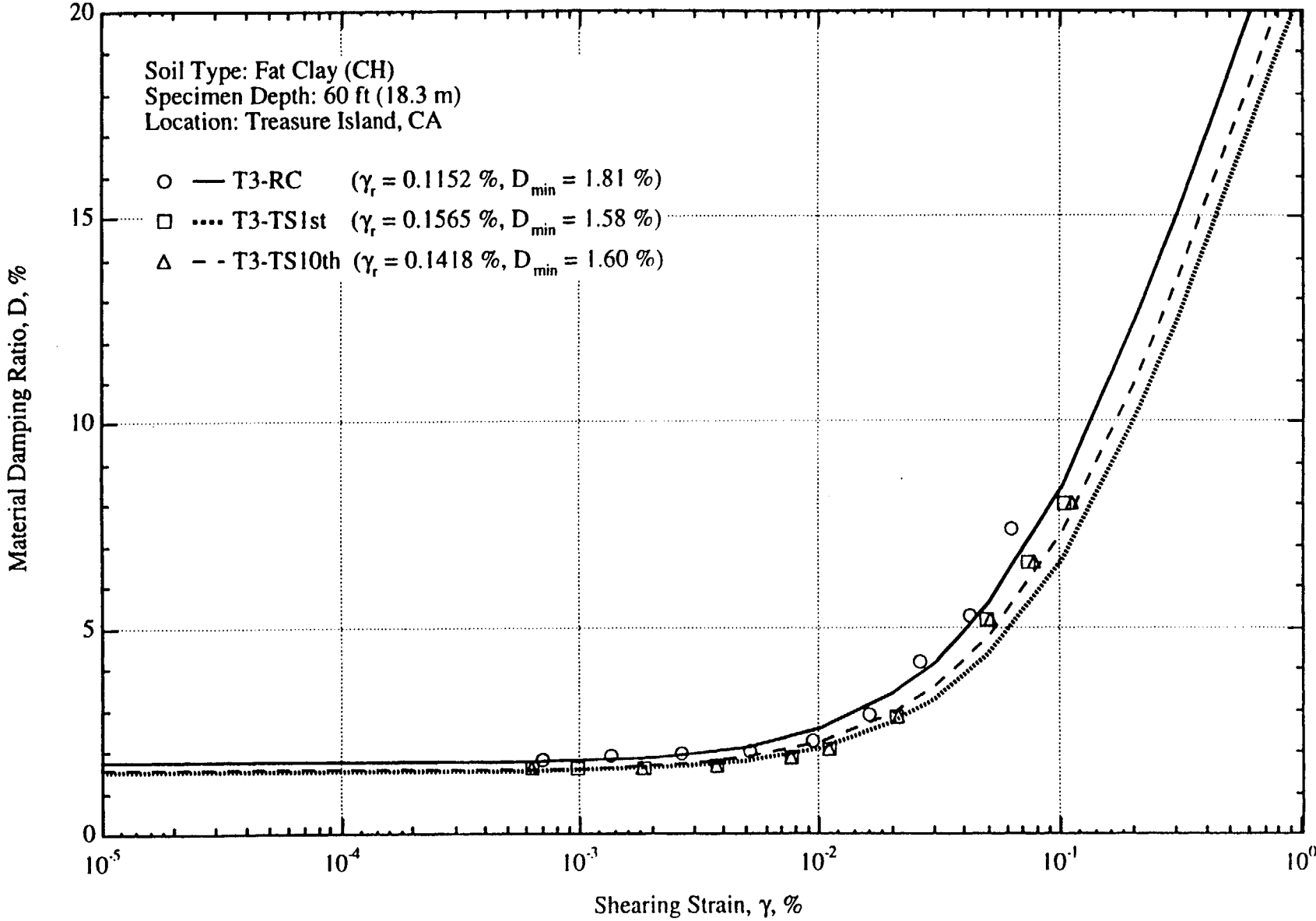


Fig. B.15 Variation in Material Damping Ratio with Shearing Strain at an Effective Confining Pressure of 18 psi(=2.59 ksf=124 kPa) from RCTS Tests of Sample T3

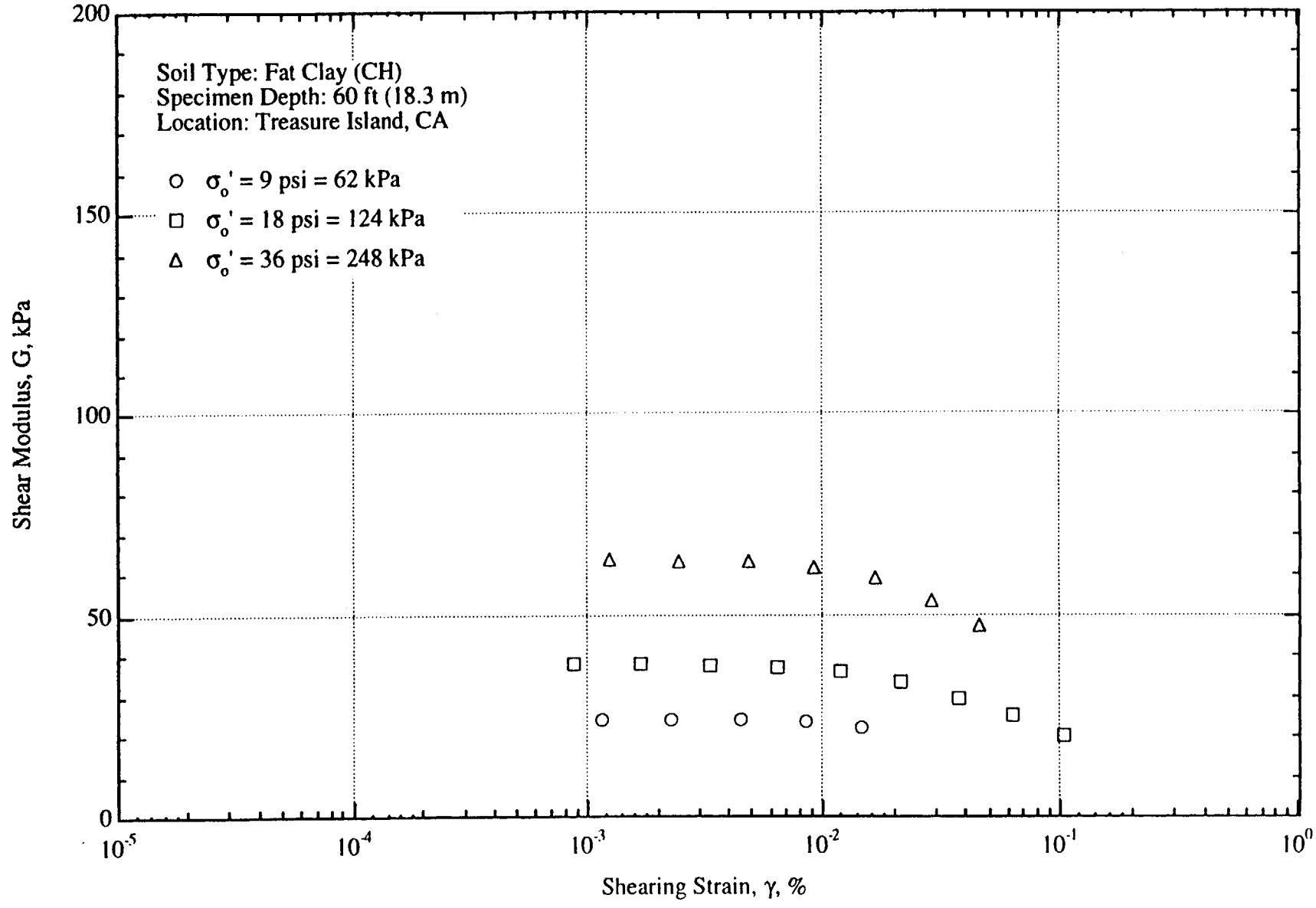


Fig. B.16 Variation in Shear Modulus with Shearing Strain and Effective Confining Pressure from Resonant Column Tests of Sample T3

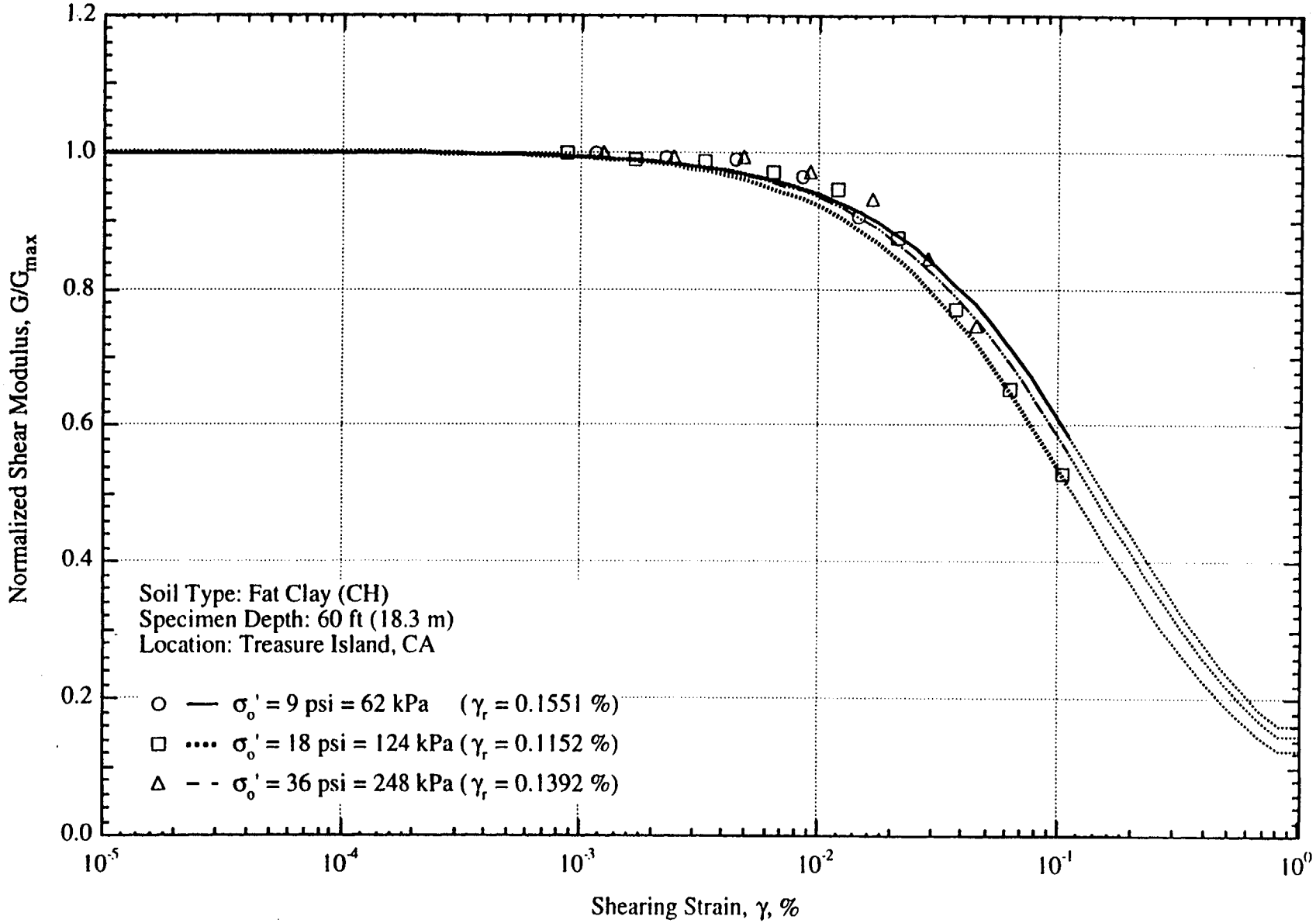


Fig. B.17 Comparison of the Variation in Normalized Shear Modulus with Shearing Strain and Effective Confining Pressure from Resonant Column Tests of Sample T3

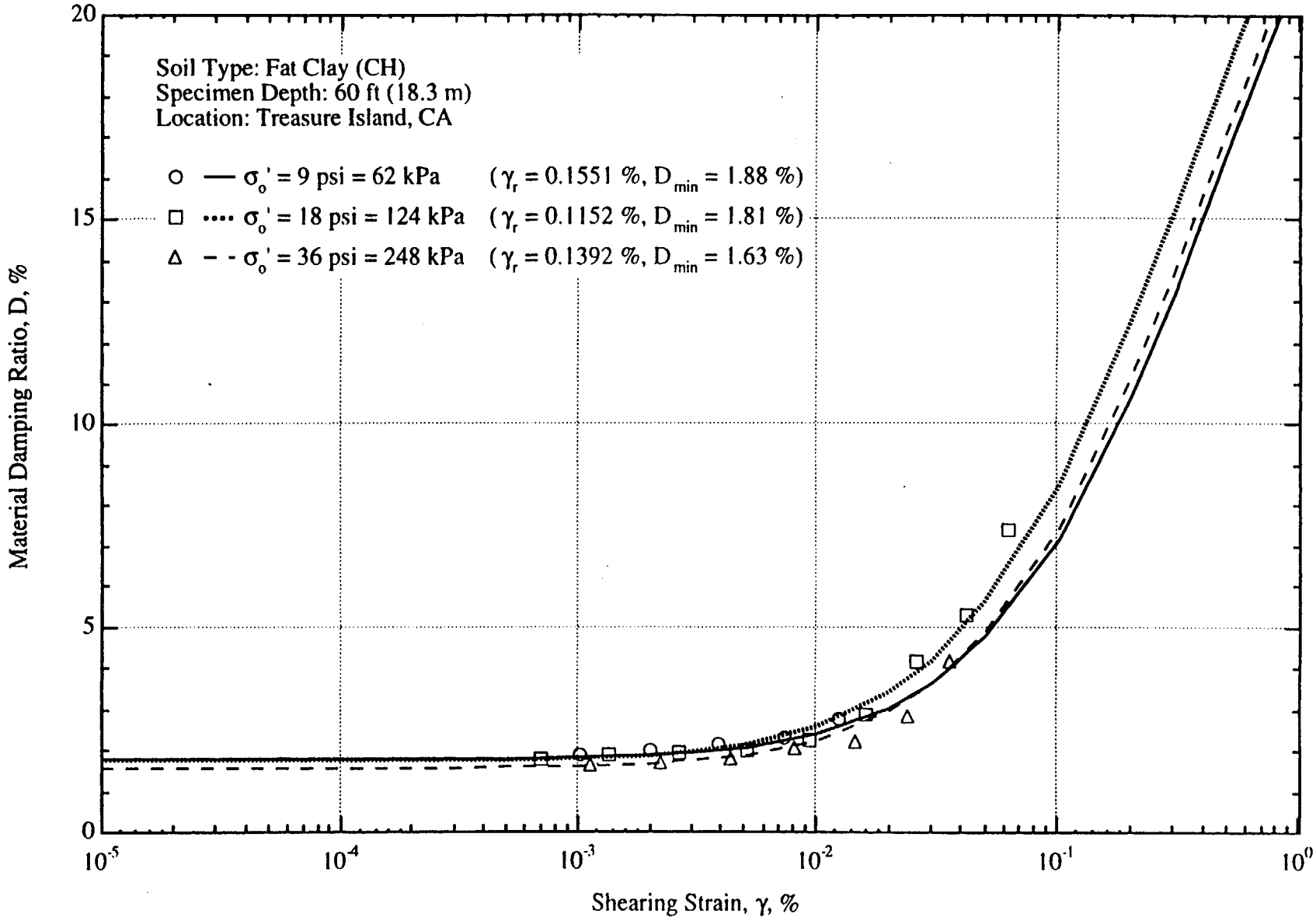


Fig. B.18 Variation in Material Damping Ratio with Shearing Strain and Effective Confining Pressure from Resonant Column Tests of Sample T3

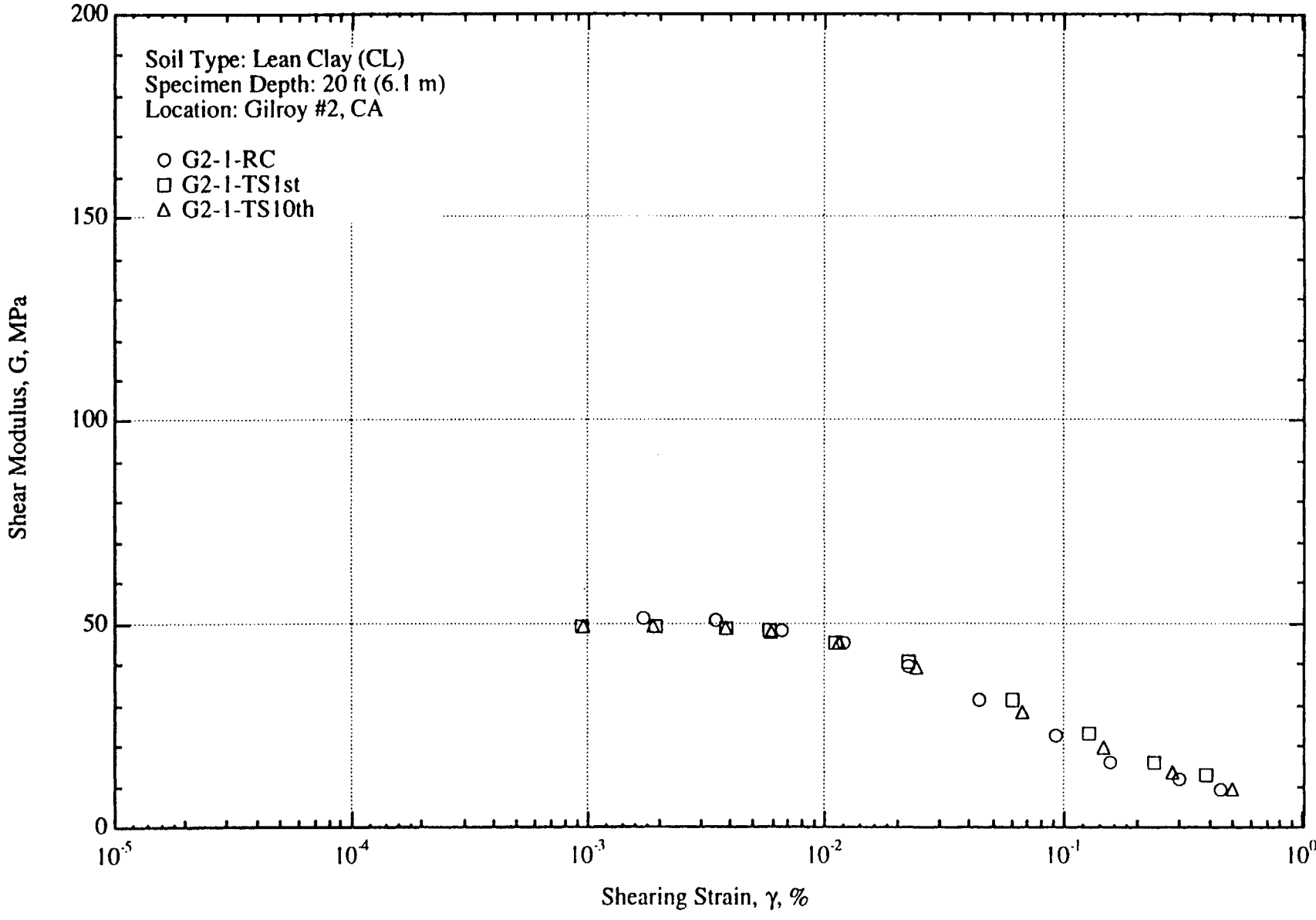


Fig. B.19 Variation in Shear Modulus with Shearing Strain at an Effective Confining Pressure of 12 psi (=1.73 ksf=83 kPa) from RCTS Tests of Sample G2-1

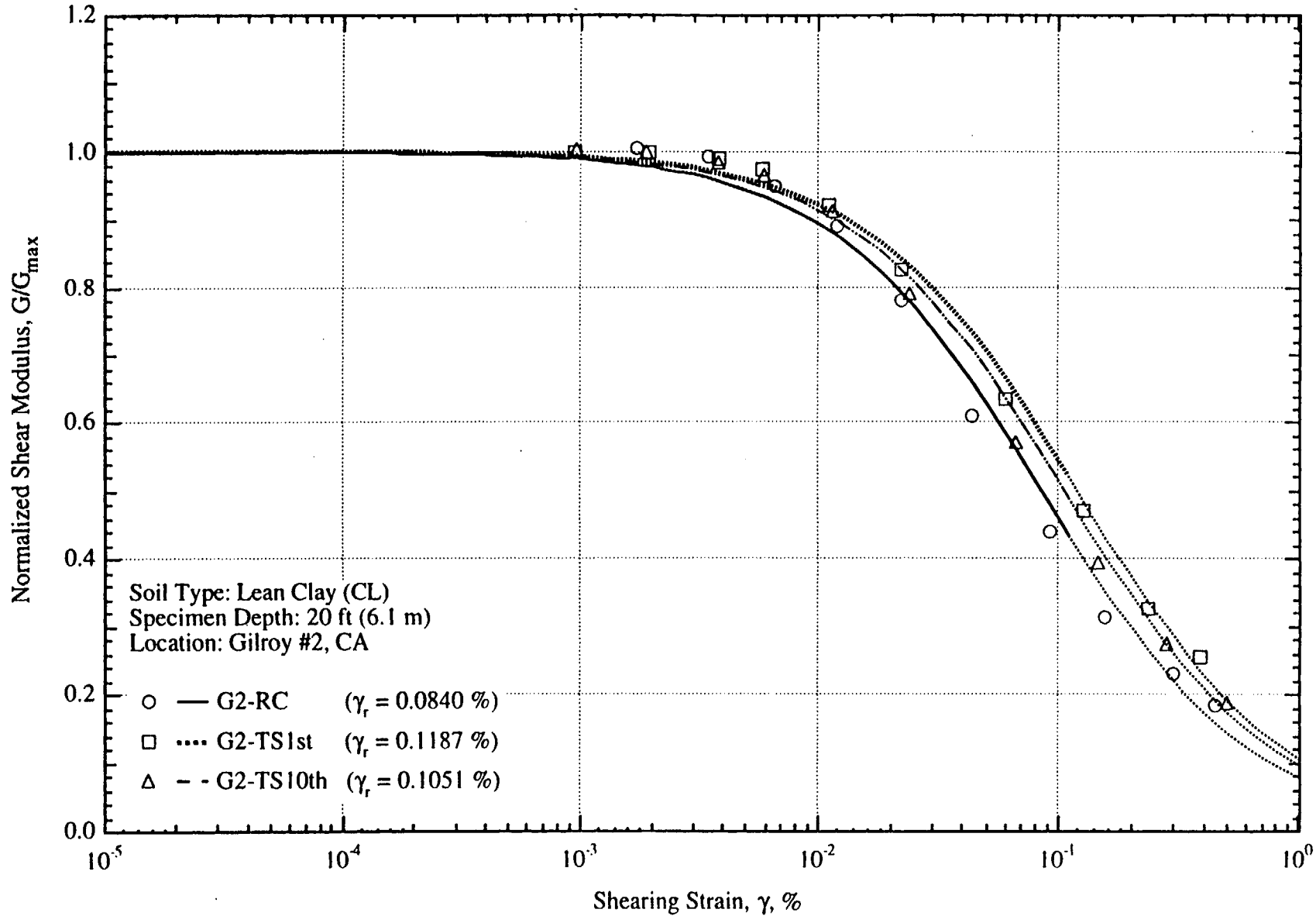


Fig. B.20 Variation in Normalized Shear Modulus with Shearing Strain at an Effective Confining Pressure of 12 psi(=1.73 ksf=83 kPa) from RCTS Tests of Sample G2-1

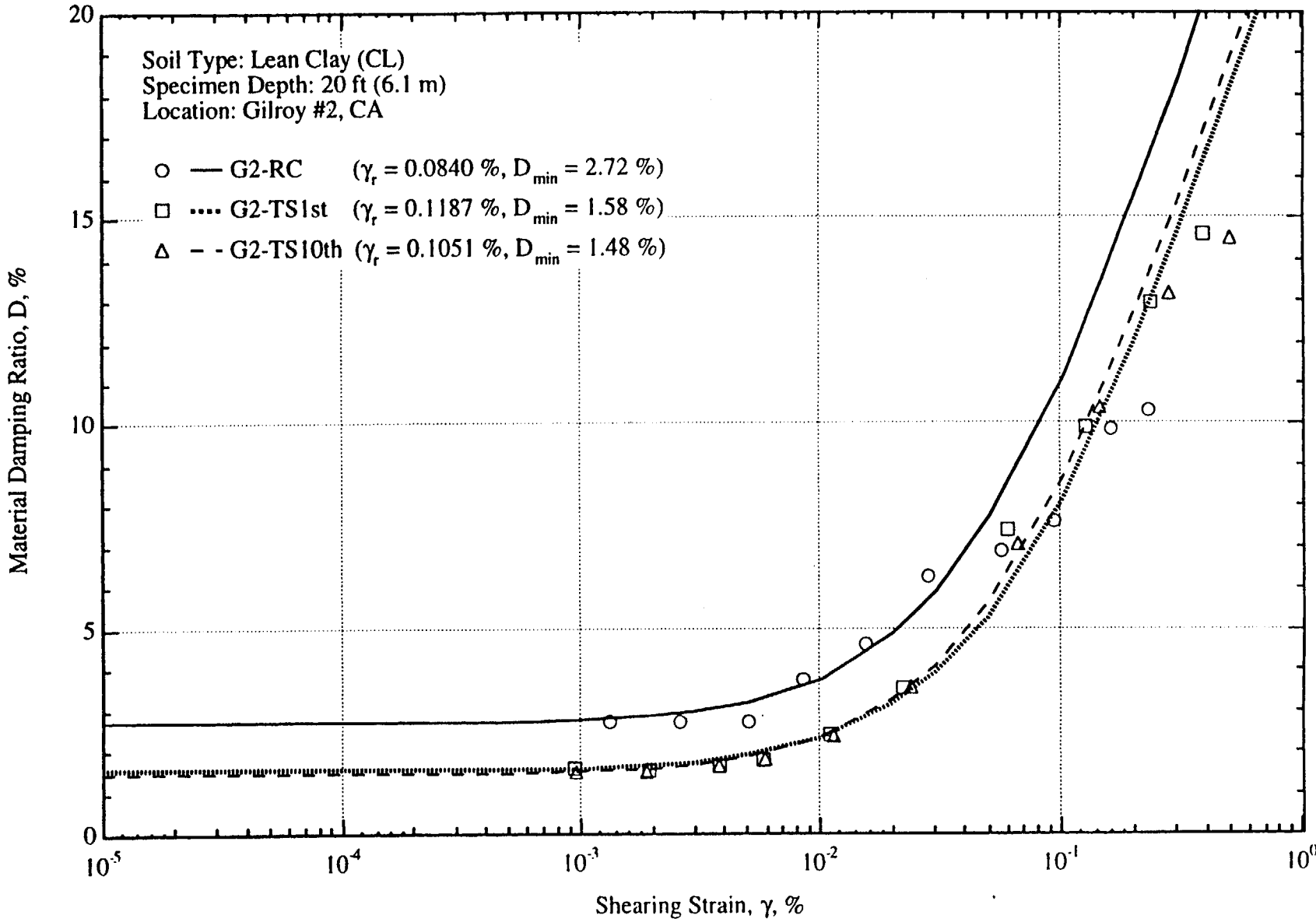


Fig. B.21 Variation in Material Damping Ratio with Shearing Strain at an Effective Confining Pressure of 12 psi(=1.73 ksf=83 kPa) from RCTS Tests of Sample G2-1

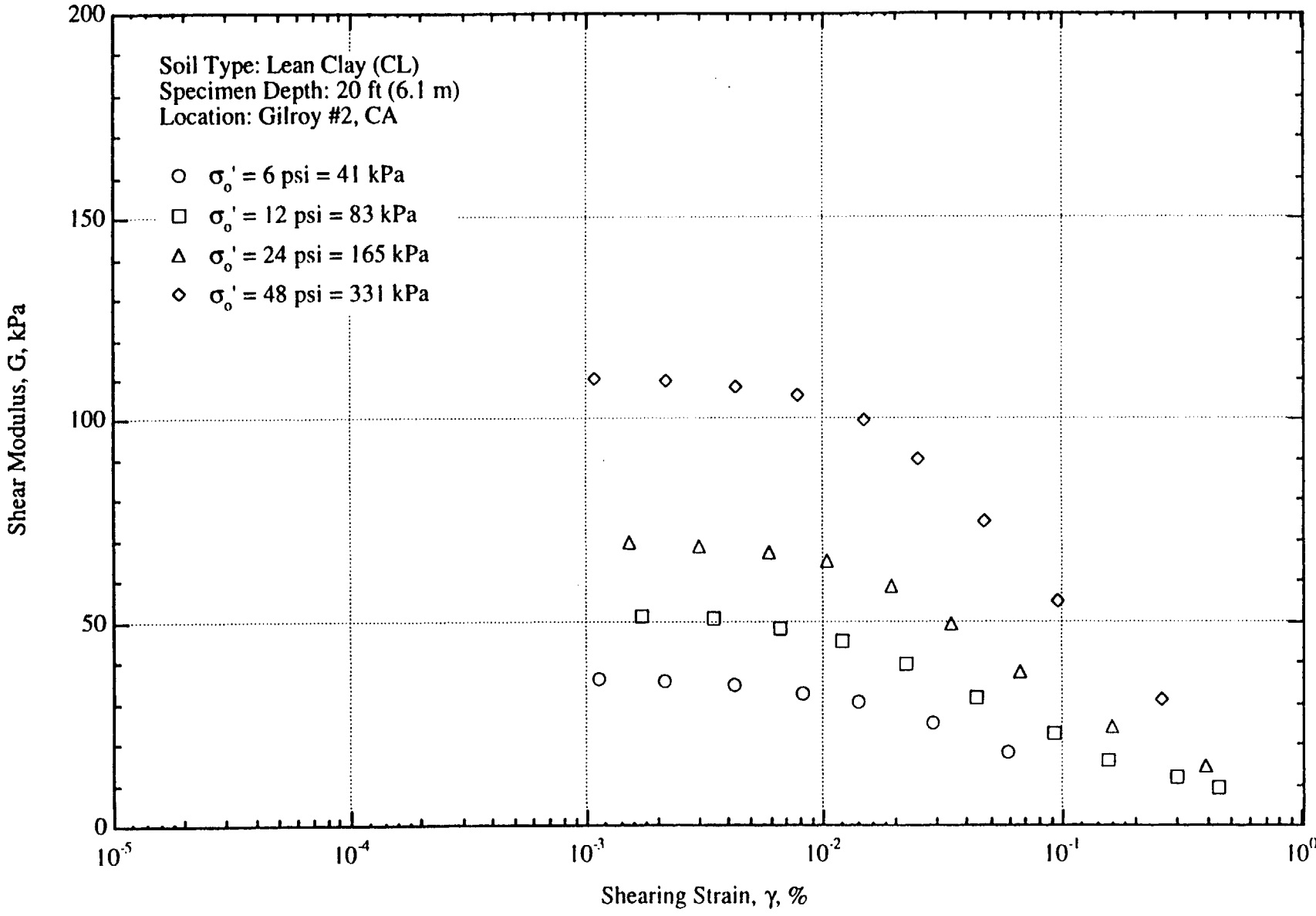


Fig. B.22 Variation in Shear Modulus with Shearing Strain and Effective Confining Pressure from Resonant Column Tests of Sample G2-1

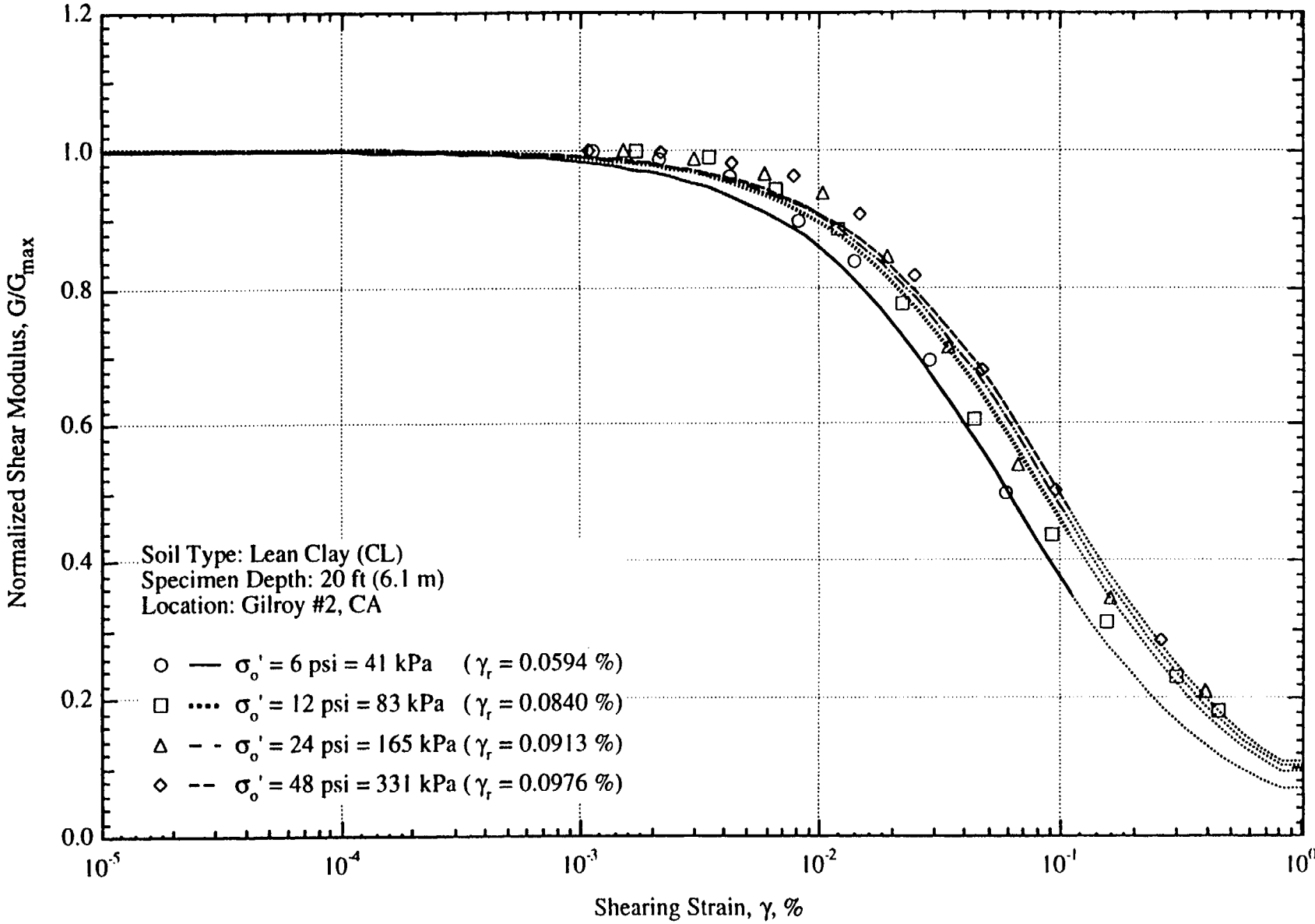


Fig. B.23 Comparison of the Variation in Normalized Shear Modulus with Shearing Strain and Effective Confining Pressure from Resonant Column Tests of Sample G2-1

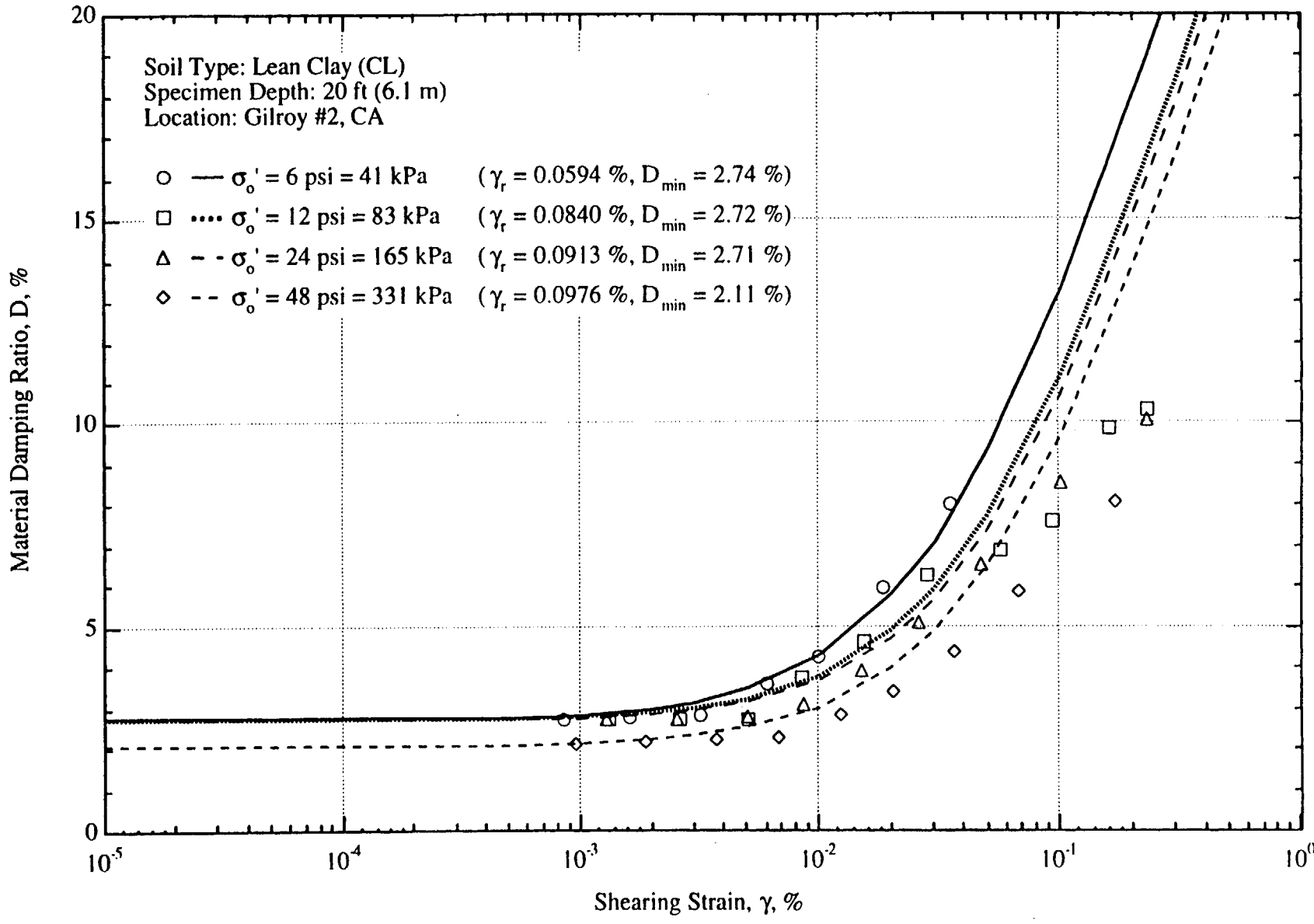


Fig. B.24 Variation in Material Damping Ratio with Shearing Strain and Effective Confining Pressure from Resonant Column Tests of Sample G2-1

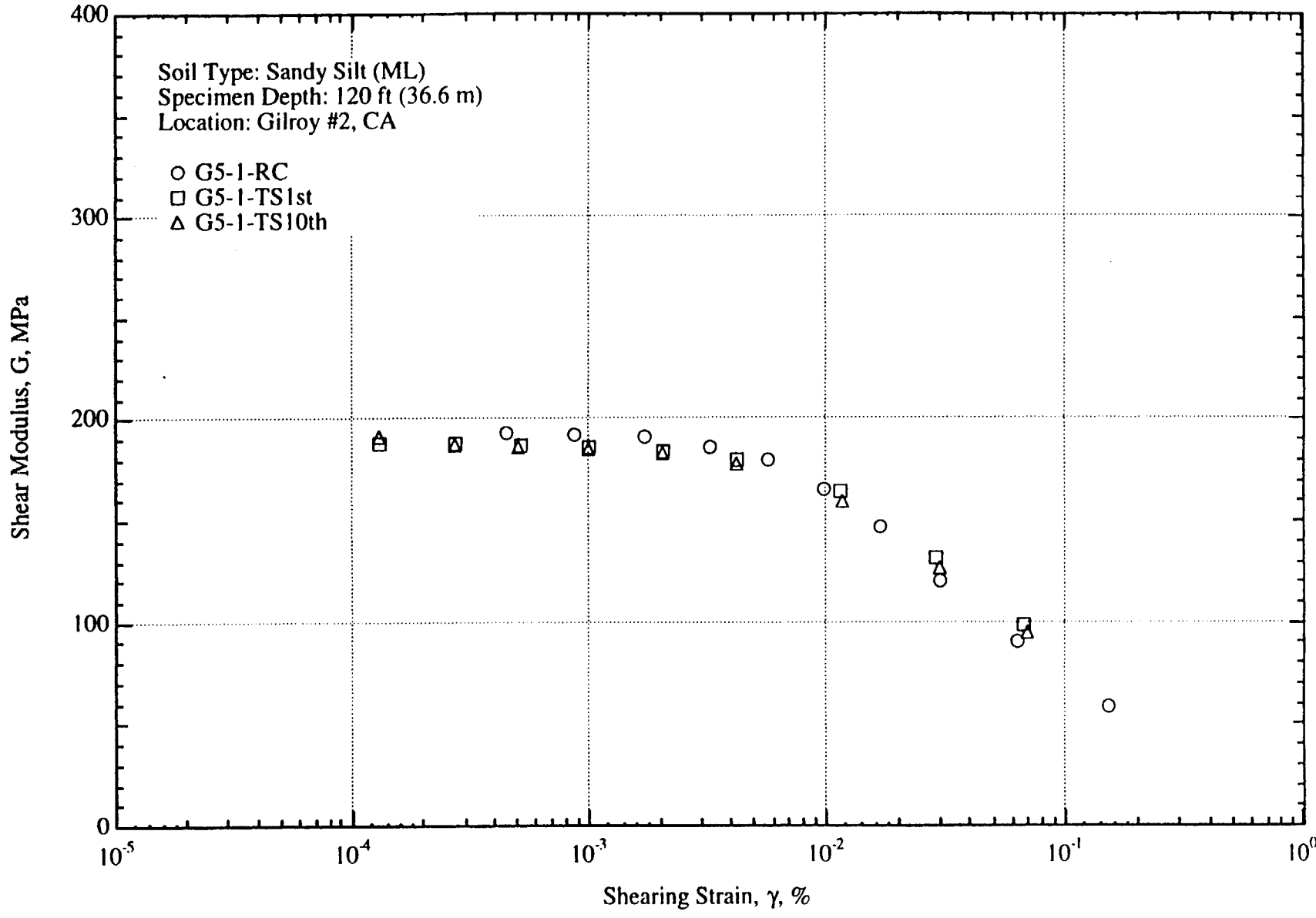


Fig. B.25 Variation in Shear Modulus with Shearing Strain at an Effective Confining Pressure of 48 psi (=6.91 ksf=331 kPa) from RCTS Tests of Sample G5-1

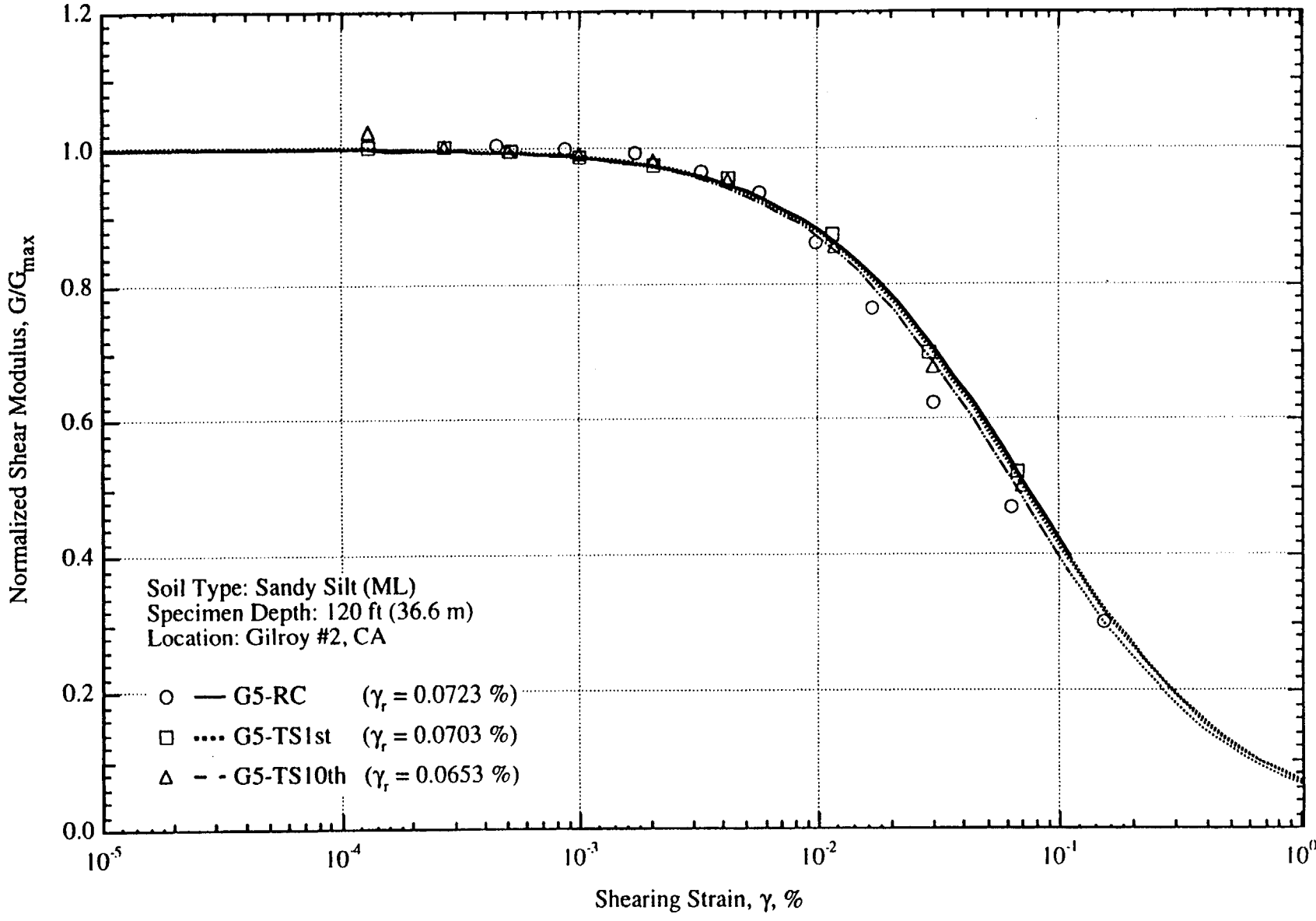


Fig. B.26 Variation in Normalized Shear Modulus with Shearing Strain at an Effective Confining Pressure of 48 psi(=6.91 ksf=331 kPa) from RCTS Tests of Sample G5-1

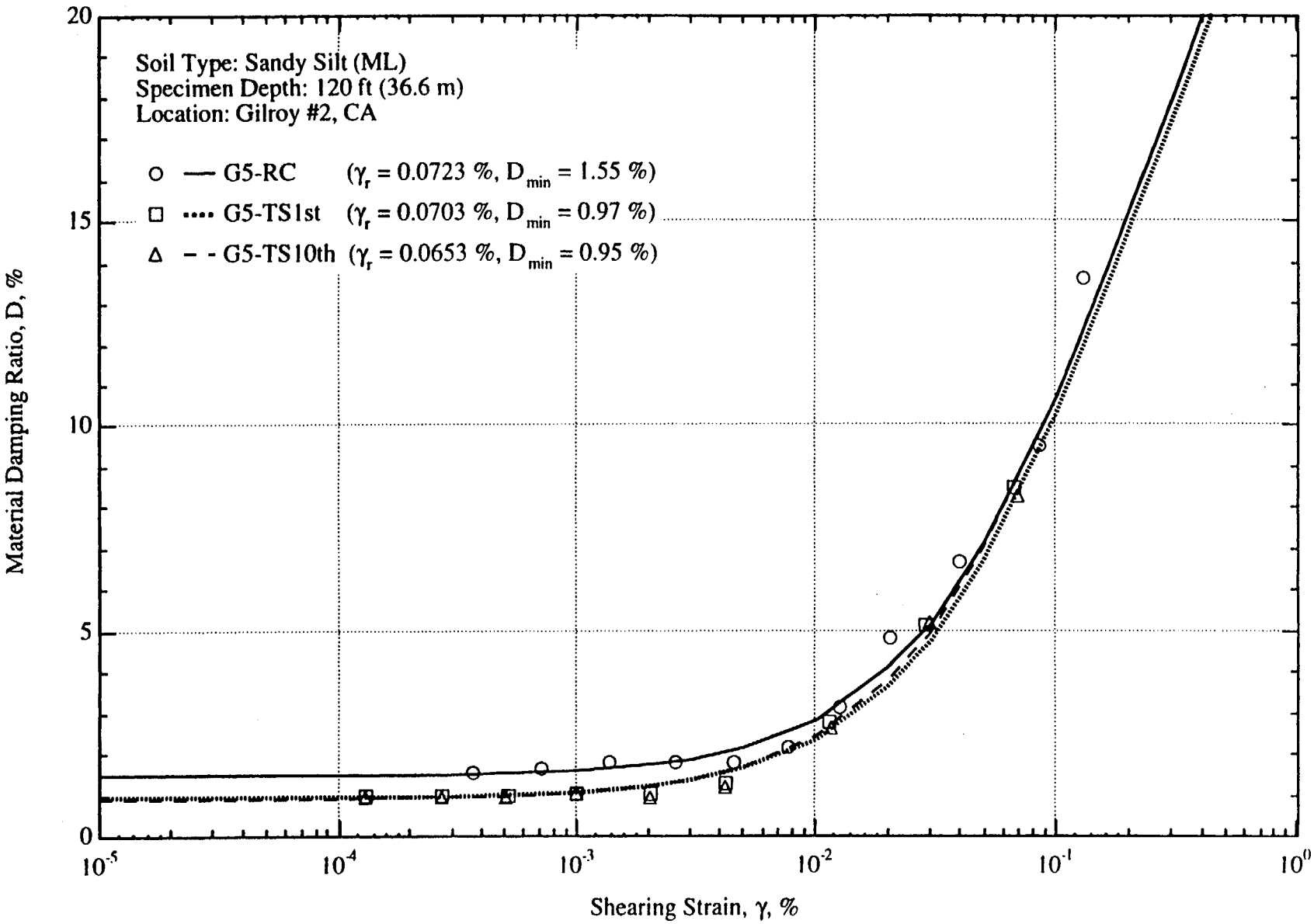


Fig. B.27 Variation in Material Damping Ratio with Shearing Strain at an Effective Confining Pressure of 48 psi(=6.91 ksf=331 kPa) from RCTS Tests of Sample G5-1

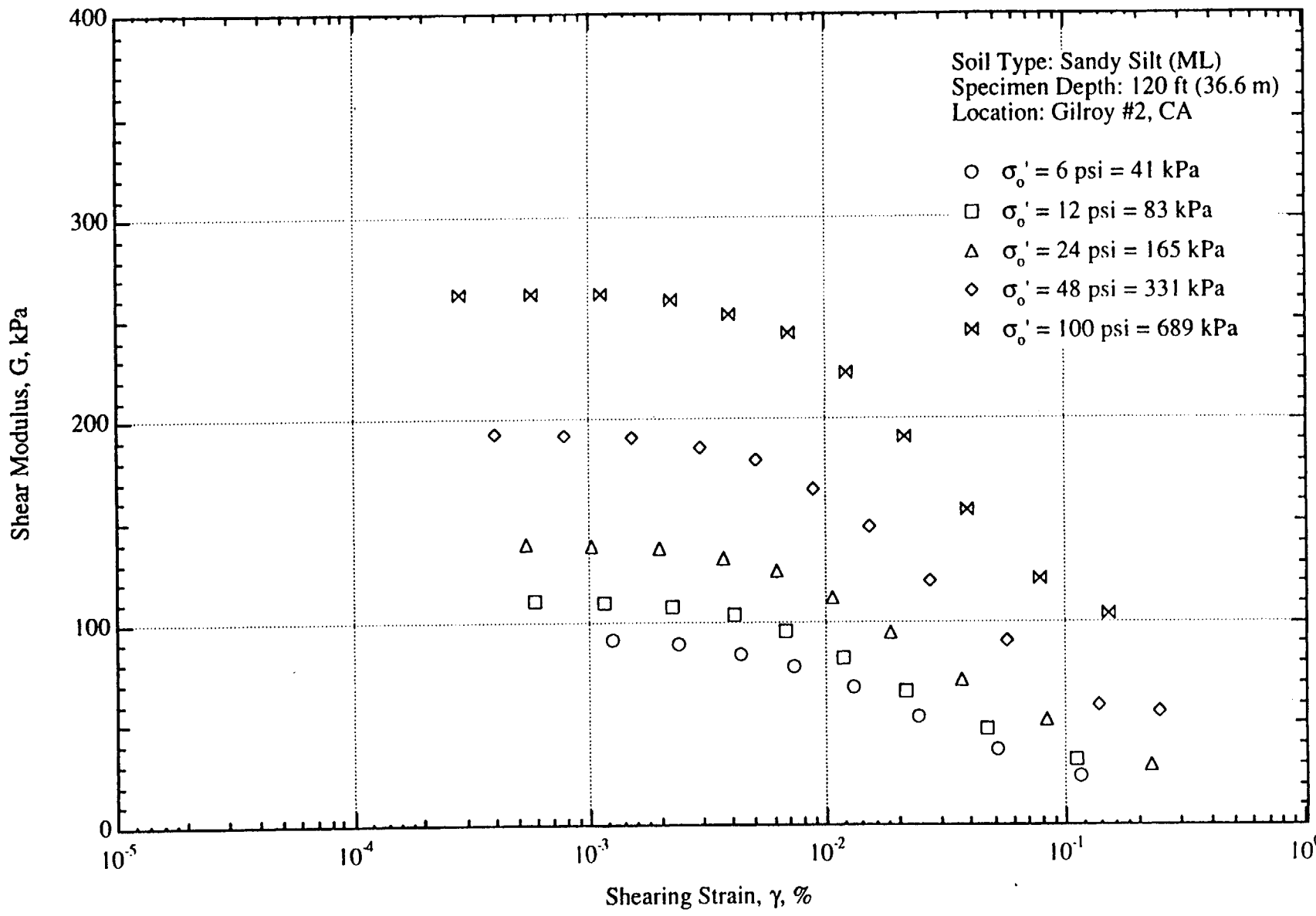


Fig. B.28 Variation in Shear Modulus with Shearing Strain and Effective Confining Pressure from Resonant Column Tests of Sample G5-1

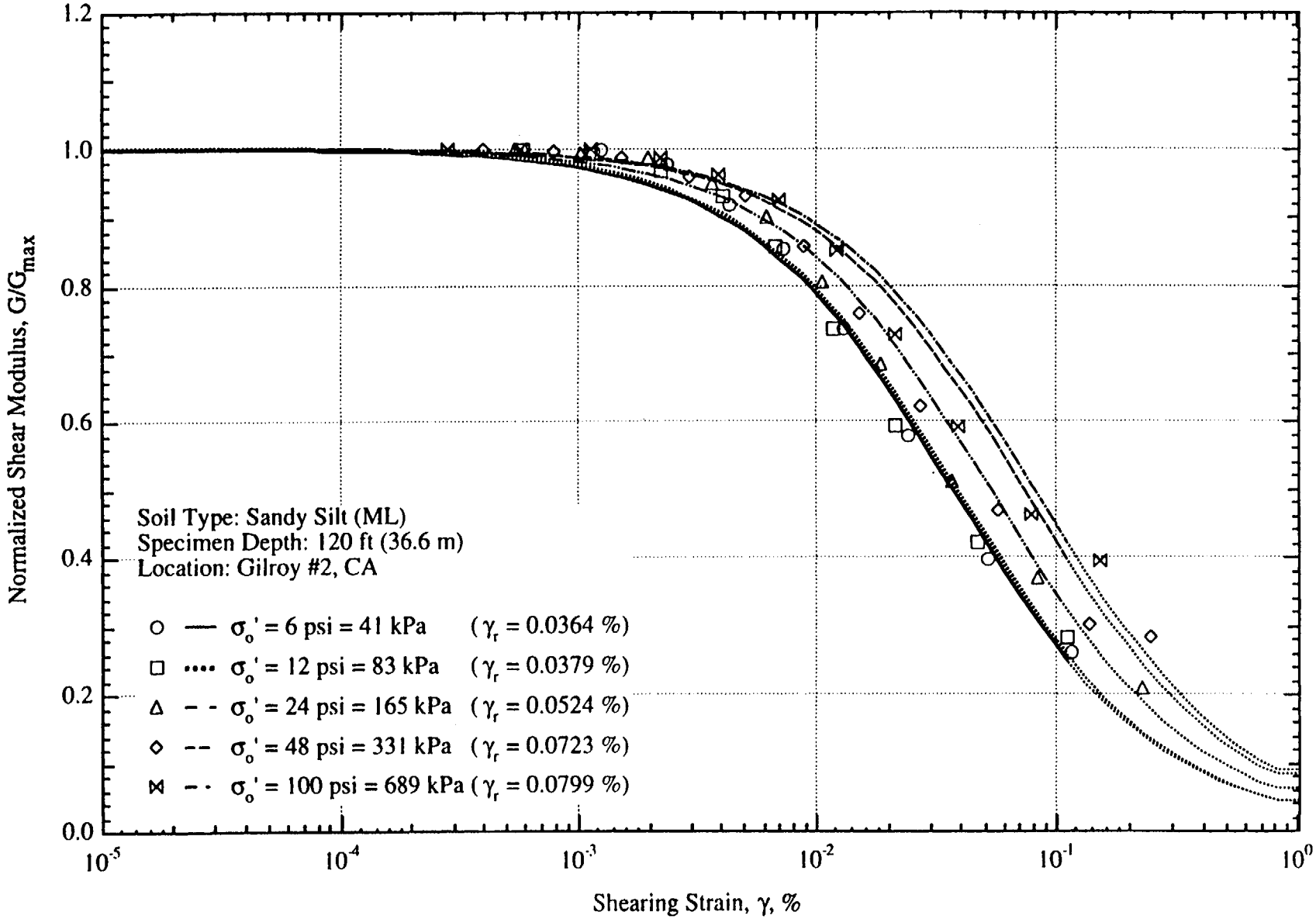


Fig. B.29 Comparison of the Variation in Normalized Shear Modulus with Shearing Strain and Effective Confining Pressure from Resonant Column Tests of Sample G5-1

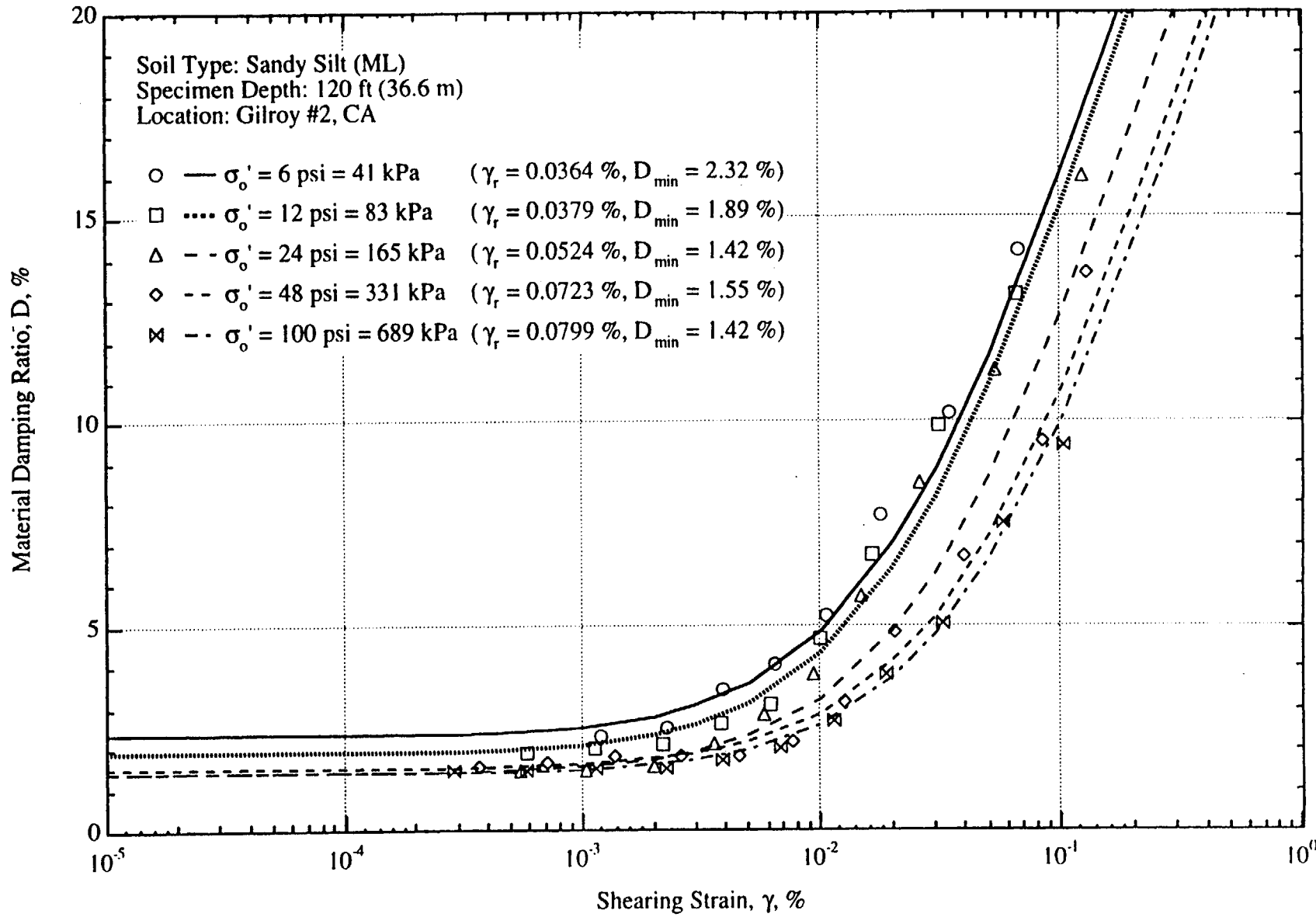


Fig. B.30 Variation in Material Damping Ratio with Shearing Strain and Effective Confining Pressure from Resonant Column Tests of Sample G5-1

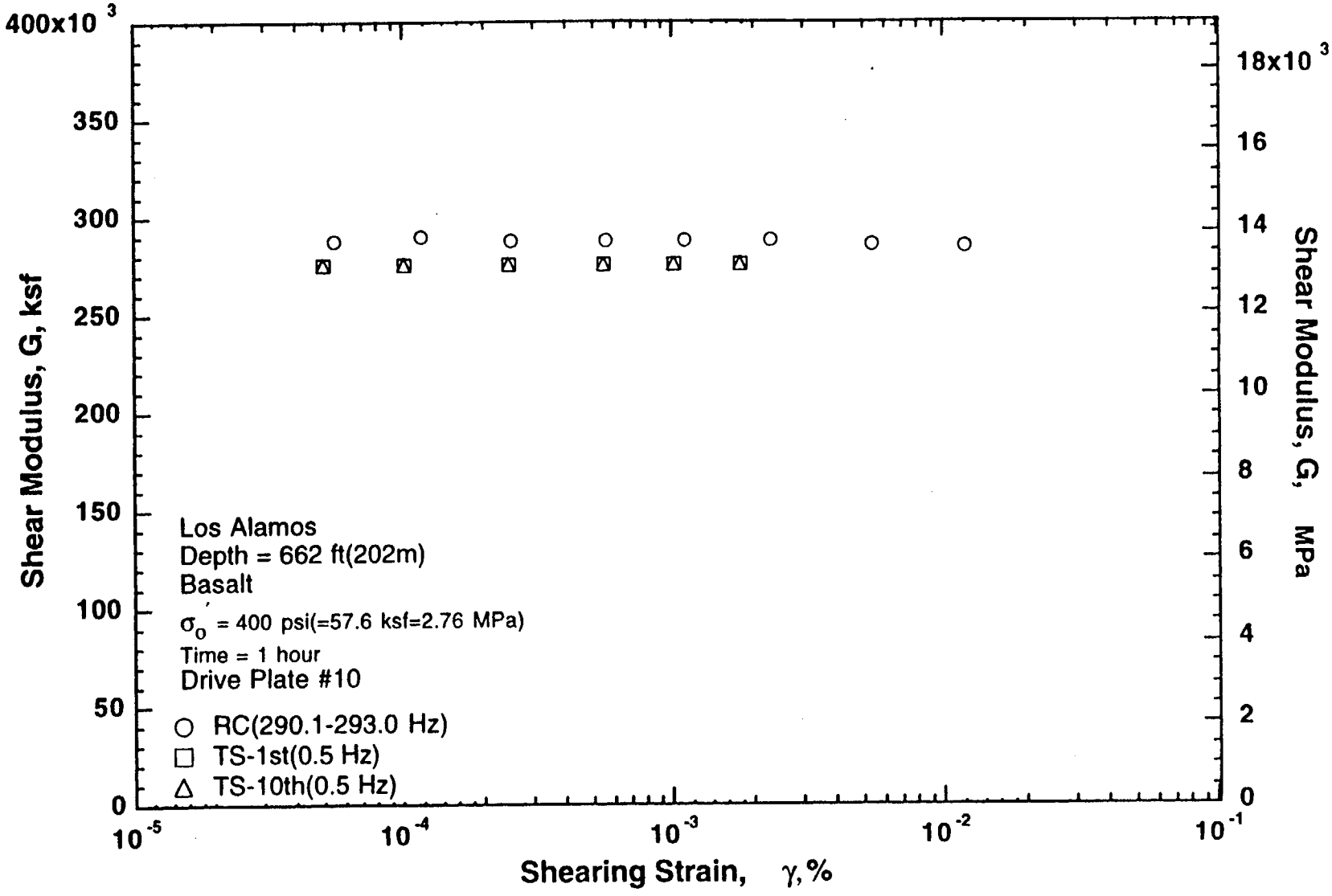


Fig. B.31 Variation in Shear Modulus with Shearing Strain at an Effective Confining Pressure of 400 psi(=57.6 ksf=2.76 MPa) from RCTS Tests of Sample HQ-146

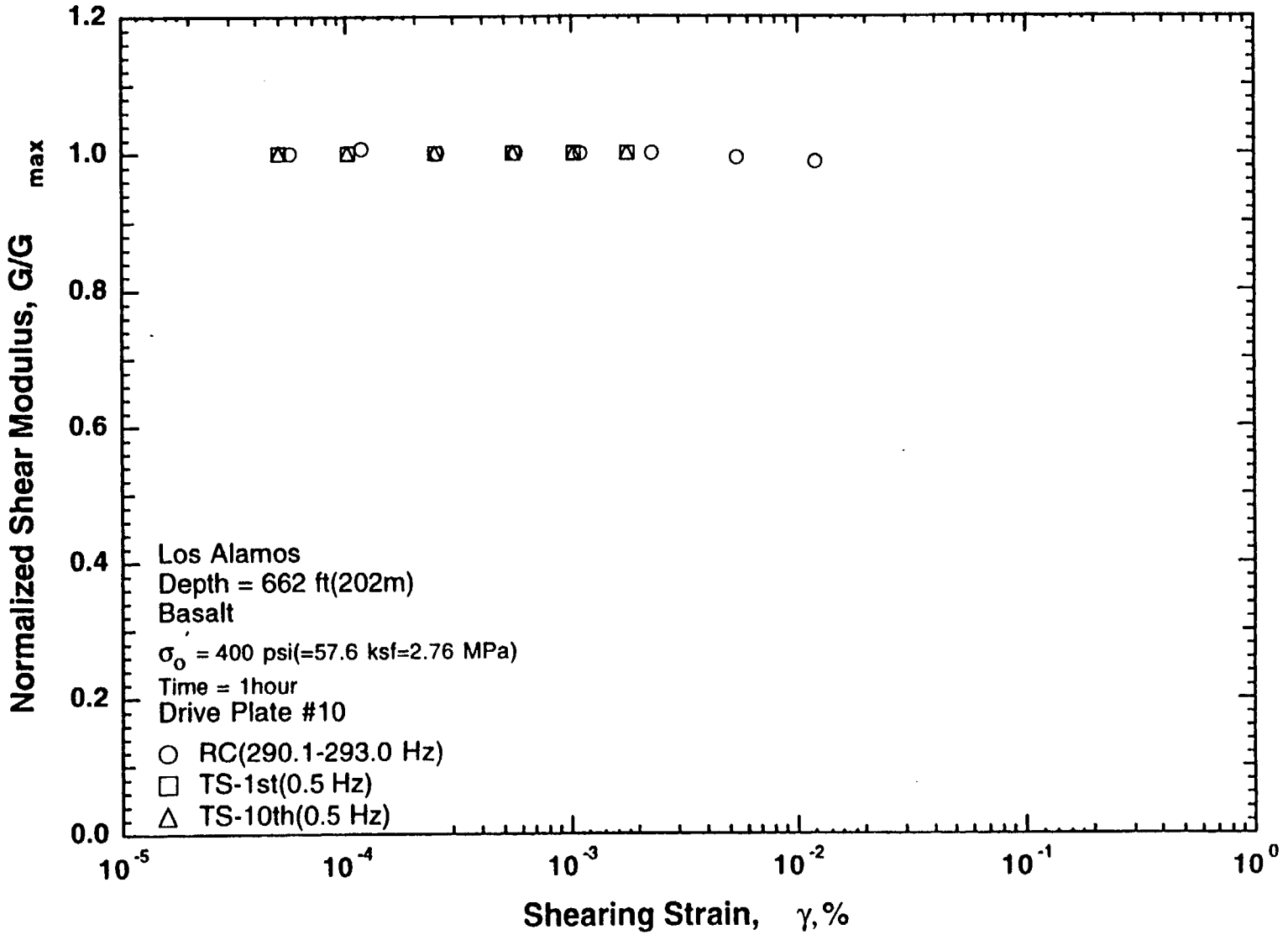


Fig. B.32 Variation in Normalized Shear Modulus with Shearing Strain at an Effective Confining Pressure of 400 psi(=57.6 ksf=2.76 MPa) from RCTS Tests of Sample HQ-146

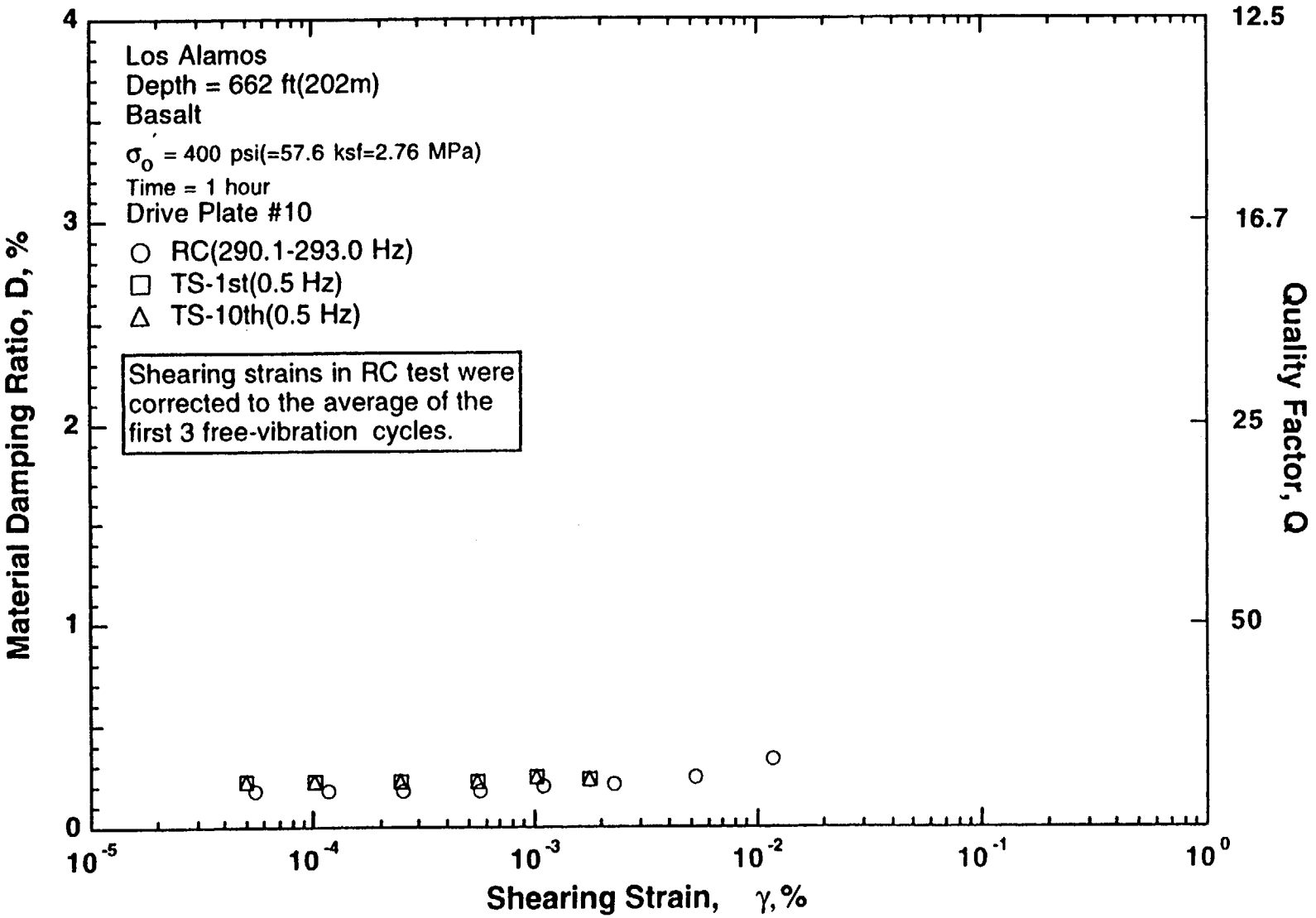


Fig. B.33 Variation in Material Damping Ratio with Shearing Strain at an Effective Confining Pressure of 400 psi(=57.6 ksf=2.76 MPa) from RCTS Tests of Sample HQ-146

# Appendix C

# Effects of Excitation Frequency, Number of Loading Cycles and Confining Pressure on the Dynamic Properties of Dry Branch and Santee Sands (Specimens CFD-4a, CFD-5a, and CFD-7a)

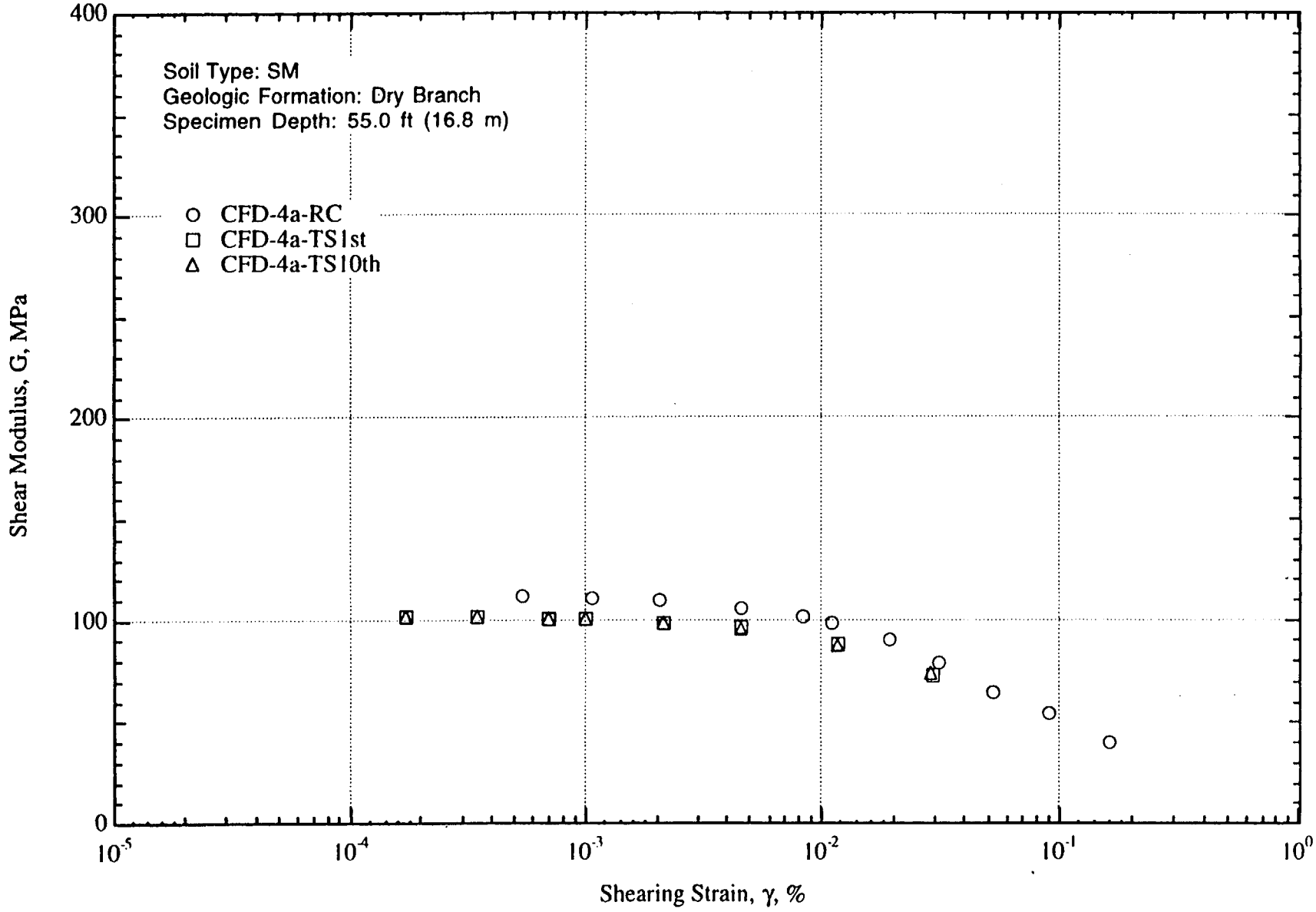


Fig. C.1 Variation in Shear Modulus with Shearing Strain at an Effective Confining Pressure of 31 psi (=4.46 ksf =214 kPa) from RCTS Tests of Specimen CFD-4a

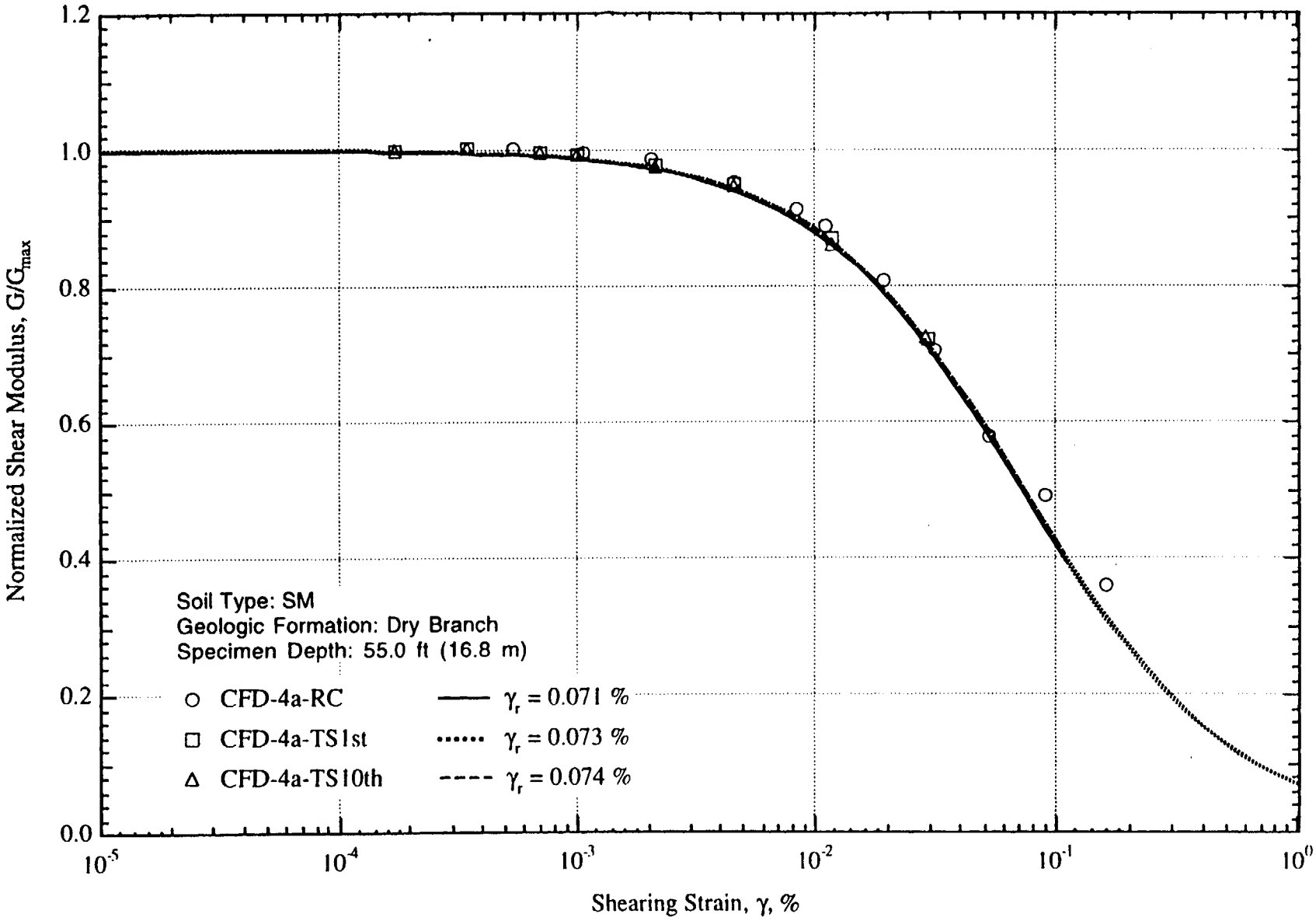


Fig. C.2 Variation in Normalized Shear Modulus with Shearing Strain at an Effective Confining Pressure of 31 psi (=4.46 ksf=214 kPa) from RCTS Tests of Specimen CFD-4a

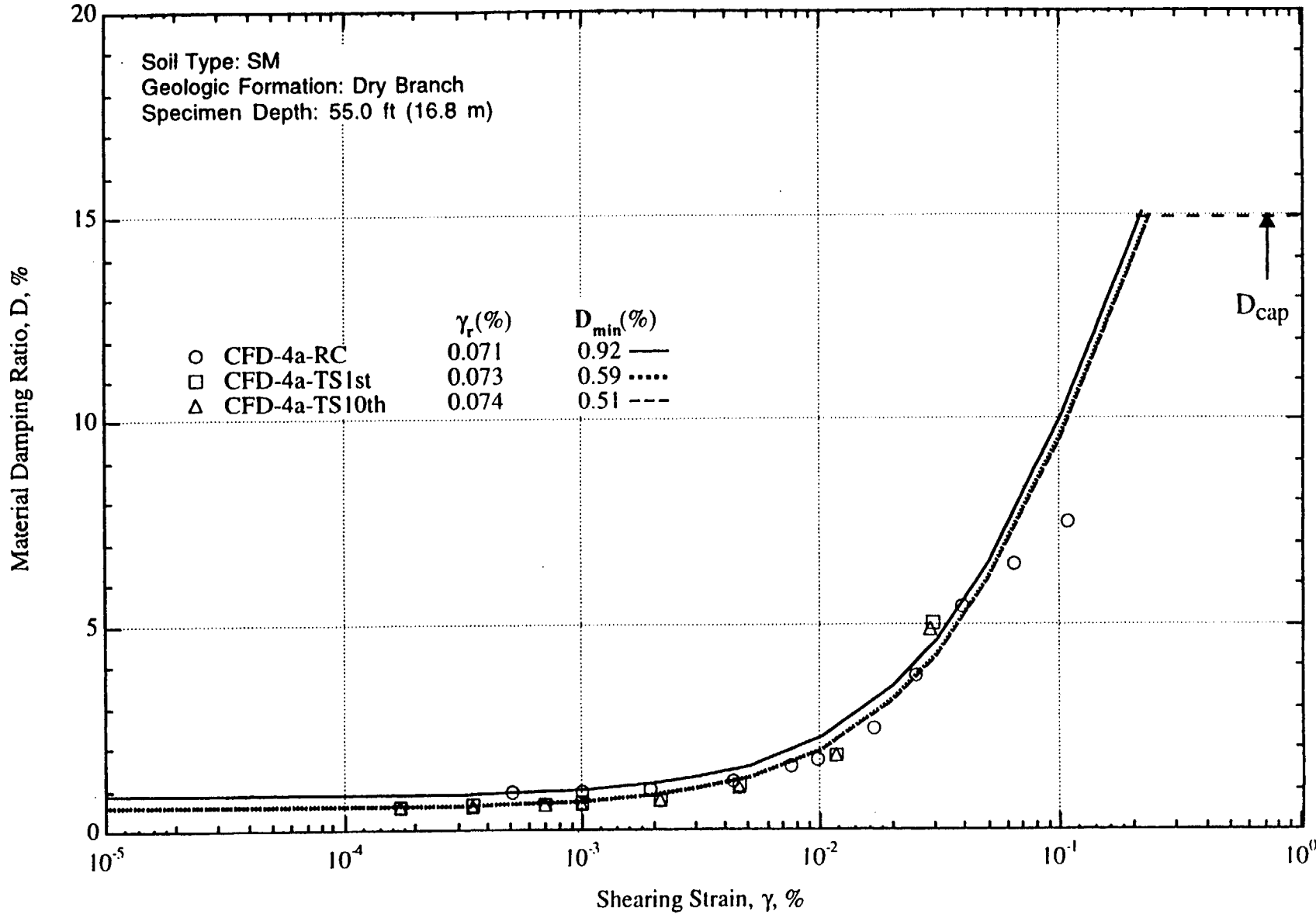


Fig. C.3 Variation in Material Damping Ratio with Shearing Strain at an Effective Confining Pressure of 31 psi (=4.46 ksf=214 kPa) from RCTS Tests of Specimen CFD-4a

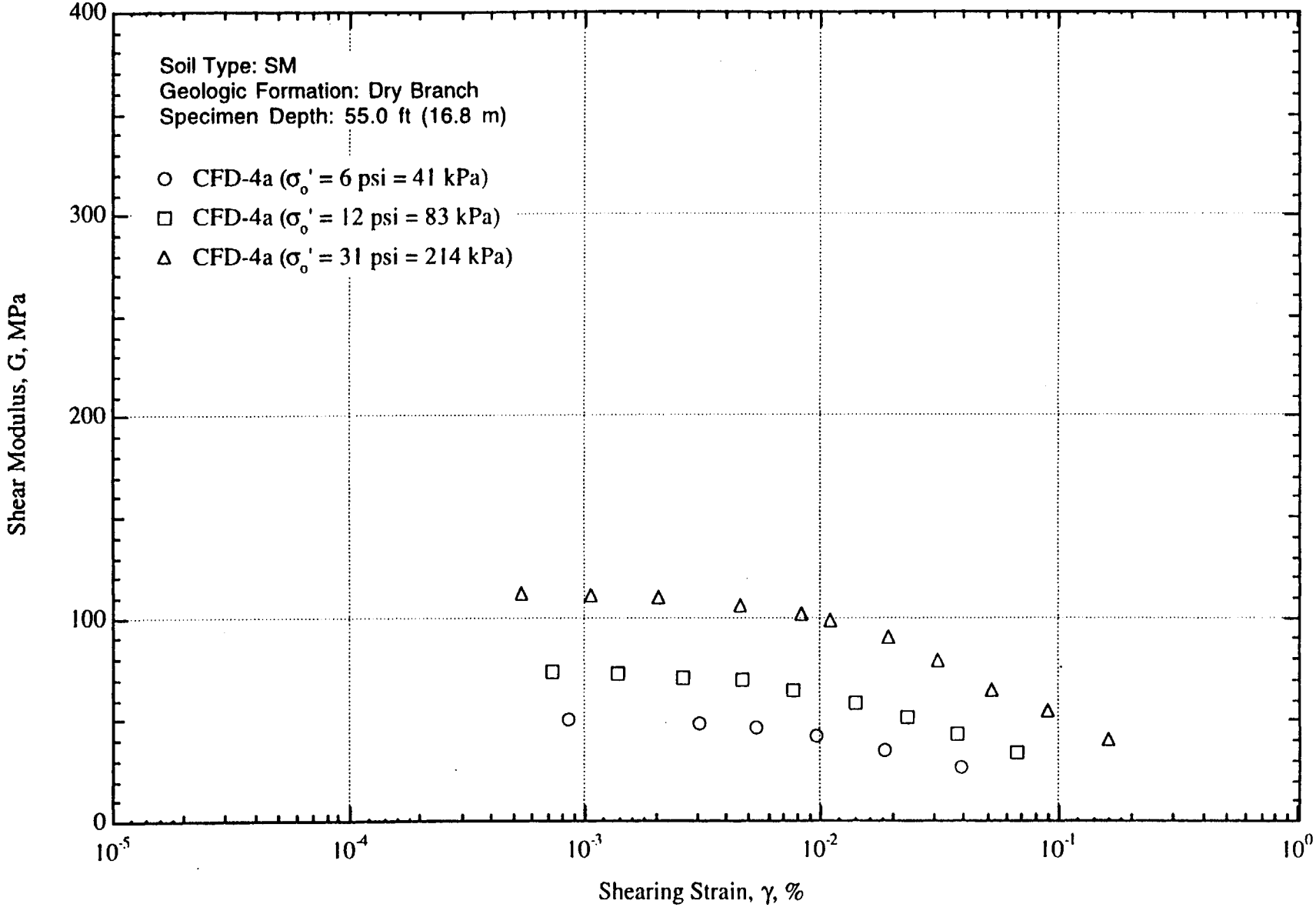


Fig. C.4 Variation in Shear Modulus with Shearing Strain and Effective Confining Pressure from Resonant Column Tests of Specimen CFD-4a

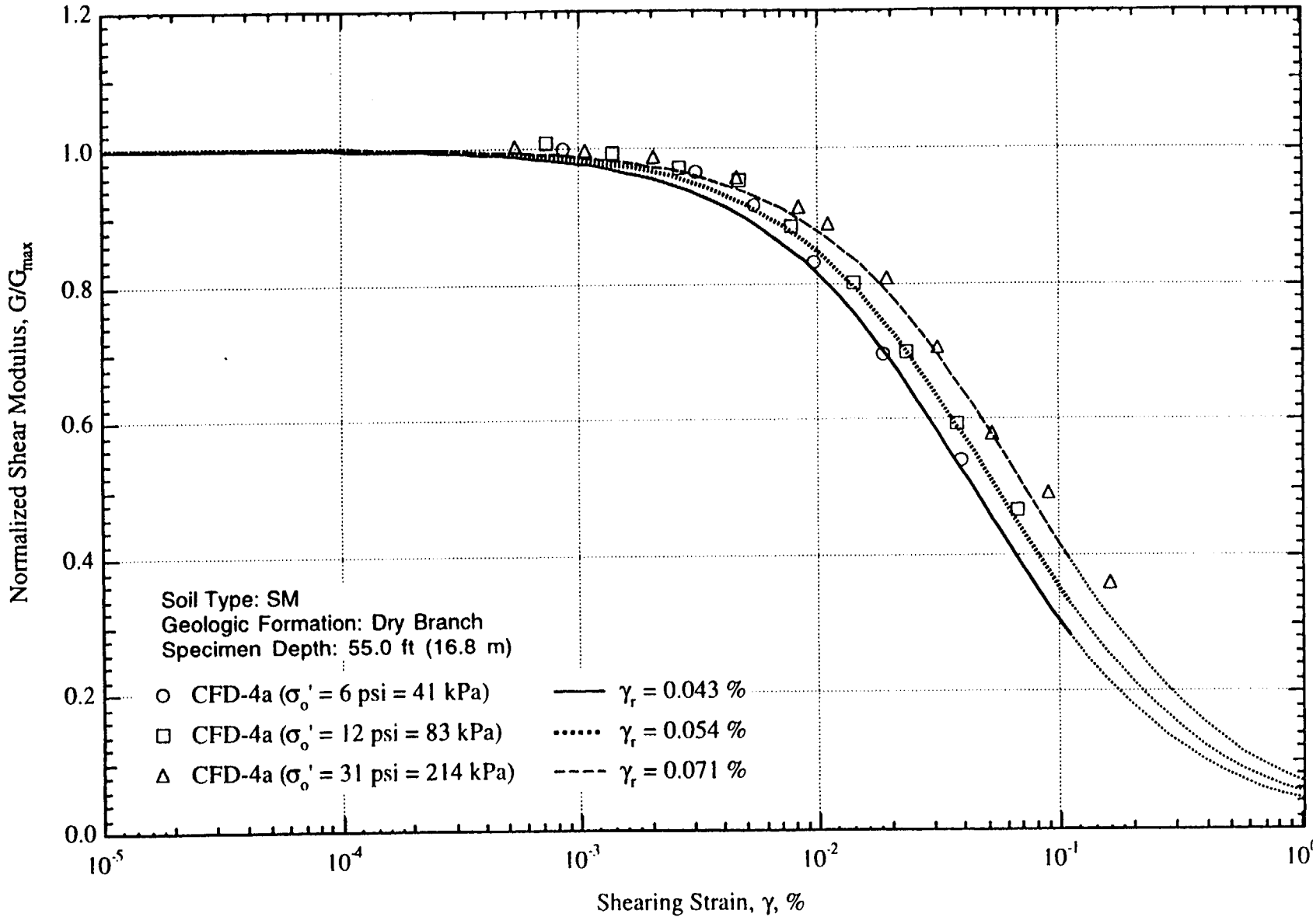


Fig. C.5 Comparison of the Variation in Normalized Shear Modulus with Shearing Strain and Effective Confining Pressure from Resonant Column Tests of Specimen CFD-4a

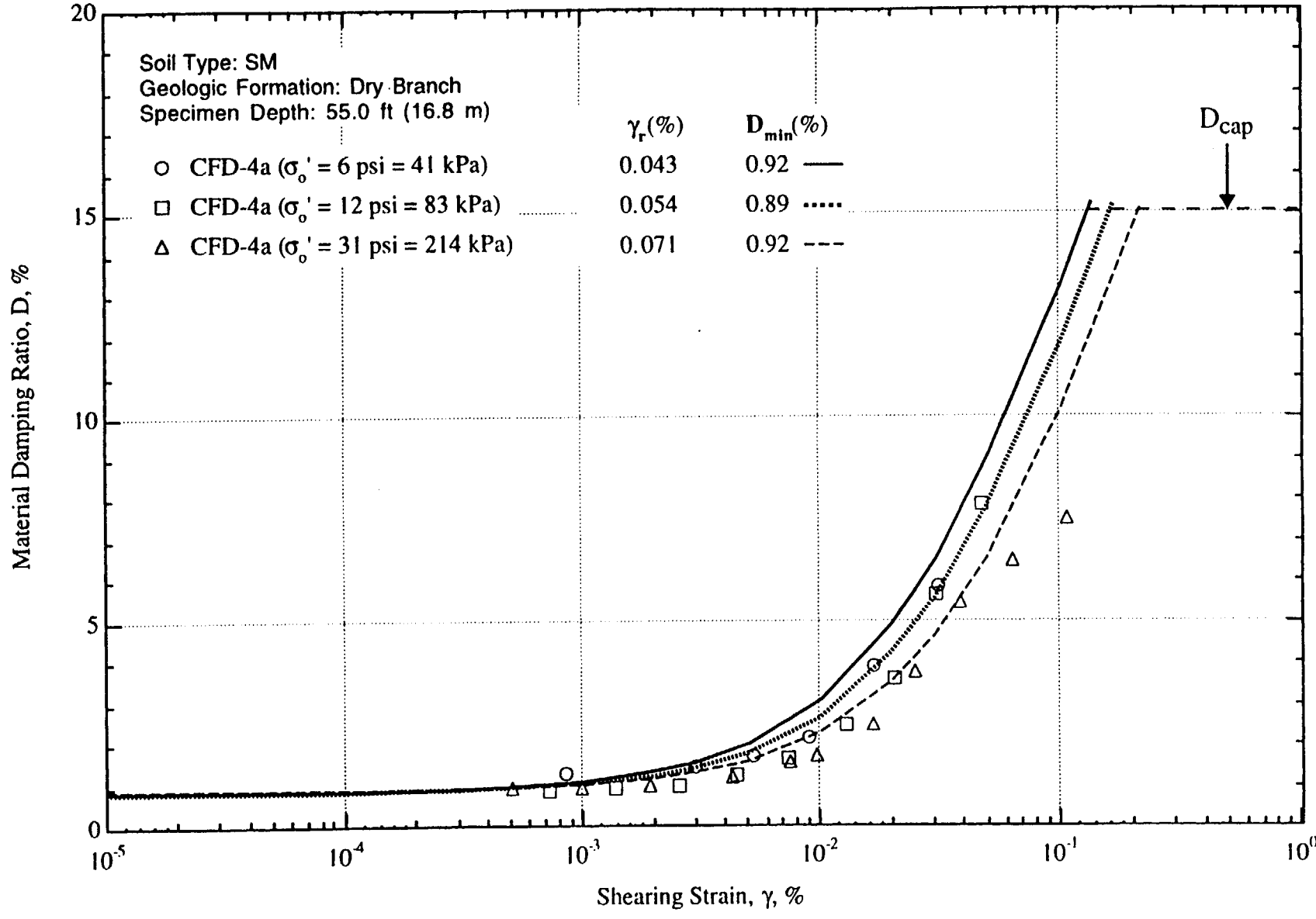


Fig. C.6 Variation in Material Damping Ratio with Shearing Strain and Effective Confining Pressure from Resonant Column Tests of Specimen CFD-4a

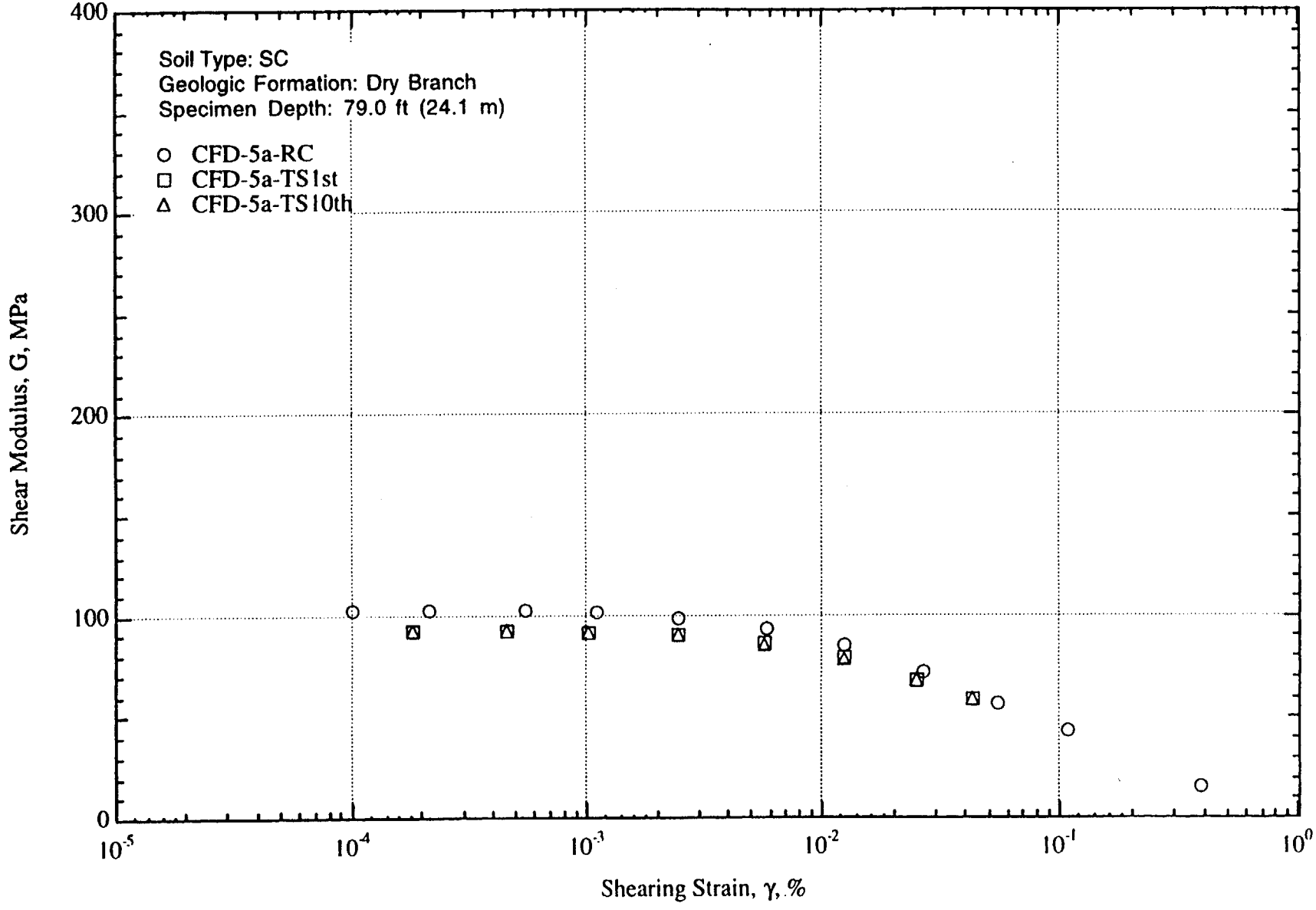


Fig. C.7 Variation in Shear Modulus with Shearing Strain at an Effective Confining Pressure of 35 psi (=5.04 ksf = 241 kPa) from RCTS Tests of Specimen CFD-5a

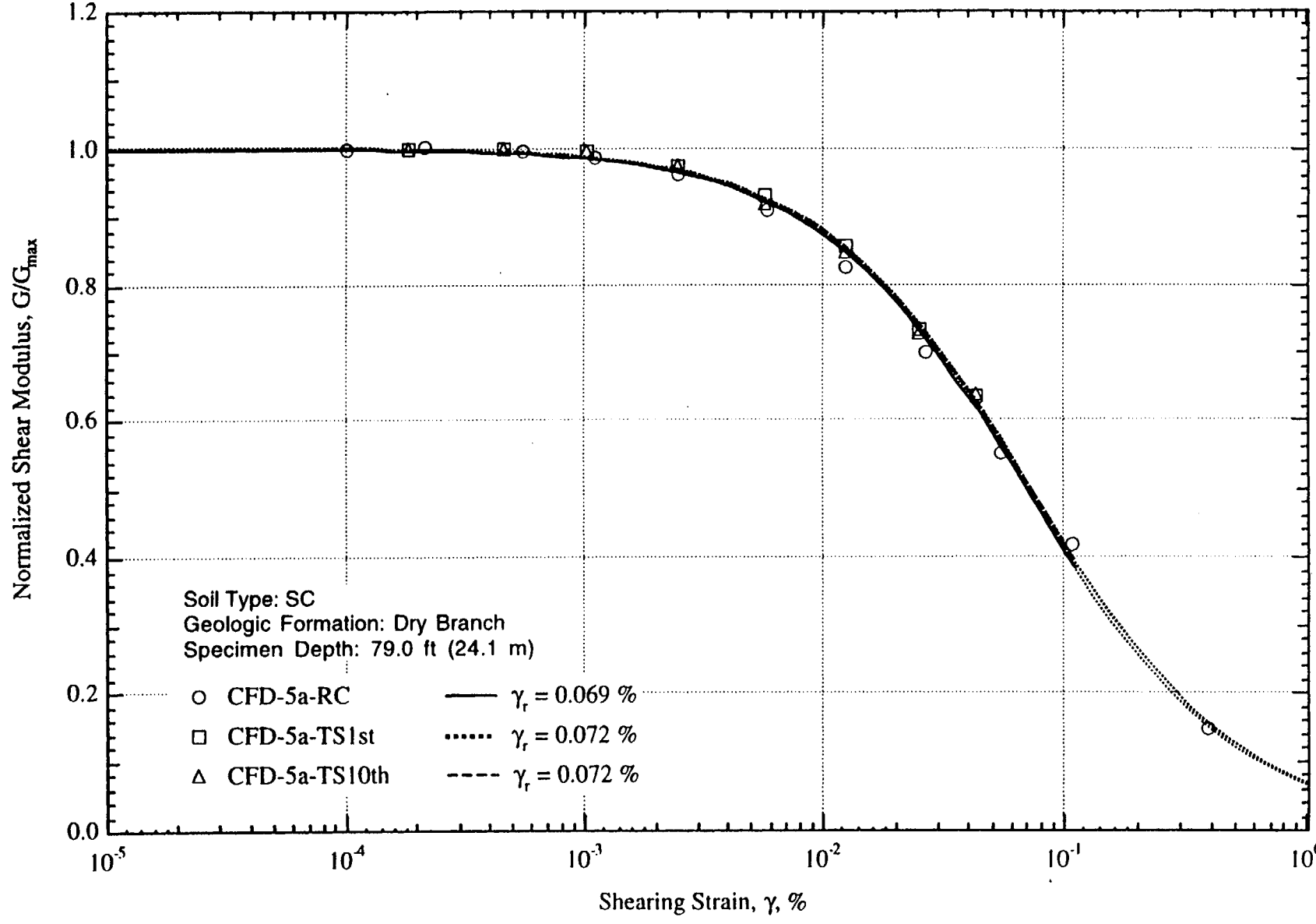


Fig. C.8 Variation in Normalized Shear Modulus with Shearing Strain at an Effective Confining Pressure of 35 psi (=5.04 ksf=241 kPa) from RCTS Tests of Specimen CFD-5a

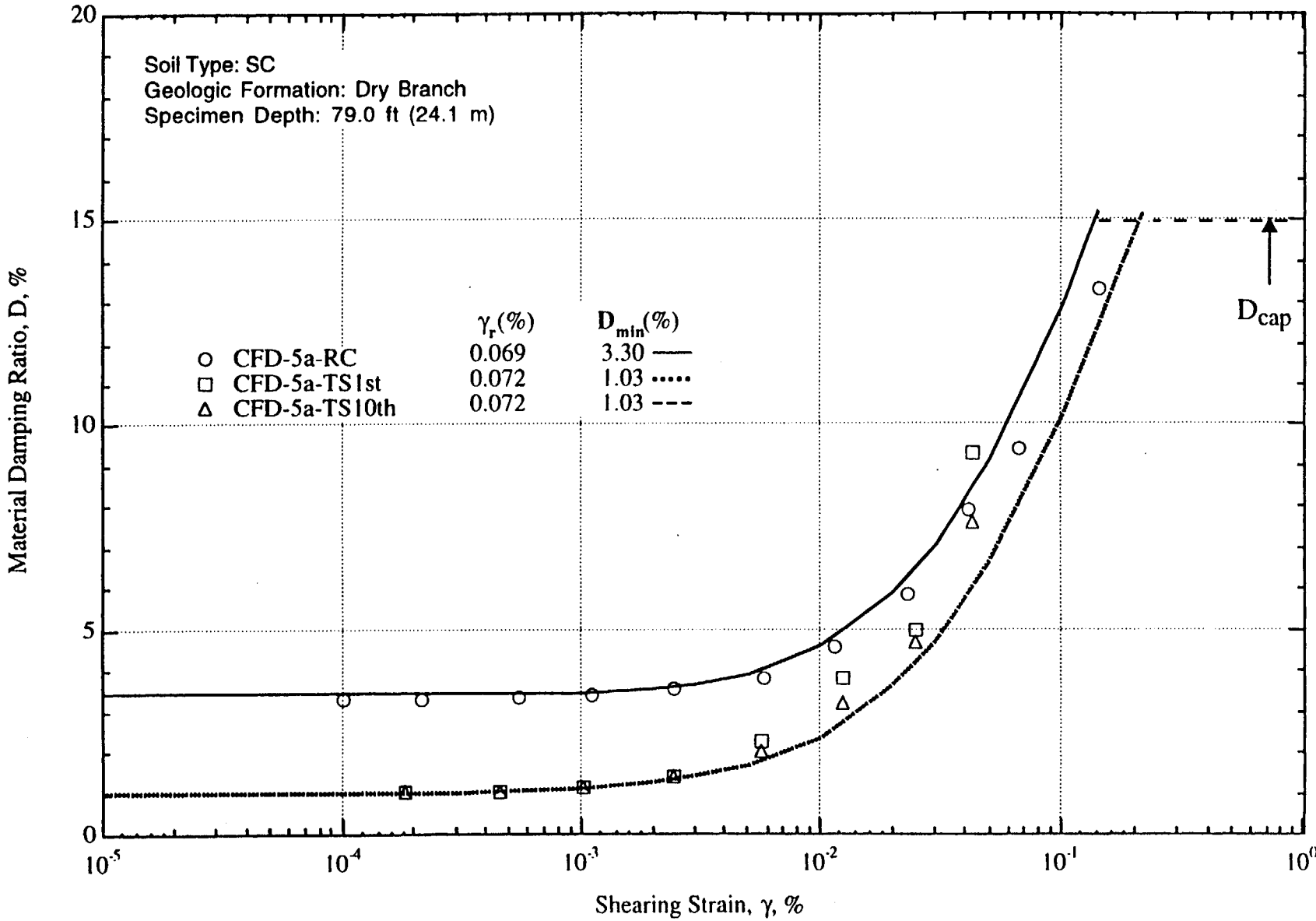


Fig. C.9 Variation in Material Damping Ratio with Shearing Strain at an Effective Confining Pressure of 35 psi (=5.04 ksf=241 kPa) from RCTS Tests of Specimen CFD-5a

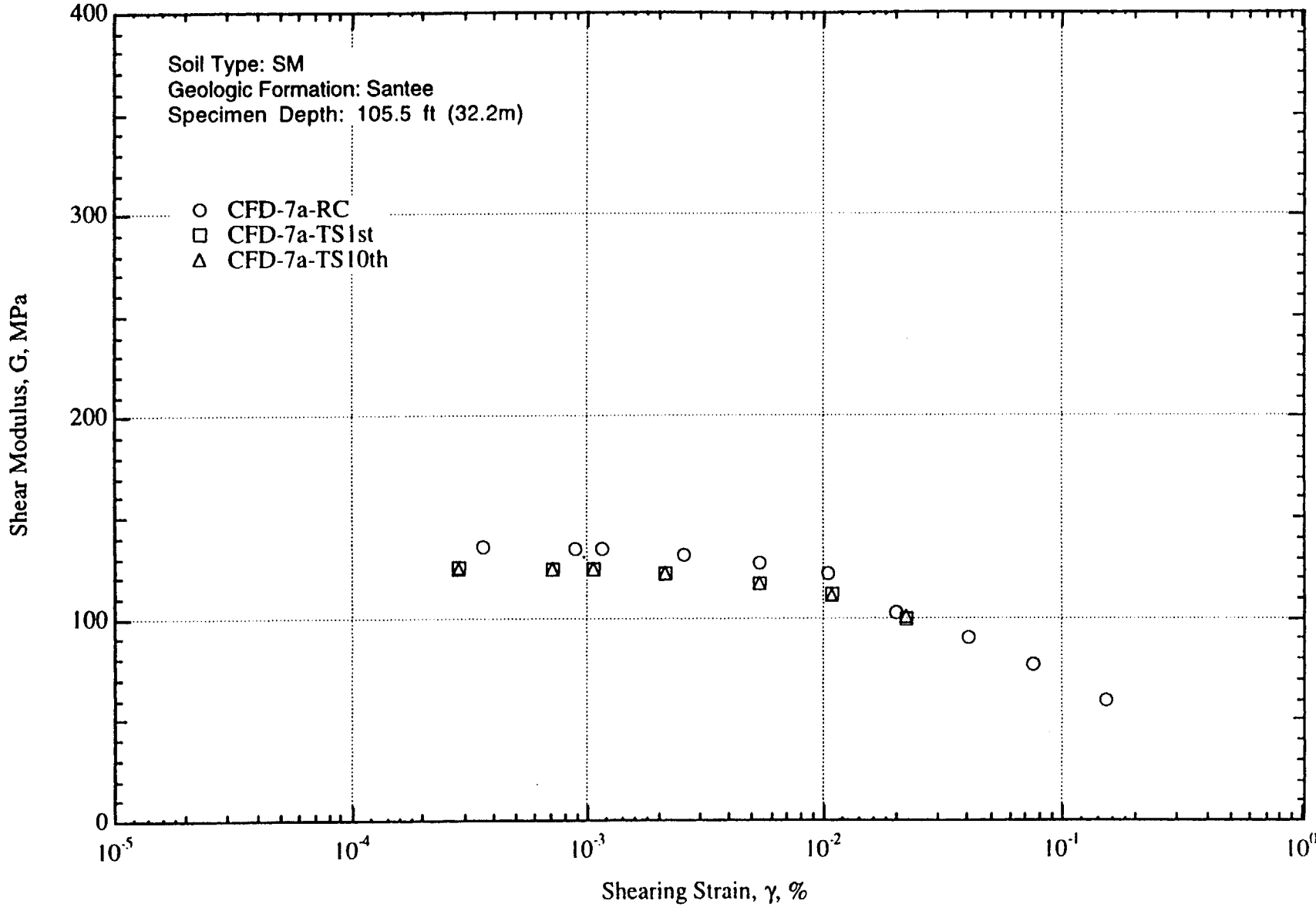


Fig. C.10 Variation in Shear Modulus with Shearing Strain at an Effective Confining Pressure of 46 psi (=6.62 ksf =317 kPa) from RCTS Tests of Specimen CFD-7a

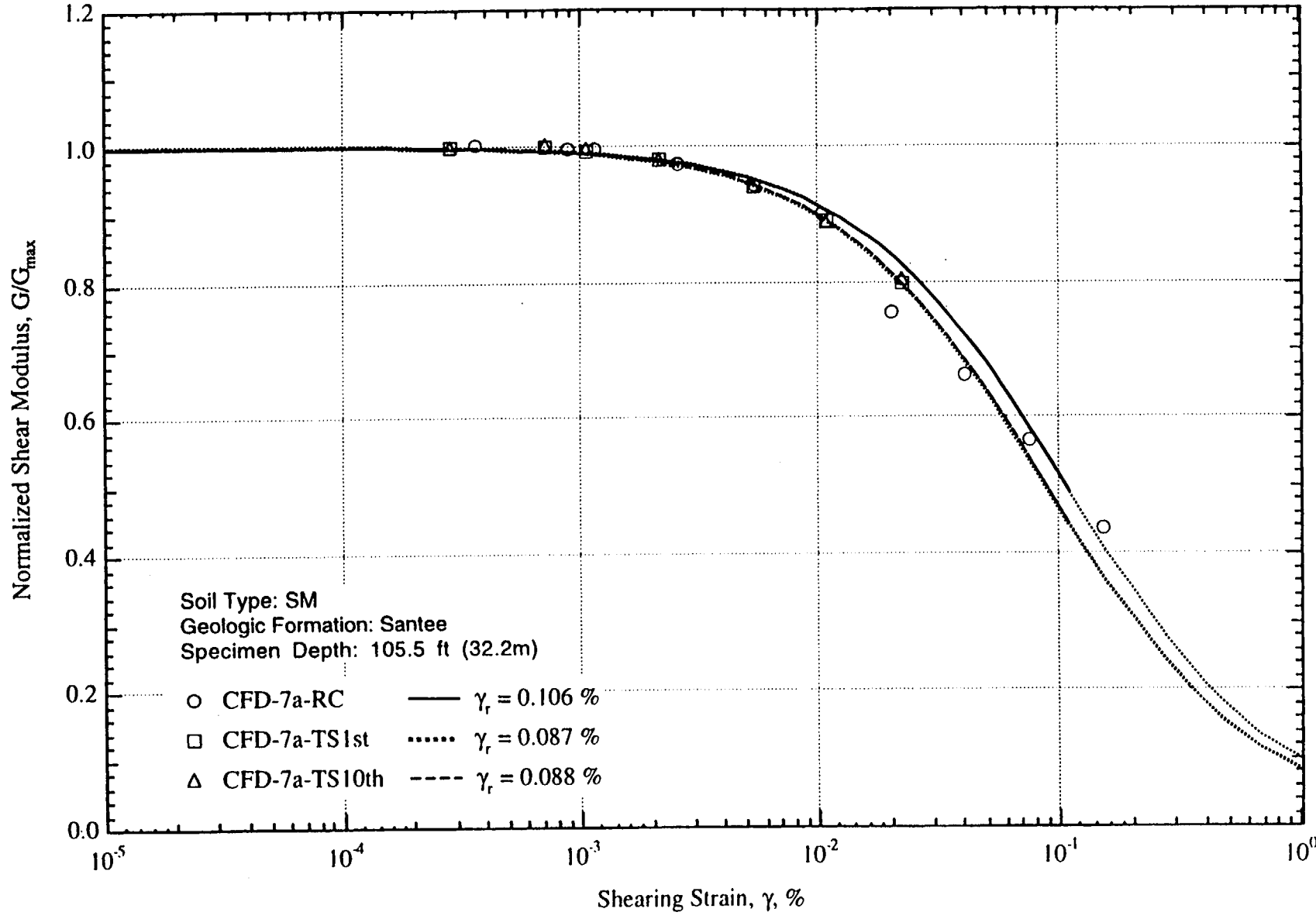


Fig. C.11 Variation in Normalized Shear Modulus with Shearing Strain at an Effective Confining Pressure of 46 psi (=6.62 ksf=317 kPa) from RCTS Tests of Specimen CFD-7a

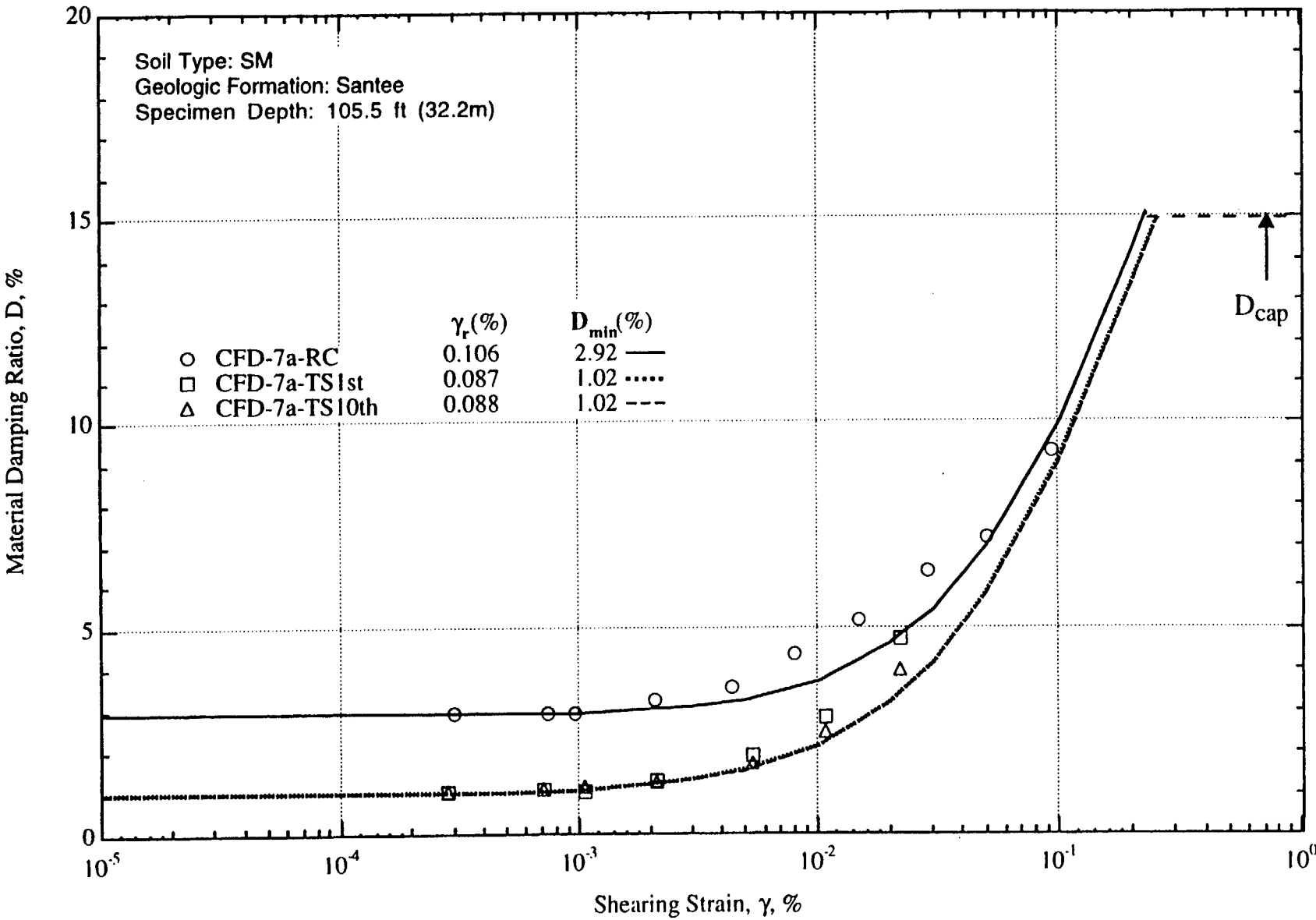


Fig. C.12 Variation in Material Damping Ratio with Shearing Strain at an Effective Confining Pressure of 46 psi (=6.62 ksf=317 kPa) from RCTS Tests of Specimen CFD-7a

# Appendix D

# Effects of Excitation Frequency, Number of Loading Cycles and Confining Pressure on the Dynamic Properties of Tobacco Road and Snapp Sands (Specimens CFD-3b, CFD-12a, and CFD-13a)

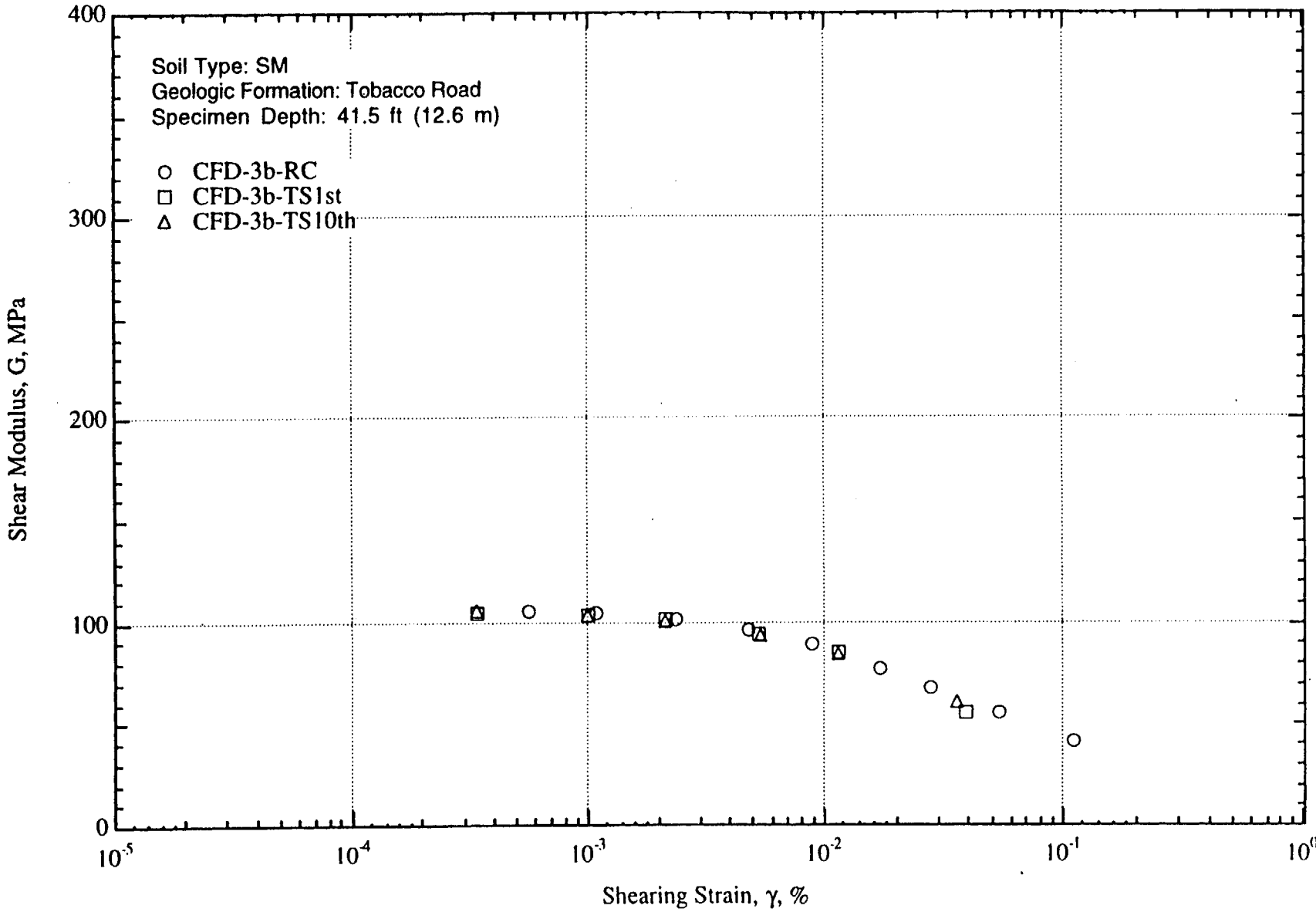


Fig. D.1 Variation in Shear Modulus with Shearing Strain at an Effective Confining Pressure of 23 psi (=3.31 ksf =159 kPa) from RCTS Tests of Specimen CFD-3b

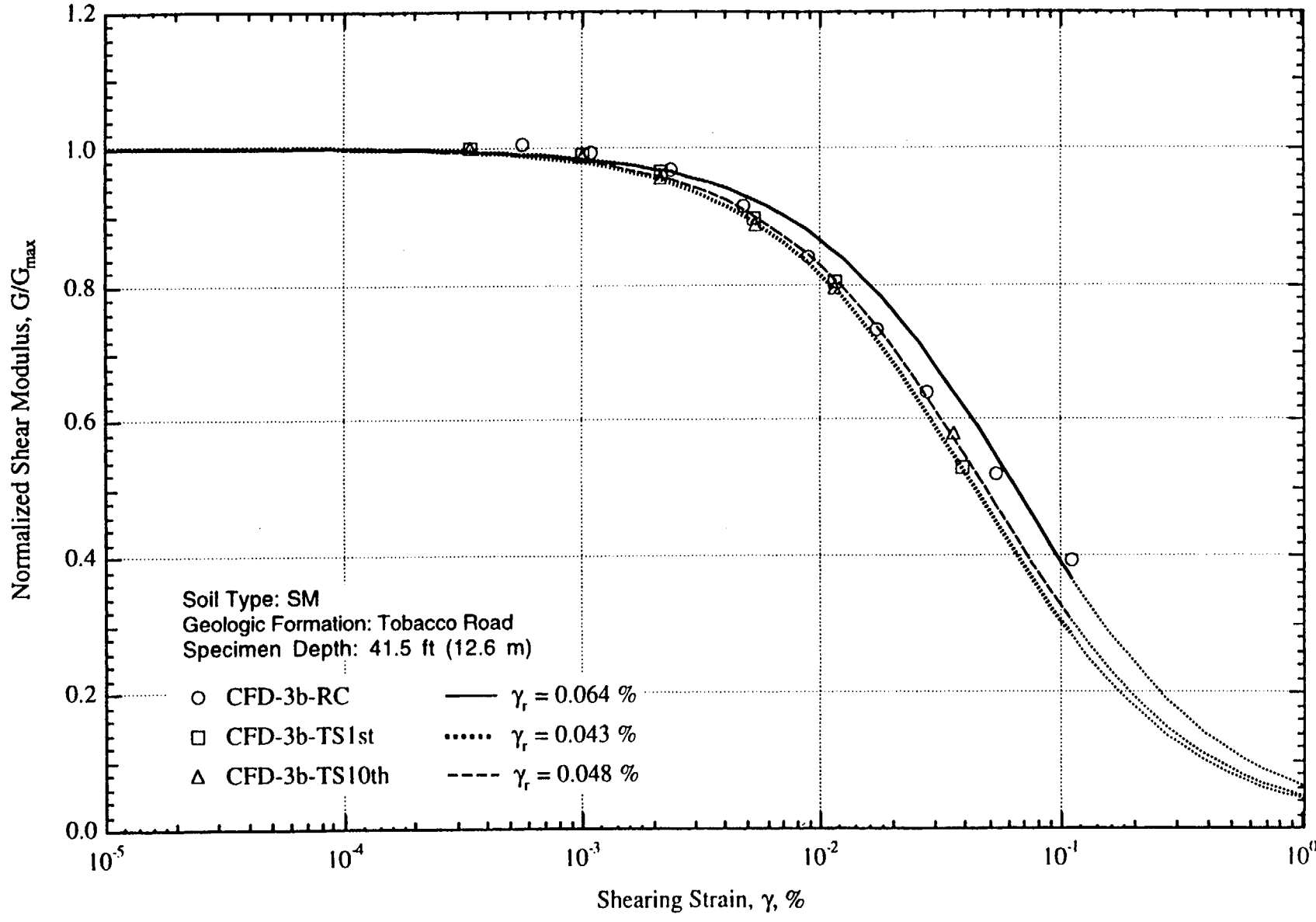


Fig. D.2 Variation in Normalized Shear Modulus with Shearing Strain at an Effective Confining Pressure of 23 psi (=3.31 ksf=159 kPa) from RCTS Tests of Specimen CFD-3b

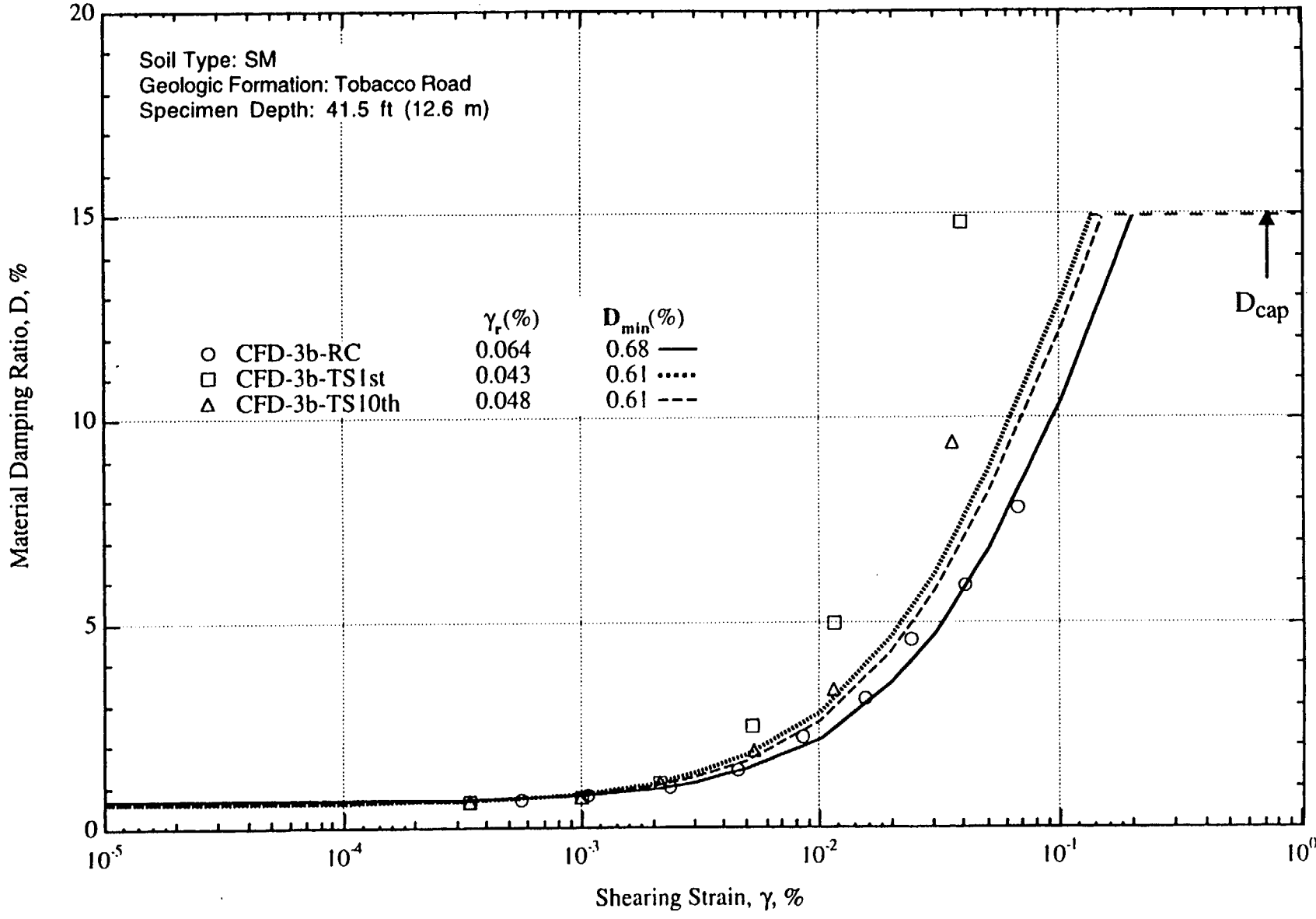


Fig. D.3 Variation in Material Damping Ratio with Shearing Strain at an Effective Confining Pressure of 23 psi (=3.31 ksf=159 kPa) from RCTS Tests of Specimen CFD-3b

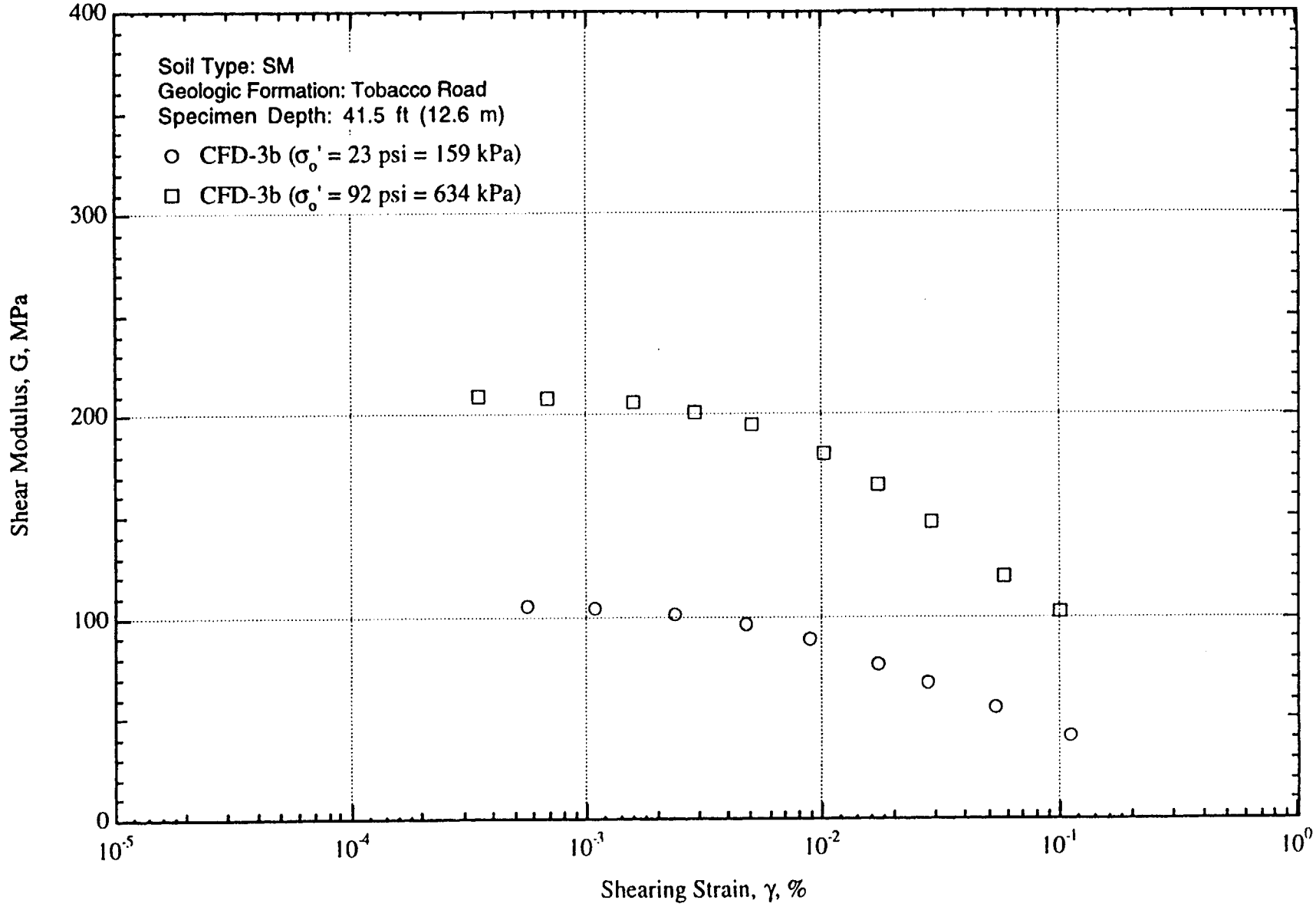


Fig. D.4 Variation in Shear Modulus with Shearing Strain and Effective Confining Pressure from Resonant Column Tests of Specimen CFD-3b

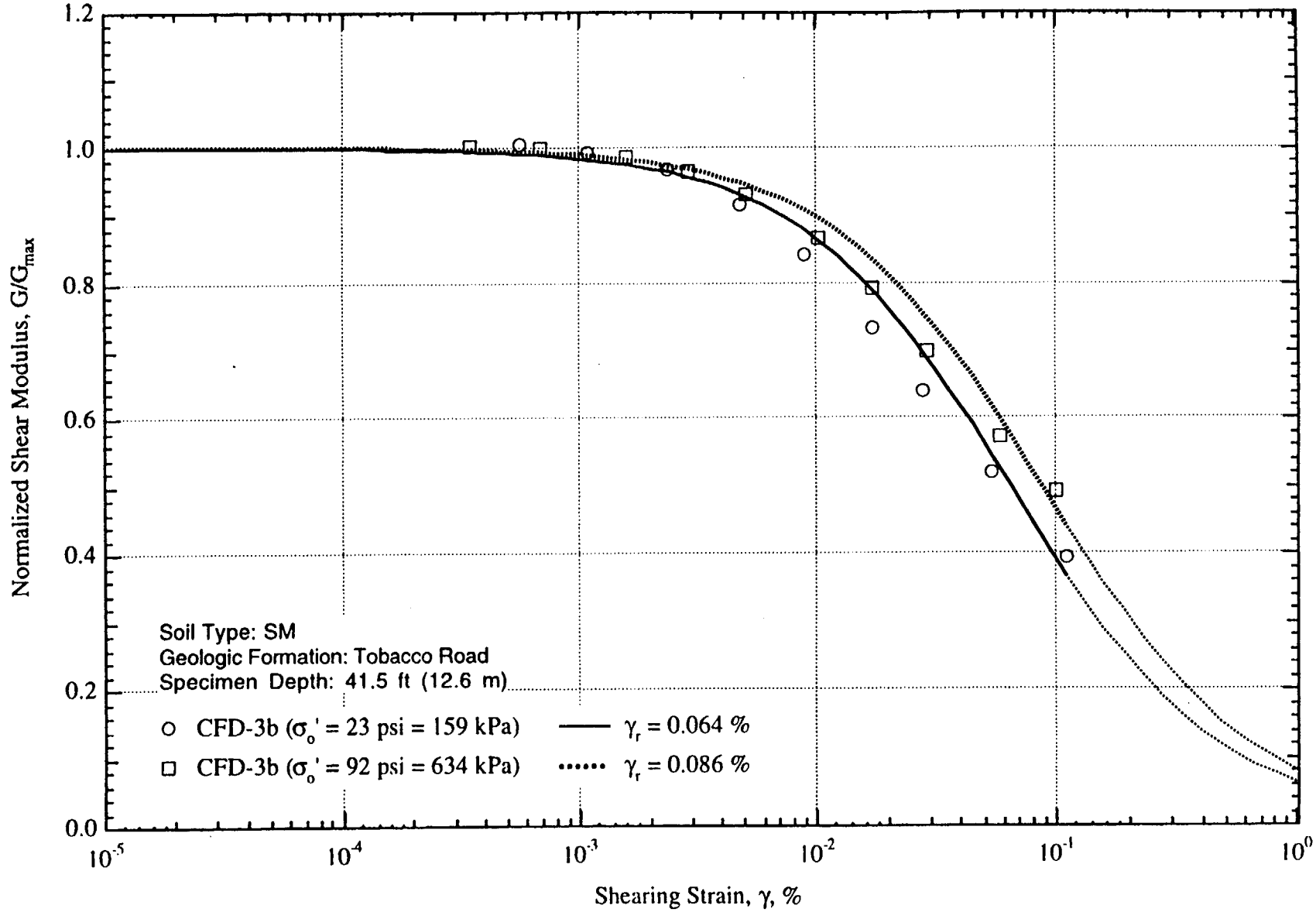


Fig. D.5 Comparison of the Variation in Normalized Shear Modulus with Shearing Strain and Effective Confining Pressure from Resonant Column Tests of Specimen CFD-3b

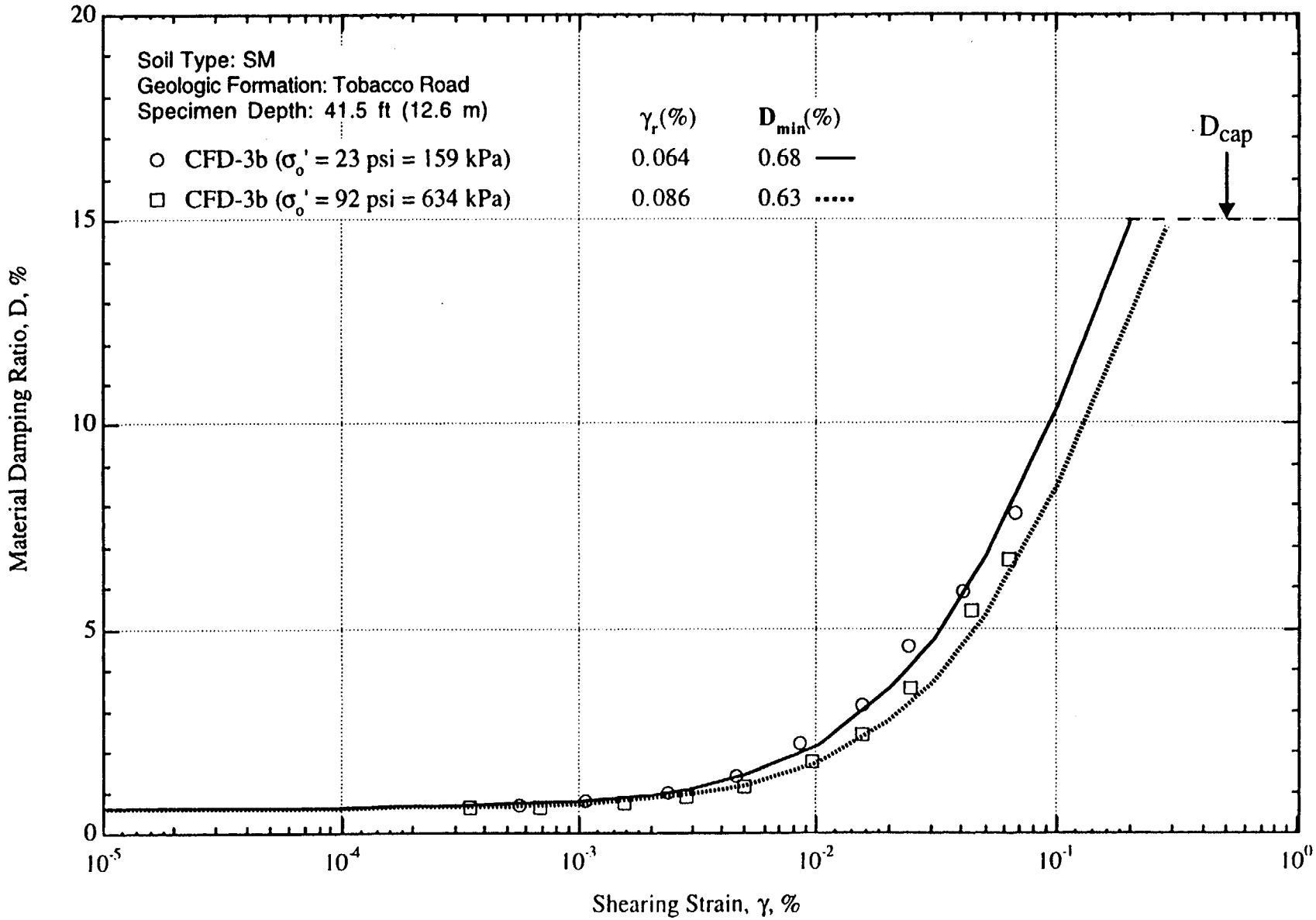


Fig. D.6 Variation in Material Damping Ratio with Shearing Strain and Effective Confining Pressure from Resonant Column Tests of Specimen CFD-3b

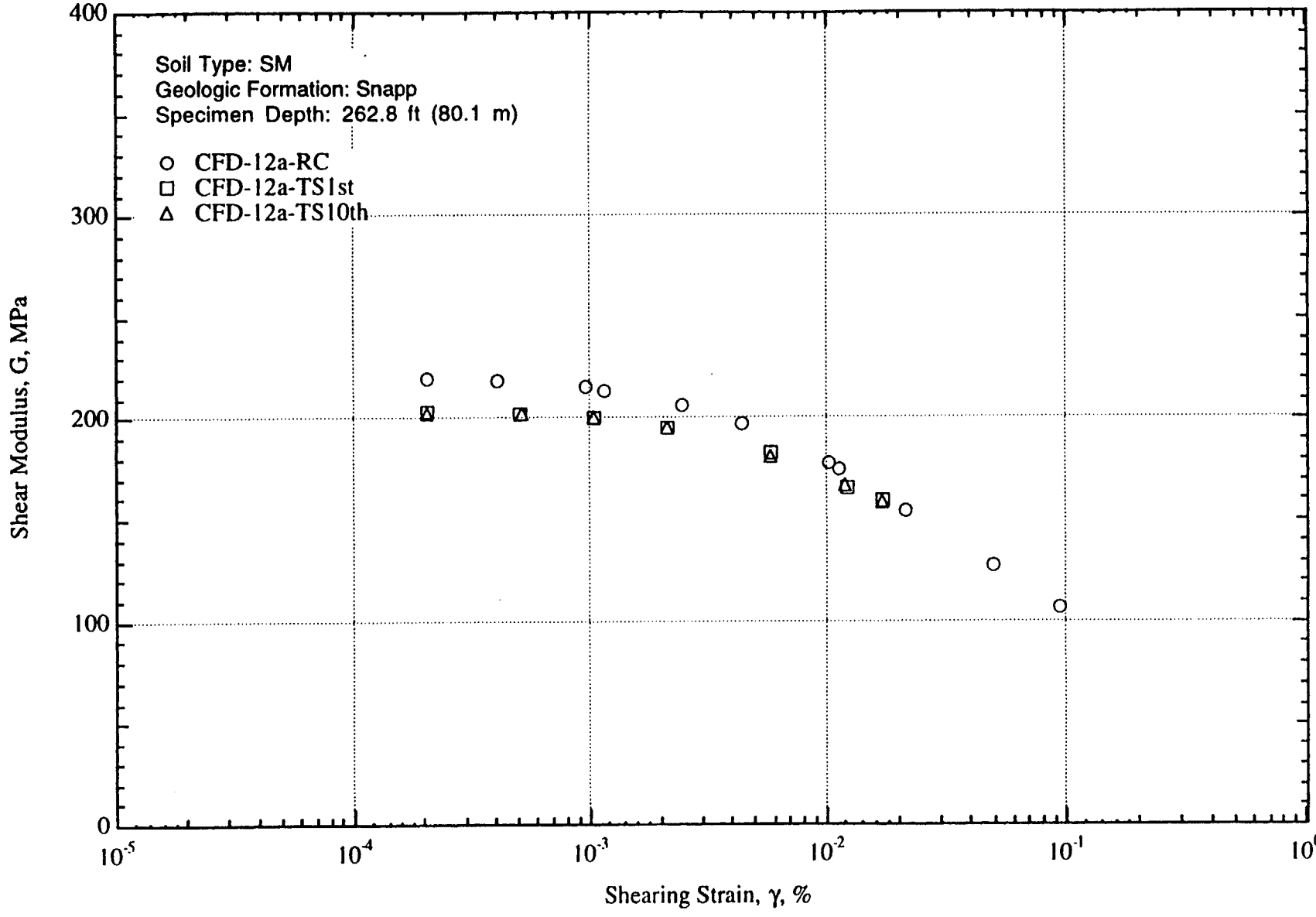


Fig. D.7 Variation in Shear Modulus with Shearing Strain at an Effective Confining Pressure of 87 psi (=12.52 ksf =600 kPa) from RCTS Tests of Specimen CFD-12a

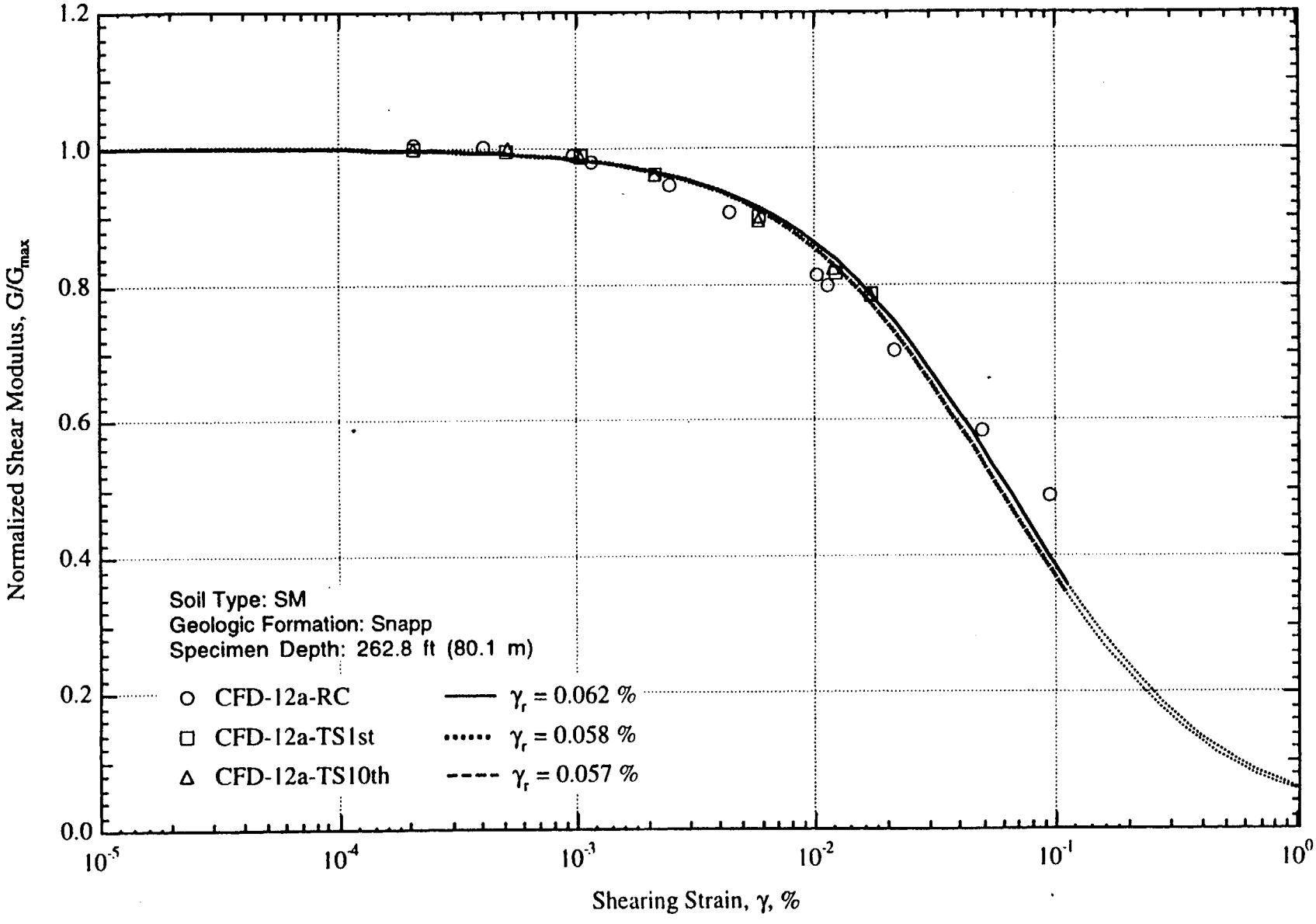


Fig. D.8 Variation in Normalized Shear Modulus with Shearing Strain at an Effective Confining Pressure of 87 psi (=12.52 ksf=600 kPa) from RCTS Tests of Specimen CFD-12a

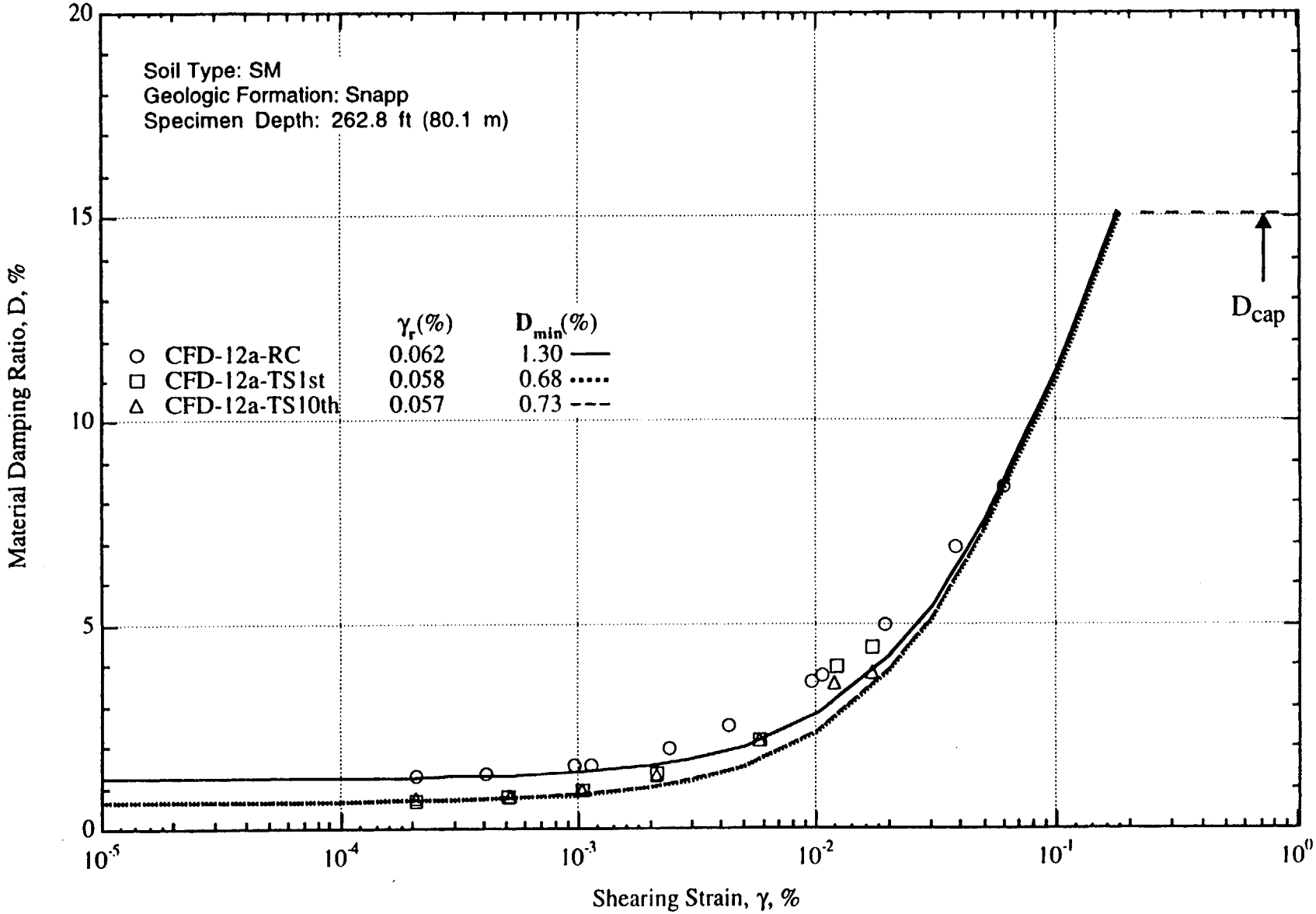


Fig. D.9 Variation in Material Damping Ratio with Shearing Strain at an Effective Confining Pressure of 87 psi (=12.52 ksf=600 kPa) from RCTS Tests of Specimen CFD-12a

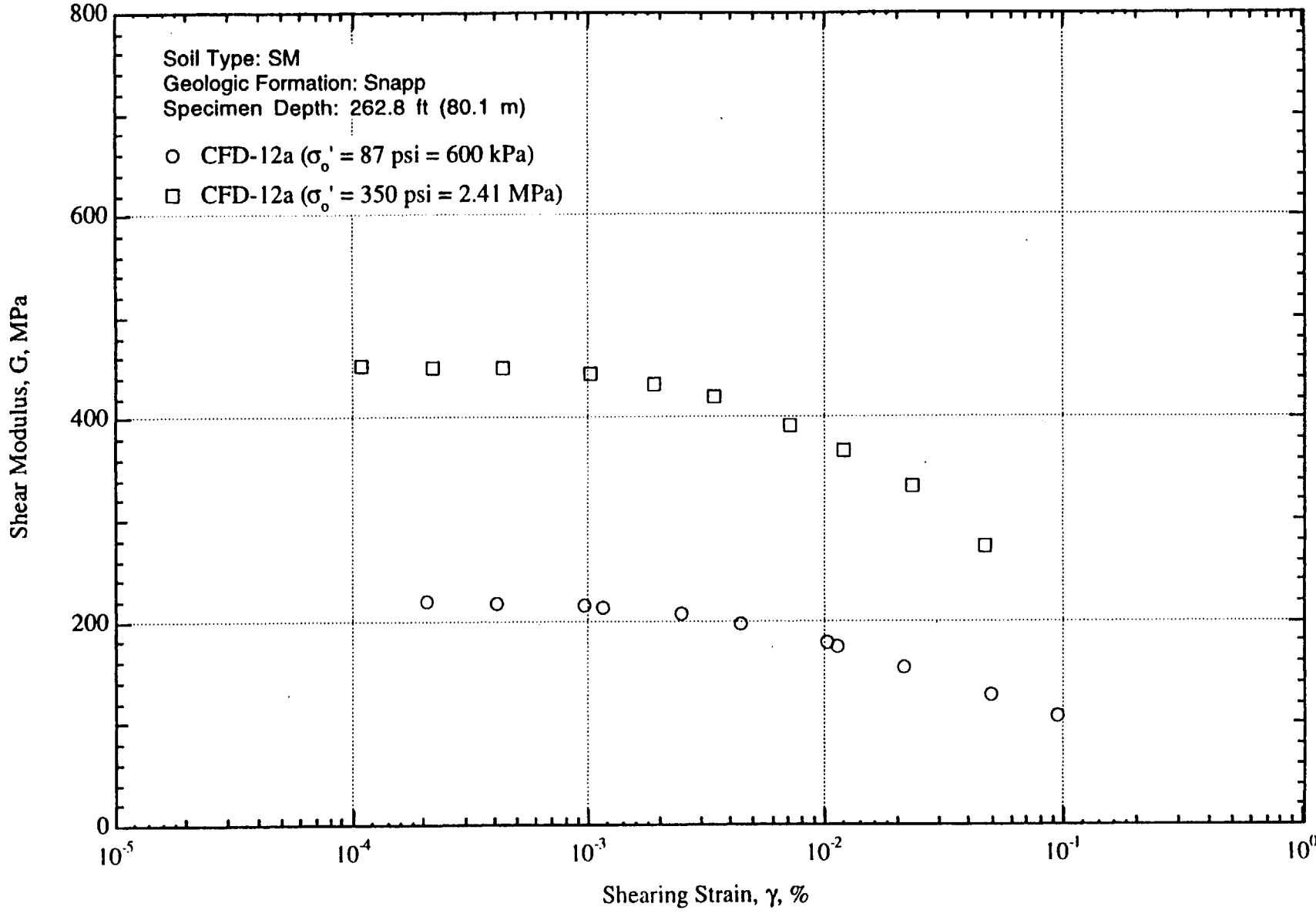


Fig. D.10 Variation in Shear Modulus with Shearing Strain and Effective Confining Pressure from Resonant Column Tests of Specimen CFD-12a

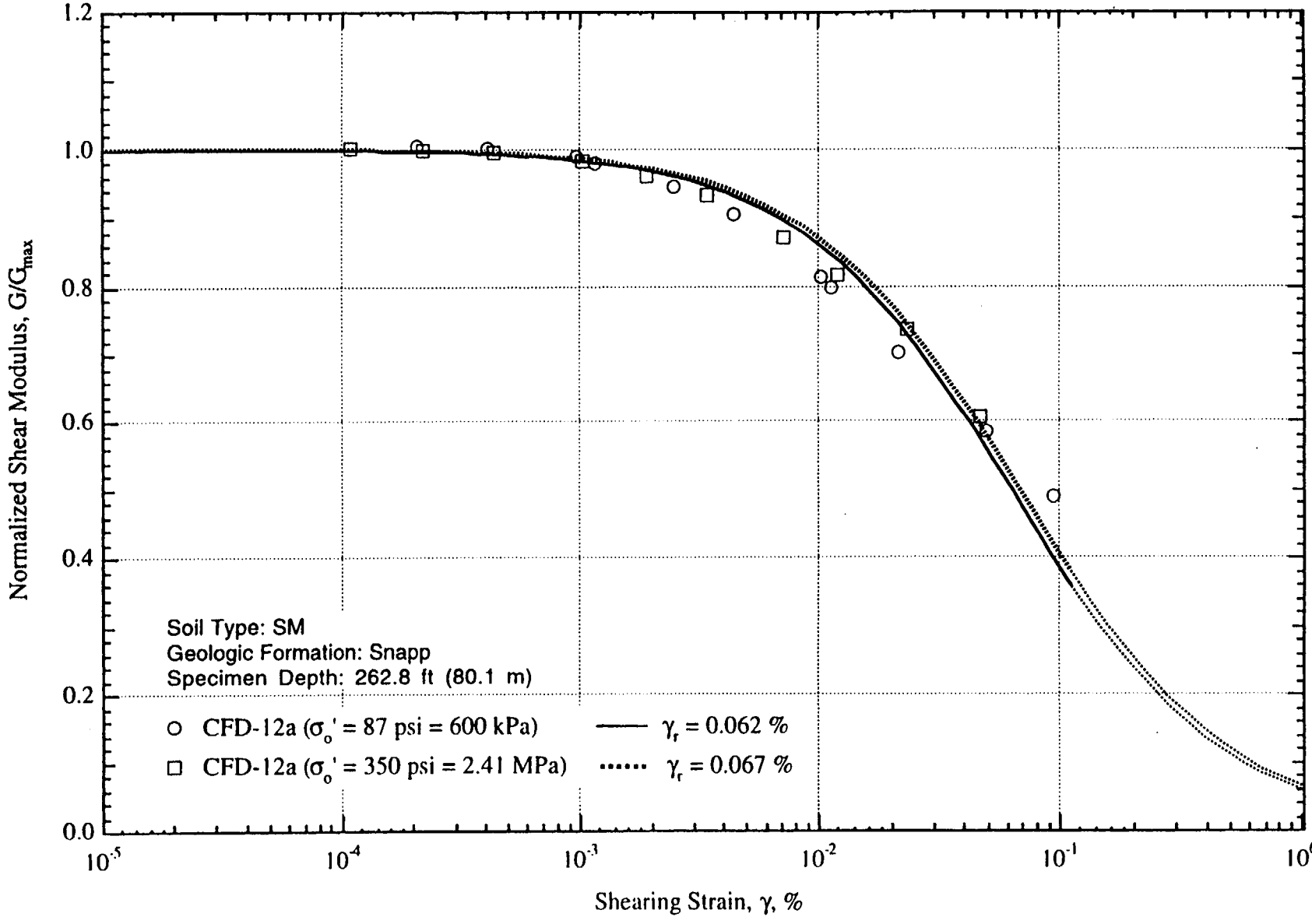


Fig. D.11 Comparison of the Variation in Normalized Shear Modulus with Shearing Strain and Effective Confining Pressure from Resonant Column Tests of Specimen CFD-12a

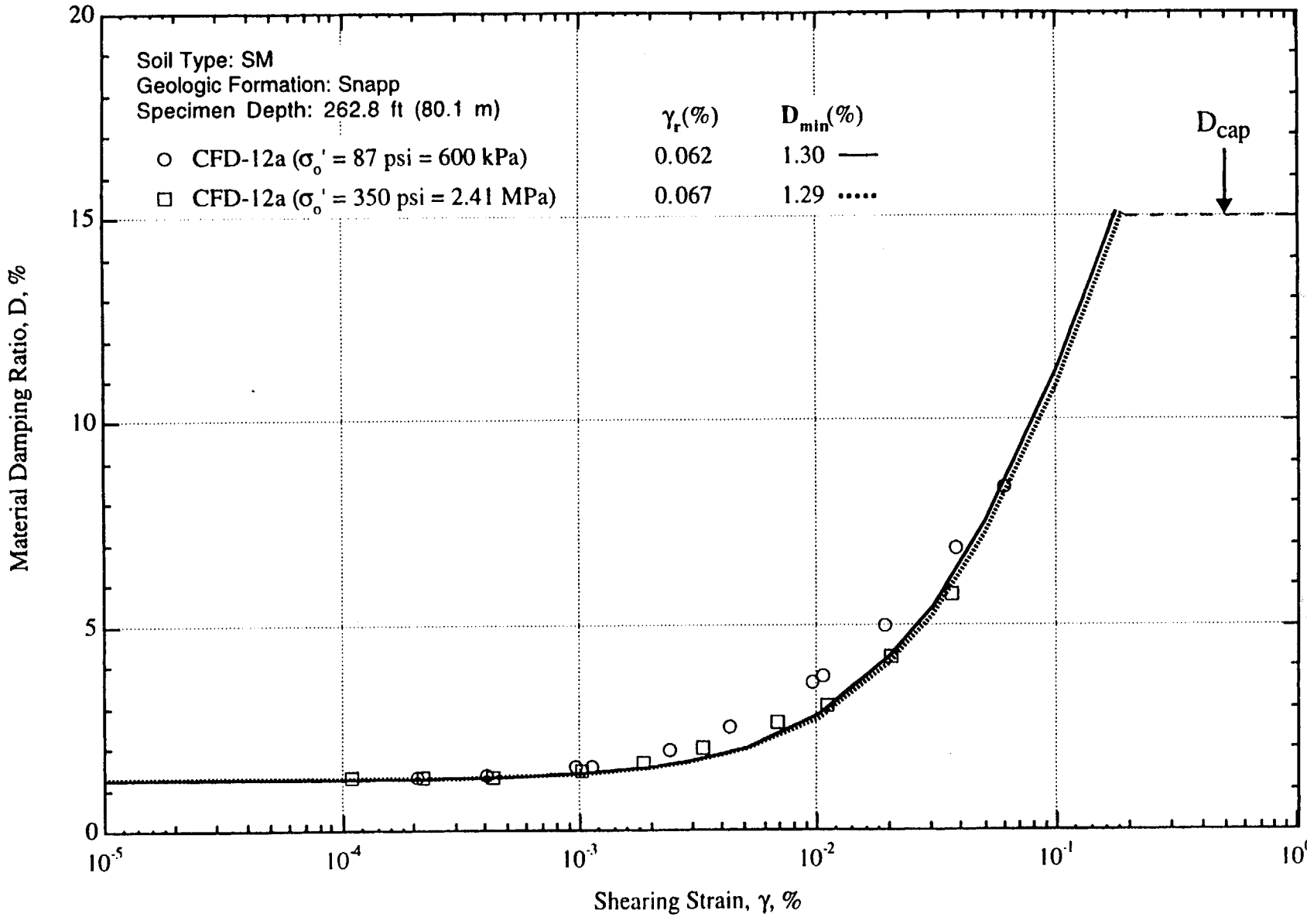


Fig. D.12 Variation in Material Damping Ratio with Shearing Strain and Effective Confining Pressure from Resonant Column Tests of Specimen CFD-12a

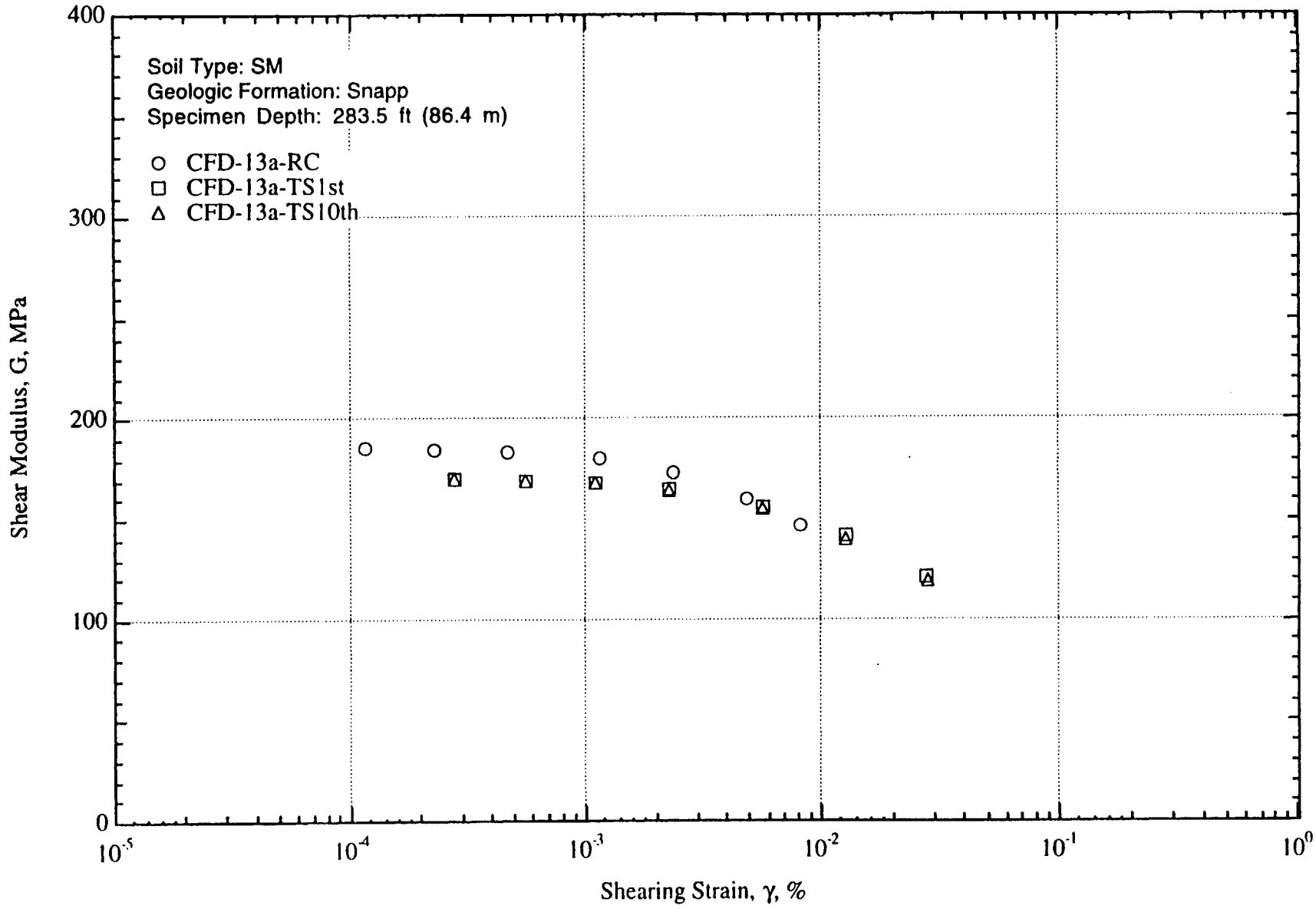


Fig. D.13 Variation in Shear Modulus with Shearing Strain at an Effective Confining Pressure of 93 psi (=13.39 ksf =641 kPa) from RCTS Tests of Specimen CFD-13a

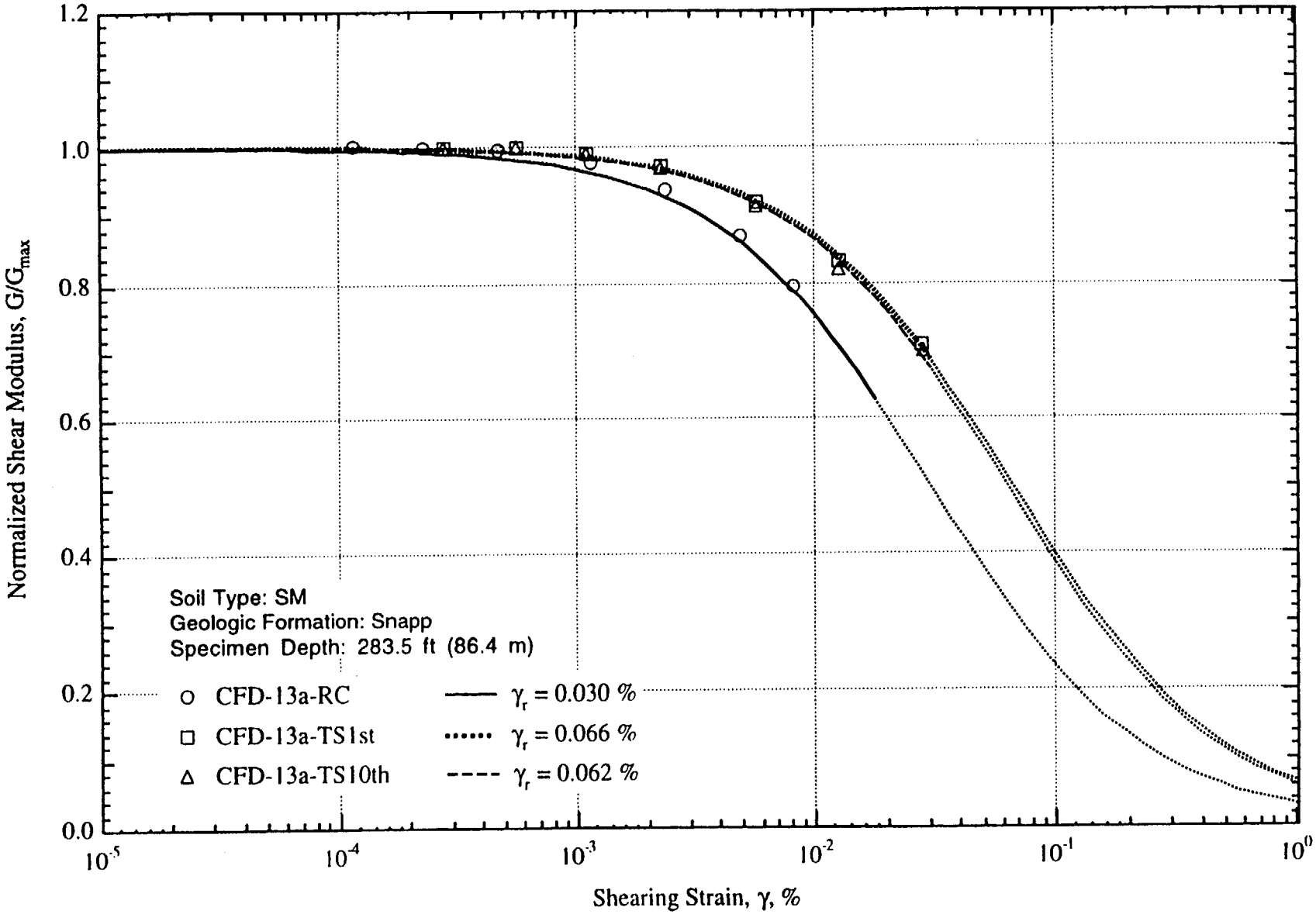


Fig. D.14 Variation in Normalized Shear Modulus with Shearing Strain at an Effective Confining Pressure of 93 psi (=13.39 ksf=641 kPa) from RCTS Tests of Specimen CFD-13a

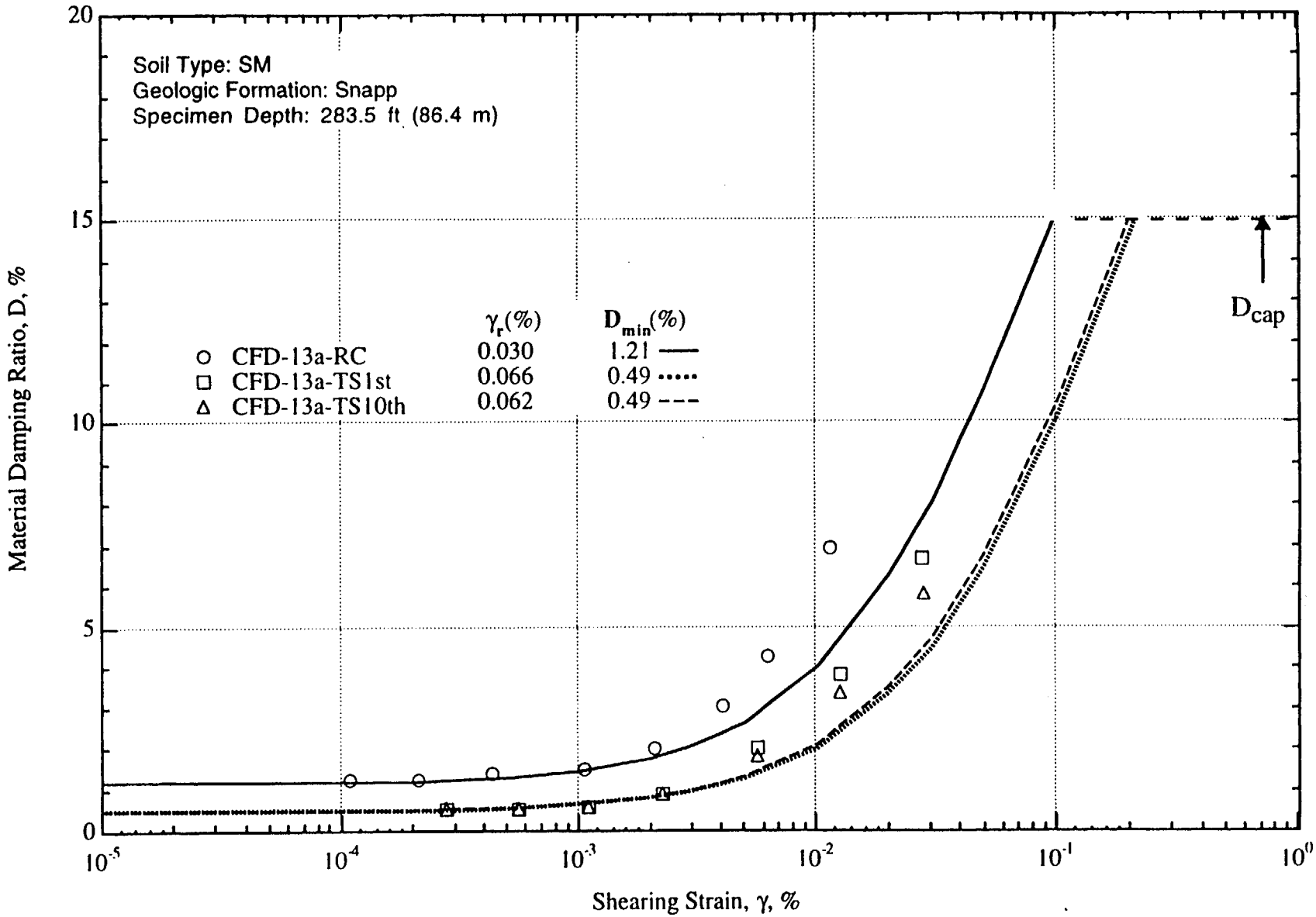


Fig. D.15 Variation in Material Damping Ratio with Shearing Strain at an Effective Confining Pressure of 93 psi (=13.39 ksf=641 kPa) from RCTS Tests of Specimen CFD-13a

# Appendix E

# Effects of Excitation Frequency, Number of Loading Cycles and Confining Pressure on the Dynamic Properties of Shallow Clays (Specimens CFD-6a and CFD-T1a)250

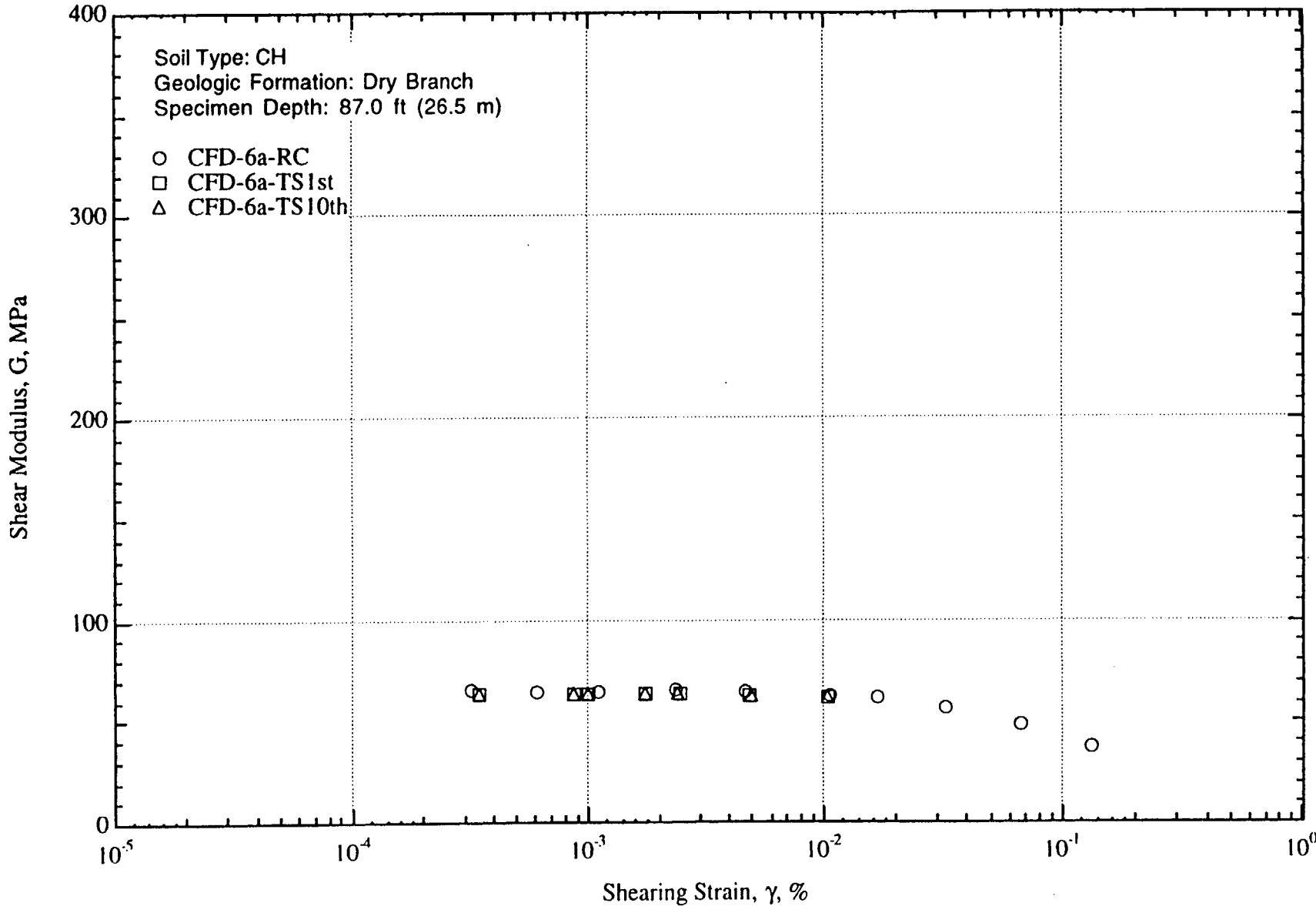


Fig. E.1 Variation in Shear Modulus with Shearing Strain at an Effective Confining Pressure of 41 psi (=5.90 ksf =283 kPa) from RCTS Tests of Specimen CFD-6a

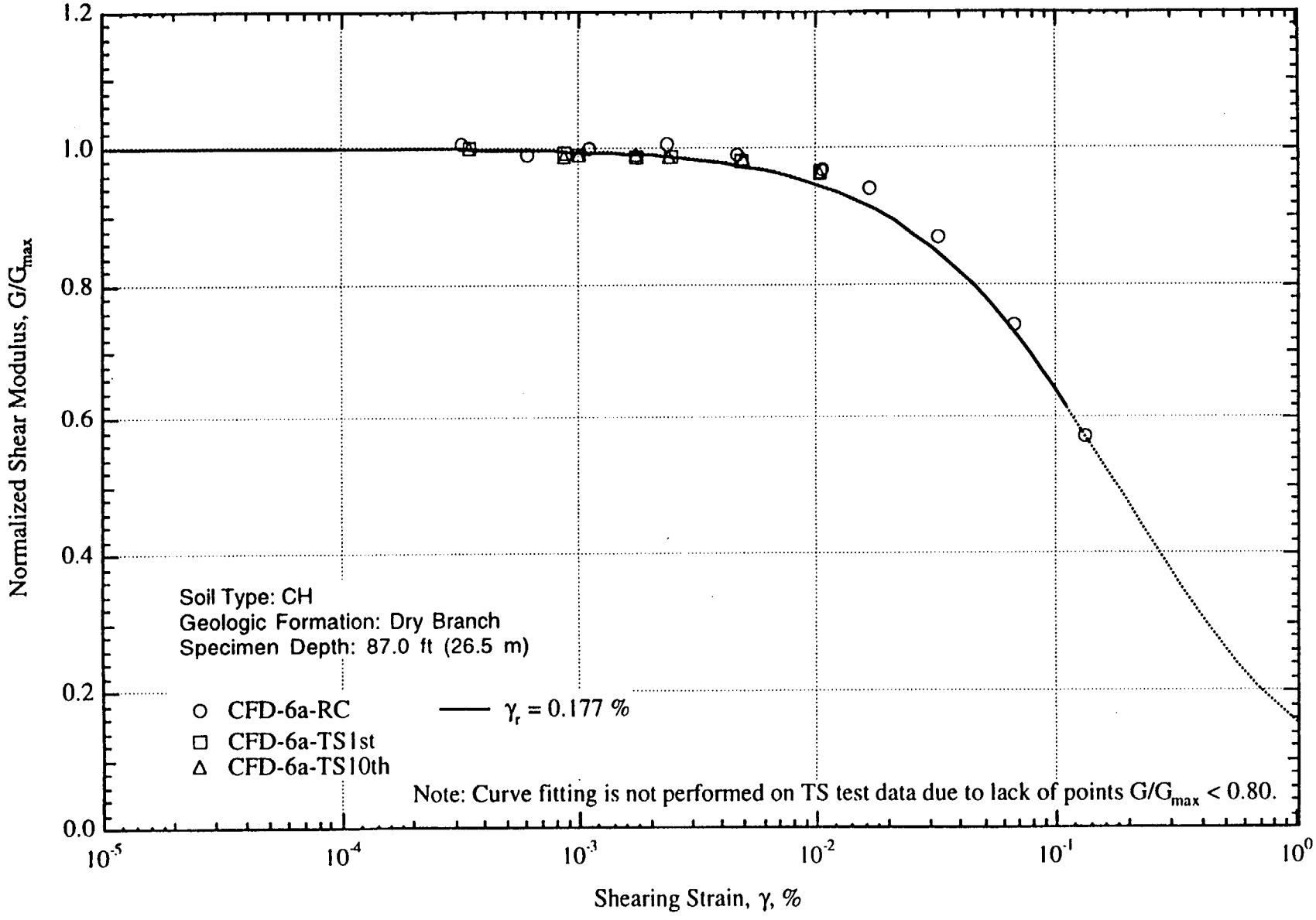


Fig. E.2 Variation in Normalized Shear Modulus with Shearing Strain at an Effective Confining Pressure of 41 psi (=5.90 ksf=283 kPa) from RCTS Tests of Specimen CFD-6a

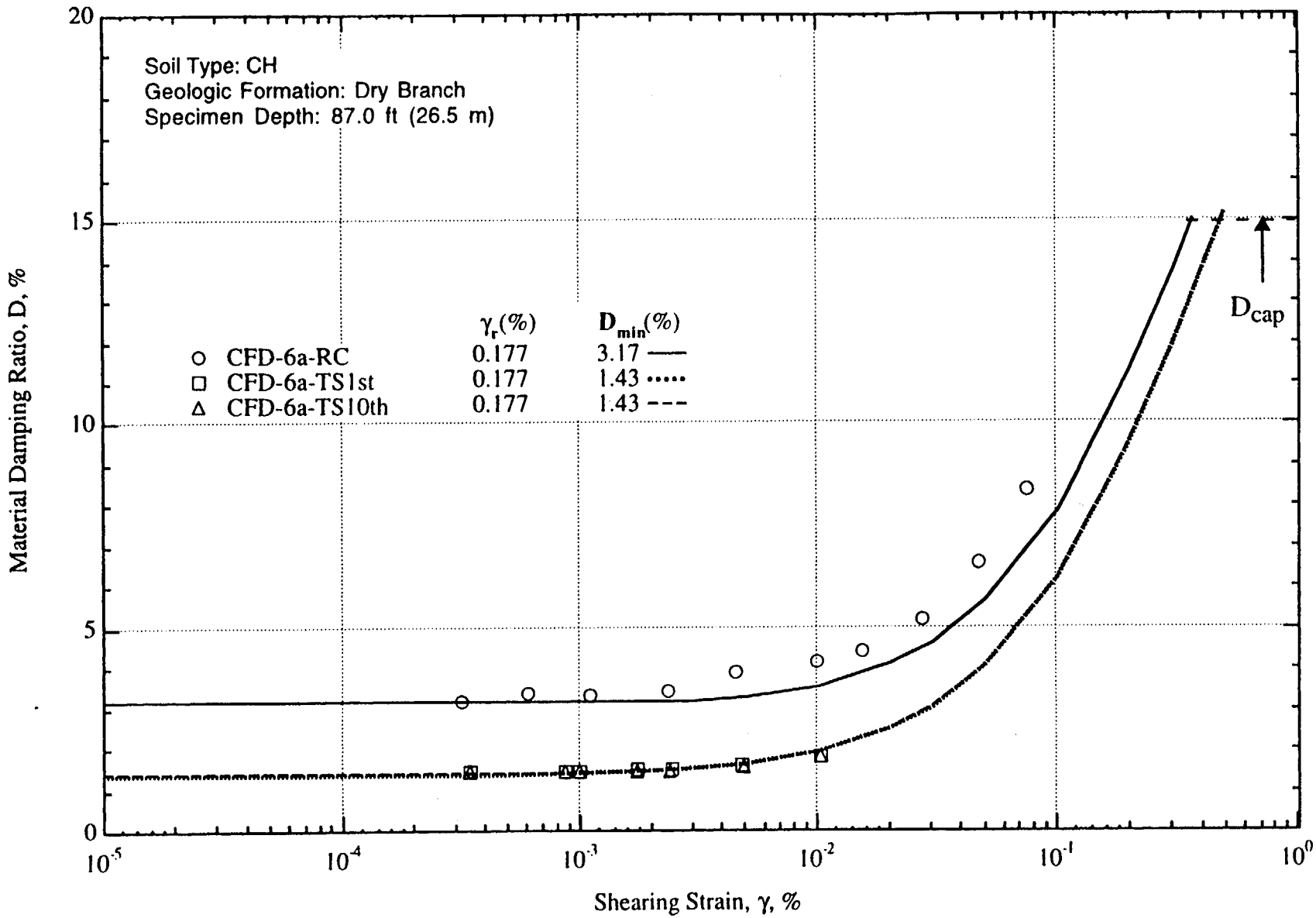


Fig. E.3 Variation in Material Damping Ratio with Shearing Strain at an Effective Confining Pressure of 41 psi (=5.90 ksf=283 kPa) from RCTS Tests of Specimen CFD-6a

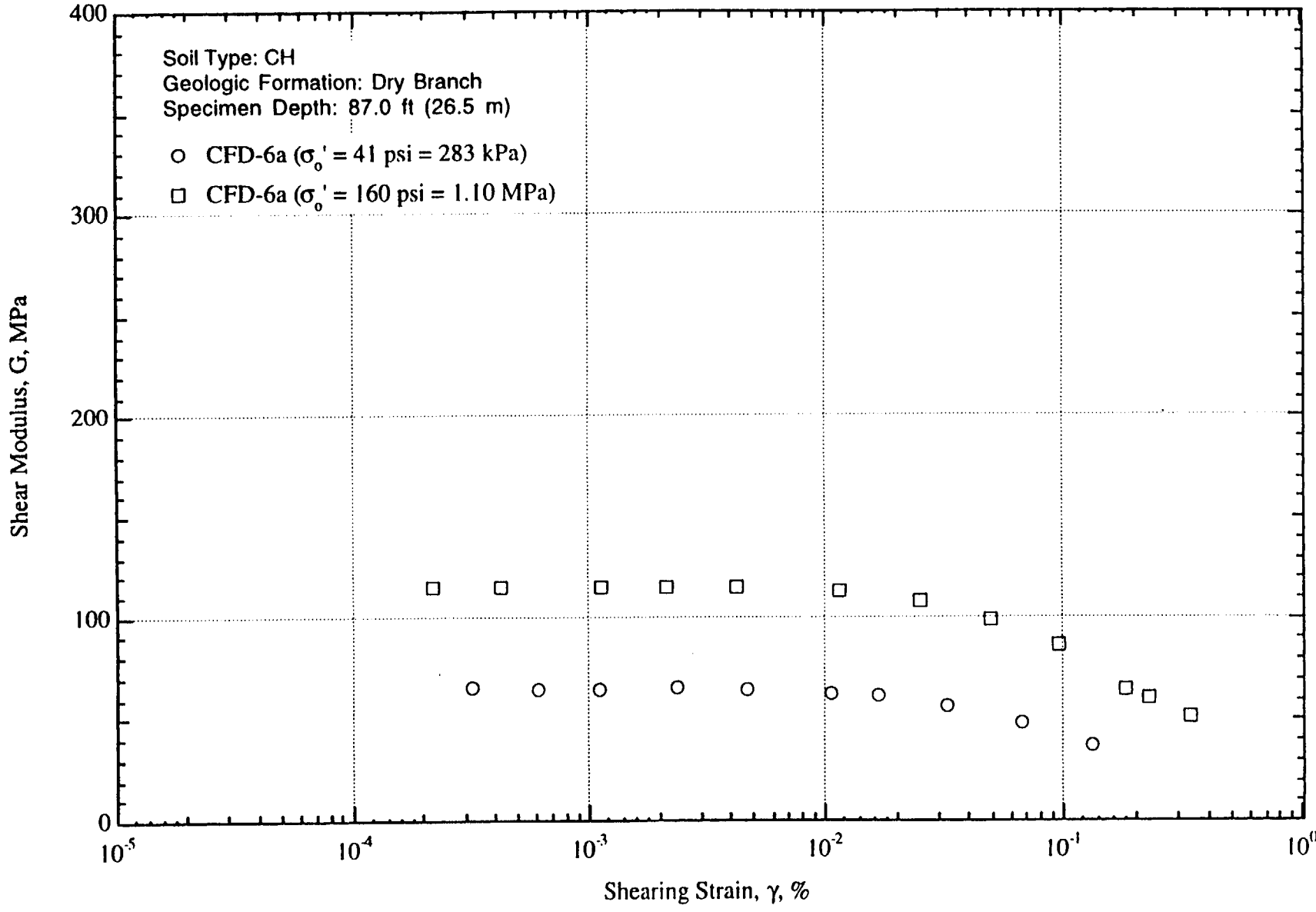


Fig. E.4 Variation in Shear Modulus with Shearing Strain and Effective Confining Pressure from Resonant Column Tests of Specimen CFD-6a

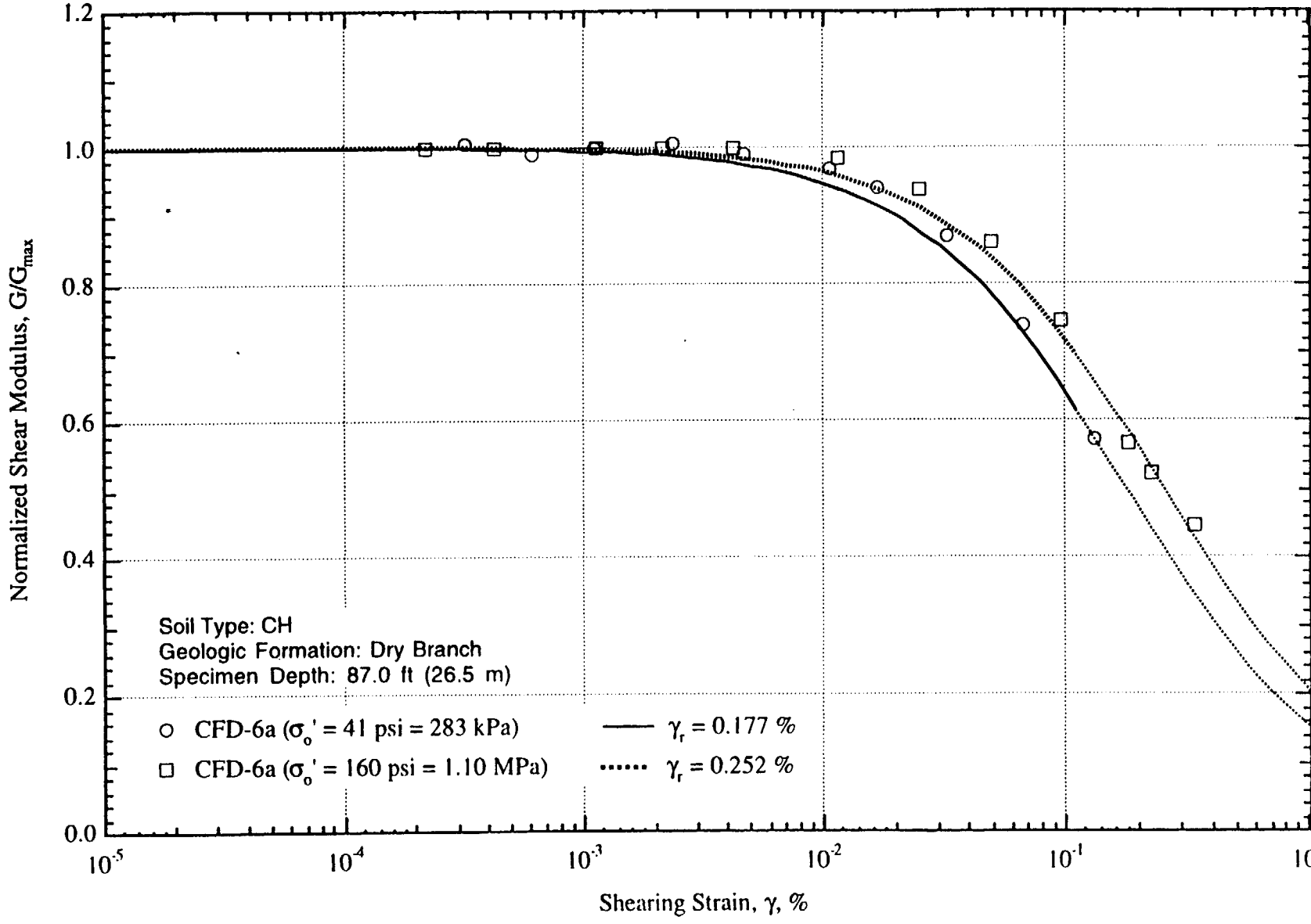


Fig. E.5 Comparison of the Variation in Normalized Shear Modulus with Shearing Strain and Effective Confining Pressure from Resonant Column Tests of Specimen CFD-6a

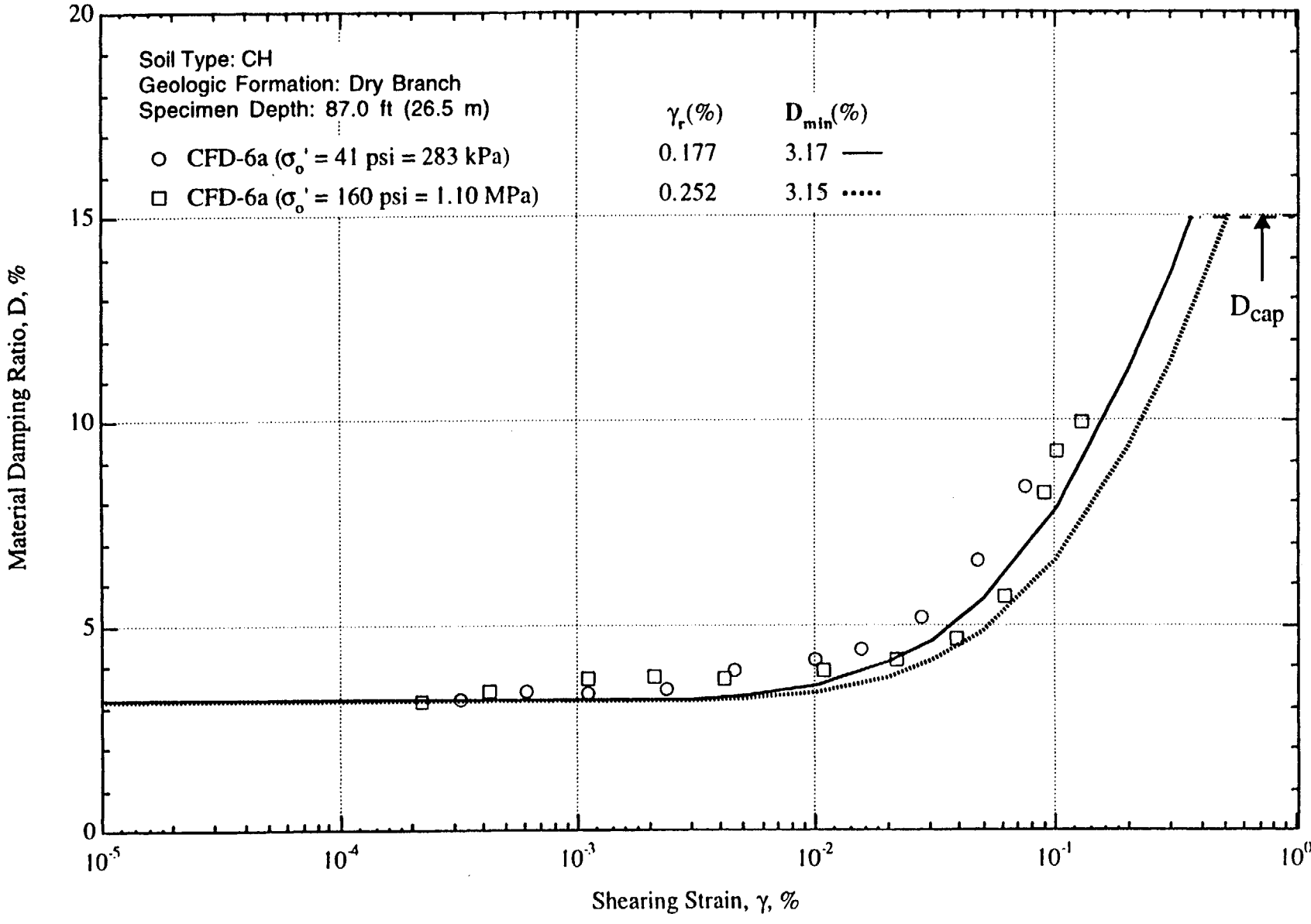


Fig. E.6 Variation in Material Damping Ratio with Shearing Strain and Effective Confining Pressure from Resonant Column Tests of Specimen CFD-6a

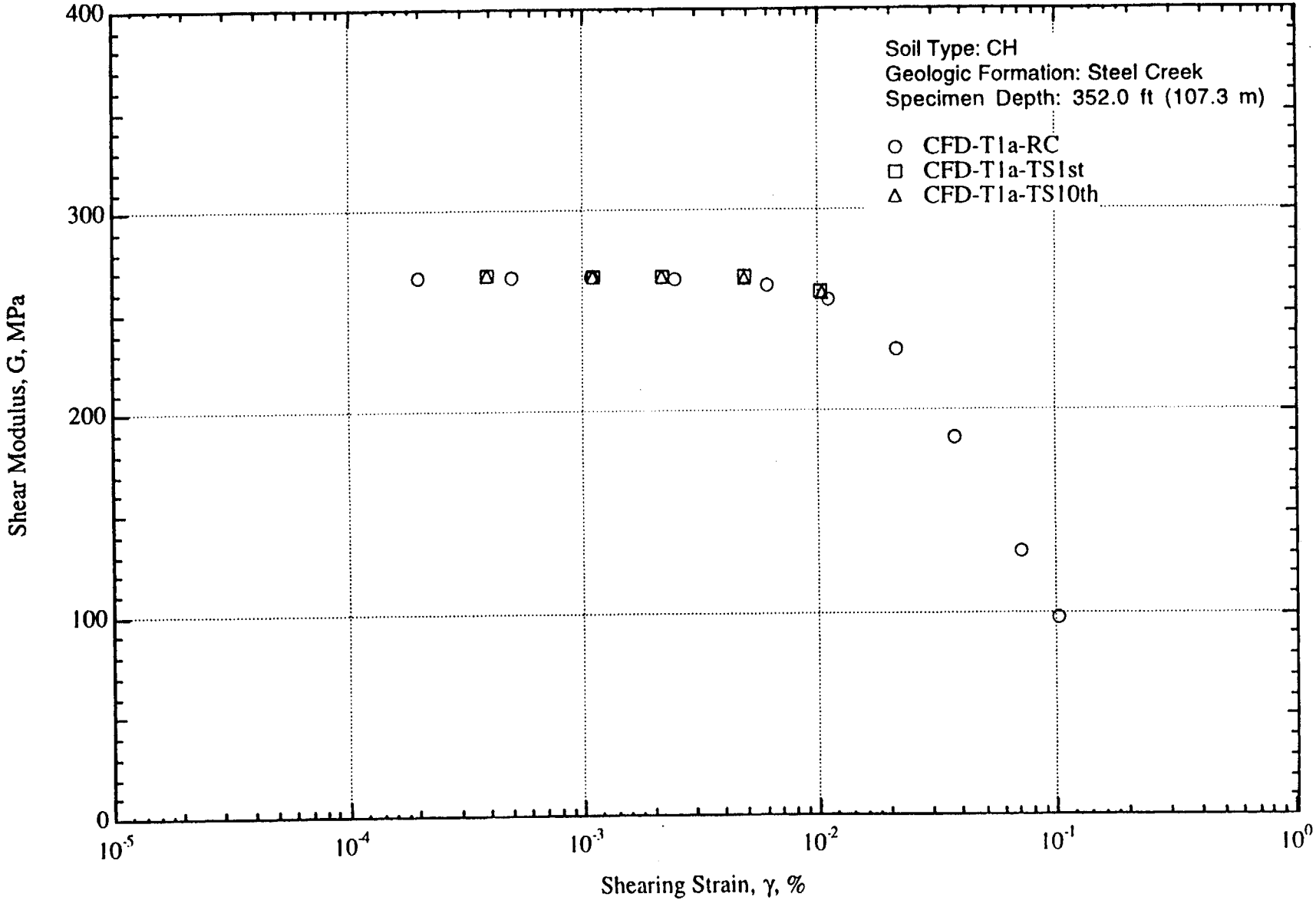


Fig. E.7 Variation in Shear Modulus with Shearing Strain at an Effective Confining Pressure of 111 psi (=15.98 ksf =765 kPa) from RCTS Tests of Specimen CFD-T1a

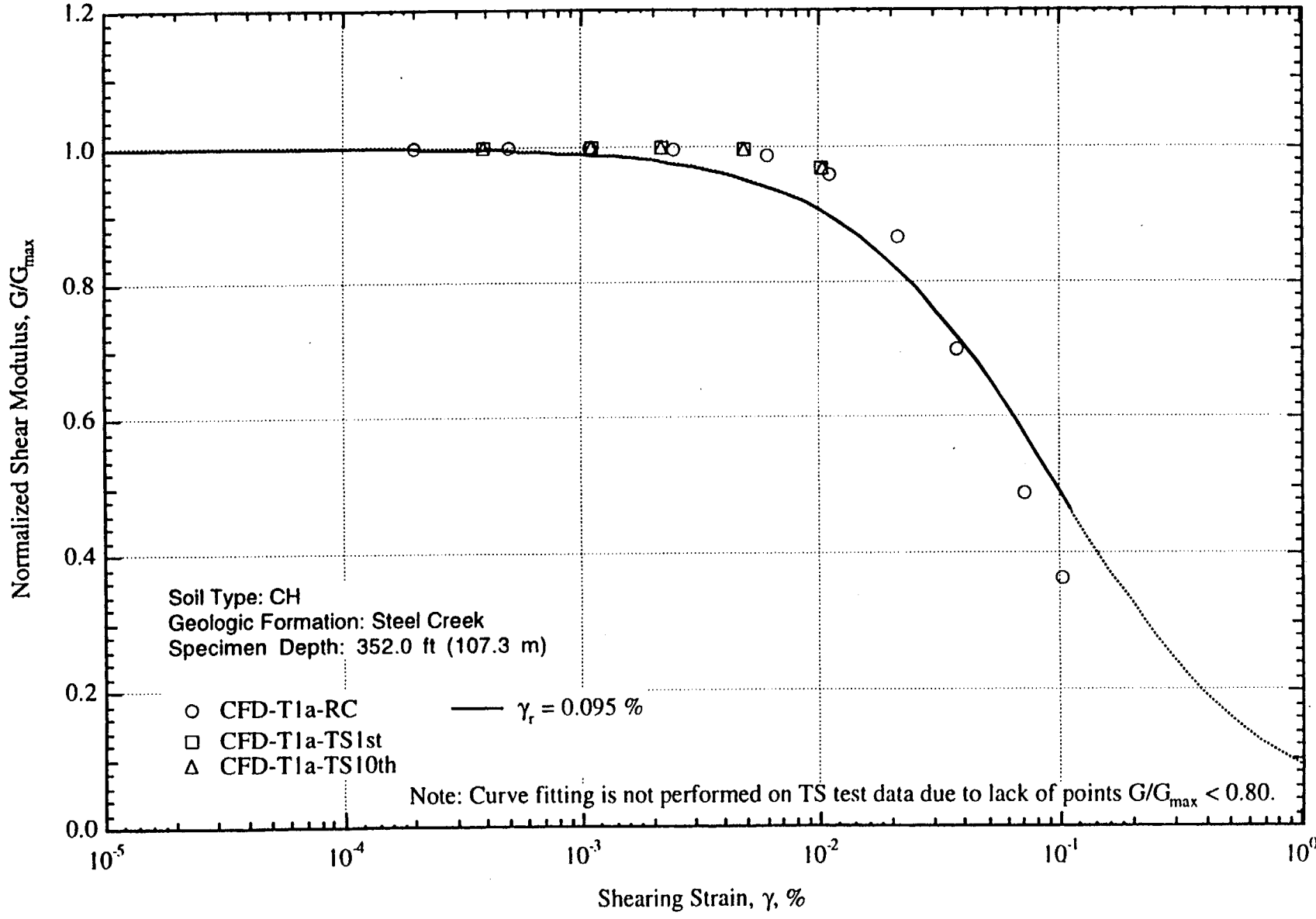


Fig. E.8 Variation in Normalized Shear Modulus with Shearing Strain at an Effective Confining Pressure of 111 psi (=15.98 ksf=765 kPa) from RCTS Tests of Specimen CFD-T1a

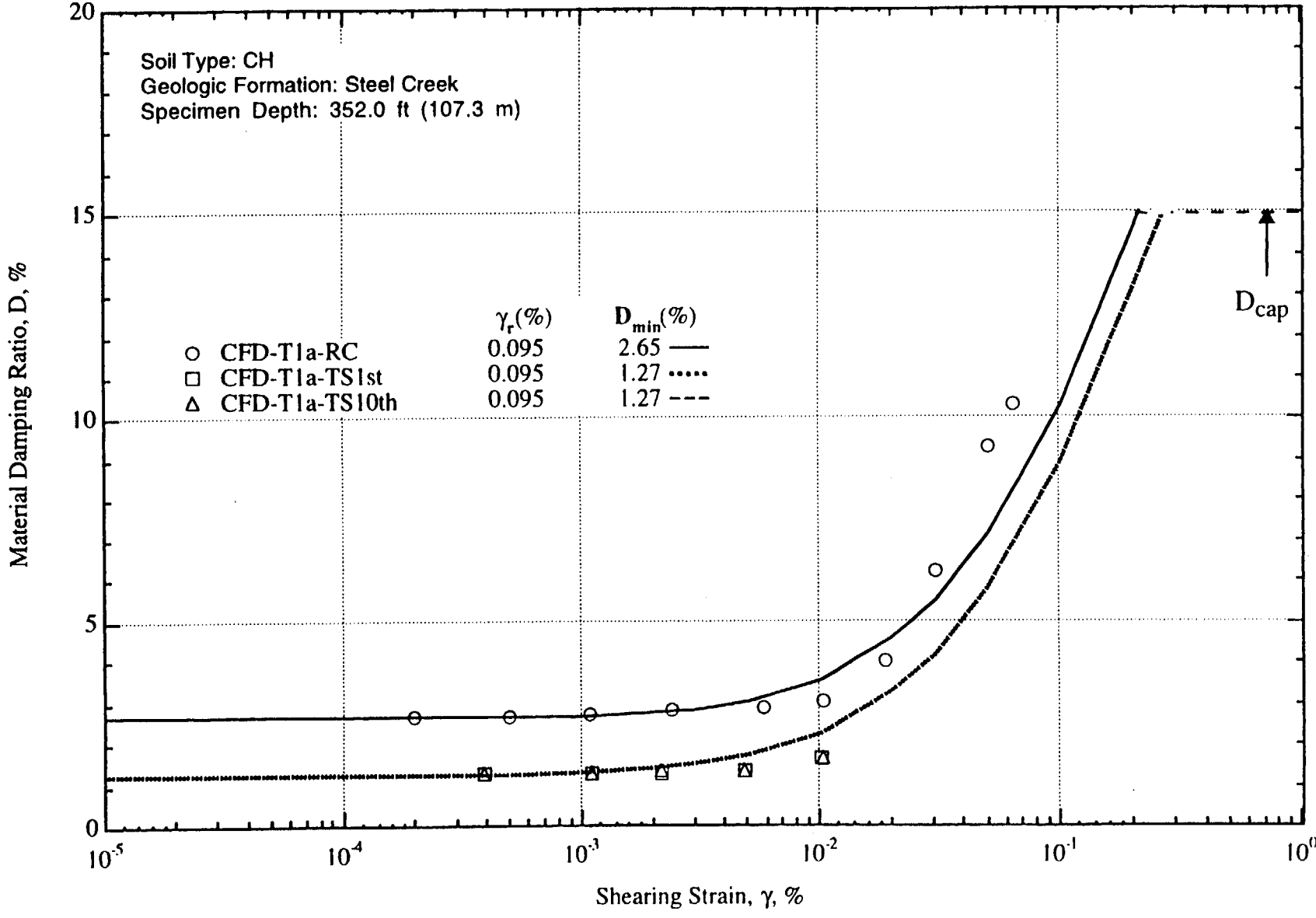


Fig. E.9 Variation in Material Damping Ratio with Shearing Strain at an Effective Confining Pressure of 111 psi (=15.98 ksf=765 kPa) from RCTS Tests of Specimen CFD-T1a

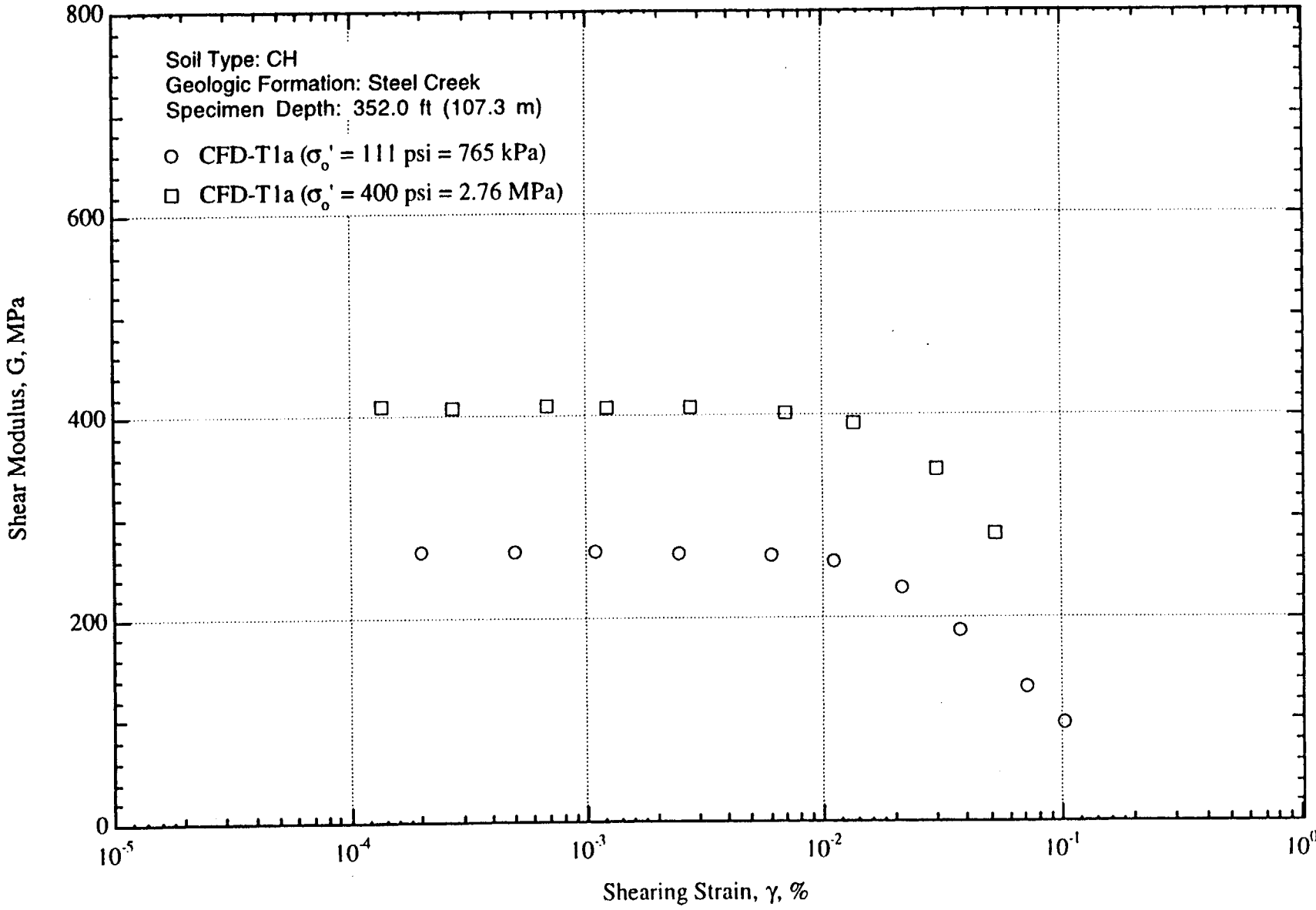


Fig. E.10 Variation in Shear Modulus with Shearing Strain and Effective Confining Pressure from Resonant Column Tests of Specimen CFD-T1a

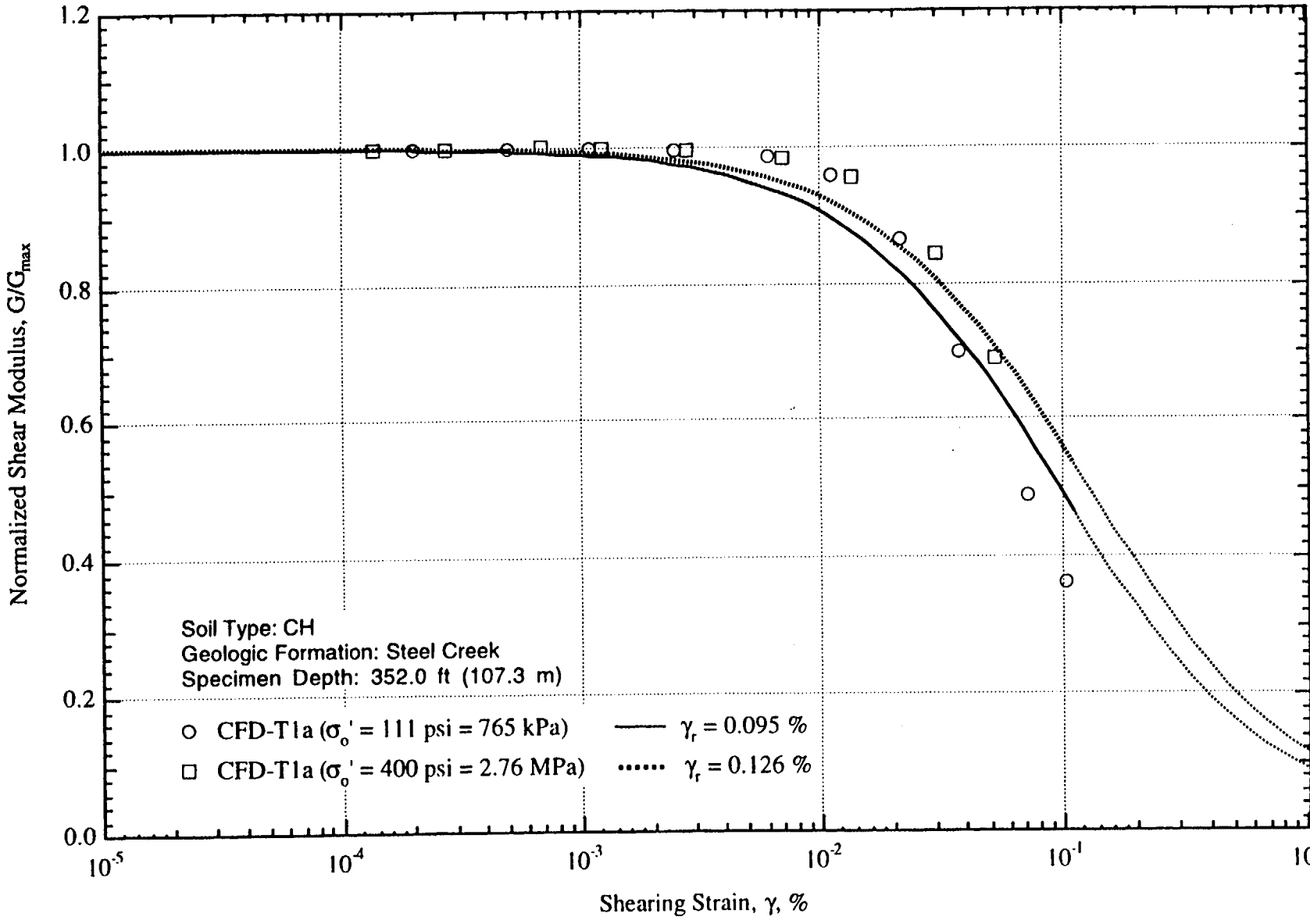


Fig. E.11 Comparison of the Variation in Normalized Shear Modulus with Shearing Strain and Effective Confining Pressure from Resonant Column Tests of Specimen CFD-T1a

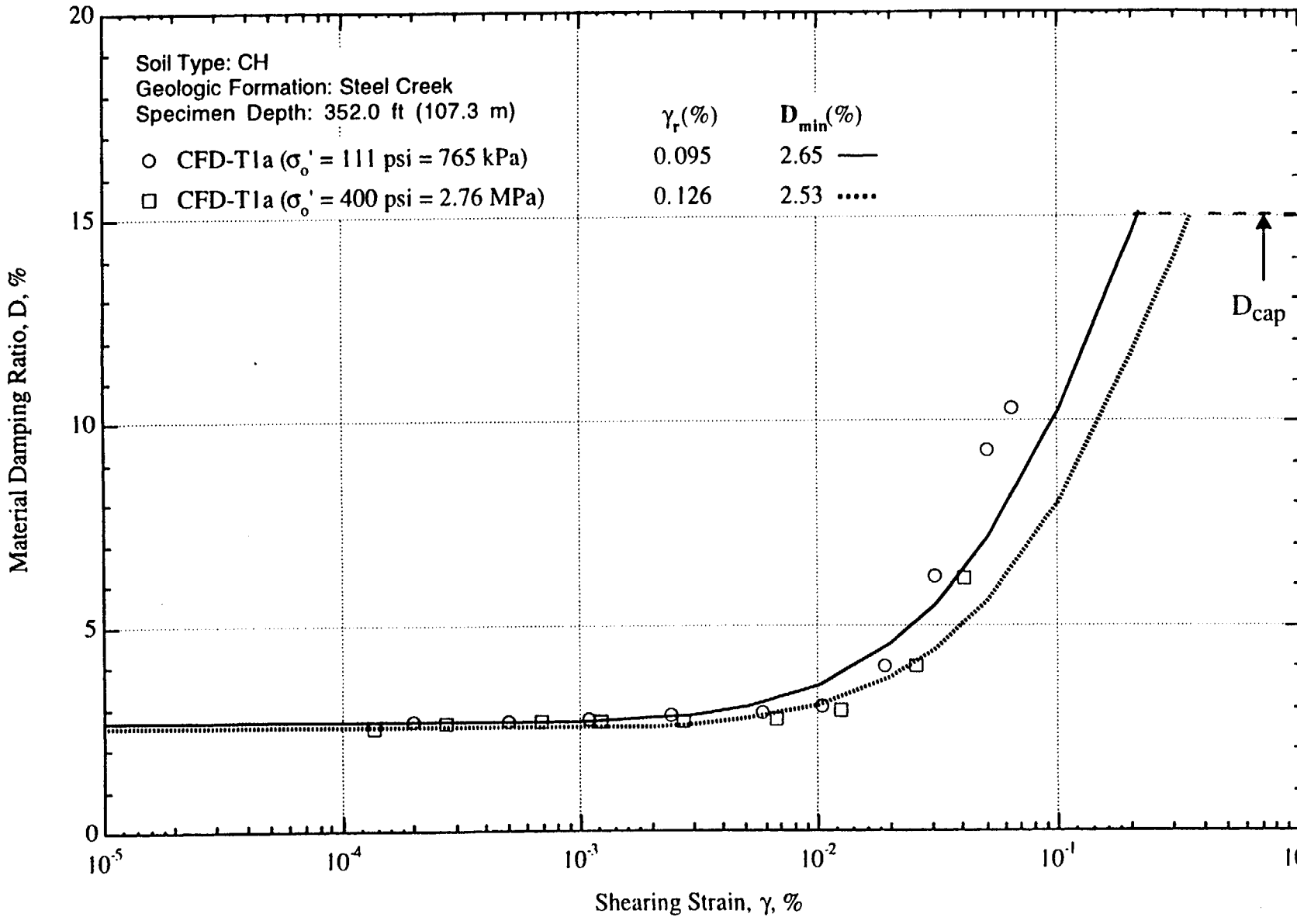


Fig. E.12 Variation in Material Damping Ratio with Shearing Strain and Effective Confining Pressure from Resonant Column Tests of Specimen CFD-T1a

# Appendix F

# Effects of Excitation Frequency, Number of Loading Cycles and Confining Pressure on the Dynamic Properties of Upland Sands (Specimens CFD-1a and CFD-2a)

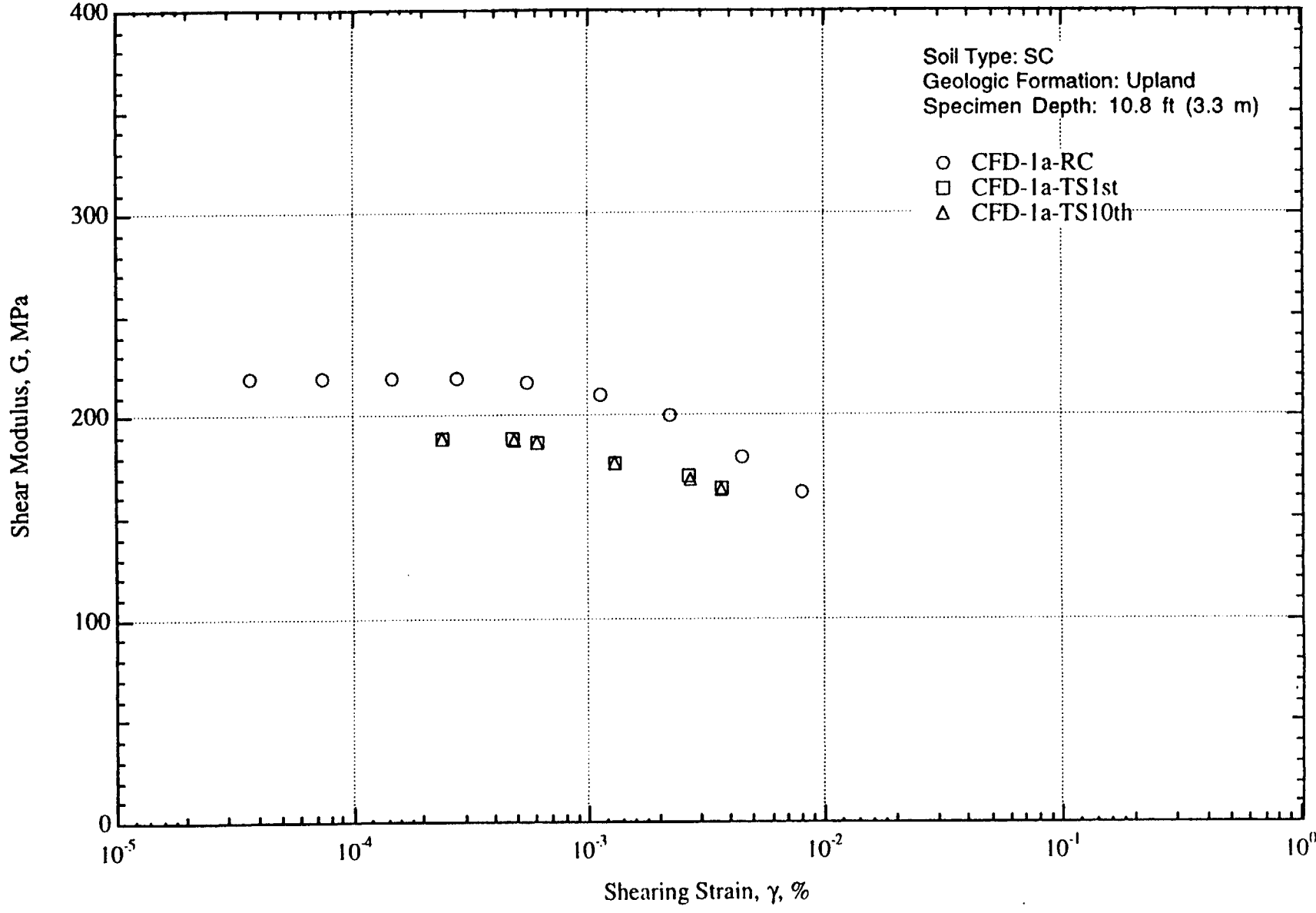


Fig. F.1 Variation in Shear Modulus with Shearing Strain at an Effective Confining Pressure of 6 psi (=864 psf =41 kPa) from RCTS Tests of Specimen CFD-1a

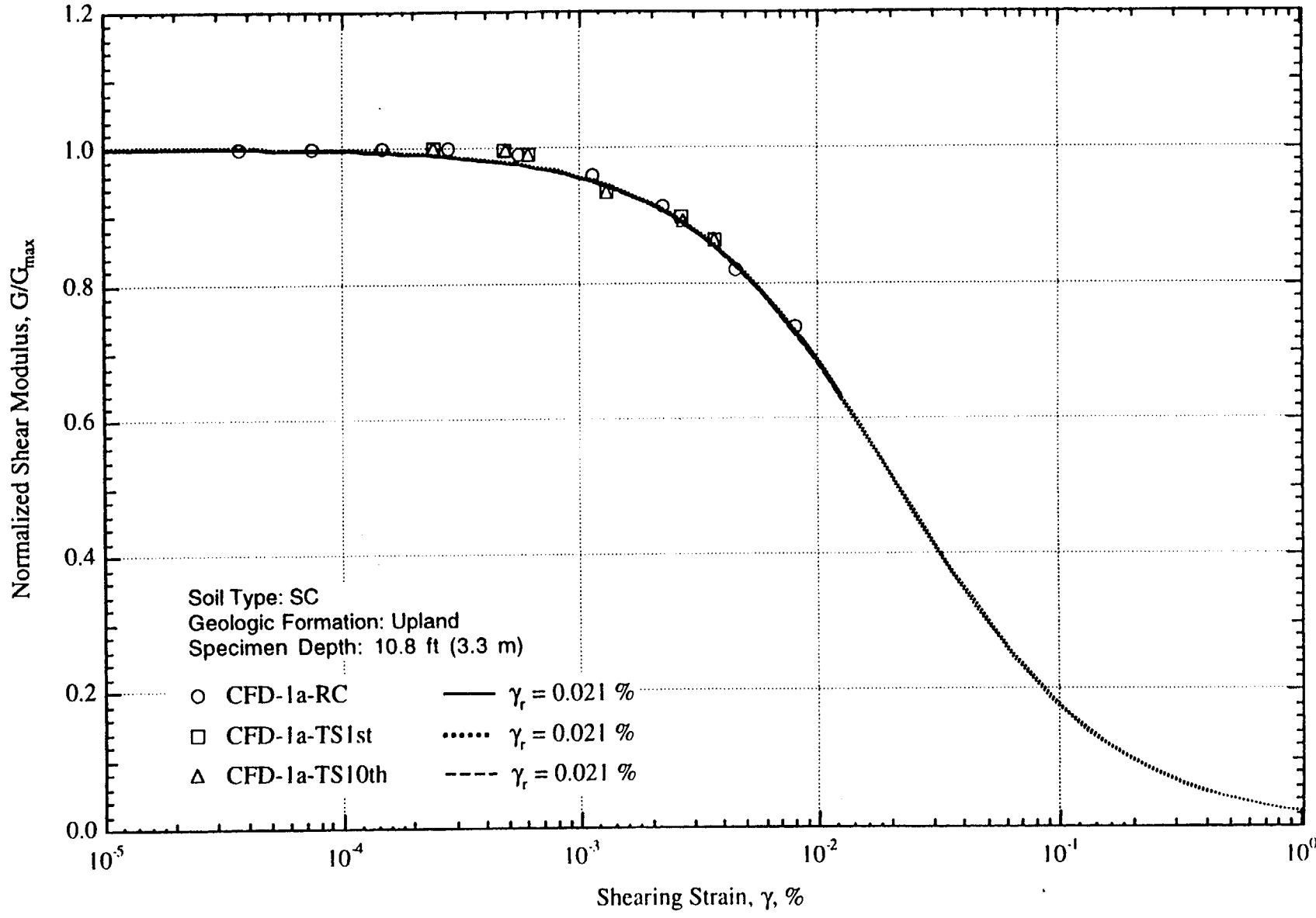


Fig. F.2 Variation in Normalized Shear Modulus with Shearing Strain at an Effective Confining Pressure of 6 psi (=864 psf=41 kPa) from RCTS Tests of Specimen CFD-1a

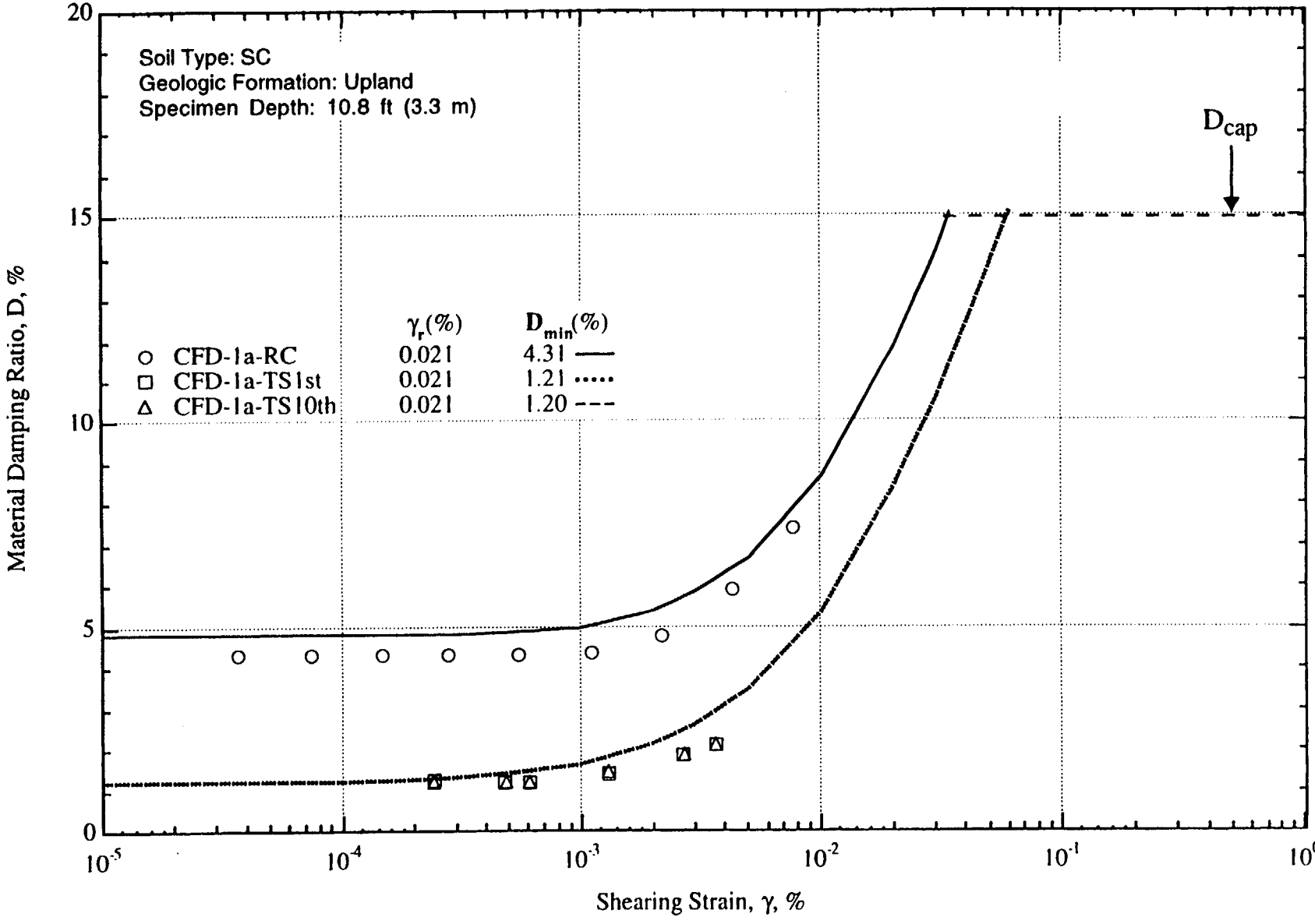


Fig. F.3 Variation in Material Damping Ratio with Shearing Strain at an Effective Confining Pressure of 6 psi (=864 psf=41 kPa) from RCTS Tests of Specimen CFD-1a

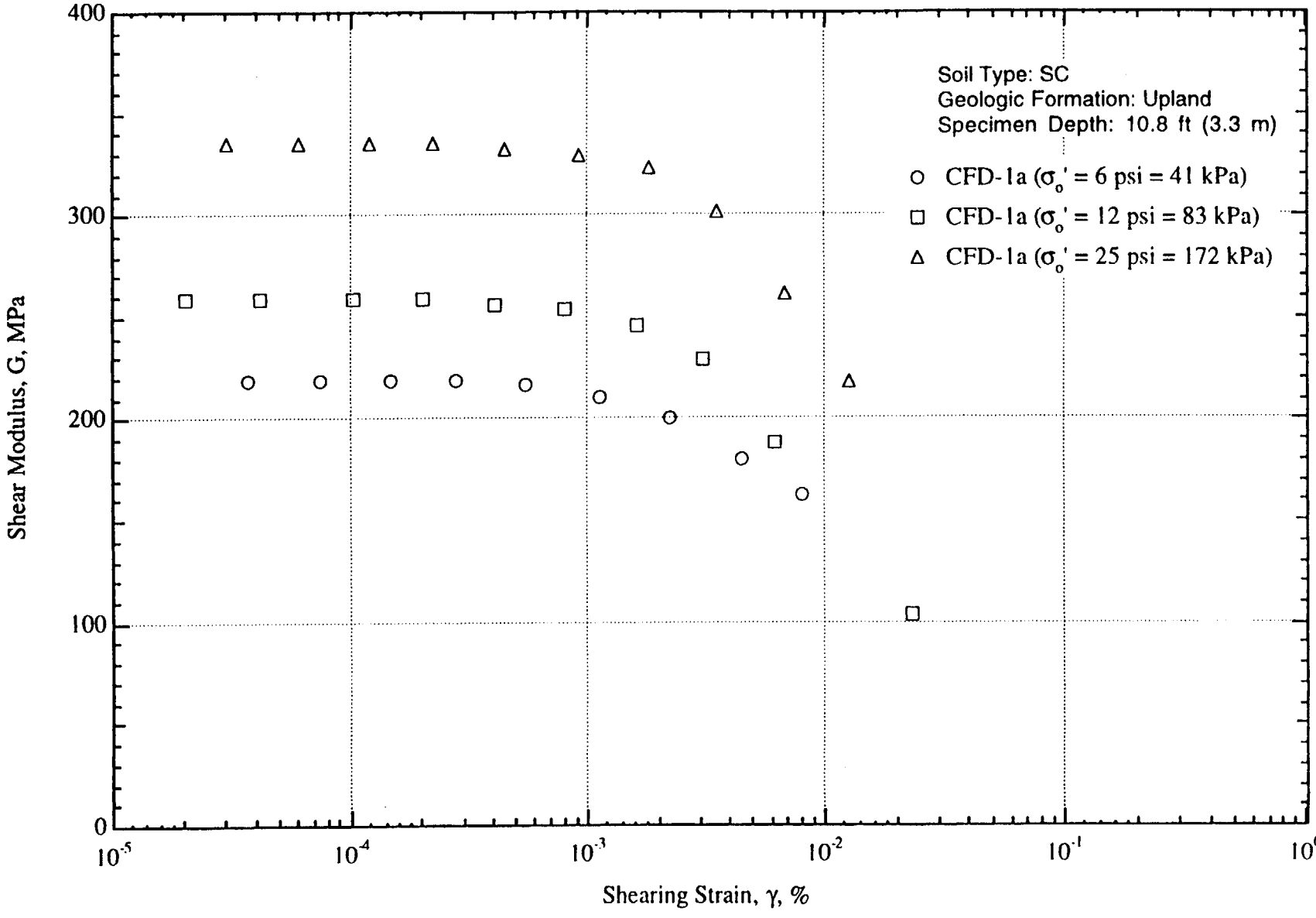


Fig. F.4 Variation in Shear Modulus with Shearing Strain and Effective Confining Pressure from Resonant Column Tests of Specimen CFD-1a

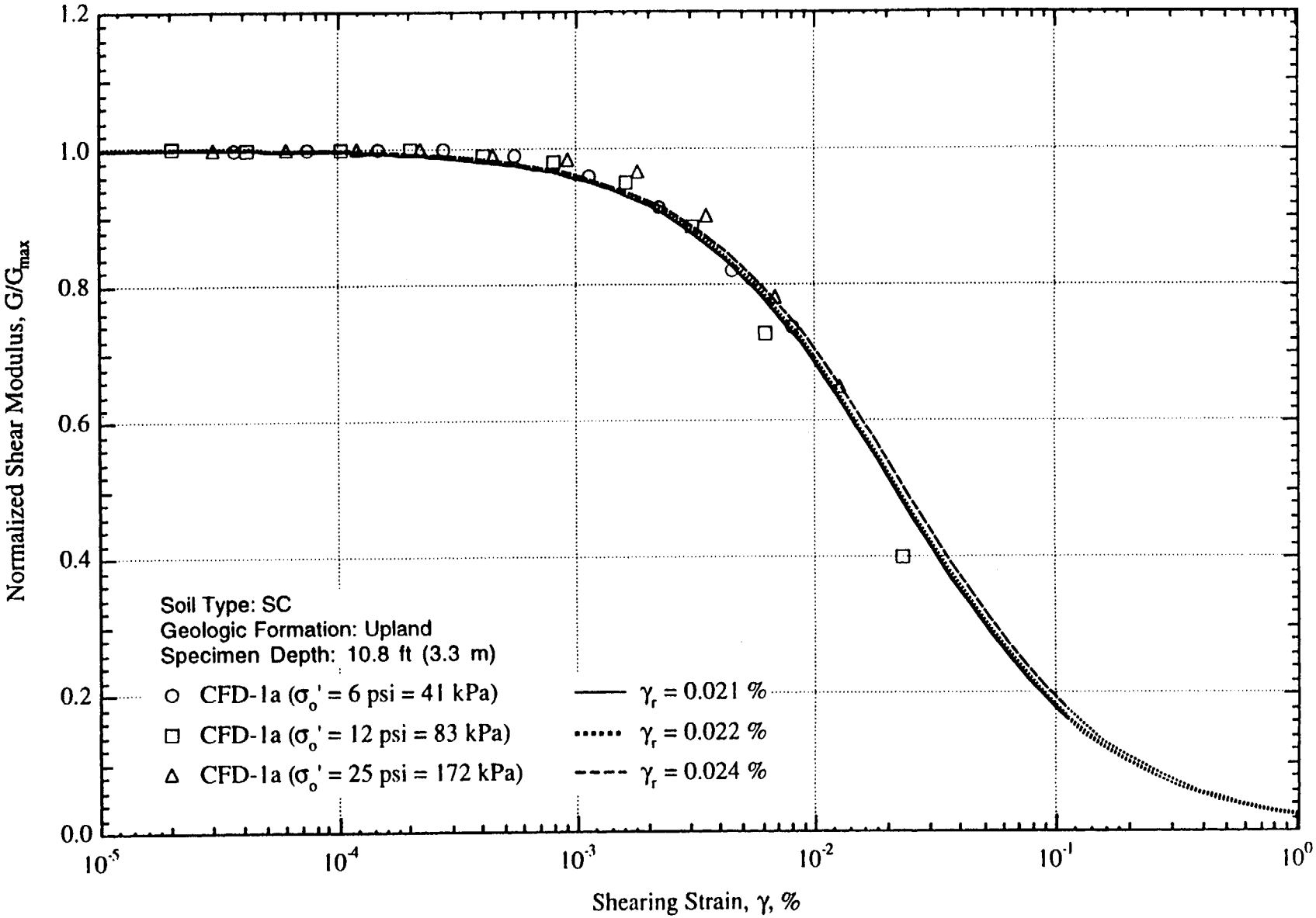


Fig. F.5 Comparison of the Variation in Normalized Shear Modulus with Shearing Strain and Effective Confining Pressure from Resonant Column Tests of Specimen CFD-1a

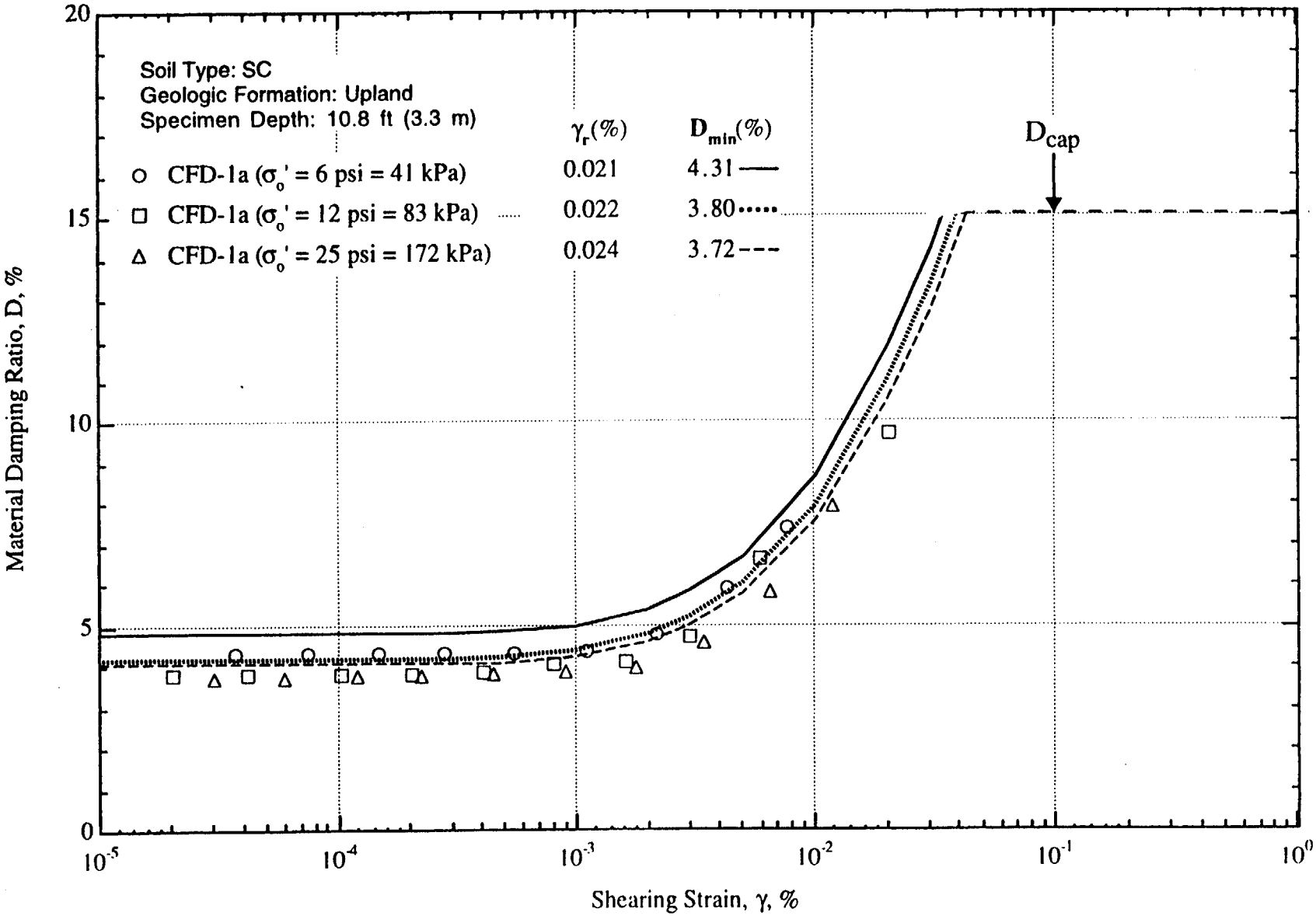


Fig. F.6 Variation in Material Damping Ratio with Shearing Strain and Effective Confining Pressure from Resonant Column Tests of Specimen CFD-1a

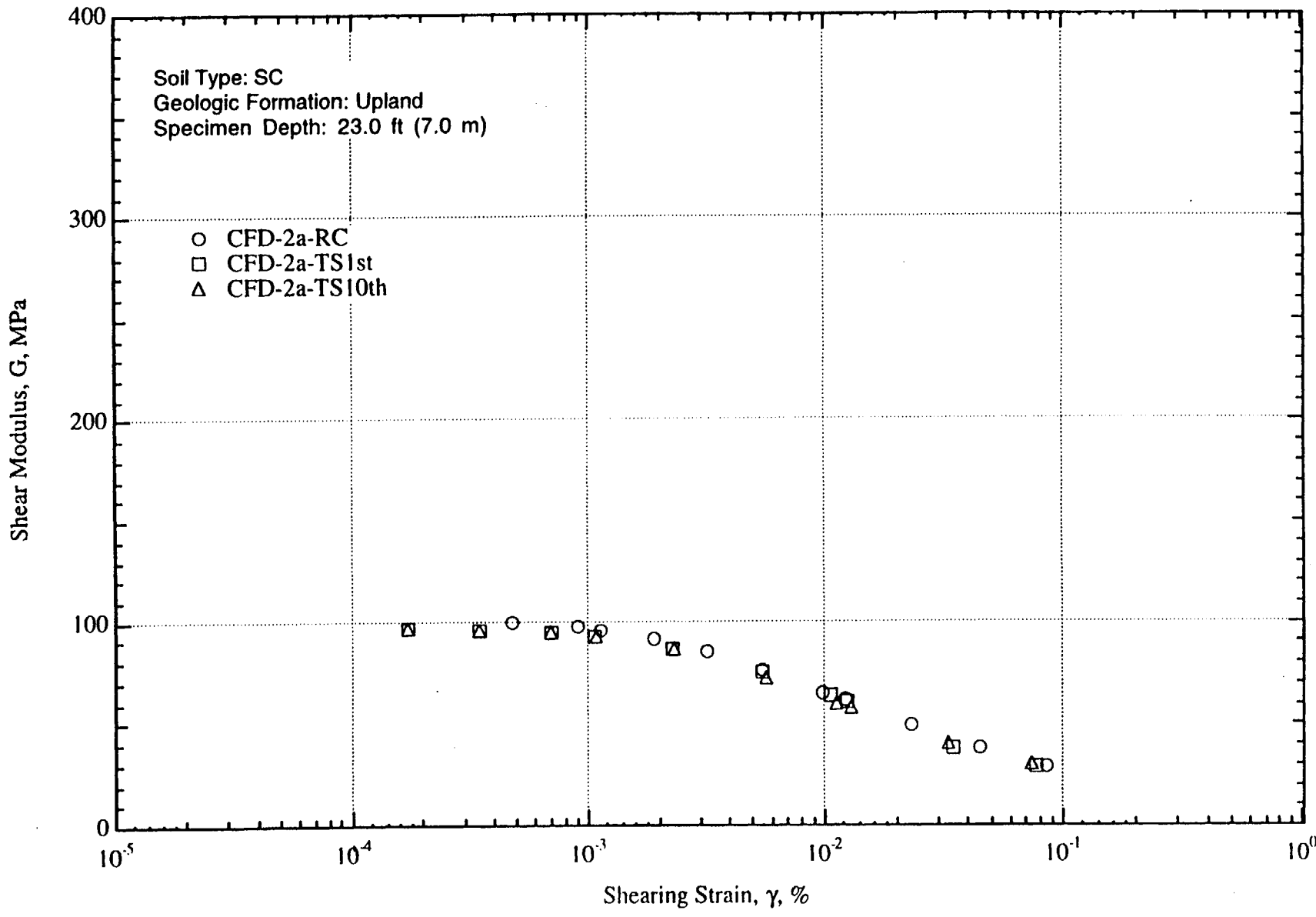


Fig. F.7 Variation in Shear Modulus with Shearing Strain at an Effective Confining Pressure of 13 psi (=1.87 ksf =90 kPa) from RCTS Tests of Specimen CFD-2a

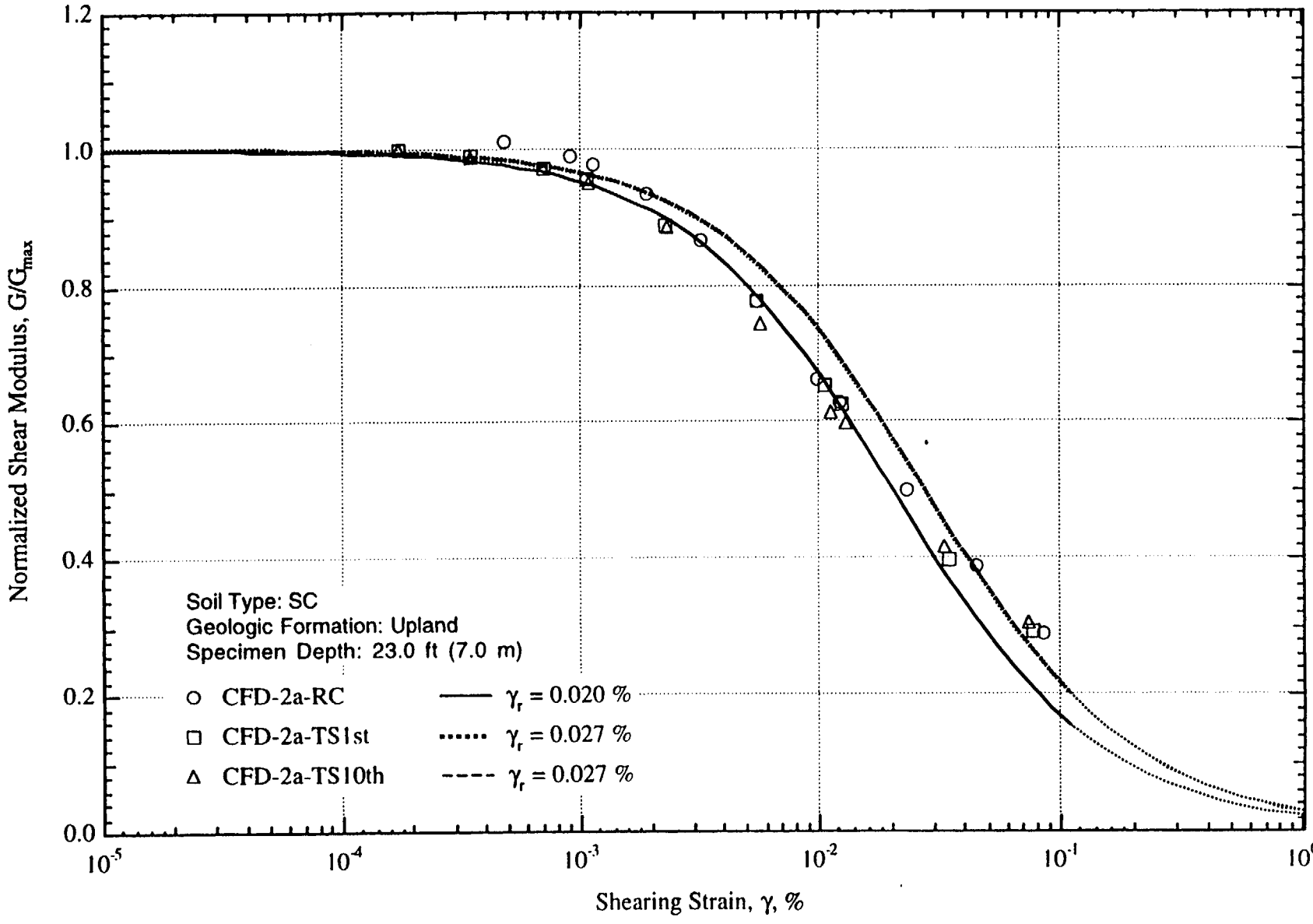


Fig. F.8 Variation in Normalized Shear Modulus with Shearing Strain at an Effective Confining Pressure of 13 psi (=1.87 ksf=90 kPa) from RCTS Tests of Specimen CFD-2a

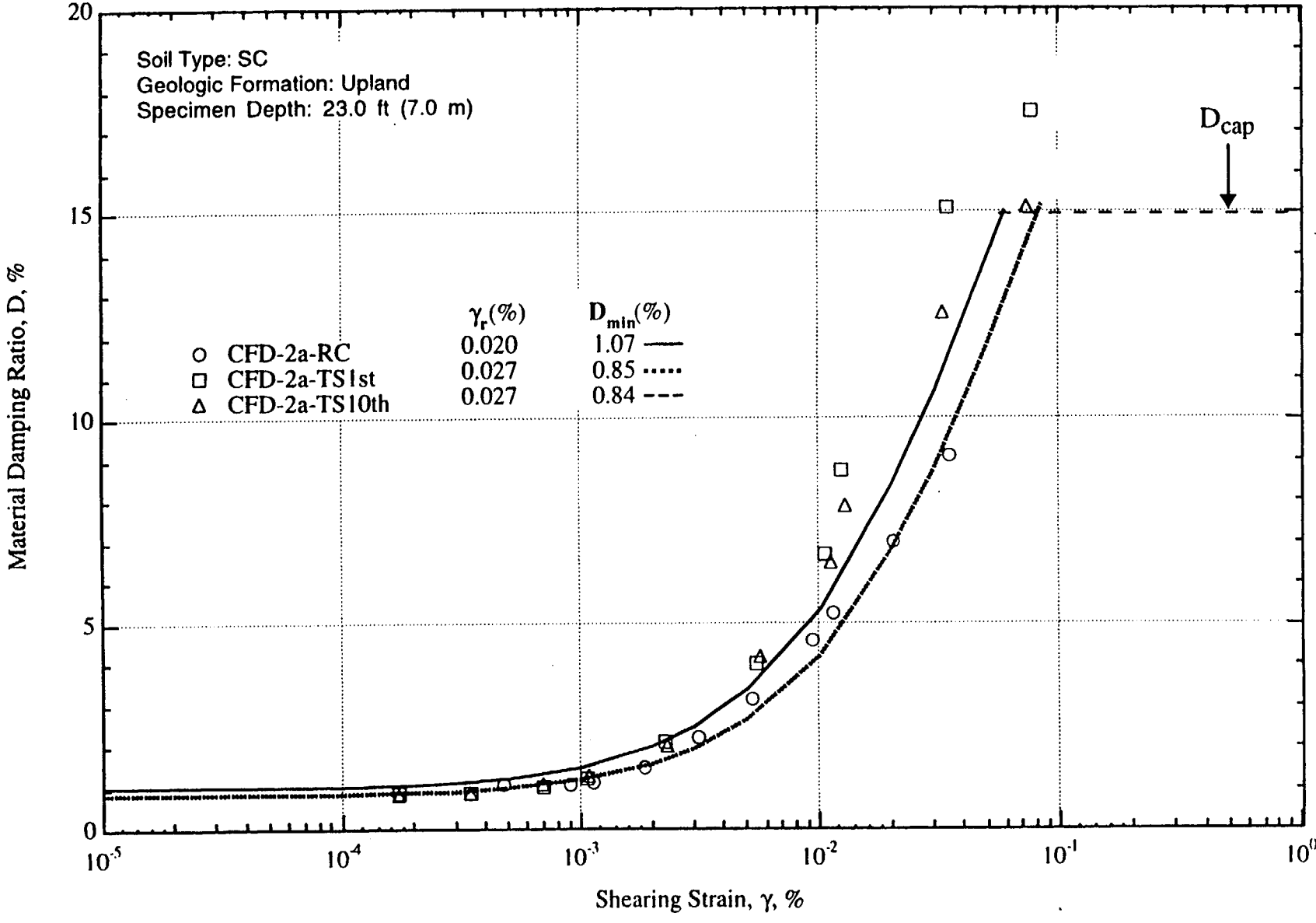


Fig. F.9 Variation in Material Damping Ratio with Shearing Strain at an Effective Confining Pressure of 13 psi (=1.87 ksf=90 kPa) from RCTS Tests of Specimen CFD-2a

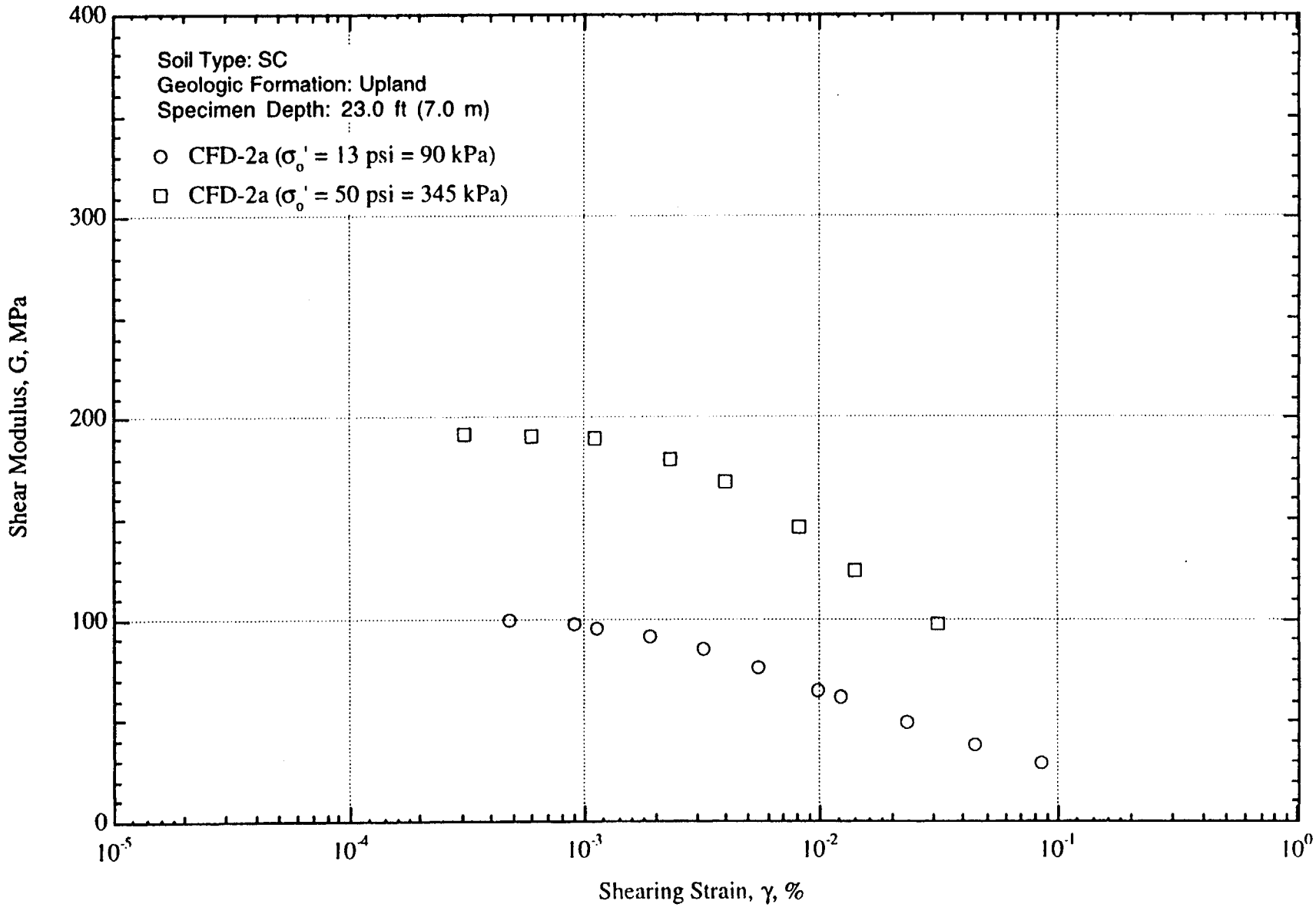


Fig. F.10 Variation in Shear Modulus with Shearing Strain and Effective Confining Pressure from Resonant Column Tests of Specimen CFD-2a

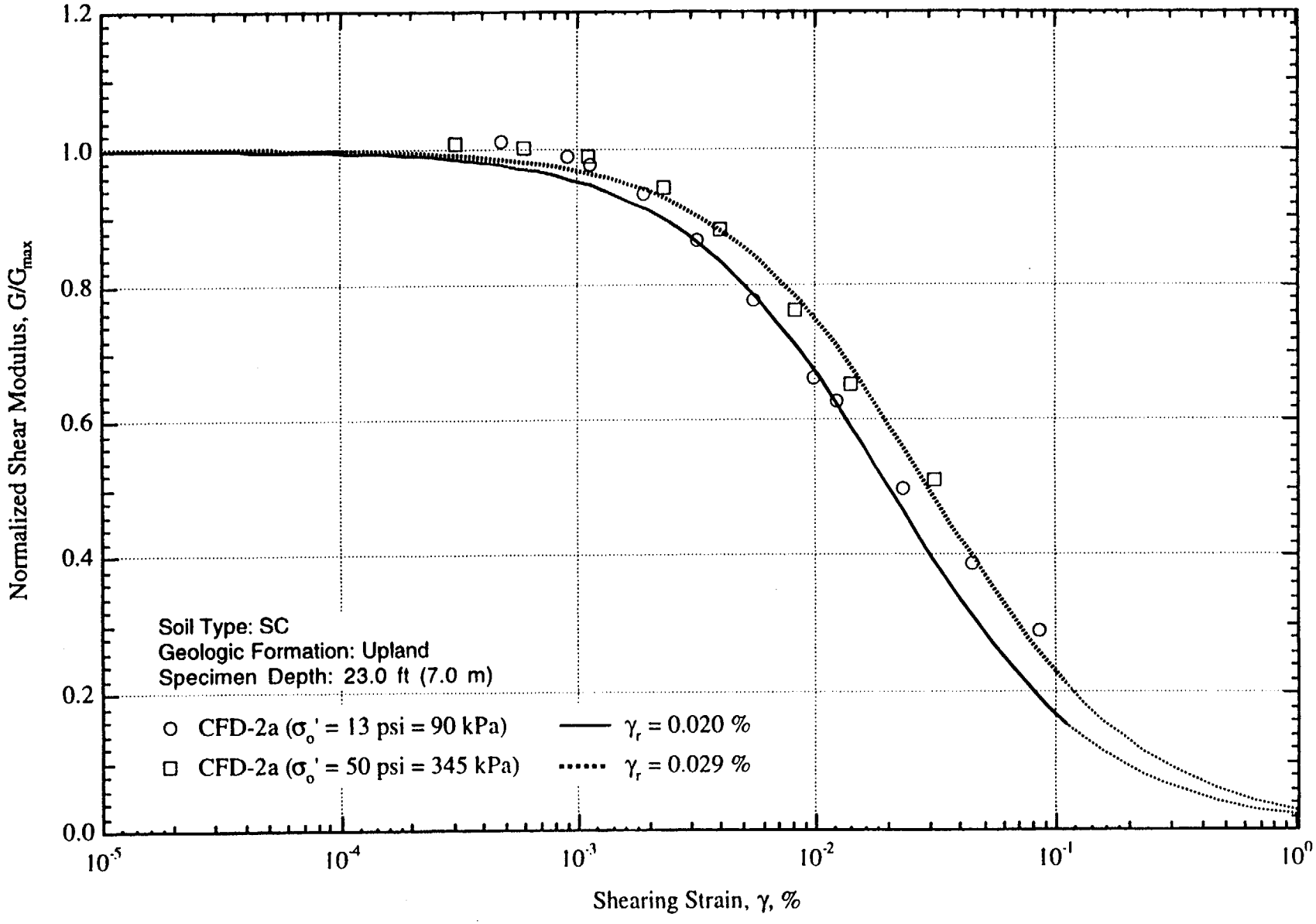


Fig. F.11 Comparison of the Variation in Normalized Shear Modulus with Shearing Strain and Effective Confining Pressure from Resonant Column Tests of Specimen CFD-2a

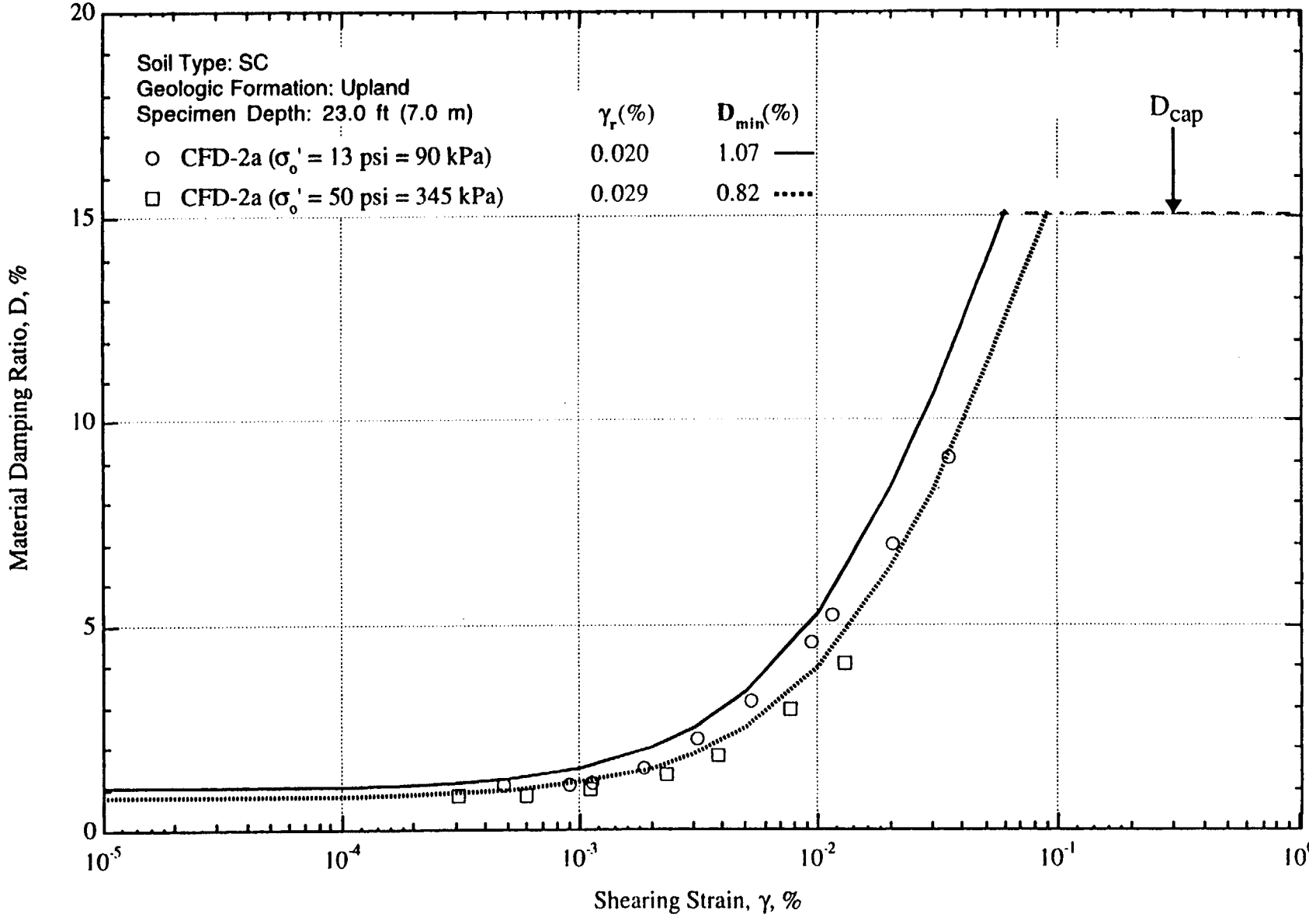


Fig. F.12 Variation in Material Damping Ratio with Shearing Strain and Effective Confining Pressure from Resonant Column Tests of Specimen CFD-2a

# Appendix G

# Effects of Excitation Frequency and Number of Loading Cycles and Confining Pressure on the Dynamic Properties of Warley Hill Sands (Specimen CFD-8a)

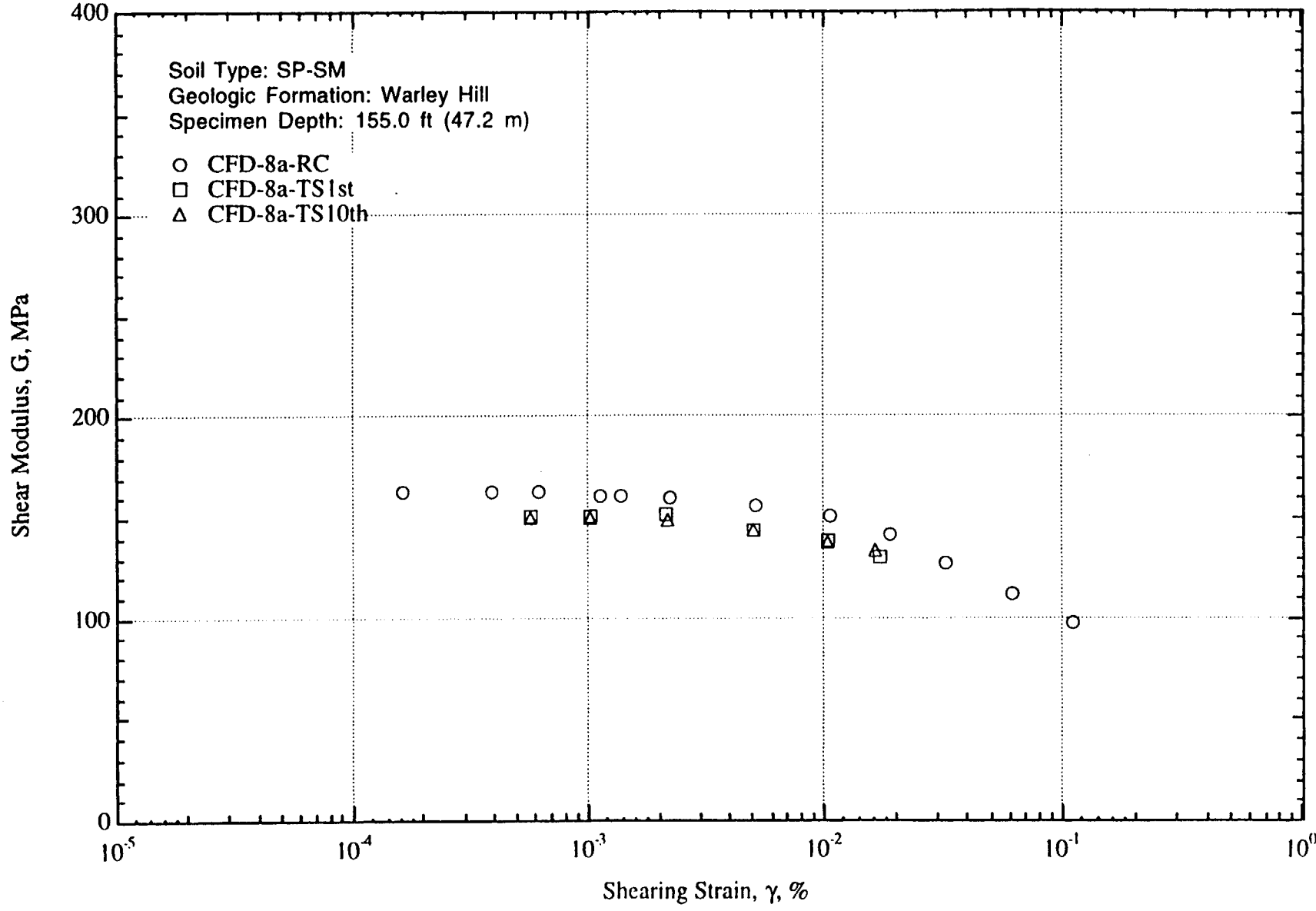


Fig. G.1 Variation in Shear Modulus with Shearing Strain at an Effective Confining Pressure of 59 psi (=8.49 ksf =407 kPa) from RCTS Tests of Specimen CFD-8a

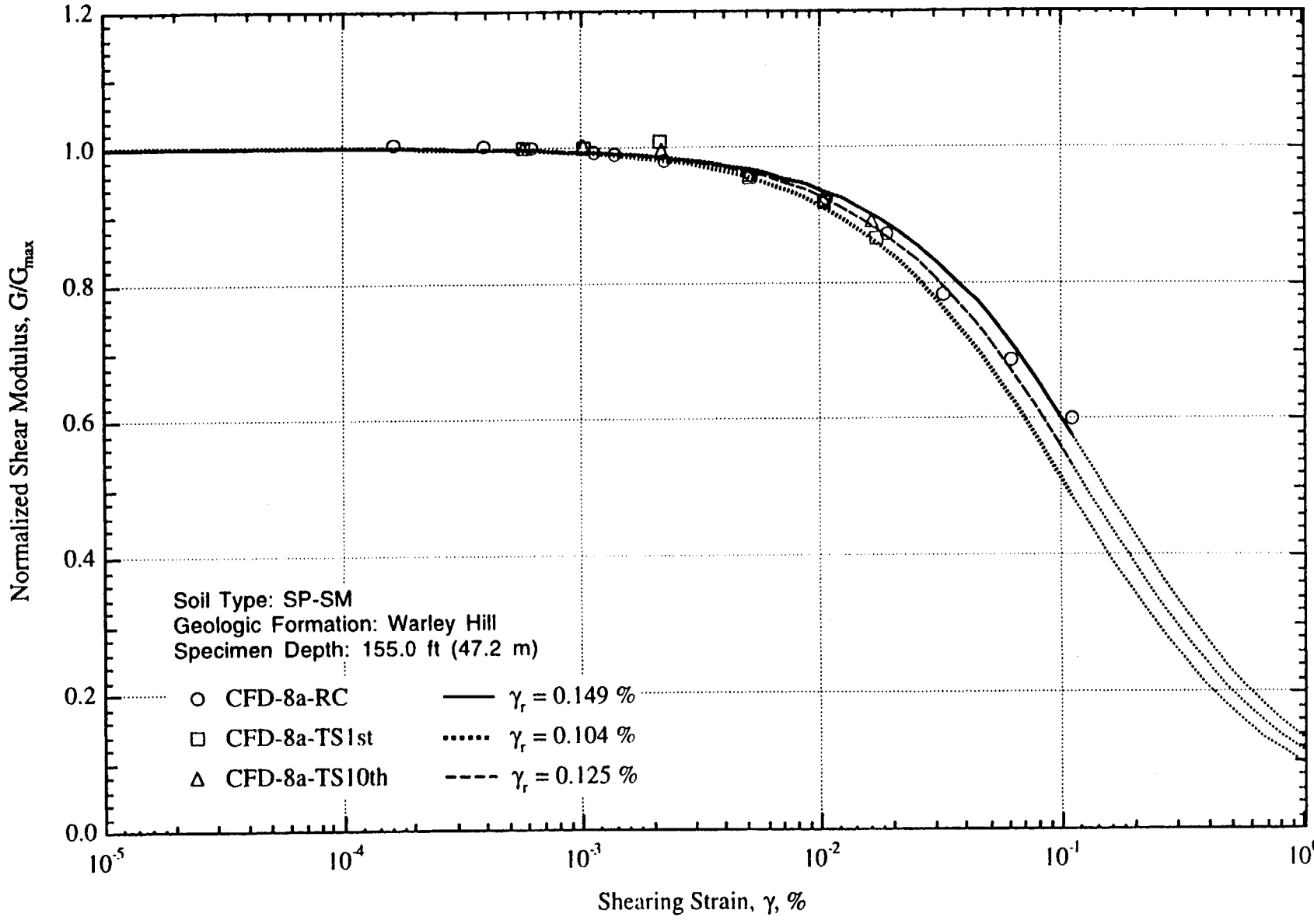


Fig. G.2 Variation in Normalized Shear Modulus with Shearing Strain at an Effective Confining Pressure of 59 psi (=8.49 ksf=407 kPa) from RCTS Tests of Specimen CFD-8a

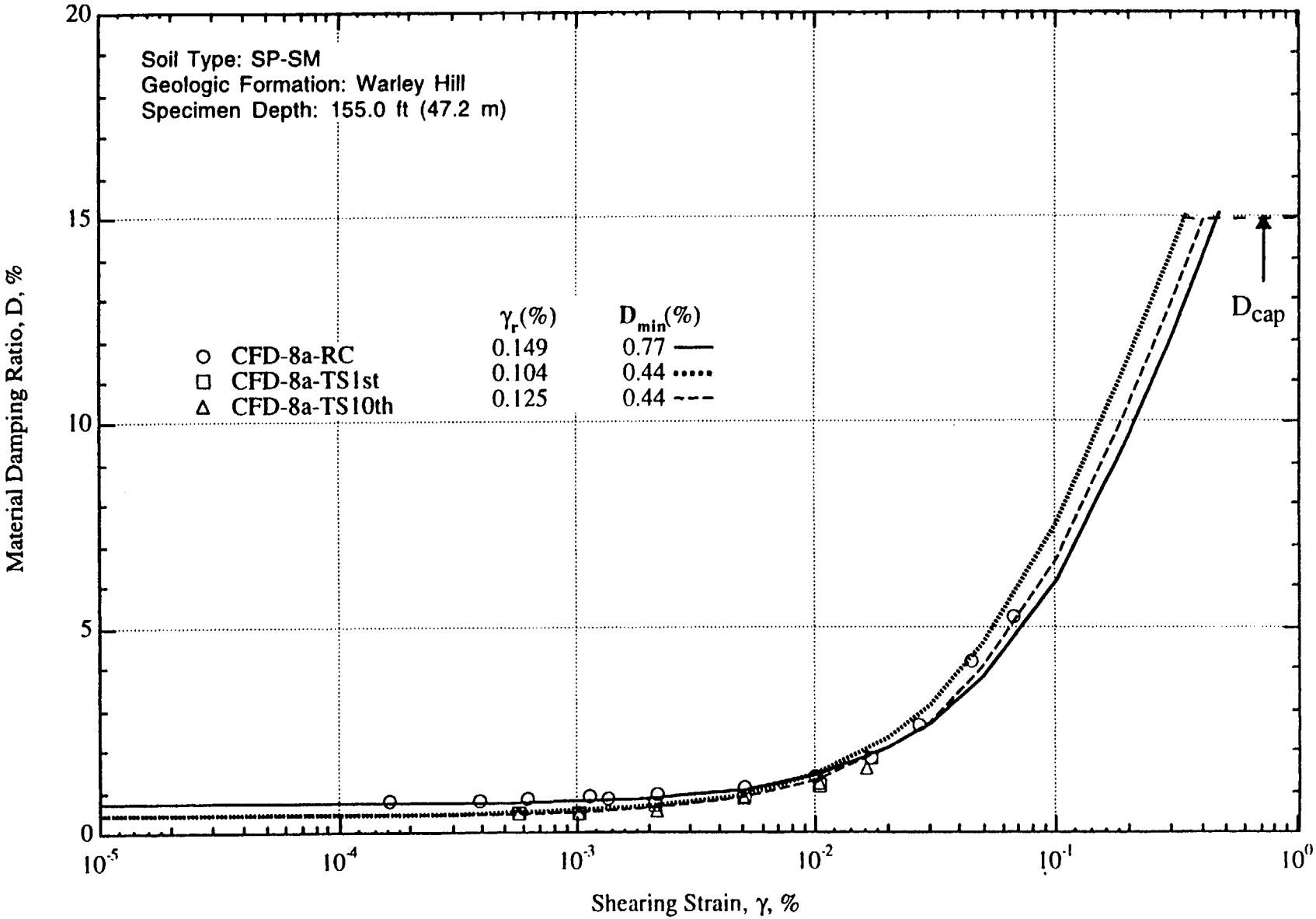


Fig. G.3 Variation in Material Damping Ratio with Shearing Strain at an Effective Confining Pressure of 59 psi (=8.49 ksf=407 kPa) from RCTS Tests of Specimen CFD-8a

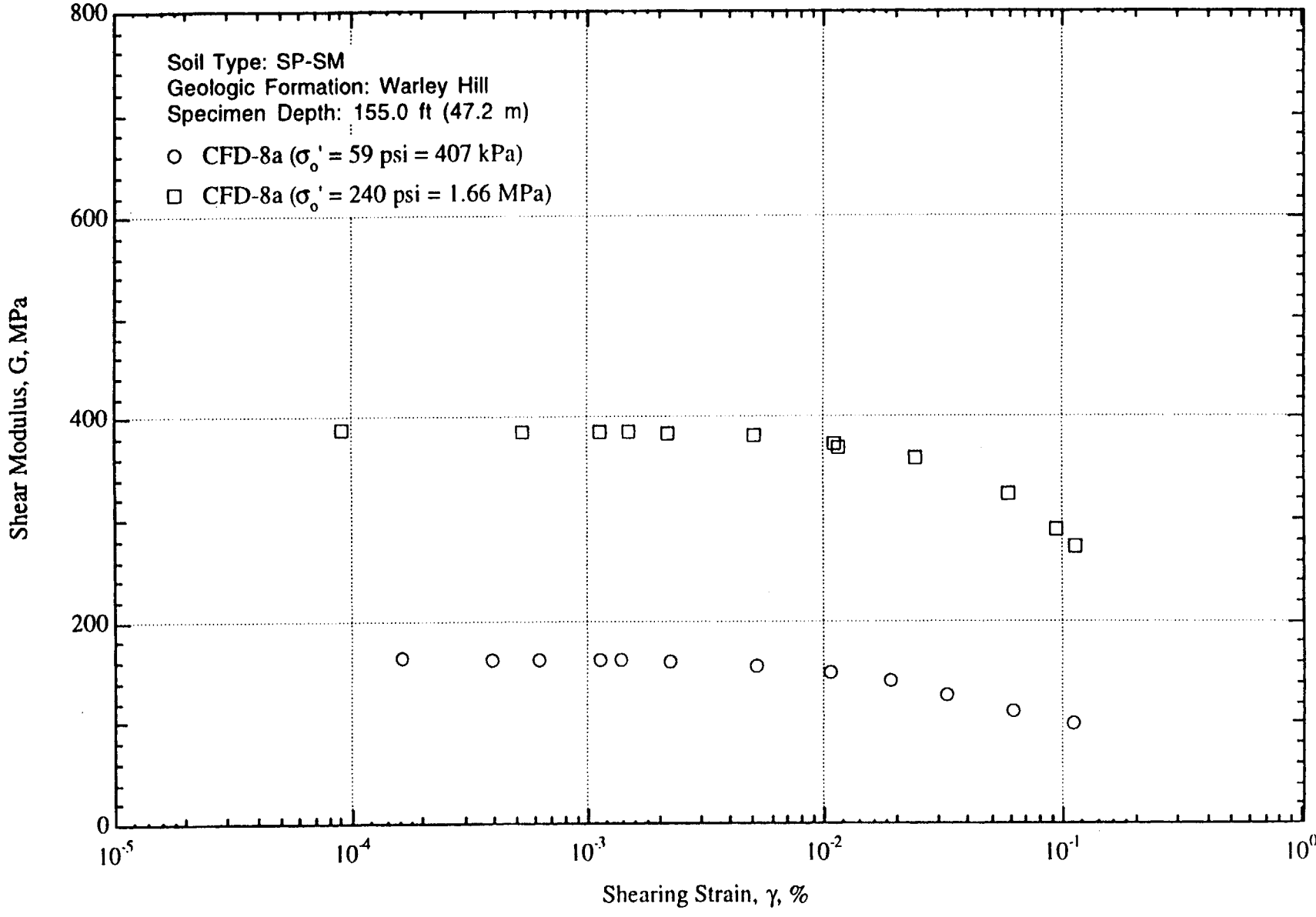


Fig. G.4 Variation in Shear Modulus with Shearing Strain and Effective Confining Pressure from Resonant Column Tests of Specimen CFD-8a

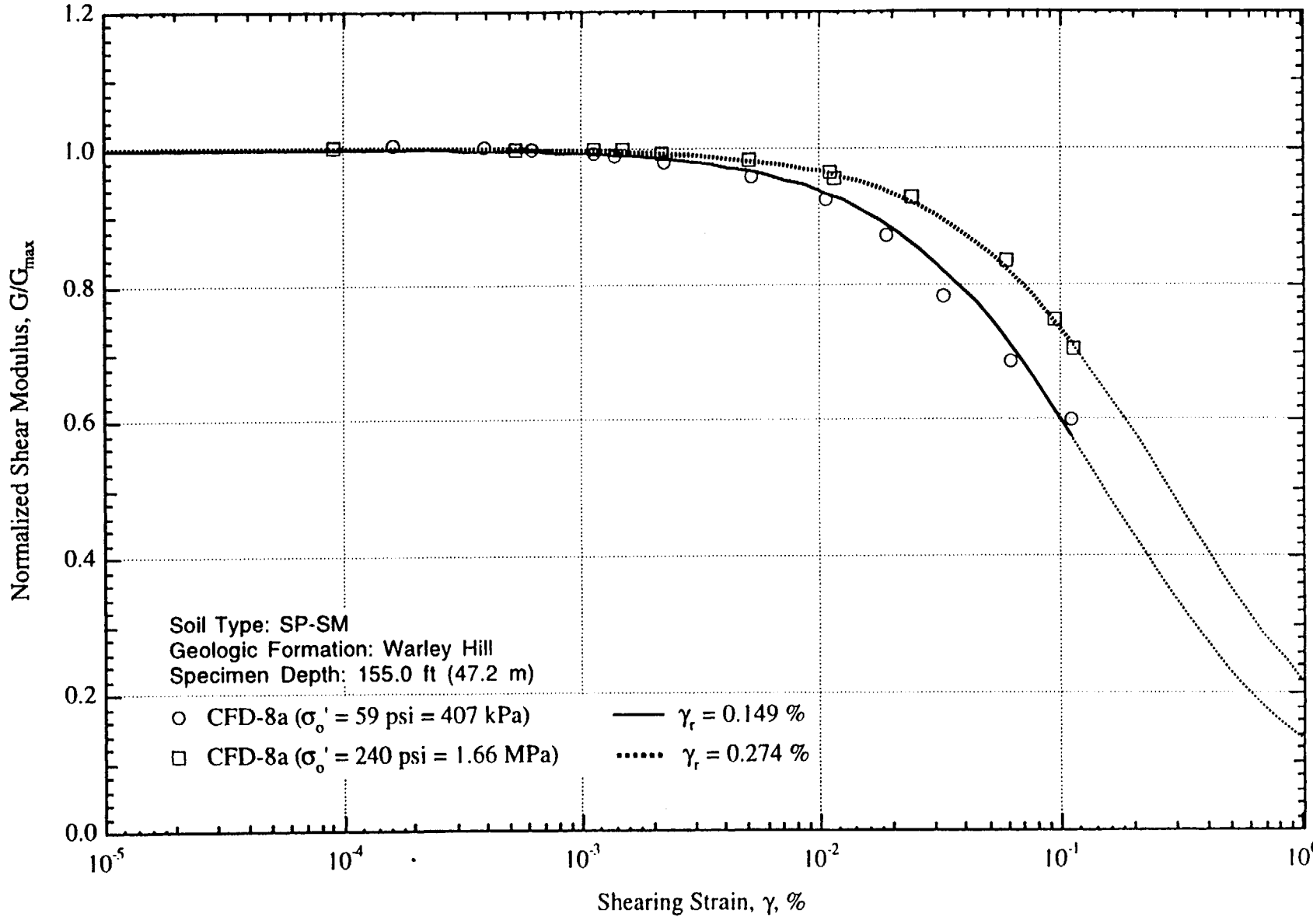


Fig. G.5 Comparison of the Variation in Normalized Shear Modulus with Shearing Strain and Effective Confining Pressure from Resonant Column Tests of Specimen CFD-8a

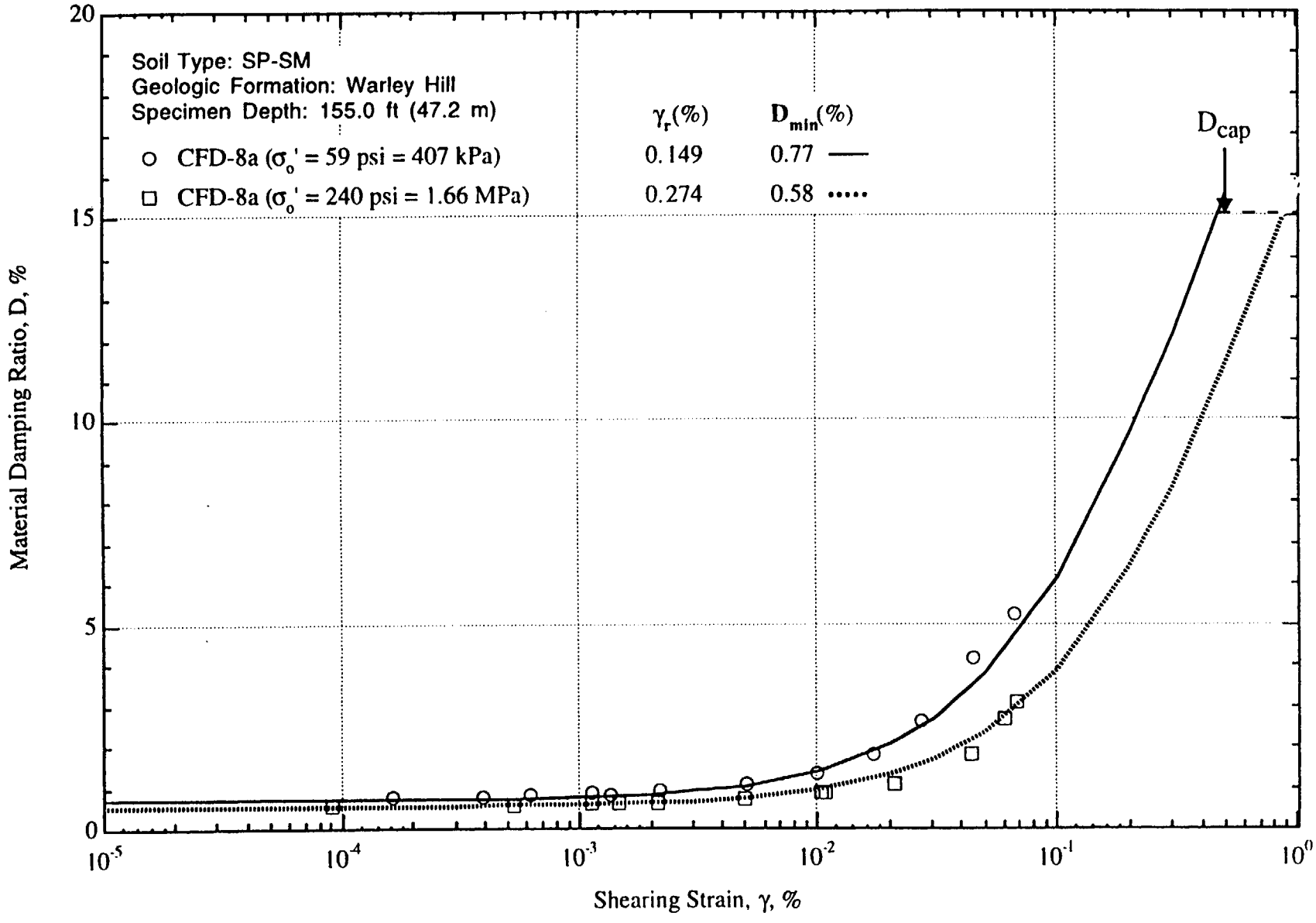


Fig. G.6 Variation in Material Damping Ratio with Shearing Strain and Effective Confining Pressure from Resonant Column Tests of Specimen CFD-8a

# Appendix H

# Effects of Excitation Frequency and Number of Loading Cycles on the Dynamic Properties of Congaree Sands

## (Specimen CFD-11a)

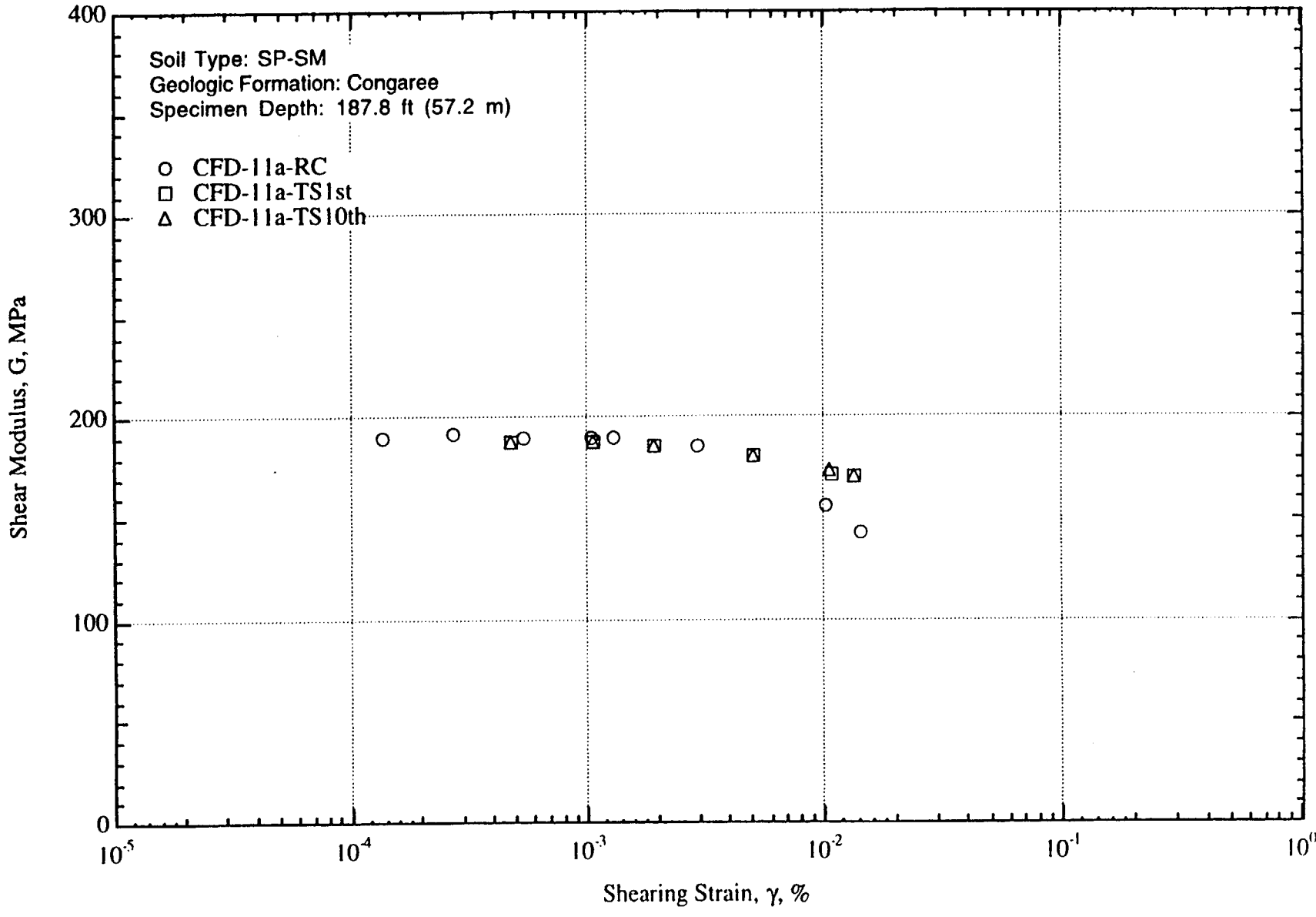


Fig. H.1 Variation in Shear Modulus with Shearing Strain at an Effective Confining Pressure of 68 psi (=9.79 ksf =469 kPa) from RCTS Tests of Specimen CFD-11a

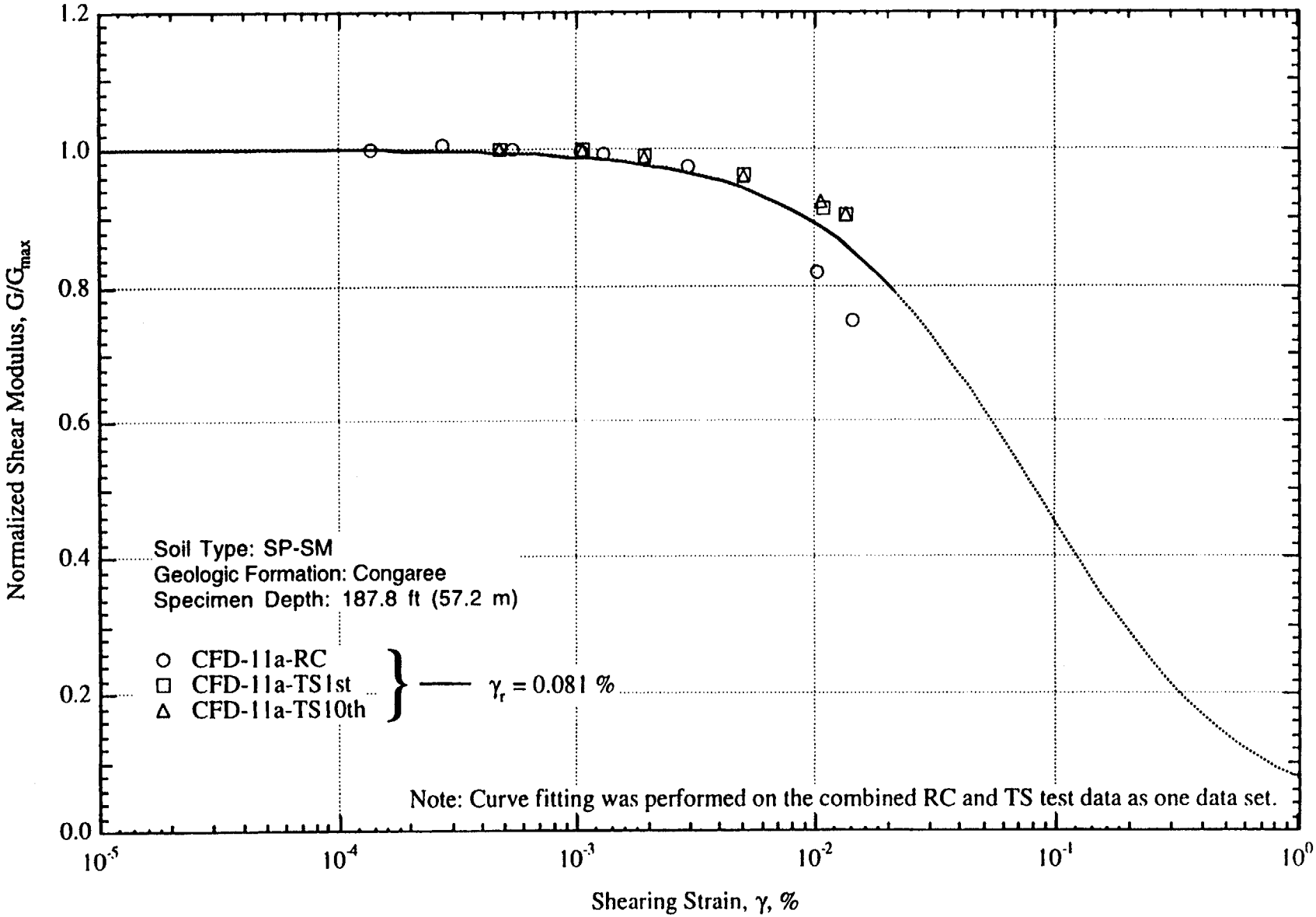


Fig. H.2 Variation in Normalized Shear Modulus with Shearing Strain at an Effective Confining Pressure of 68 psi (=9.79 ksf=469 kPa) from RCTS Tests of Specimen CFD-11a

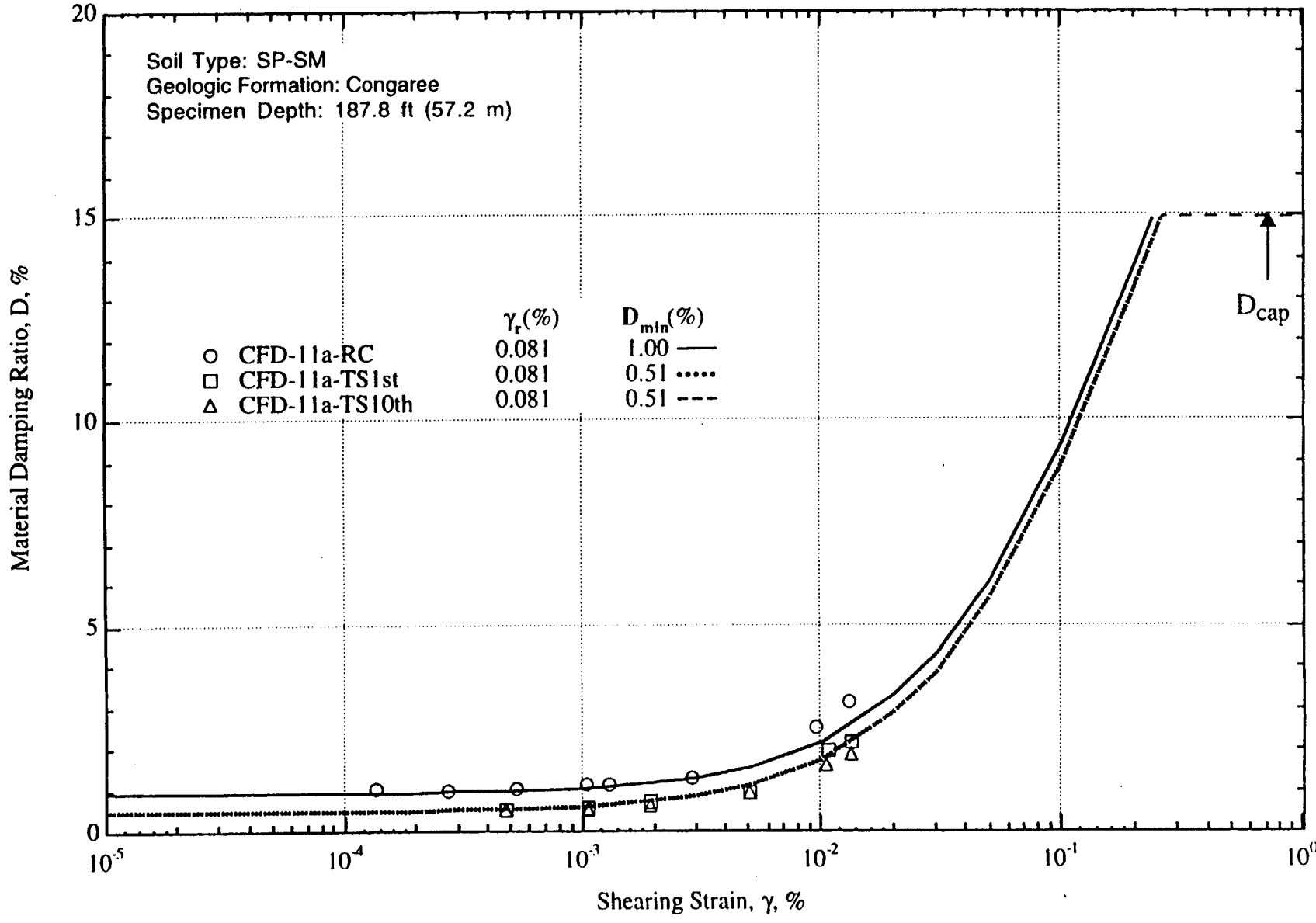


Fig. H.3 Variation in Material Damping Ratio with Shearing Strain at an Effective Confining Pressure of 68 psi (=9.79 ksf=469 kPa) from RCTS Tests of Specimen CFD-11a

# Appendix I

# Effects of Excitation Frequency and Number of Loading Cycles on the Dynamic Properties of Deep Sands (Specimens CFD-T6c)

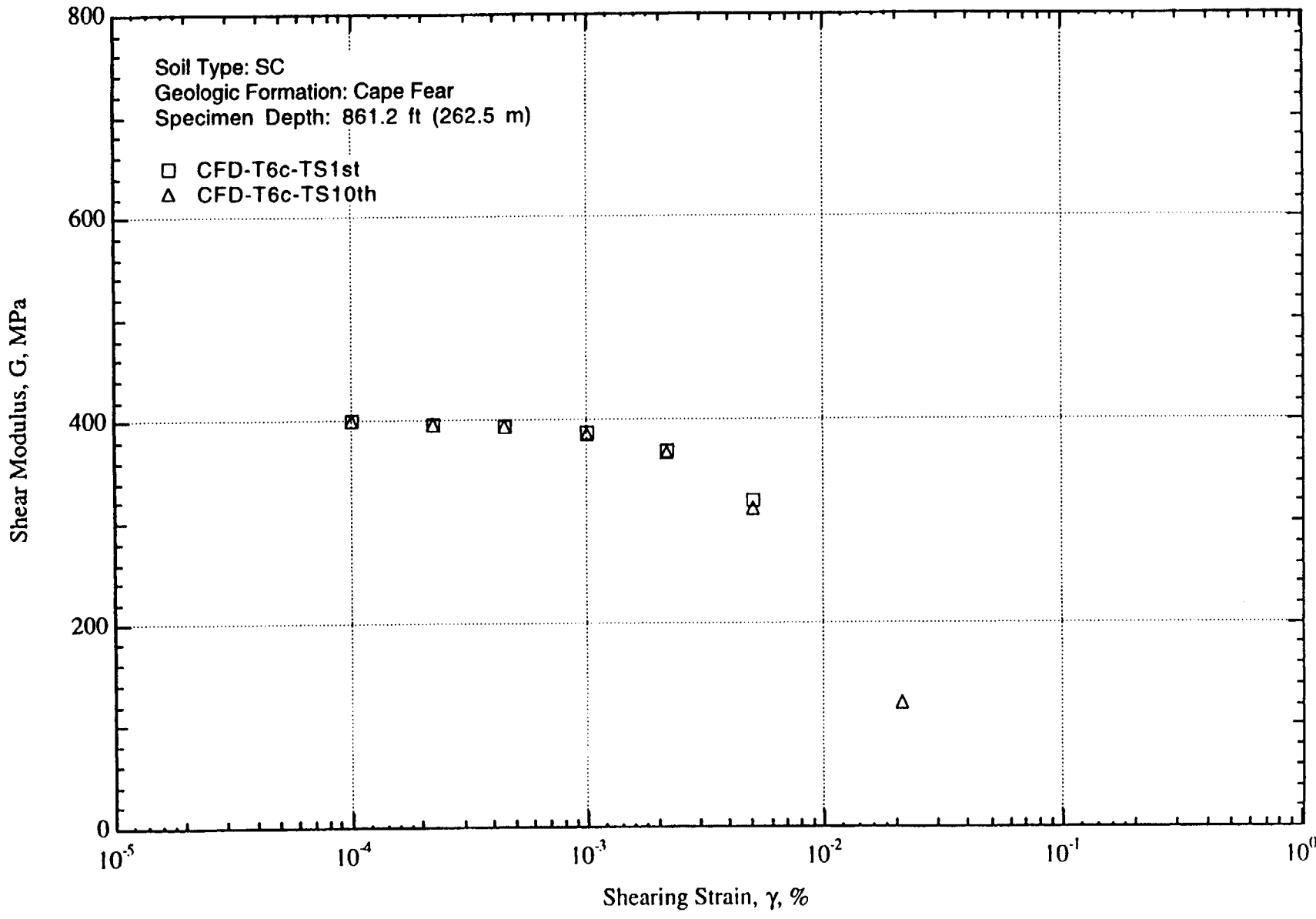


Fig. I.1 Variation in Shear Modulus with Shearing Strain at an Effective Confining Pressure of 247 psi (=35.56 ksf =1.70 MPa) from RCTS Tests of Specimen CFD-T6c

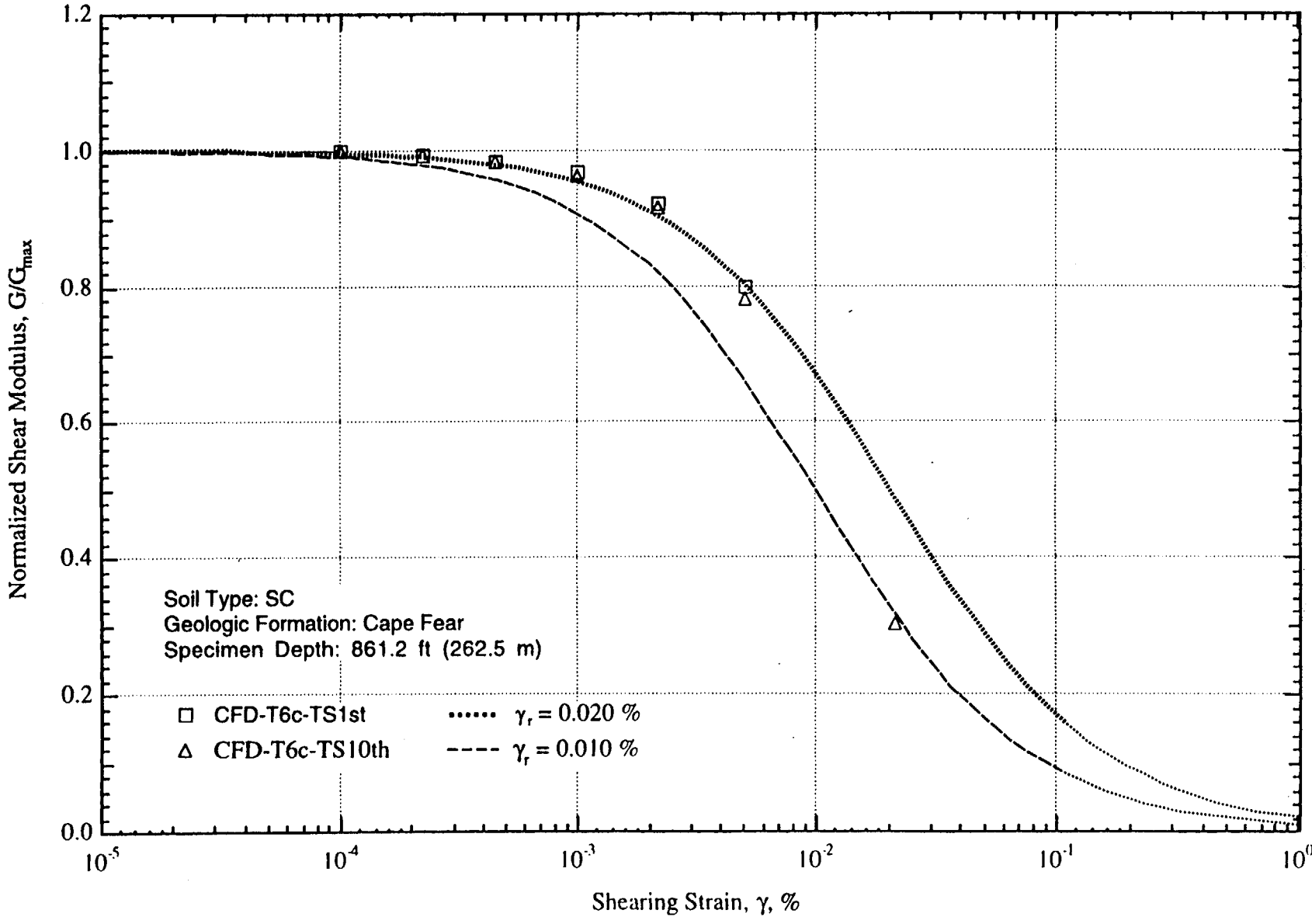


Fig. I.2 Variation in Normalized Shear Modulus with Shearing Strain at an Effective Confining Pressure of 247 psi (=35.56 ksf=1.70 MPa) from RCTS Tests of Specimen CFD-T6c

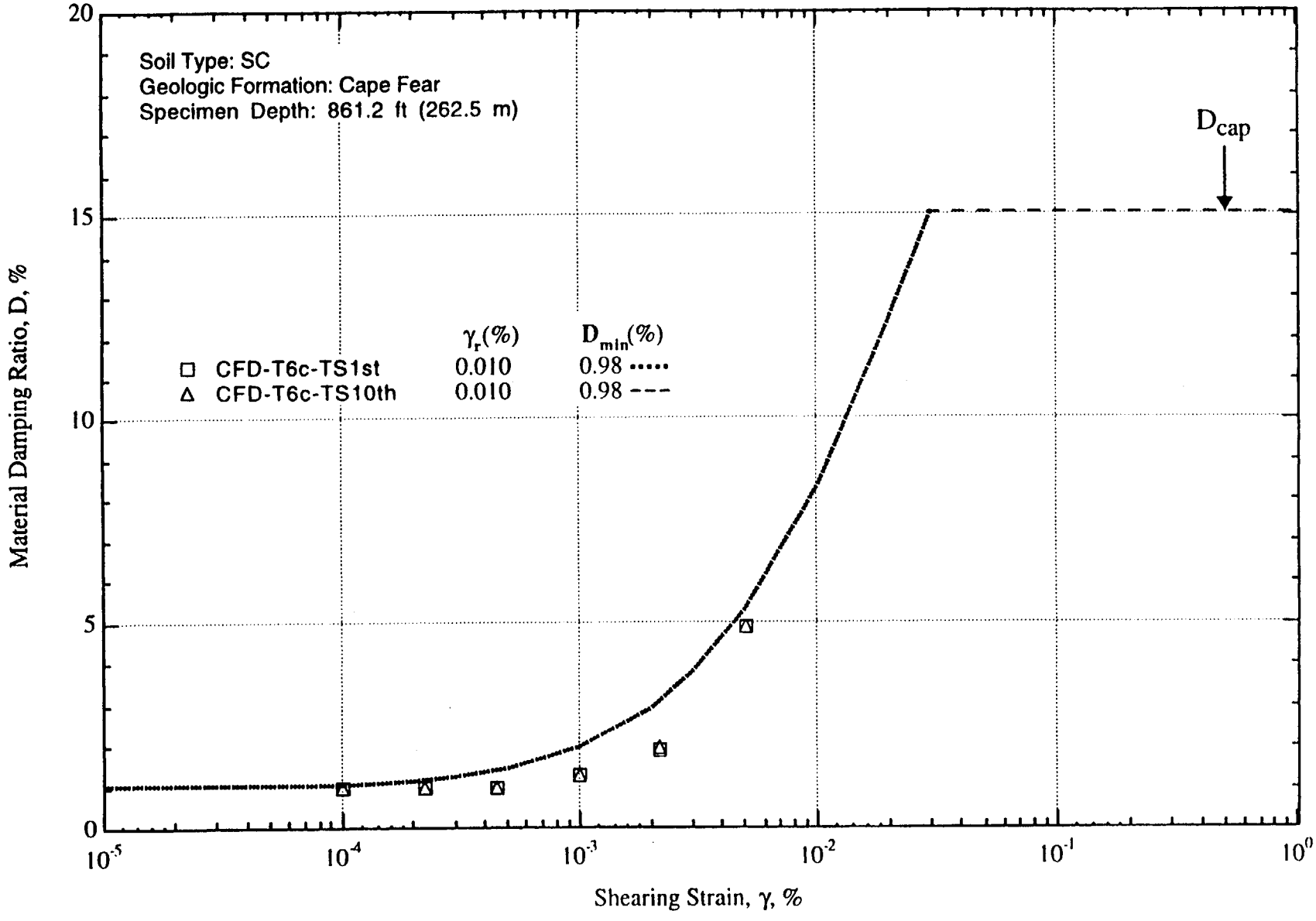


Fig. I.3 Variation in Material Damping Ratio with Shearing Strain at an Effective Confining Pressure of 247 psi (=35.56 ksf=1.70 MPa) from RCTS Tests of Specimen CFD-T6c

# Appendix J
# Effects of Excitation Frequency and Number of Loading Cycles on the Dynamic Properties of Deep Clays (Specimens CFD-T4a and CFD-T5b)

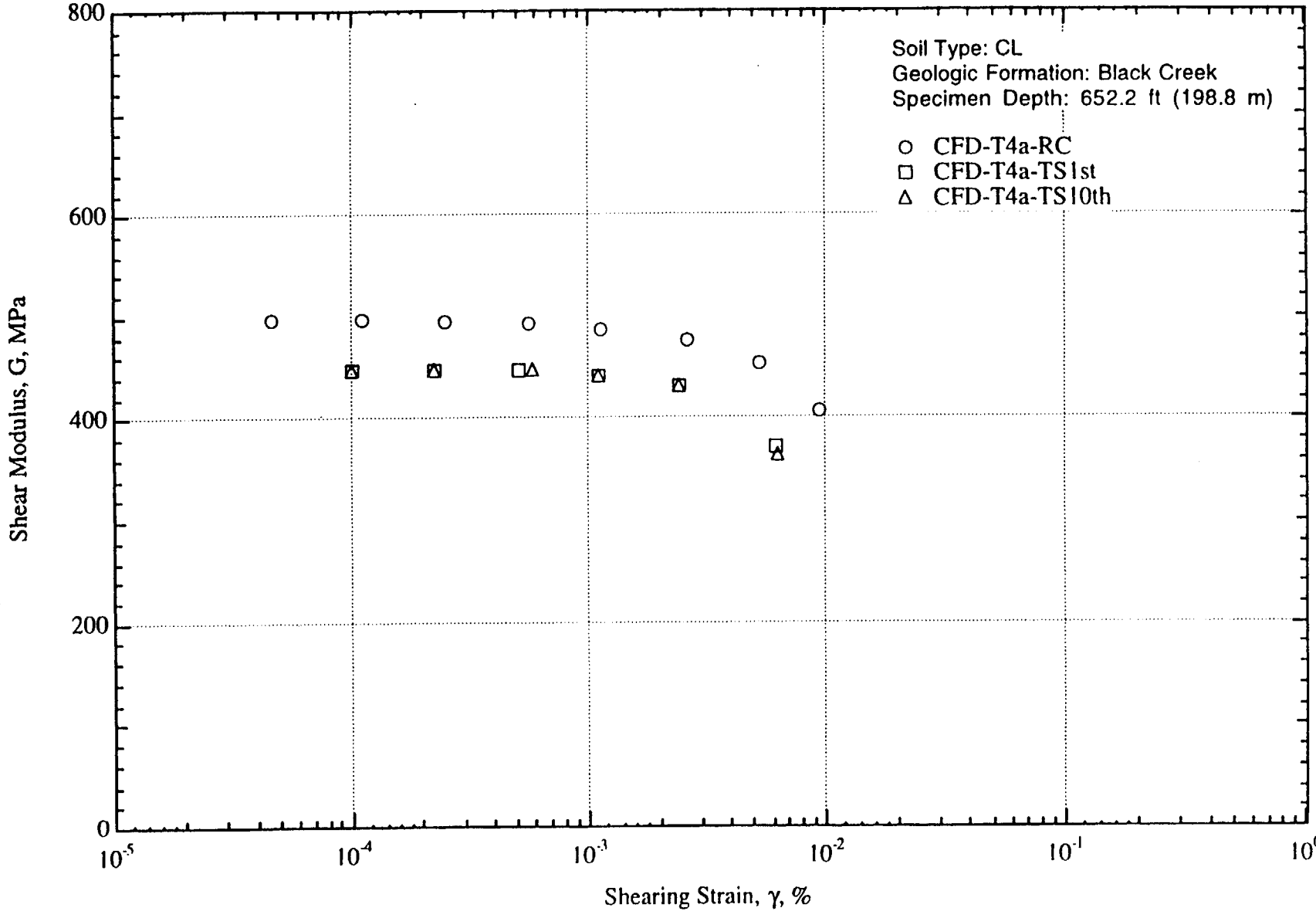


Fig. J.1 Variation in Shear Modulus with Shearing Strain at an Effective Confining Pressure of 191 psi (=27.50 ksf =1.32 MPa) from RCTS Tests of Specimen CFD-T4a

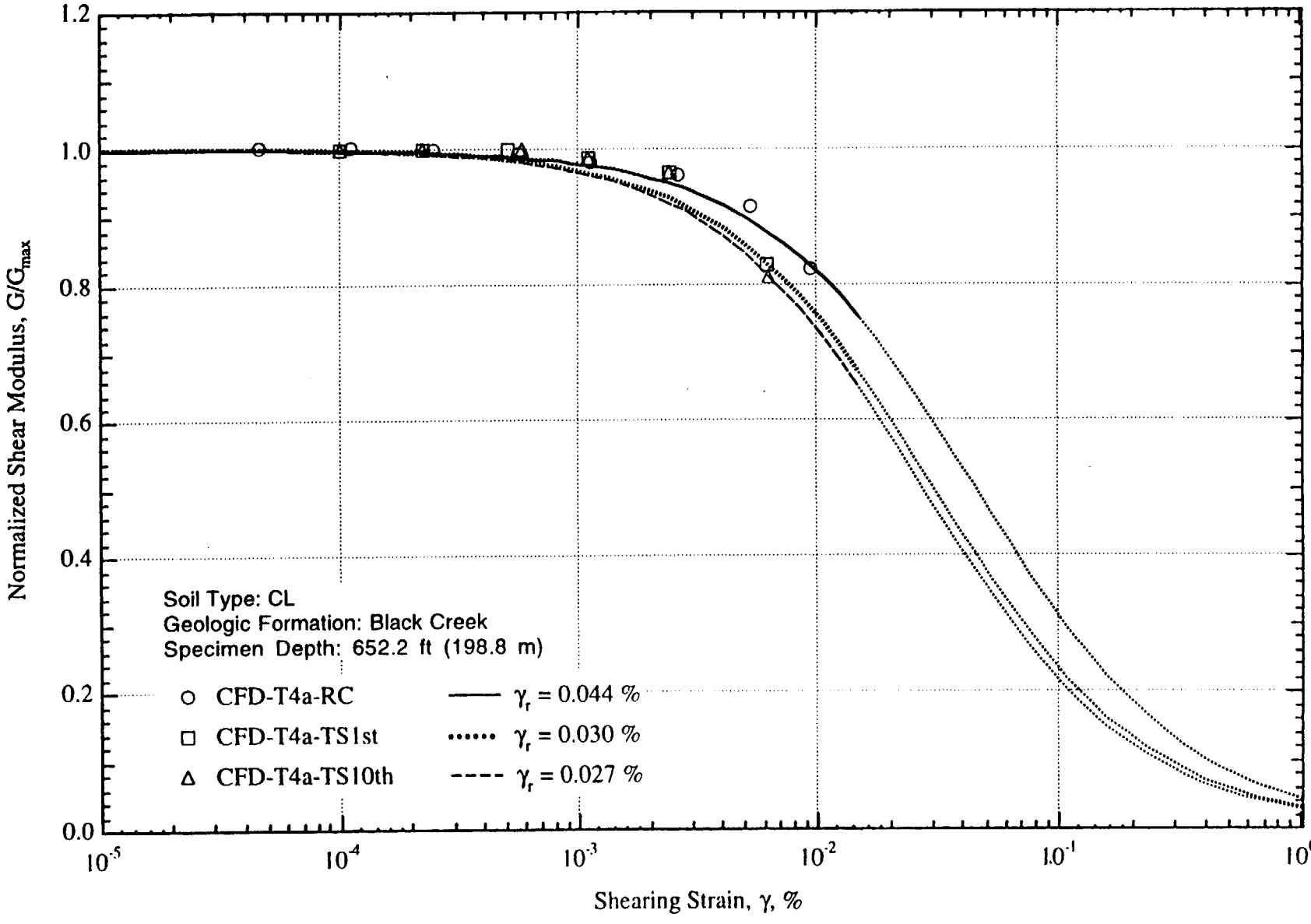


Fig. J.2 Variation in Normalized Shear Modulus with Shearing Strain at an Effective Confining Pressure of 191 psi (=27.50 ksf=1.32 MPa) from RCTS Tests of Specimen CFD-T4a

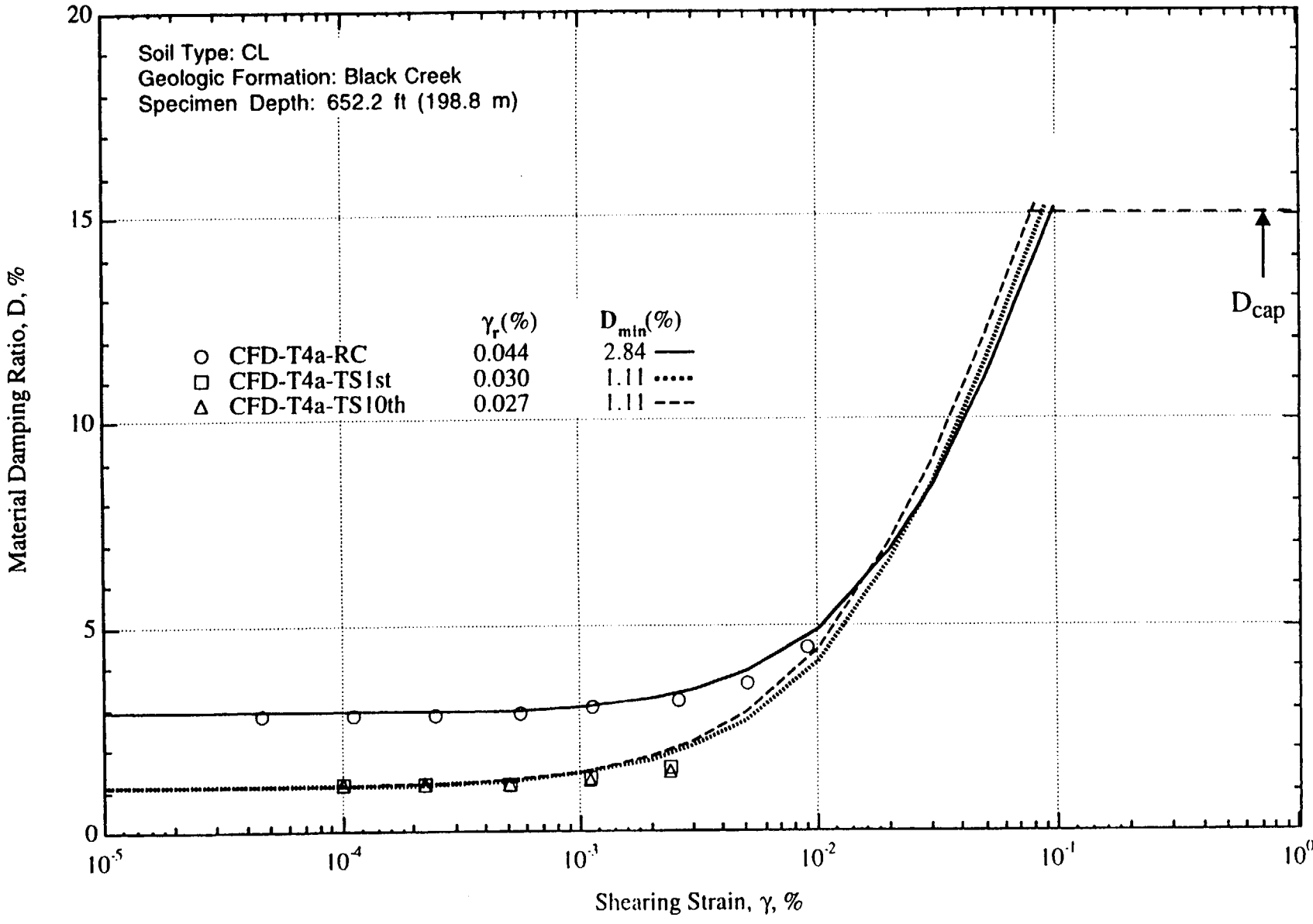


Fig. J.3 Variation in Material Damping Ratio with Shearing Strain at an Effective Confining Pressure of 191 psi (=27.50 ksf=1.32 MPa) from RCTS Tests of Specimen CFD-T4a

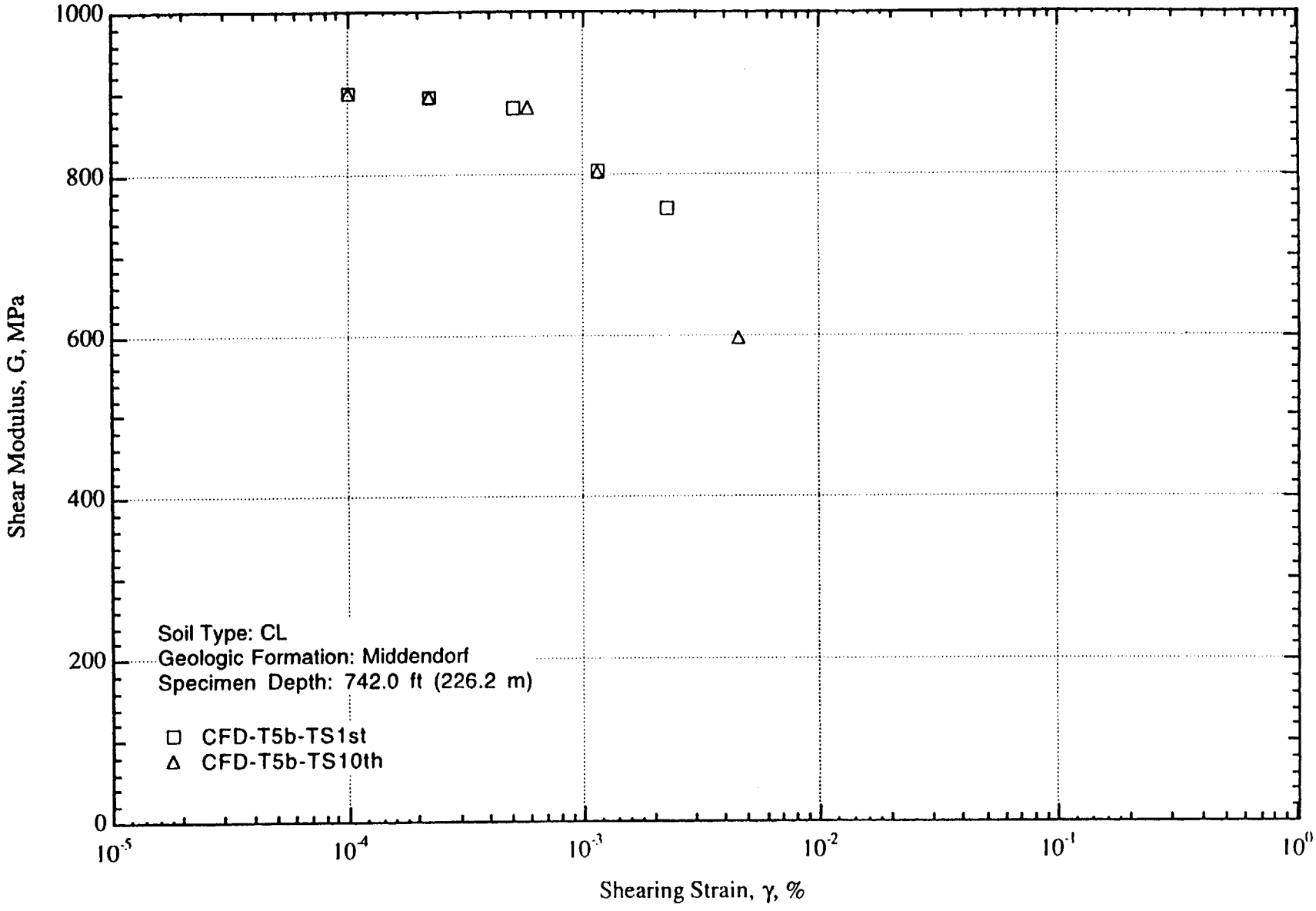


Fig. J.4 Variation in Shear Modulus with Shearing Strain at an Effective Confining Pressure of 215 psi (=30.95 ksf =1.48 MPa) from RCTS Tests of Specimen CFD-T5b

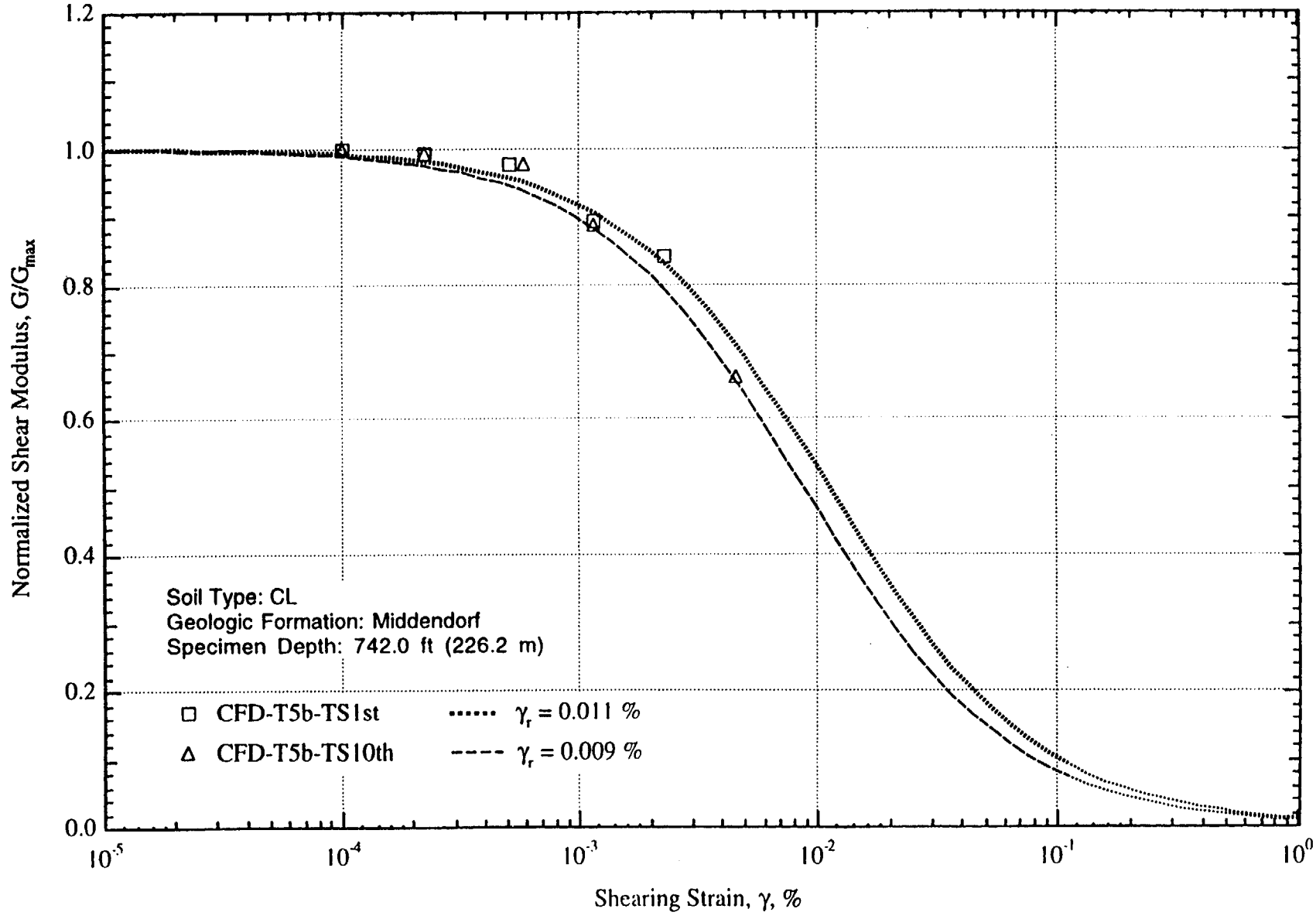


Fig. J.5 Variation in Normalized Shear Modulus with Shearing Strain at an Effective Confining Pressure of 215 psi (=30.95 ksf=1.48 MPa) from RCTS Tests of Specimen CFD-T5b

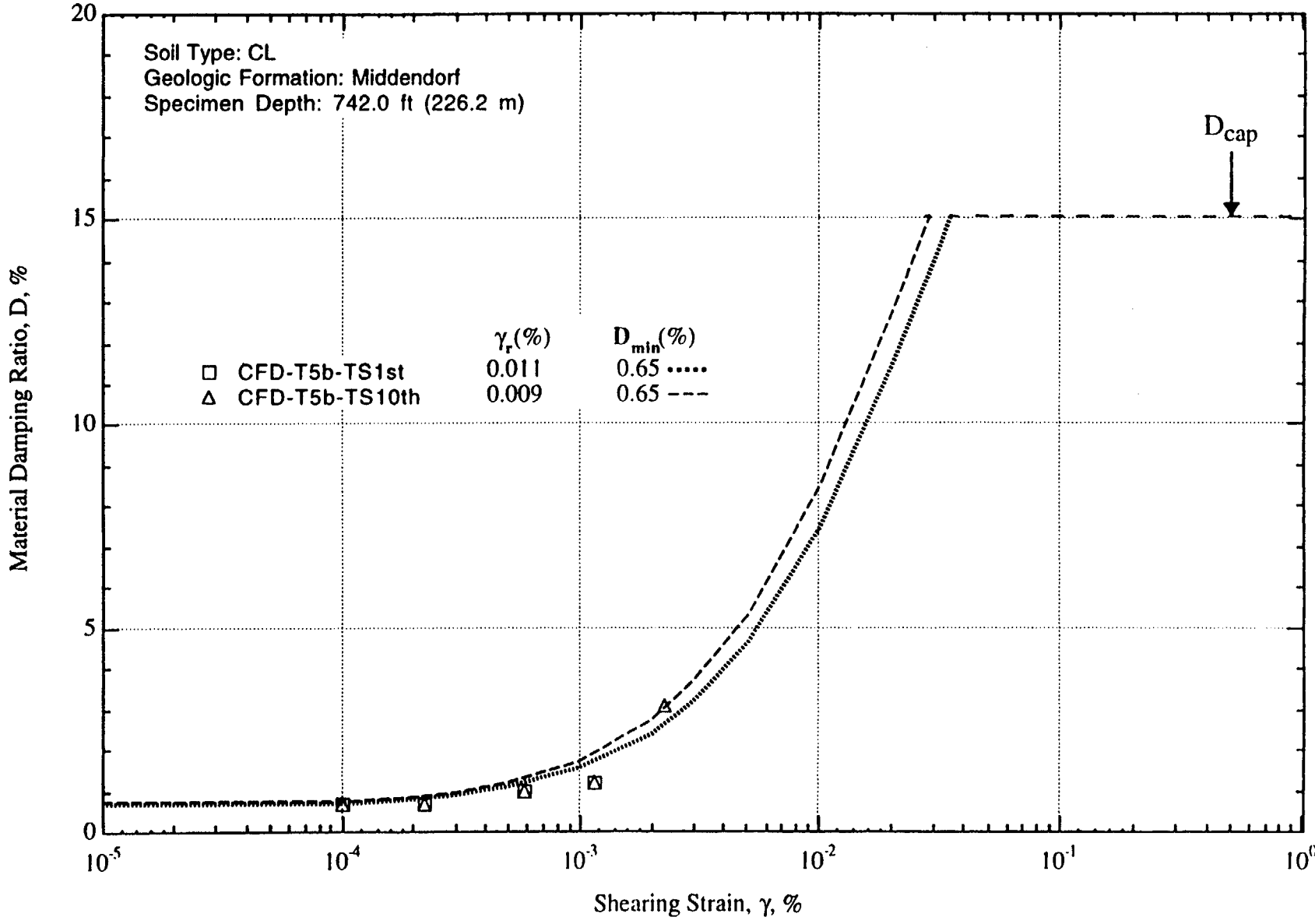


Fig. J.6 Variation in Material Damping Ratio with Shearing Strain at an Effective Confining Pressure of 215 psi (=30.95 ksf=1.48 MPa) from RCTS Tests of Specimen CFD-T5b

WSRC-TR-96-0062
Rev. 0
March 22, 1996

# Investigations of Nonlinear Dynamic Soil Properties at the Savannah River Site (U)

Westinghouse Savannah River Company
Savannah River Site
Aiken, SC 29808

Prepared for the U.S. Department of Energy under contract no. DE-AC09-89SR18035

Westinghouse
Savannah River Company

P.O. Box 616
Aiken, SC 29808

ECSD-SGS-96-0107

March 28, 1996

Brent J. Gutierrez, P.E.
U.S. Department of Energy
Savannah River Operations Office
Post Office Box A
Aiken, SC 29802

Dear Mr. Gutierrez:

ITEM 1- SIGNIFICANT ACCOMPLISHMENT FOR PERIOD 14 - CORRELATION STUDY OF NONLINEAR DYNAMIC SOIL PROPERTIES (U)

The University of Texas, Austin (UTA) final report, "Correlation Study of Nonlinear Dynamic Soil Properties", is enclosed. The purpose of the report is to summarize measurements of SRS soil dynamic properties (including those measured by the UTA) and to make specific recommendations on soil dynamic properties to be used in ground motion predictions. The UTA analysis and recommendations represent a significant advancement in the measurement and application of soil dynamic properties in soils.

A summary document, entitled "Investigations of Nonlinear Dynamic Soil Properties at the Savannah River Site", has been prepared with the assistance and concurrence of a Peer Review Panel, which is documented by their signatures. This summary document reflects and extends the major conclusions of the UTA report.

If you should have any questions, please contact M. E. Maryak (2-6846) or R. C. Lee (2-6938) of my staff.

Very truly yours,

Lawrence A. Salomone

Lawrence A. Salomone
SRS Chief Geotechnical Engineer

LAS:kbk
Att.

CC: J. Kimball, DOE-Germantown, w/o Att.
E. P. Rahe, Jr., 730-B, w/o Att.
S. K. Formby, 730-B, w/o Att.
M. R. Lewis, 730-2B, w/o Att.
F. Loceff, 730-B, w/o Att.
R. C. Lee, 730-2B, w/o Att.

## Disclaimer

WSRC-TR-96-0062
Rev. 0

# Investigations of Nonlinear Dynamic Soil Properties at the Savannah River Site

R.C. Lee

Approved by: Laurence A. Salomone

Prepared for the U.S. Department of Energy under contract no. DE-AC09-89SR18035

## Introduction

This document summarizes laboratory dynamic soil testing investigations conducted by the University of Texas at Austin (UTA) for the Savannah River Site (SRS) (Stokoe et al., 1995a, Stokoe et al., 1995b, Sponseller and Stokoe, 1995). The purpose of the investigations is to provide an evaluation of past testing results in the context of new test data and the development of consistent site wide models of material strain dependencies based upon geologic formation, depth, and relevant index properties. The resulting sets of modulus reduction and damping curves and their uncertainties (Figures 3 through 9; Tables 1 through 3) are intended to provide valuable baseline data for guidance in future analyses of site effects as well as the evaluation of previous site response studies. For future applications, the recommended dynamic properties and their uncertainties are specifically intended for SRS site evaluations and should be appropriately updated when site specific data are collected.

The UTA results and recommendations incorporated in this summary have been reviewed by consultants employed by Westinghouse Savannah River Company (WSRC) or the Department of Energy (DOE), namely, Prof. Carl Costantino, Dr. Robert Pyke, and Dr. Walter Silva. Together with Prof. Kenneth Stokoe, II of the UTA, their signatures at the end of this summary constitute concurrence with the results and recommendations.

The UTA (Stokoe et al., 1995a) summarized various studies conducted for the SRS together with results of new dynamic measurements made from samples taken during the Pen Branch Confirmatory Drilling Program. The particular properties of interest are the non-linear behavior in shear modulus (G) (or normalized shear modulus $G/G_{max}$) and hysteretic damping ratio (D) as functions of induced maximum shear strain ($\gamma$). The data used to assess these relationships were obtained from cyclic triaxial, torsional resonant column and cyclic torsional shear tests conducted on "undisturbed" samples taken at various SRS sites. The data were taken from 29 reports for 17 different site areas at the SRS together with the results from the investigations conducted by UTA for the Pen Branch Fault Confirmatory Drilling Program. The objectives of the program were: (1) to review existing SRS dynamic soil properties test data for the purpose of incorporating the data in a database; (2) to test Pen Branch Fault Confirmatory Drilling Program samples using the latest dynamic testing technology; (3) to construct a dynamic soil properties database with the purpose of deriving possible formation or soil specific correlations of nonlinear dynamic soil properties with parameters of the SRS Coastal Plain sediments; and (4) to provide recommendations for dynamic soil properties associated with the SRS soil column.

## SRS Dynamic Soil Testing Data Review and Database

A dynamic soil properties database was compiled from available SRS reports on dynamic soil properties (Stokoe et al., 1995b). The SRS areas from which data were obtained are: (1) area of the Pen Branch Fault Confirmatory Drilling Program; (2) H-Area In-Tank Precipitation Facility; (3) H-Area Replacement Tritium Facility; (4) H-Area, Building 221-H (5) Proposed New Production Reactor; (6) Par Pond Dam; (7) K-Reactor Area; (8) Burial Ground Expansion; (9) L-Reactor Area; (10) L-Area Cooling Pond Dam; and (11) F-Area, Sand Filter Structure. These 11 areas represent 8 general locations at the SRS and are shown in Figure 1.

### Test Data Limitations

Based on review of the test data presented in these reports, the following conclusions were reached regarding test procedures or methodology in the evaluations of soil properties.

1. All cyclic triaxial test data, previously measured, were excluded based upon a review of the hysteretic data presented in these reports. Equipment related complications are apparent in the hysteretic loops presented in some reports which indicate that piston friction and/or top-cap lifting may have influenced the resultant data generated. These results require a more extensive investigation of the raw data before they could be incorporated into the database.

2. Some resonant column test data, previously measured, were excluded. Three tests which were performed on samples of reconstituted materials were excluded, and 10 tests were excluded which had data presented in graphical form only, making it difficult to evaluate the non-linear behavior.

3. All resonant column damping data were excluded because of strong frequency dependencies observed in the data. Because there were not sufficient data to model the frequency dependence of $D(\log \gamma)$, the higher frequency RC damping measurements made by all organizations (other than UTA) compiled in the database, could not be corrected to the desired lower frequencies typical of TS measurements. Therefore, the recommended $D(\log \gamma)$ functions were estimated from TS measurements only which were performed by UTA at $f < 1$ Hz..

### Dynamic Property Database

Based upon a review of the site descriptions at the SRS facility areas, a general stratigraphic description of the site has been formulated in which the order of the soil layers through the overburden is considered reasonably consistent across the SRS (Figure 2). The specific depths and thickness of the various units, however, are expected to vary somewhat depending upon the particular location at the site. A total of 72 resonant

column (RC) and 15 cyclic torsional shear (TS) tests on "undisturbed" samples were obtained for the various locations at the SRS. Of the 72 samples evaluated, 51 are sand samples taken from the Tobacco Road, Dry Branch, Santee and Snapp formations as shown in Figure 2. The remaining 21 samples were relatively uniformly distributed throughout the other soil layers or are clay samples within these formations.

**Dynamic Soil Testing**

The UTA measured strain dependency of the soil shear modulus ($G(\log \gamma)$) and material damping ($D(\log \gamma)$) by two independent methods (Resonant Column and Torsional Shear) on the same sample and in the same apparatus. Because the RC technique excites the sample at resonance, the frequency (f) of the measurement is inherently higher than the TS frequency. In general, it has been found that both the TS and RC testing lead to similar evaluation of strain dependent shear modulus degradation properties or the strain dependent $G/G_{max}$ ratios. However, significant frequency dependent effects can distort the corresponding hysteretic damping evaluation. These parallel measurements have identified clear first-order dependence of hysteretic damping on excitation frequency. For either the low frequency TS ($f < 1Hz$) or corresponding higher frequency RC testing, machine losses and/or frequency dependent effects associated with the cyclic testing must be quantified to ensure that the measured cyclic loss data are appropriate for application for site response analyses. Therefore, to confidently use the results from RC testing, these frequency dependent effects, if any, must be established and quantified. This can be done by performing complementary TS testing on the same samples.

These experimental results, as well as those from other studies, indicate that for either sands or clays, the cyclic properties are sensitive to the applied loading cycle (N) selected, particularly at the higher level of shear strain. This effect is a result of volume and pore-pressure changes with loading cycle. It is therefore recommended that the values of $G/G_{max}(\log \gamma)$ and $D(\log \gamma)$ be computed from the tenth load cycle ($N=10$) for use in site seismic response analyses. The tenth load cycle was judged to be most appropriate for application to magnitude 6-7 earthquakes. In addition, it is recommended that the highest value of hysteretic damping ratio (D) used in these analyses be limited to 15% since laboratory measurements at higher strain levels are complicated by degeneration of the shape of the stress-strain loops and the applicability of the damping ratio as used in equivalent linear analysis becomes questionable.

**Dynamic Soil Property Correlation and Modeling Results**

The effects of geologic and geotechnical variables on $G/G_{max}(\log \gamma)$ and $D(\log \gamma)$ were considered in this evaluation. Considerations were made on the dependencies by soil type, plasticity index, fines content, small-strain stiffness, state of stress, specimen depth, boring location, geologic age, and geologic formation. From the review of these experimental results, it is observed that the $G/G_{max}(\log \gamma)$ and $D(\log \gamma)$ relationships are primarily dependent on the particular soil type and geologic formation from which the sample was obtained. The Unified Soil Classification system was used to establish soil type for sands

and clays. Effects of plasticity index, fines content, and state of stress are implicitly included in the formation dependency. Confining pressure has only minor effects on $G/G_{max}(\log \gamma)$ and $D(\log \gamma)$. The "sands" and "clays" databases were additionally subdivided into shallow (< 150 m (500 ft)) and deep (>150 m (500 ft) sample depth) categories. Sufficient data were available to establish statistical confidence bands for analysis of correlated data subsets of shallow sands: (1) Tobacco Road; (2) Dry Branch; (3) Santee; and (4) Snapp. There are however, several formations missing from the sands and clays databases. Statistical summaries for $G/G_{max}(\log \gamma)$ and $D(\log \gamma)$ were also compiled for deep sands, shallow clays, and deep clays. Application of specific nonlinear strain dependence is based solely on the soil type and stratigraphy as described in Figure 2.

The experimentally determined cyclic data has been found to be reasonably approximated by the hyperbolic stress-strain model (Hardin and Drnevich, 1972, and Pyke, 1993). Pyke (1993) extended this model to provide a unique and consistent relationship between $G(\log \gamma)$ and $D(\log \gamma)$, given the specific values of the three parameters $G_{max}$ (low strain shear modulus), $D_{min}$ (low-strain hysteretic damping ratio) and $\gamma_r$ (the reference strain defined as the maximum shear stress divided by $G_{max}$) for a particular soil. In general, it has been found that for sands at depths less than 90 m (300 ft), the value of the reference strain increases with depth or mean effective confining pressure. This is similar to the results and recommendations of other studies (e.g., EPRI, 1993). The results for the deeper sands and clays of SRS, however, did not follow this trend. This discrepancy may be due to sample disturbance effects inherent in the procedures used to retrieve samples at these deeper depths, the limitations of the testing procedures for the deep samples or both.

All data (sands and clays) from the deep soil specimens were discarded, and dynamic properties for deeper portions of the soil column were extrapolated from the shallow correlations. To account for the effects of increased confining pressure at the deeper portions of the column, a normalized power law relationship was derived between $\gamma_r$ and the mean effective stress ($\sigma_o'$) and $D_{min}$ and $\sigma_o'$ using test data:

$$\gamma_r / \gamma_{r,m} = ( \sigma_o' / \sigma_m' )^{0.28}$$

and

$$D_{min} = 3.2 \, (\sigma_o')^{-0.16} \quad \text{for clays}$$

$$D_{min} = 1.6 \, (\sigma_o')^{-0.16} \quad \text{for sands}$$

where $\sigma_m'$ is the in situ mean effective stress and $\gamma_{r,m}$ is the reference strain corresponding to the in situ mean effective stress. The dynamic properties ($G/G_{max}(\log \gamma)$and $D(\log \gamma)$) from these samples have been correlated with the site stratigraphy and are presented in terms of best-estimate values together with their variability. Figures 3 through 6 illustrate

the recommended dynamic properties for the following shallow sands:

1. Stiff Upland ($G_{max}$>200MPa)
2. Tobacco Road and Snapp
3. Dry Branch, Santee, Warley Hill, and Congaree Sands (and soft Upland)
4. Unrepresented Shallow Sands (average depth of specimens 35m (116 ft))

The figures show fits to the mean and +- $\sigma$ of the data using the hyperbolic model. In addition, recommendations are presented in Figure 7 for the shallow clays (average depth of 48 m (156 ft)), the deep sands (extrapolated from the shallow sands) and the deep clays (extrapolated from the shallow clays) (Figures 8 & 9 respectively). Figures 10 & 11 illustrate best estimate $G/G_{max}$ and damping curves for the same general site stratigraphy. Comparison of the recommended SRS $G/G_{max}$ curves with those from EPRI (1993) are shown in Figures 12 and 13. Comparisons with EPRI (1993) damping are shown in Figures 14 and 15.

Estimates of the statistical variability in $G/G_{max}$ data are included in Table 1 for the formations described in the general site stratigraphy recommended for the SRS. These estimates are based upon the analysis of data from both RC and TS tests conducted on these formations. Estimates of variability of hysteretic damping ratio are less robust since so few torsional shear test data are available for inclusion in the database. However, based upon the analysis of damping data from seven TS sand samples taken from several formations of the soil column, it is recommended that the standard deviation (natural log) of D (in percent) be set to about 0.3 for strain levels in the range of $1 \times 10^{-4}$ to $1 \times 10^{-2}$ percent. It is recommended that this value be used for all formations in site response calculations until further test data become available or further statistical analysis is pursued (Table 2).

Finally, it has been noted that a rough inverse correlation exists between shear stiffness and hysteretic damping ratio from the TS test data. Based upon this result as well as the subjective judgment of its appropriateness, these correlations may be accommodated in selection of percentiles for $G/G_{max}$ and D in any site response calculations.

**Comparison To Prior SRS Dynamic Soil Models**

Comparisons of these recommendations to a previously developed degradation model for the SRS, known as the GEI (1991) model with its depth dependent factor, are shown in Figures 16 & 17. The GEI model has been used in a number of site response evaluations. The experimental results described above indicate that the degradation properties are related to stratigraphy rather than to a single parameter such as depth. The GEI results compare favorably with the recommended values except that degradation data for the shallow Upland unit and for the shallow and deep clay samples do not correlate well with the GEI model used previously, as can be seen from Figure 16.

Prior ground motion investigations for the SRS that use the GEI recommendations are not expected to differ significantly as a result of this recommendation. Anticipated earthquake-induced strains in the shallow Upland unit are low, further, the GEI shallow dynamic property recommendations were more linear so that ground motion predictions for the Upland formation are conservative. The shallow and deep clay modulus and damping relationship are more linear than GEI (Figures 16 & 17). However, there are no known SRS facility soil column's that have thick clay deposits (that could tend to under-predict larger-strain ground motions using GEI recommended soil properties).

## Conclusions

For application of dynamic soil properties to critical facilities at the SRS, formation dependent degradation models reported herein (Figures 3 through 9; Tables 1 through 3) are considered appropriate for soils or structural analysis. If, for higher hazard facilities, additional site specific sampling and testing is performed, then data correlations described herein should be validated by the new data. If testing is done, additional validation should be done for the recommended variability in D(log $\gamma$) and coupling between $G/G_{max}$(log $\gamma$)and D(log $\gamma$).

For future site characterization or confirmatory analysis, selection of depths for fixed-piston samples should be made on the basis of geologic formation and observed fluctuations in low-strain shear modulus or the occurrence of clay layers with significant thickness (for seismic response purposes, a layer having thickness of one-half of the seismic wavelength or greater at the frequencies of interest). Fixed piston or other samples taken for dynamic testing should not be attempted for depths greater than about 90 m (300 ft) without additional justification or modification of procedures that may insure that disturbance is minimized.

If cyclic triaxial tests are to be used in the future, deformation measurements must be performed on the soil specimen (not platen-to-platen) and the load cell must be placed inside the confining chamber. The resultant loops should be carefully scrutinized to ensure that (a) the loops are reasonably stable for the initial 10 to 15 load cycles, and (b) no particular machine dependent anomalies are apparent in the data generated in the individual loops. It is recommended that the values of $G/G_{max}$ (log $\gamma$) and D(log $\gamma$) be computed from the tenth load cycle (N=10) and measured at $f < 1$ Hz for use in seismic site response analyses. In addition, it is recommended that the highest value of hysteretic damping ratio (D) used in these analyses be limited to 15%. The low-strain damping ($D_{min}$) and D(log $\gamma$) for all specimens were found to be strongly dependent on frequency of the cyclic test. All future dynamic soil testing should account for this dependency by measuring properties at a suite of frequencies (including the site response analysis frequencies) and in-situ stress levels. The frequency effects can be accounted for by a combination of TS and RC tests on all samples.

Kenneth H. Stokoe, II
Department of Civil Engineering
University of Texas at Austin
Austin, TX 78712

Carl Costantino
Department of Civil Engineering
City College of New York
New York, NY 10031

Robert Pyke
Consulting Engineer
1076 Carol Lane #136
Lafayette, CA 94549

Walter Silva
Pacific Engineering and Analysis
311 Pamona Ave.
El Cerrito, CA 94530

## References

Electric Power Research Institute (1993).Guidelines for determining design basis ground motions, EPRI TR-102293, Nov. 1993.

GEI (1991). K-Reactor Area, Geotechnical Investigation for Seismic Issues-Technical Evaluation, Savannah River Site," Project 90375, March. In Volume 1, Part II, Appendix A of K Reactor Area, Geotechnical Investigation for Seismic Issues, Savannah River Site by WSRC, Report WSRC-TR-91-47, March 1991.

Pyke, R.M. (1993). Modeling of Dynamic Soil Properties, Appendix 7.A in Guidelines for Determining Design Basis Ground Motions, Electric Power Research Institute, J.F. Schneider EPRI Project Manager, pp. 7.A-1 - 7.A-90.

Sponseller, T.E. and K.H. Stokoe II (1995). Evaluation of Transportation Vibrations and Laboratory Handling Activities On the Shear Modulus and Material Damping Ratio of Uncemented and Lightly Cemented Loose Sand, University of Texas at Austin report for WSRC.

Stokoe, K.H., S.K. Hwang, M. Darendeli, and N.J. Lee (1995). Correlation Study of Nonlinear Dynamic Soil Properties, University of Texas at Austin Final Report for WSRC, October, 1995.

Stokoe, K.H., II, N.-K. J. Lee, and R.D. Andrus (1995). Review of Dynamic Soil Properties Determined in Previous Studies, University of Texas at Austin report for WSRC.

**Table 1. Statistics Associated with the $G/G_{max}$; Relationships Determined by RC Testing**

| | | Reference Strain[1] $\gamma_r$ (%) | | |
|---|---|---|---|---|
| Formation Description | n | mean | mean + $\sigma$ | mean - $\sigma$ |
| Stiff Upland Sands | 3 | 0.021 | (0.031)[2] | (0.014) |
| Tobacco Road and Snapp Sands | 18 | 0.044 | 0.059 | 0.033 |
| Dry Branch, Santee, Warley Hill and Congaree Sands | 25 | 0.077 | 0.109 | 0.051 |
| Four Mile Sands and any other Unrepresented Shallow Sands | 46 | 0.066 | (0.107) | (0.044) |
| Shallow Clays | 4 | 0.148 | 0.246 | 0.103 |
| Deep Sands | - | 0.111 | 0.221 | 0.068 |
| Deep Clays | - | 0.230 | 0.493 | 0.143 |

Notes: (1) Computation of $G/G_{max}$ mean and +- $\sigma$ for selected value of shear strain is:

$$G/G_{max} = 1/(1+\gamma/\gamma_r)$$

where $\gamma$ is the desired value of shear strain in percent and $\gamma_r$ is the reference strain tabulated. Fit to the mean and +- $\sigma$ of the data was made using hyperbolic model (Pyke, 1993).

(2) Reference strains in parenthesis's were derived on the basis of small sample data sets.

## Table 2. Statistics Associated with the D (log-γ); Relationships Determined by TS Testing

| Formation Description | Ref. Strain $\gamma_r$ (%) | Mean $D_{min}$ (%) | $\sigma^{(1)}$ |
|---|---|---|---|
| Stiff Upland Sands | 0.021 | 1.03 | 0.3 |
| Tobacco Road and Snapp Sands | 0.044 | 0.61 | 0.3 |
| Dry Branch, Santee, Warley Hill and Congaree Sands | 0.077 | 0.88 | 0.3 |
| Four Mile Sands and any other Unrepresented Shallow Sands | 0.066 | 0.71 | 0.3 |
| Shallow Clays | 0.148 | 1.36 | 0.3 |
| Deep Sands | 0.111 | 0.53 | 0.3 |
| Deep Clays | 0.230 | 1.06 | 0.3 |

Notes: (1) σ is ln-normal value that can be applied throughout the strain-range.

## Table 3. Recommended[1] Damping Ratio vs Shear-Strain

Formation Description

| Strain (%) | Upland | Tobacco Rd/Snapp | Dry Branch/Santee | Shallow Sand |
|---|---|---|---|---|
| 0.00001 | 1.059 | 0.625 | 0.825 | 0.674 |
| 0.0001 | 1.059 | 0.625 | 0.825 | 0.674 |
| 0.0002 | 1.103 | 0.647 | 0.835 | 0.687 |
| 0.0003 | 1.151 | 0.67 | 0.846 | 0.702 |
| 0.0005 | 1.248 | 0.717 | 0.871 | 0.733 |
| 0.001 | 1.493 | 0.835 | 0.936 | 0.811 |
| 0.002 | 1.973 | 1.07 | 1.07 | 0.97 |
| 0.003 | 2.434 | 1.3 | 1.205 | 1.127 |
| 0.005 | 3.302 | 1.747 | 1.47 | 1.435 |
| 0.01 | 5.201 | 2.79 | 2.108 | 2.171 |
| 0.02 | 8.165 | 4.605 | 3.281 | 3.505 |
| 0.03 | 10.407 | 6.139 | 4.336 | 4.686 |
| 0.05 | 13.639 | 8.614 | 6.162 | 6.692 |
| 0.1 | 18.317 | 12.799 | 9.605 | 10.363 |
| 0.2 | | 17.425 | 13.951 | 14.825 |
| 0.3 | | | 16.683 | |

Formation Description

| Strain (%) | Shallow Clay | Deep Sand | Deep Clay |
|---|---|---|---|
| 0.00001 | 1.296 | 0.489 | 0.992 |
| 0.0001 | 1.296 | 0.489 | 0.992 |
| 0.0002 | 1.292 | 0.497 | 0.99 |
| 0.0003 | 1.293 | 0.505 | 0.991 |
| 0.0005 | 1.3 | 0.524 | 0.995 |
| 0.001 | 1.326 | 0.57 | 1.013 |
| 0.002 | 1.389 | 0.665 | 1.054 |
| 0.003 | 1.456 | 0.759 | 1.097 |
| 0.005 | 1.594 | 0.945 | 1.186 |
| 0.01 | 1.938 | 1.398 | 1.410 |
| 0.02 | 2.603 | 2.251 | 1.851 |
| 0.03 | 3.233 | 3.039 | 2.276 |
| 0.05 | 4.392 | 4.453 | 3.08 |
| 0.1 | 6.82 | 7.289 | 4.856 |
| 0.2 | 10.356 | 11.179 | 7.671 |
| 0.3 | 12.884 | 13.799 | 9.833 |
| 0.5 | 16.317 | 17.21 | 12.995 |

Notes: (1) Recommended curves derived using hyperbolic model (Pyke, 1993).

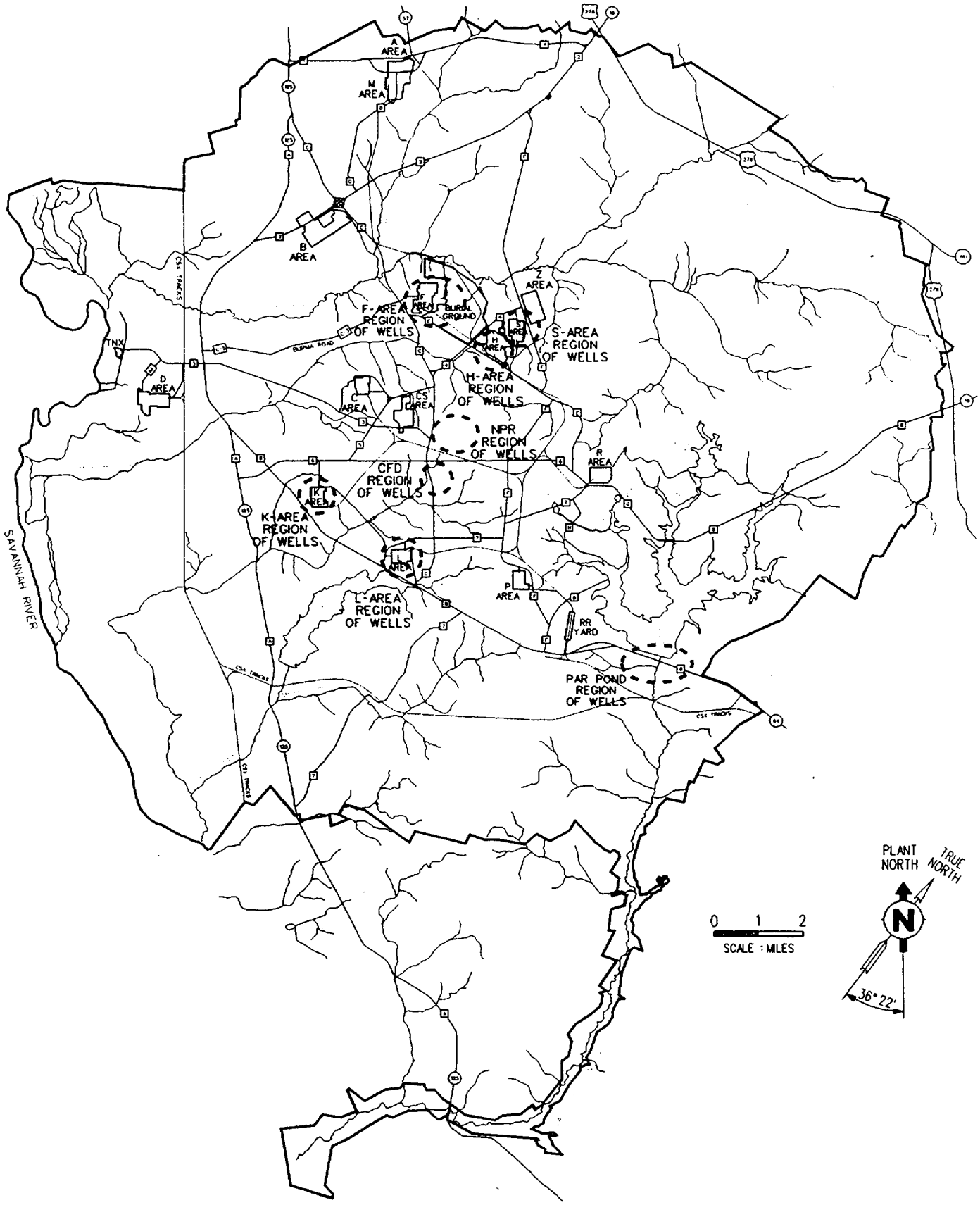


Fig. 1 Map of Savannah River Site Showing the General Boring (Well) Locations of All Specimens Used in the Correlation Database.

| Elevation (ft) | Geologic Formation | Depth (ft) | Number of Specimens | |
|---|---|---|---|---|
| | | | Sand | Clay |
| 248 | | 0 | (3) | (0) |
| 218 | Upland | 30 | (18) | (1) |
| | Tobacco Road | | | |
| 174 | | 74 | (13) | (2) |
| | Dry Branch | | | |
| 125 | | 123 | | |
| | Santee | | (16) | (0) |
| 58 | | 190 | (2) | (0) |
| 43 | Warley Hill | 205 | | |
| | Congaree | | (1) | (0) |
| -4 | | 252 | (0) | (0) |
| -30 | Four Mile | 278 | (4) | (1) |
| -55 | Snapp | 303 | | |
| | Sawdust Landing | | (0) | (0) |
| -122 | | 370 | | |
| | Steel Creek | | (0) | (1) |
| -242 | | 490 | | |
| | Black Creek | | (4) | (1) |
| -517 | | 765 | | |
| | Middendorf | | (1) | (1) |
| -657 | | 905 | | |
| | Cape Fear | | (3) | (0) |
| -795 | | 1043 | | |
| | Basement | | | |

Note: Stratigraphic profile taken from boring CFD 18.

Fig. 2 General Stratigraphic Profile of the Savannah River Site.

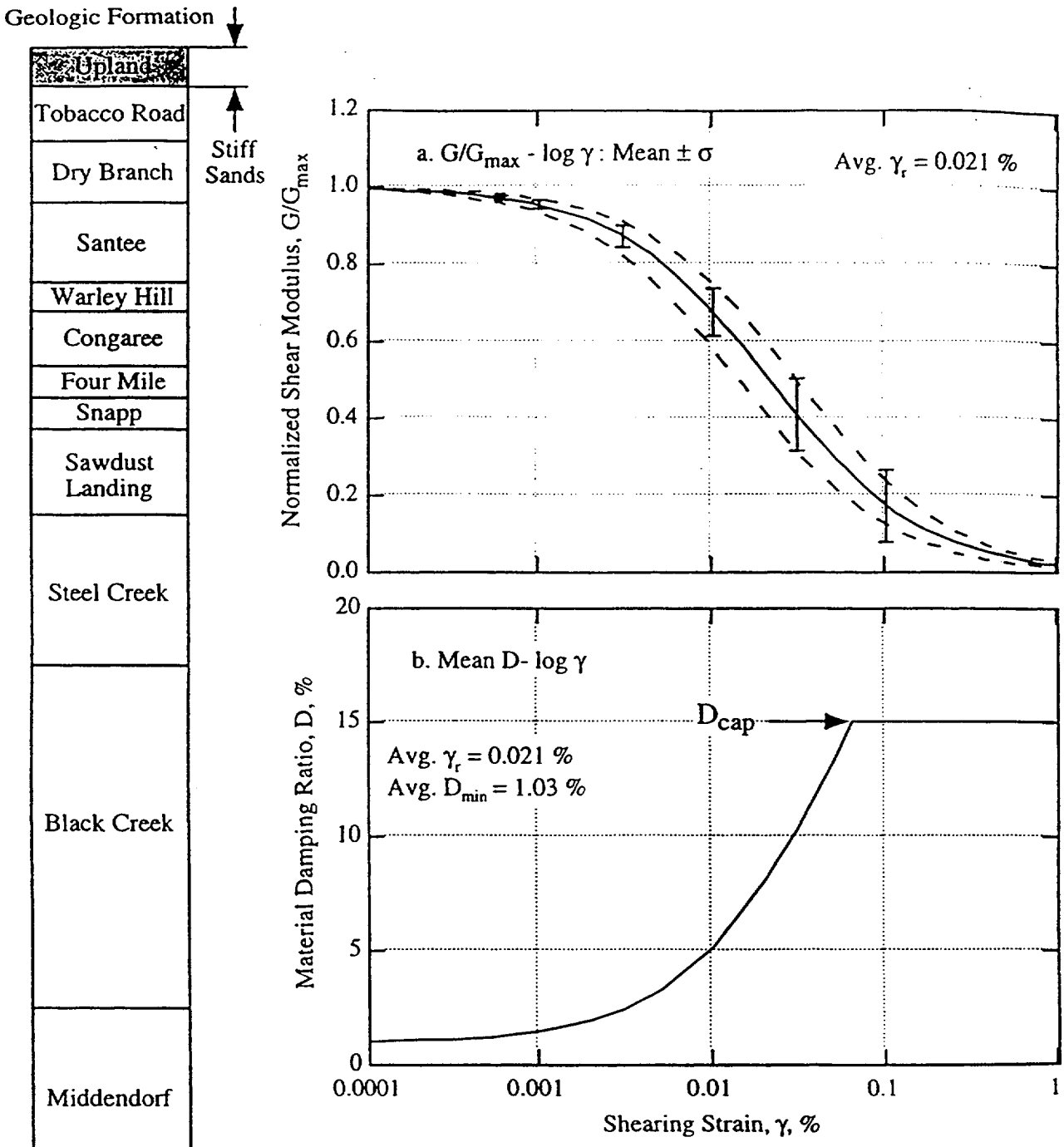


Notes: 1. Stratigraphic profile taken from boring CFD 18.
2. Standard deviations taken from generic shallow sand relationship shown in Fig. 119 and given in Table 24.
3. Stiff sands are defined as those with $G_{max} > 200$ MPa.
4. For soft Upland sands ($G_{max} < 100$ MPa) use relationships shown in Fig. 123.
5. Values of D evaluated at f ≤1 Hz.

Fig. 3 Recommended $G/G_{max}$ (log-γ) and D (log-γ) relationships for Stiff Upland Sands at SRS (taken from Stokoe et al., 1995). Numerical values for best estimates and uncertainties for $G/G_{max}$ (log-γ) and D (log-γ) can be determined from Tables 1, 2, and 3.

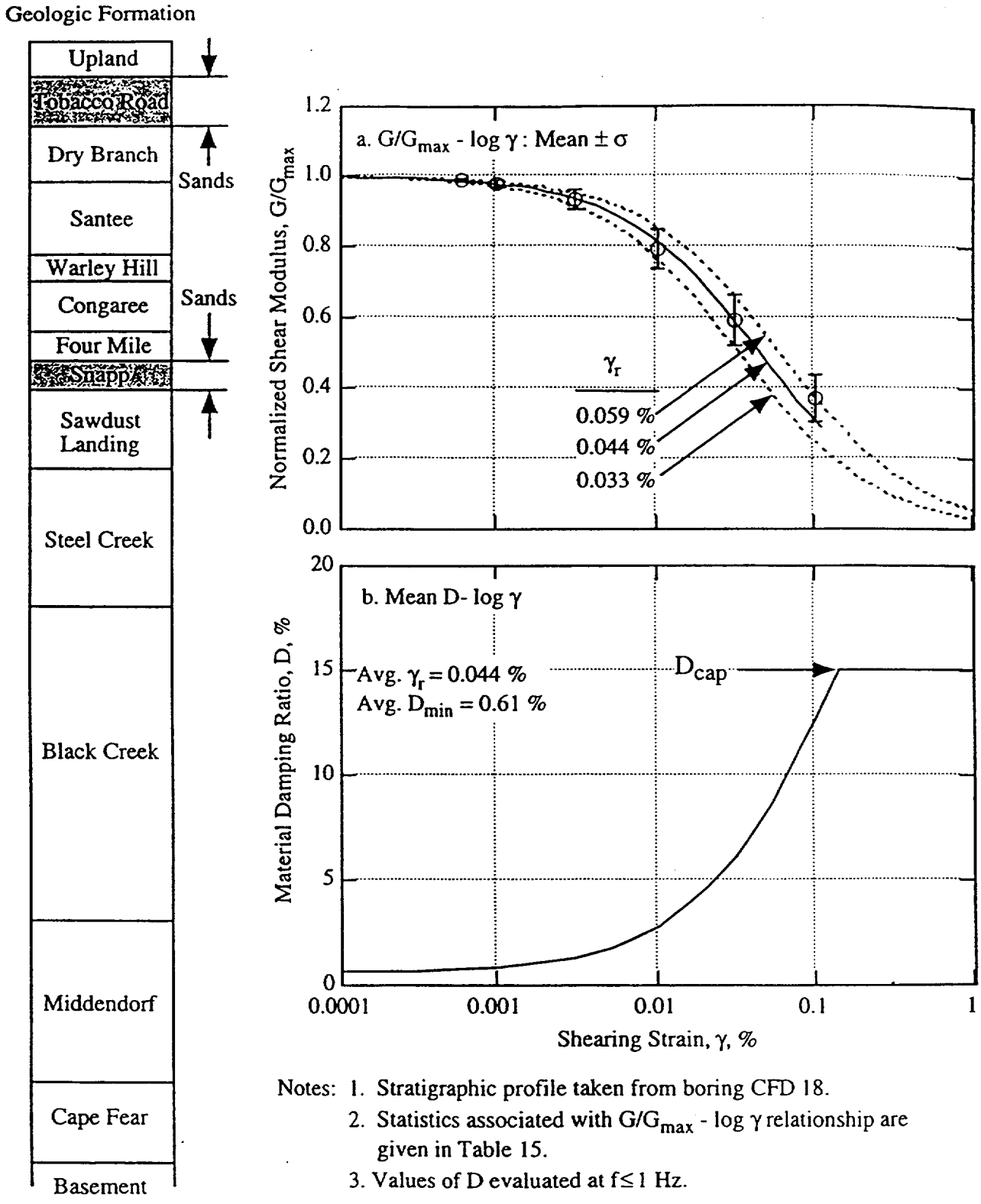


Notes: 1. Stratigraphic profile taken from boring CFD 18.
2. Statistics associated with $G/G_{max}$ - log γ relationship are given in Table 15.
3. Values of D evaluated at f≤1 Hz.

Fig. 4 Recommended $G/G_{max}$ (log-γ) and D (log-γ) relationships for Tobacco Road and Snapp Sands at SRS (taken from Stokoe et al., 1995). Numerical values for best estimates and uncertainties for $G/G_{max}$ (log-γ) and D (log-γ) can be determined from Tables 1, 2, and 3.

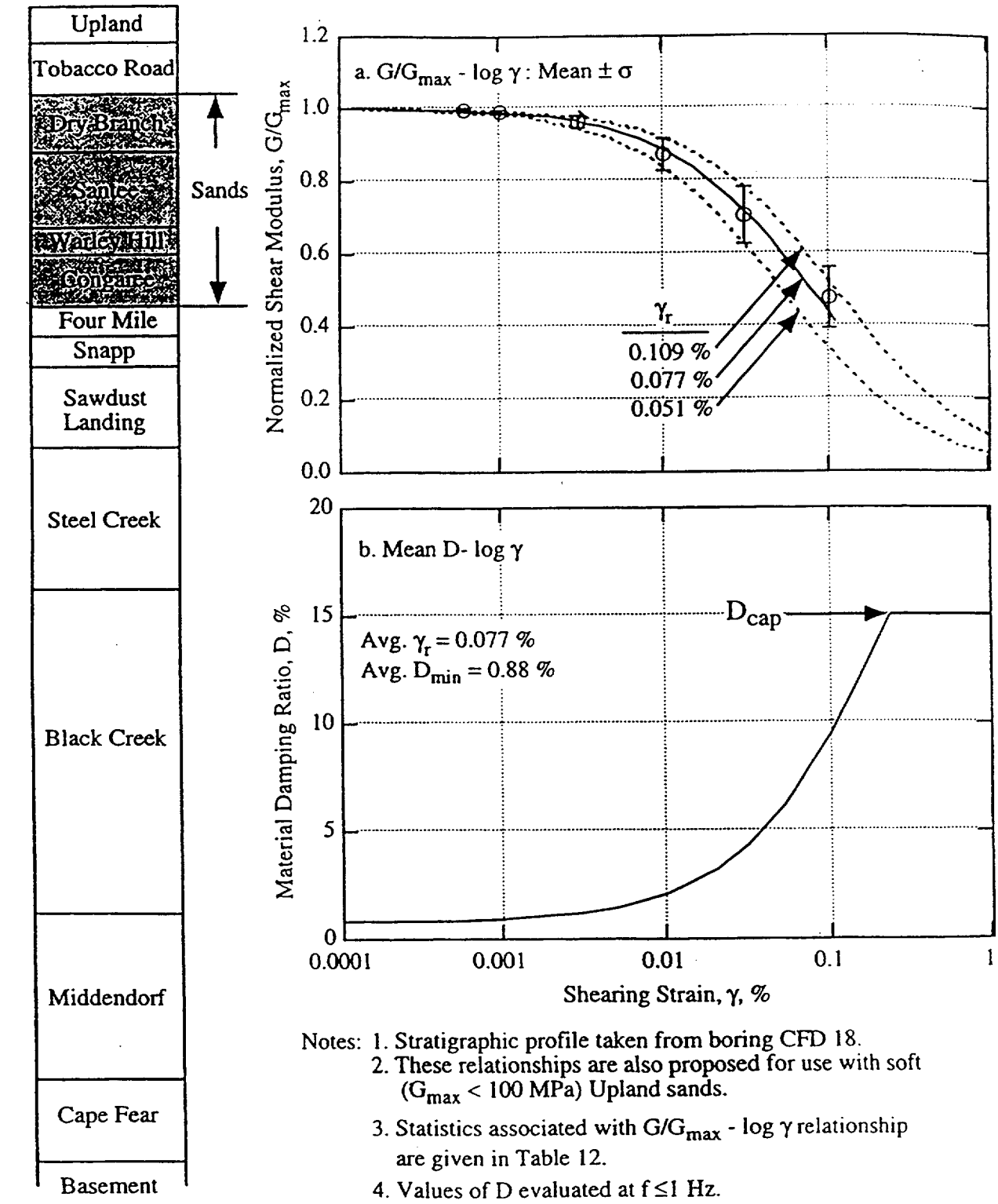


Notes: 1. Stratigraphic profile taken from boring CFD 18.
2. These relationships are also proposed for use with soft ($G_{max}$ < 100 MPa) Upland sands.
3. Statistics associated with $G/G_{max}$ - log γ relationship are given in Table 12.
4. Values of D evaluated at f ≤1 Hz.

Fig. 5 Recommended $G/G_{max}$ (log-γ) and D (log-γ) relationships for Dry Branch, Santee, Warley Hill and Congaree Sands at SRS (taken from Stokoe et al., 1995). Numerical values for best estimates and uncertainties for $G/G_{max}$ (log-γ) and D (log-γ) can be determined from Tables 1, 2, and 3.

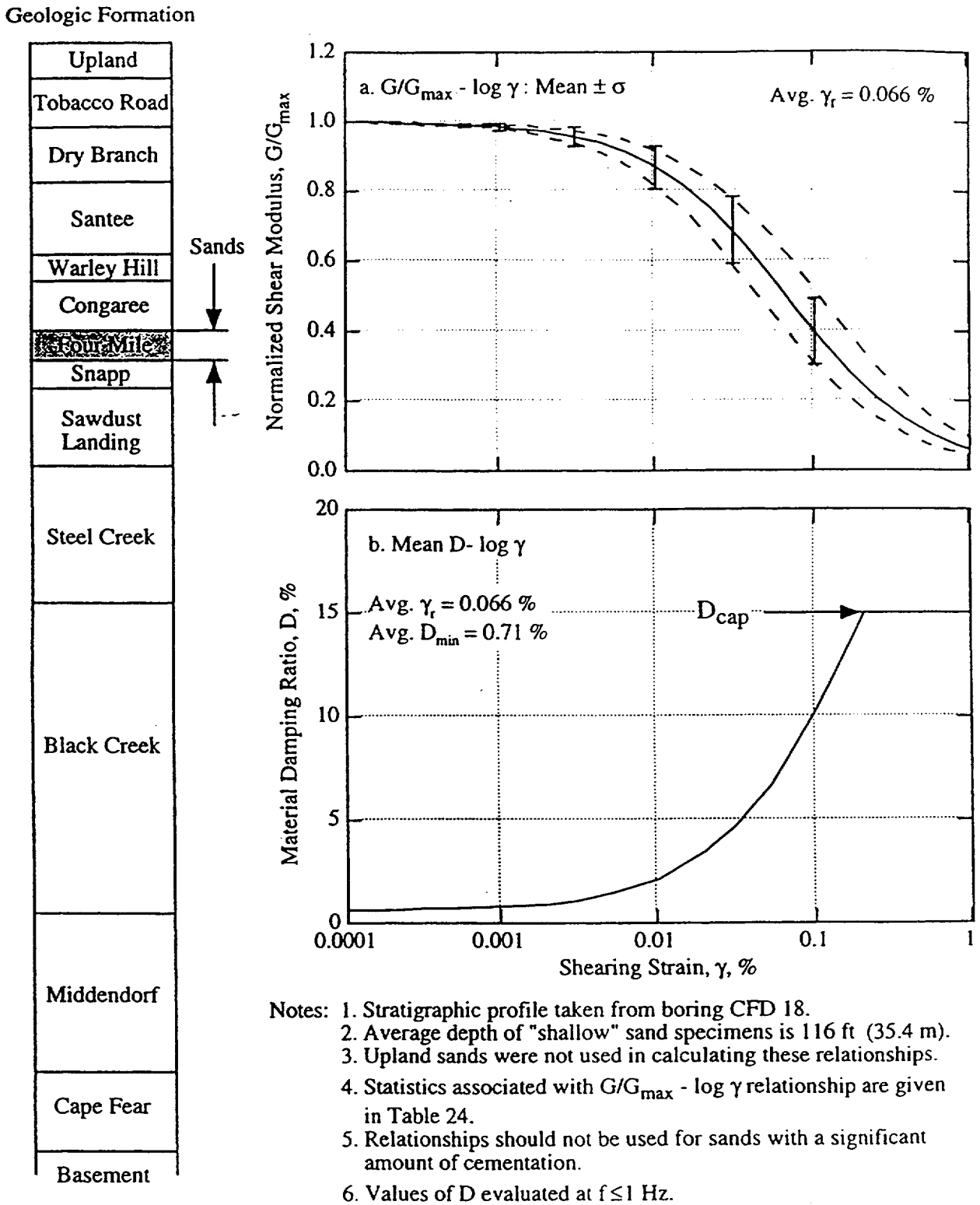


Notes:
1. Stratigraphic profile taken from boring CFD 18.
2. Average depth of "shallow" sand specimens is 116 ft (35.4 m).
3. Upland sands were not used in calculating these relationships.
4. Statistics associated with $G/G_{max}$ - log γ relationship are given in Table 24.
5. Relationships should not be used for sands with a significant amount of cementation.
6. Values of D evaluated at $f \leq 1$ Hz.

Fig. 6 Recommended $G/G_{max}$ (log-γ) and D (log-γ) relationships for Four Mile Sands and any other unrepresented shallow sand formation at SRS (taken from Stokoe et al., 1995). Numerical values for best estimates and uncertainties for $G/G_{max}$ (log-γ) and D (log-γ) can be determined from Tables 1, 2, and 3.

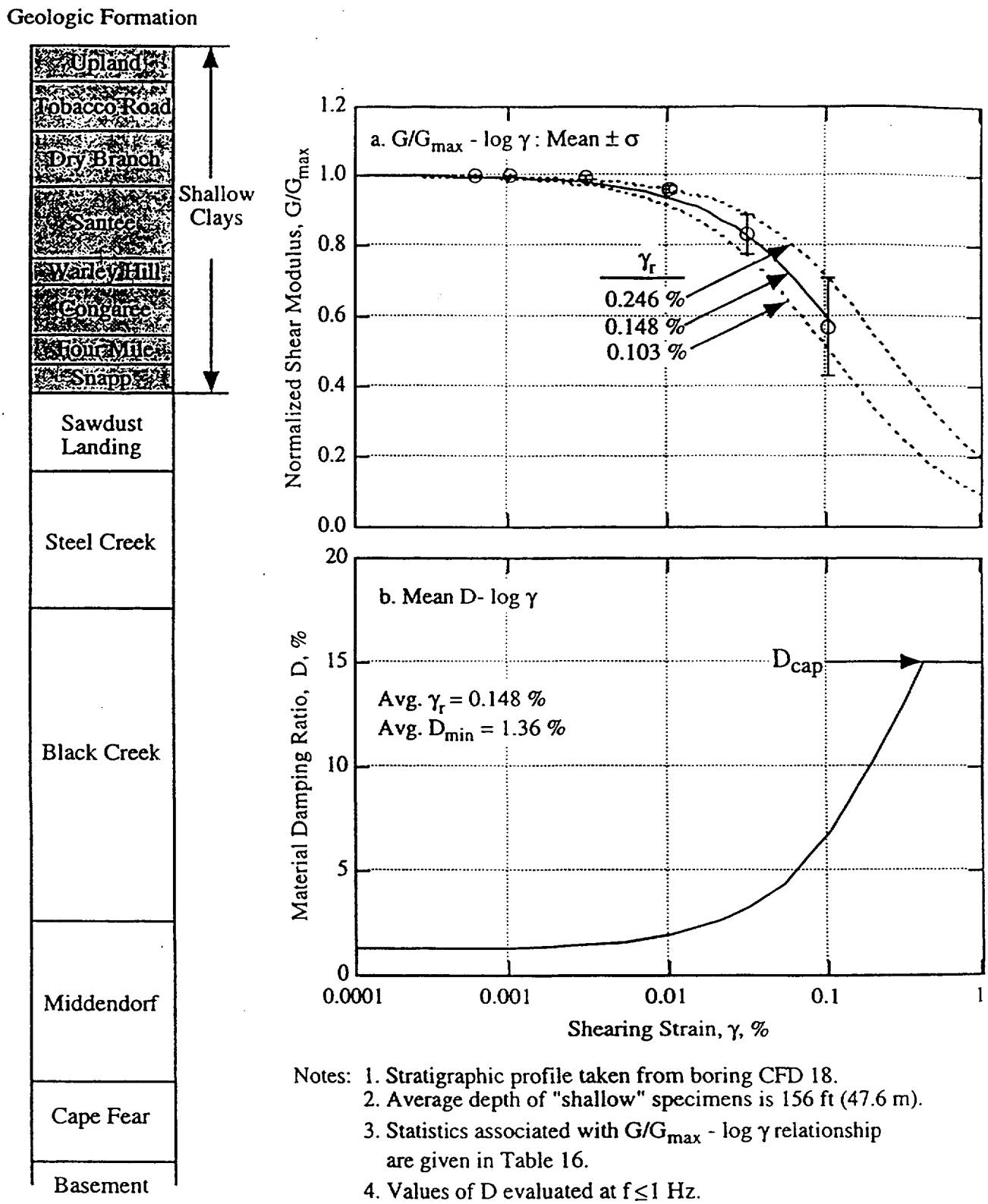


Notes: 1. Stratigraphic profile taken from boring CFD 18.
2. Average depth of "shallow" specimens is 156 ft (47.6 m).
3. Statistics associated with $G/G_{max}$ - log γ relationship are given in Table 16.
4. Values of D evaluated at f ≤ 1 Hz.

Fig. 7 Recommended $G/G_{max}$ (log-γ) and D (log-γ) relationships for Shallow Clays at SRS (taken from Stokoe et al., 1995). Numerical values for best estimates and uncertainties for $G/G_{max}$ (log-γ) and D (log-γ) can be determined from Tables 1, 2, and 3.

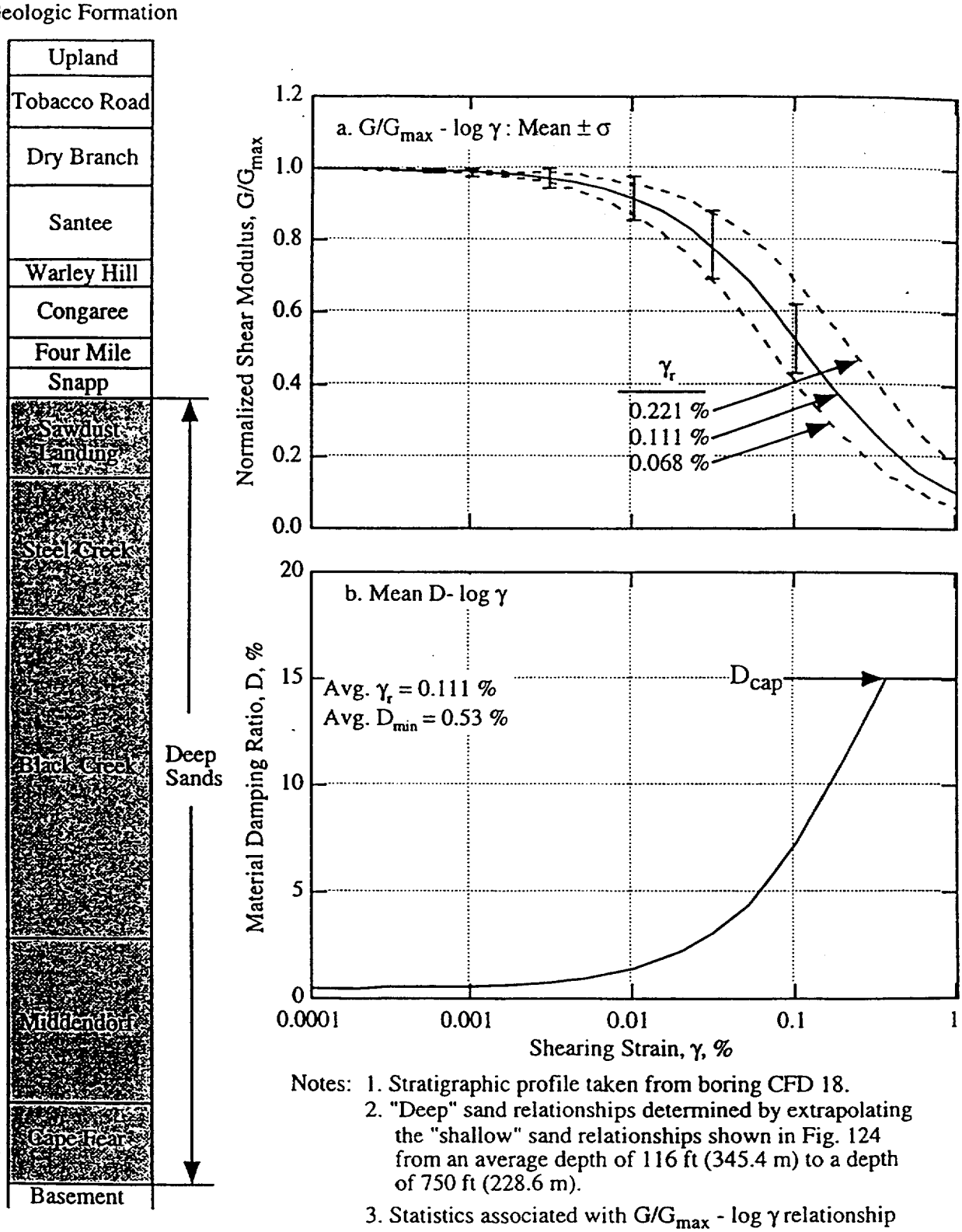


Notes:
1. Stratigraphic profile taken from boring CFD 18.
2. "Deep" sand relationships determined by extrapolating the "shallow" sand relationships shown in Fig. 124 from an average depth of 116 ft (345.4 m) to a depth of 750 ft (228.6 m).
3. Statistics associated with $G/G_{max}$ - log γ relationship are given in Table 24.
4. Values of D evaluated at f ≤ 1 Hz.

Fig. 8 Recommended $G/G_{max}$ (log-γ) and D (log-γ) relationships for Deep Sands at SRS (taken from Stokoe et al., 1995). Numerical values for best estimates and uncertainties for $G/G_{max}$ (log-γ) and D (log-γ) can be determined from Tables 1, 2, and 3.

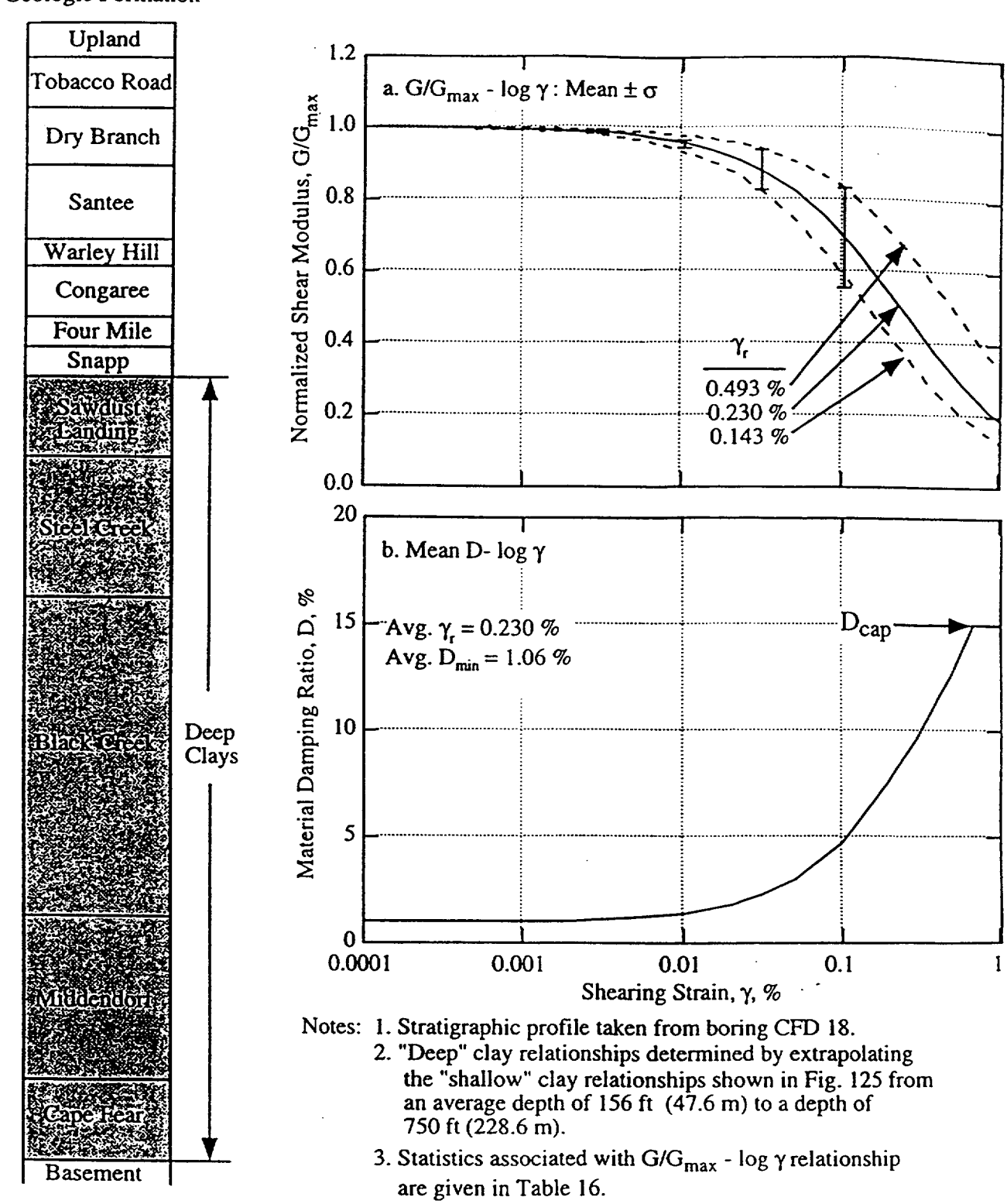


Notes:
1. Stratigraphic profile taken from boring CFD 18.
2. "Deep" clay relationships determined by extrapolating the "shallow" clay relationships shown in Fig. 125 from an average depth of 156 ft (47.6 m) to a depth of 750 ft (228.6 m).
3. Statistics associated with $G/G_{max}$ - log γ relationship are given in Table 16.
4. Values of D evaluated at f ≤ 1 Hz.

Fig. 9 Recommended $G/G_{max}$ (log-γ) and D (log-γ) relationships for Deep Clays at SRS (taken from Stokoe et al., 1995). Numerical values for best estimates and uncertainties for $G/G_{max}$ (log-γ) and D (log-γ) can be determined from Tables 1, 2, and 3.

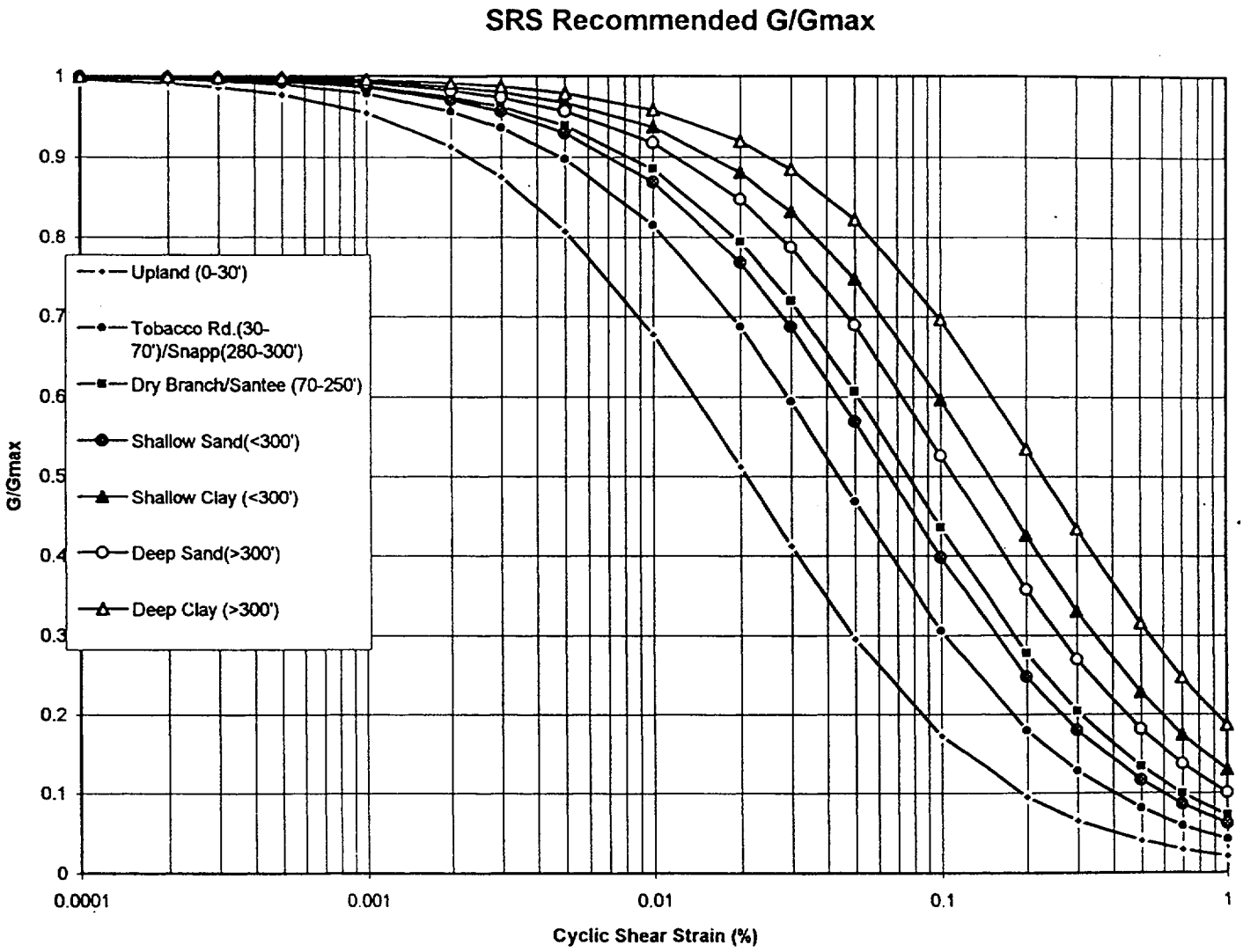


Fig. 10 SRS best estimate normalized shear-modulus curves, by formation.

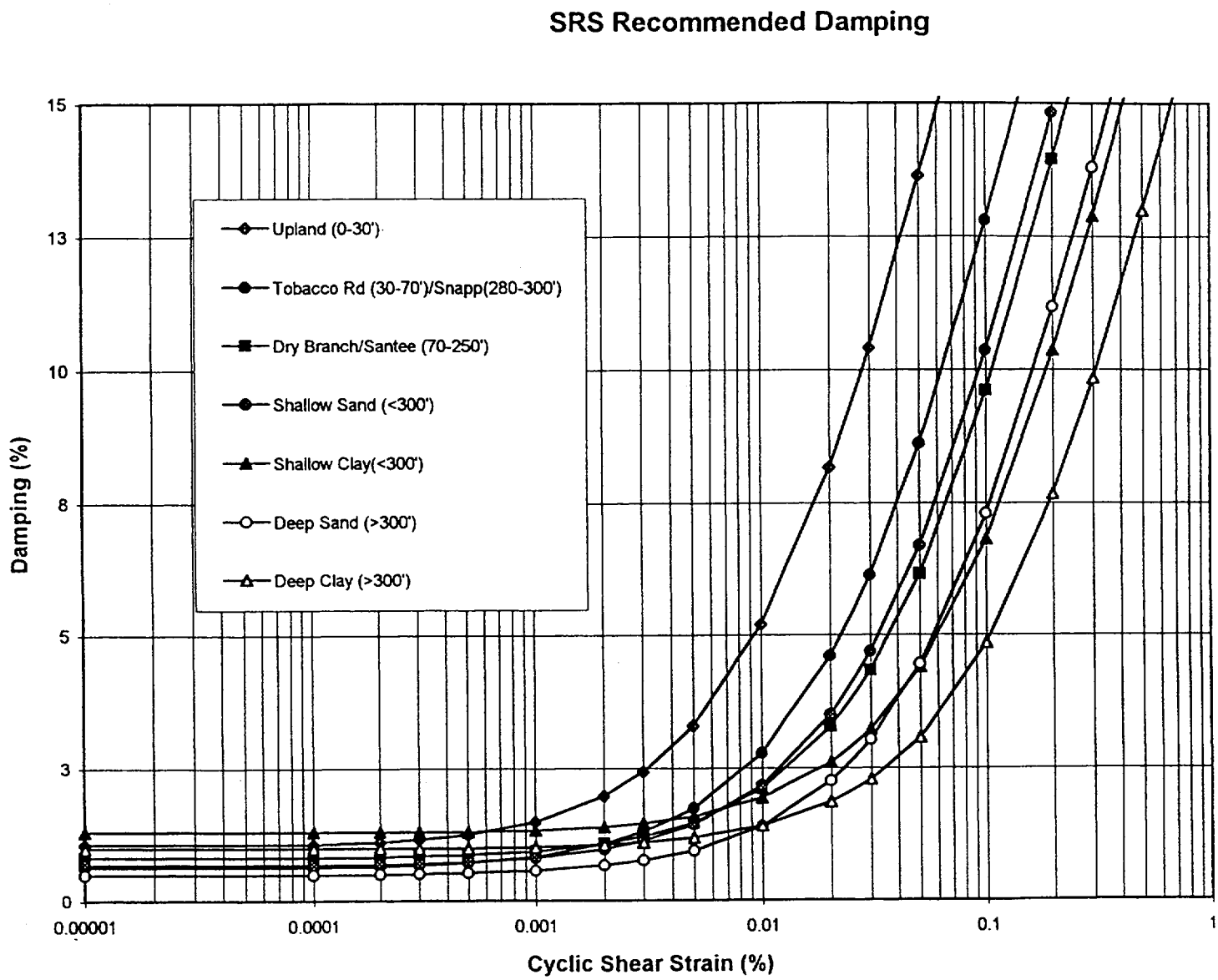


Fig. 11 SRS best estimate damping curves, by formation.

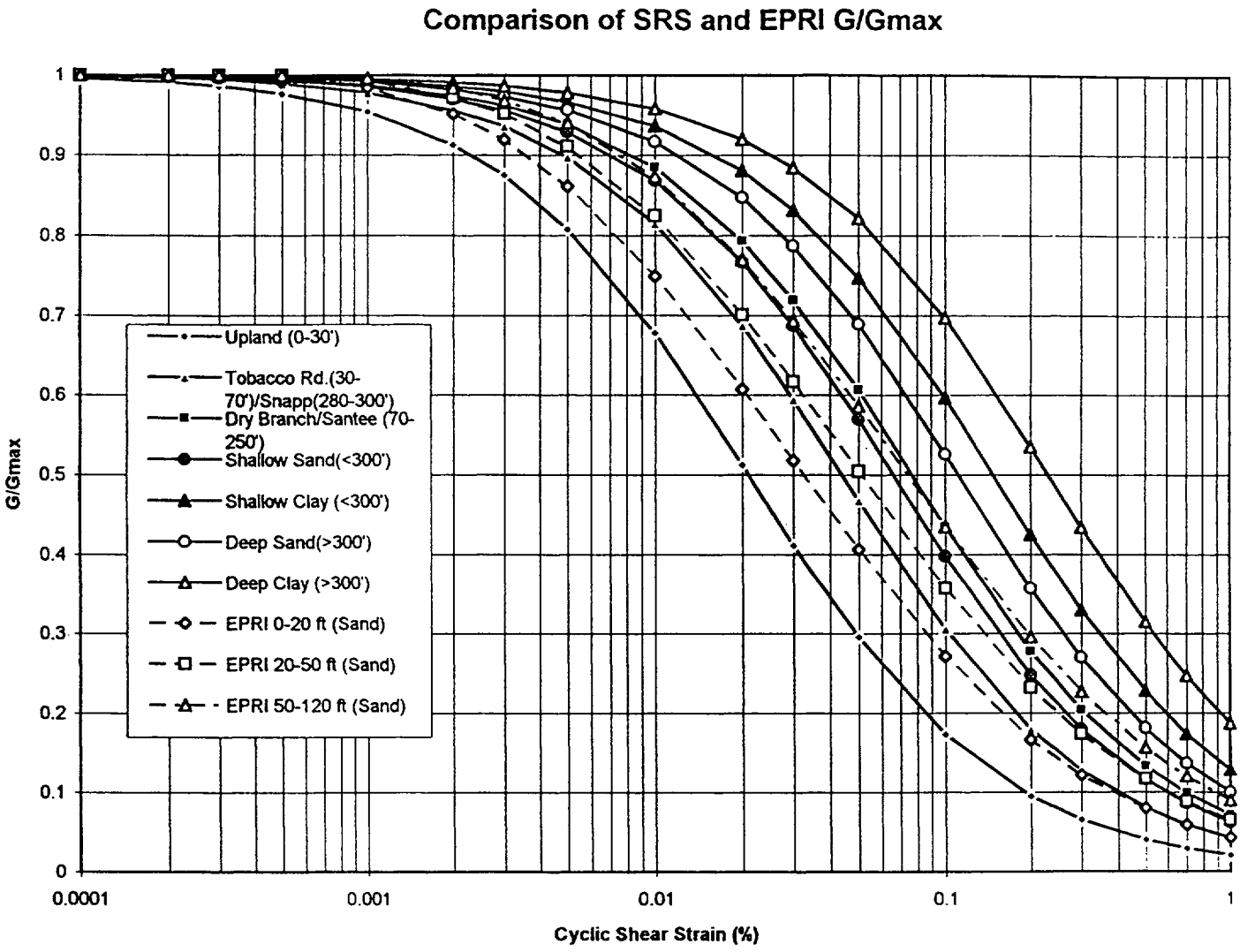


Fig. 12 Comparison of SRS best estimate G/Gmax (Solid Curves) with shallow EPRI (1993) (dashed).

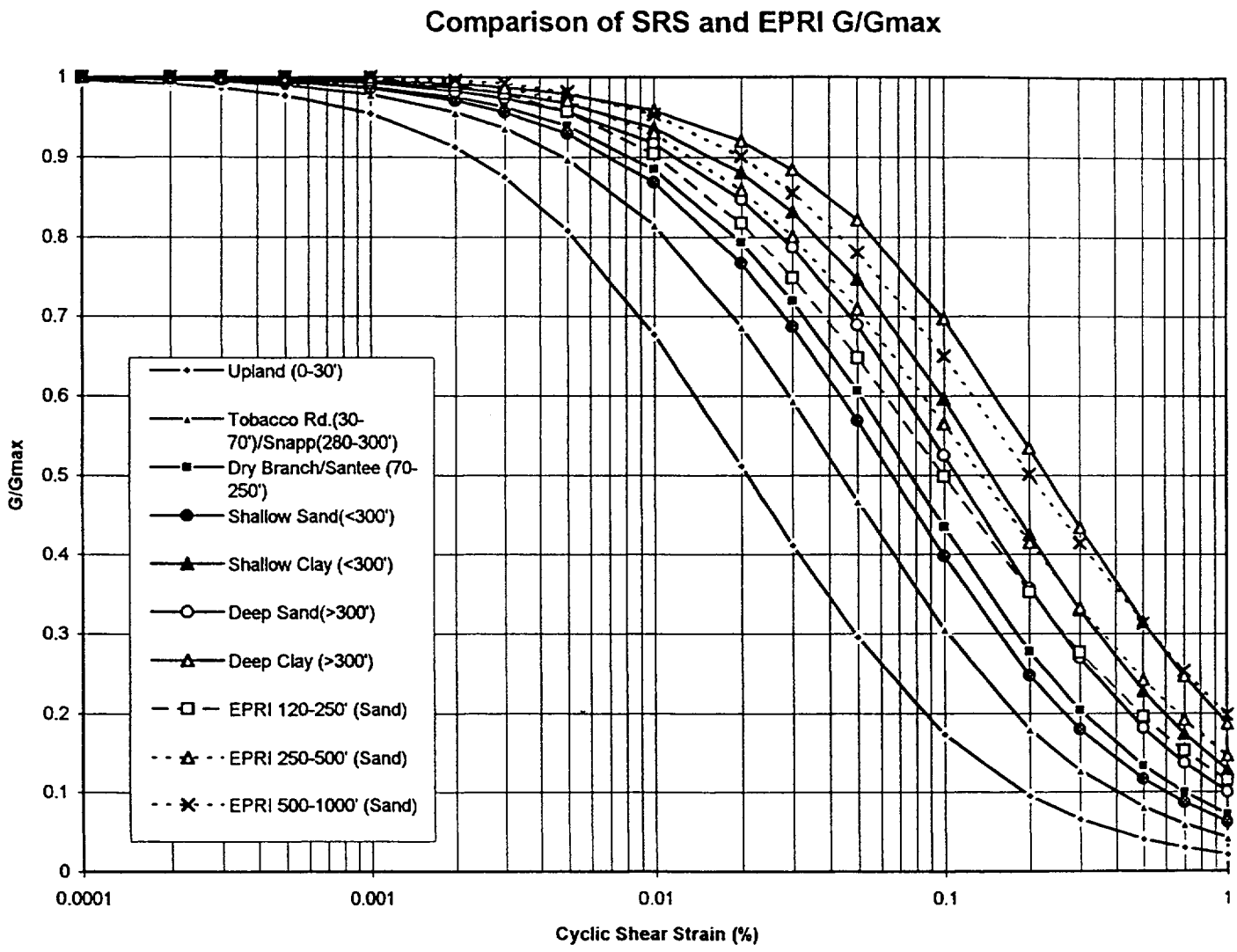


Fig. 13 Comparison of SRS best estimate G/Gmax (Solid Curves) with deep EPRI (1993) (dashed).

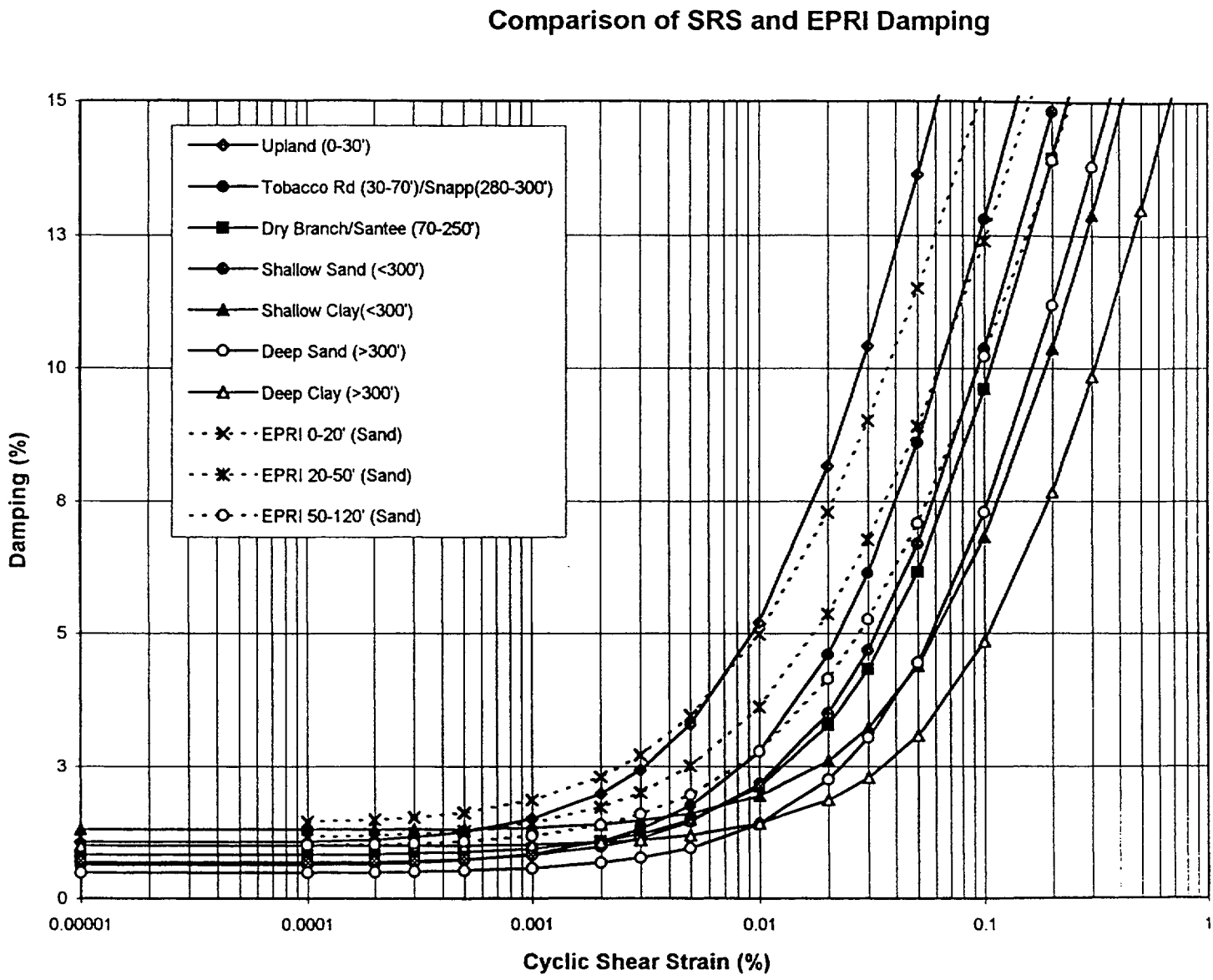


Fig. 14 Comparison of SRS best estimate damping (Solid Curves) with shallow EPRI (1993) (dashed).

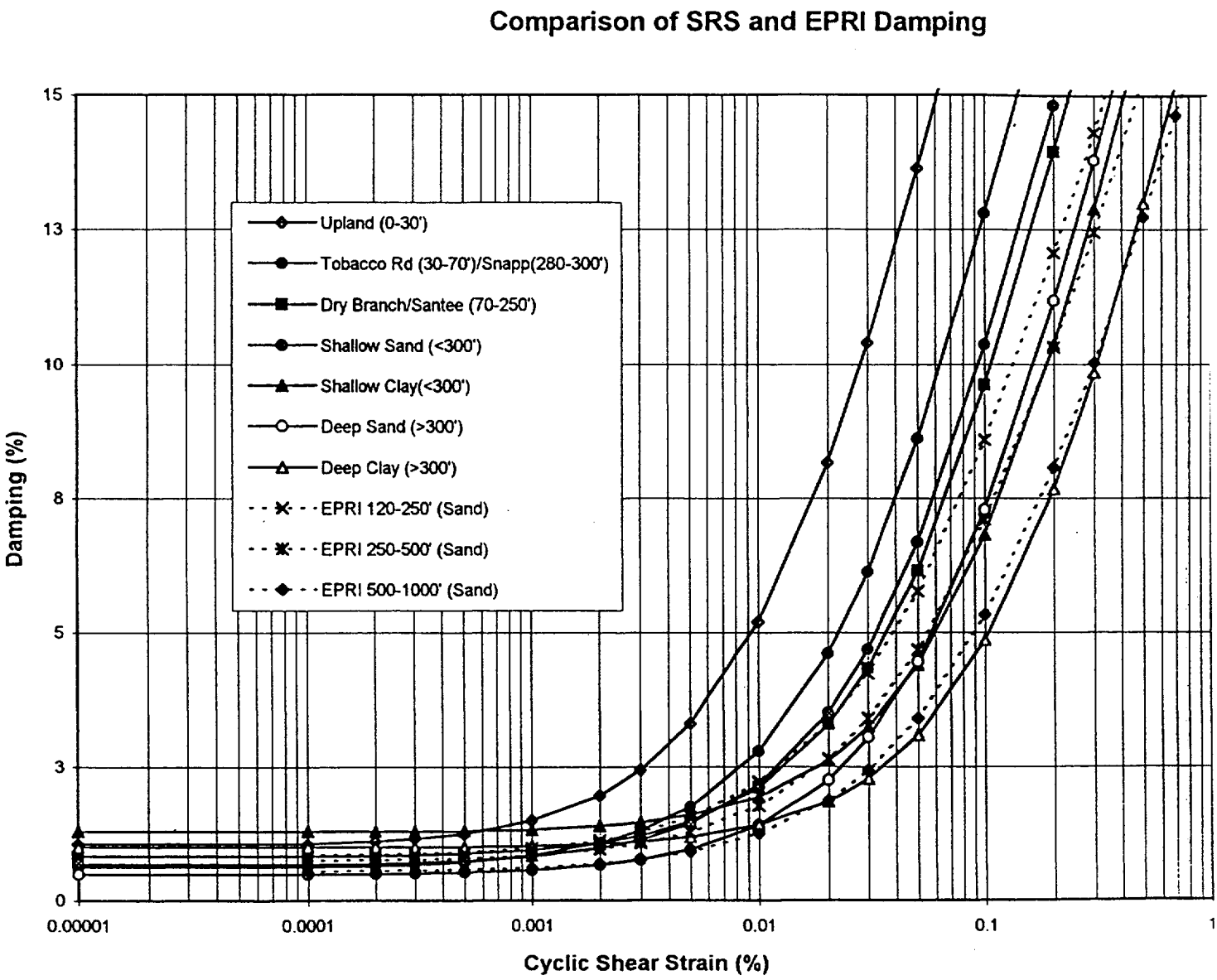


Fig. 15 Comparison of SRS best estimate damping (Solid Curves) with deep EPRI (1993) (dashed).

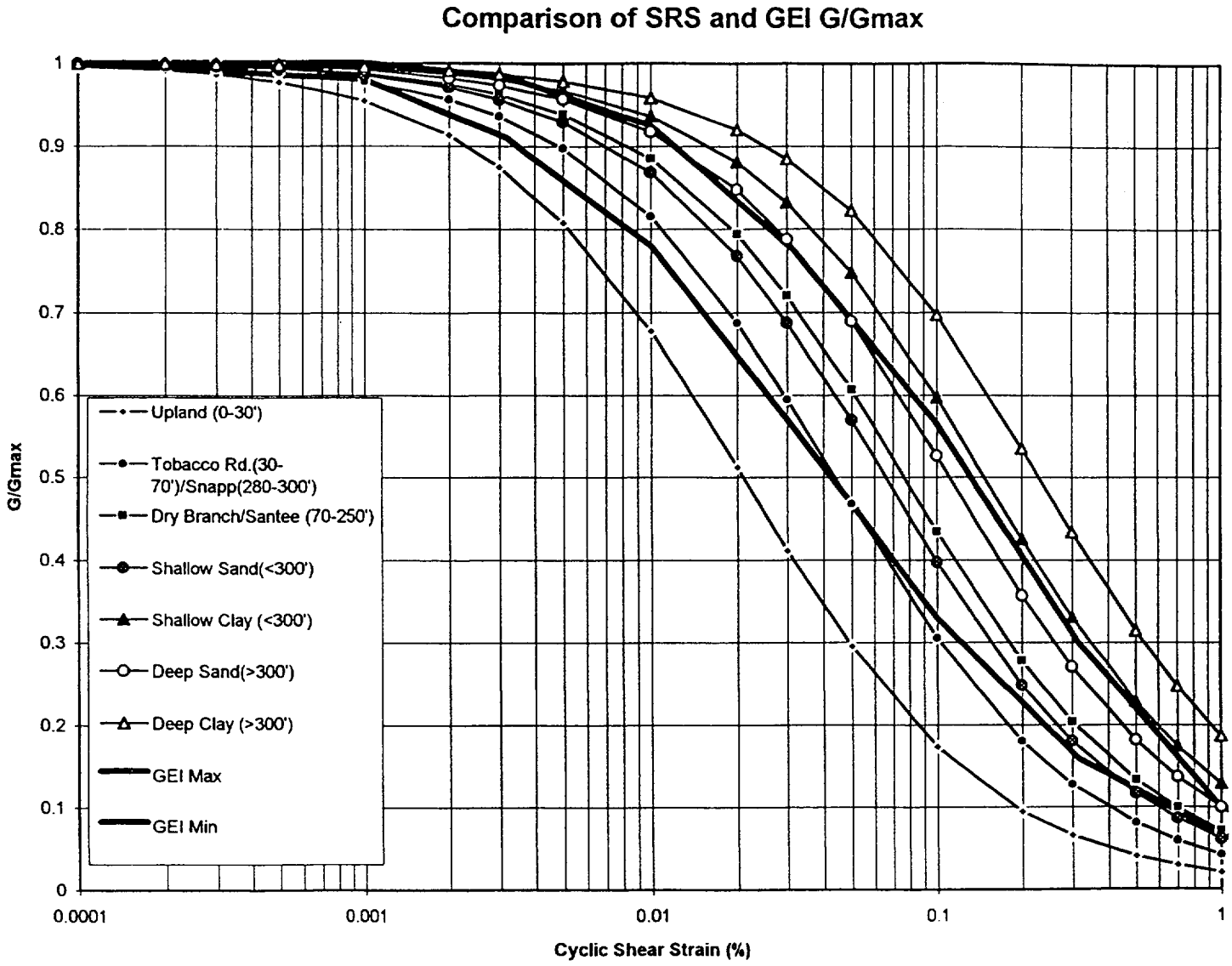


Fig. 16 Comparison of SRS best estimate G/Gmax (Solid Curves) with minimum and maximum GEI (1991) (bold).

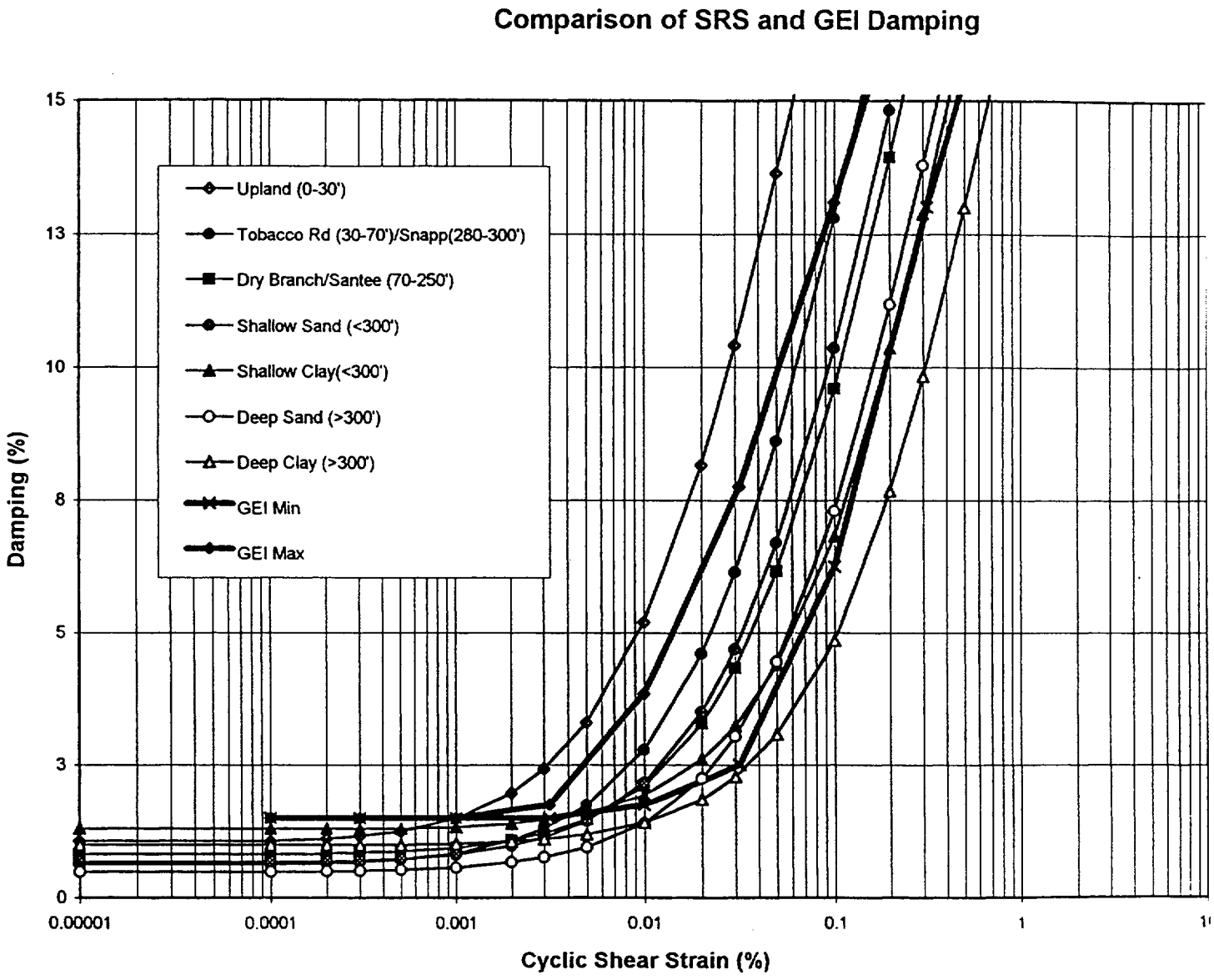


Fig. 17 Comparison of SRS best estimate damping (Solid Curves) with minimum and maximum GEI (1991) (bold).